Tesis de Doctorado

en Ciencias Biológicas

VALIDACIÓN DE LA GLUCOSA-6-FOSFATO DESHIDROGENASA

DE *TRYPANOSOMA CRUZI*,

COMO BLANCO PARA EL DISEÑO RACIONAL

DE FÁRMACOS ANTICHAGÁSICOS.

Lic. Cecilia Ortiz Carrión
Orientador: Dr. Marcelo A. Comini
PEDECIBA – Biología, Universidad de la República, Uruguay
Junio 2017

TRIBUNAL

Dra. Margot Paulino (Facultad de Química, Universidad de la República)

Dr. Sergio Pantano (Institut Pasteur de Montevideo)

Dr. Carlos Robello (Facultad de Medicina, Universidad de la República)

RESUMEN

La enfermedad de Chagas, causada por el parásito *Trypanosoma cruzi*, es endémica de América Latina y presenta elevados índices de mortalidad y morbilidad. La búsqueda y caracterización de nuevos blancos moleculares que contribuyan a la generación de fármacos o estrategias terapéuticas es una meta prioritaria para esta enfermedad. En este sentido, la enzima glucosa-6-fosfato deshidrogenasa (G6PDH), cuya función es catalizar la primera reacción de la vía de las pentosas-5-fosfato donde se generan equivalentes de reducción (NADPH), ribosa-5-fosfato e intermediarios de la glicólisis, ha mostrado ser un factor determinante para la supervivencia de *Trypanosoma brucei* y de virulencia para las formas infectivas de *T. cruzi* y *Leishmania donovani*. Gran parte de su importancia biológica radica en aportar poder reductor para el mantenimiento de la homeostasis redox intracelular.

Nuestro objetivo ha sido caracterizar desde el punto de vista bioquímico, estructural y biológico a la G6PDH de *T. cruzi*, de manera tal de profundizar en el conocimiento sobre esta enzima y, eventualmente, validarla como blanco farmacológico.

Entre los principales resultados obtenidos durante la misma se destacan: (**1**) la cristalización y resolución de la primera estructura atómica de una G6PDH proveniente de un organismo patógeno, *T. cruzi*; (**2**) la identificación y el estudio de la relevancia funcional y estructural de varias regiones y residuos diferenciales entre la proteína de *T. cruzi* y su homóloga humana; (**3**) la dilucidación del sitio de unión de inhibidores esteroideos a la G6PDH de *T. cruzi*, el cual difiere de aquel propuesto para las enzimas de *Leishmania infantum* y humana; y (**4**) la confirmación que la G6PDH es una enzima predominantemente citosólica y blanco molecular de la epiandrosterona en epimastigotas de diferentes cepas de *T. cruzi*.

De esta forma, este trabajo ha realizado aportes importantes respecto a la caracterización molecular de este blanco farmacológico, permitiendo la identificación de diferentes características estructurales distintivas que pueden ser explotadas en el diseño racional de inhibidores.

ABSTRACT

Chagas disease is caused by the parasite Trypanosoma cruzi, which is endemic to Latin America, and present high rates of mortality and morbidity. The identification and characterization of new molecular targets that may lead to the generation of new drugs or therapeutic strategies is of upmost importance to combat this disease. The enzyme glucose-6-phosphate dehydrogenase (G6PDH) catalyzes the first reaction of the pentose-5-phosphate pathway that generates important metabolites such as NADPH, ribose-5-phosphate and glycolytic intermediates. G6PDH has been shown to be a determinant factor for the survival of *Trypanosoma brucei* and a virulence factor in the infective forms of *T. cruzi* and *Leishmania donovani*. The biological relevance of this enzyme lies on supplying reducing power for the maintenance of the intracellular redox homeostasis.

The main goal of this study was to undertake the biochemical, structural and biological characterization of G6PDH from *T. cruzi*, in order to reach a comprehensive knowledge on the molecular aspects that distinguish this enzyme and, eventually, contribute to its validation as a drug target candidate.

The main results obtained during this thesis are: (**1**) the crystallization and resolution of the first atomic structure of a G6PDH from a pathogenic organism, *T. cruzi*; (**2**) the identification and study of structural and functional relevance of several regions and residues that are distinctive between *T. cruzi* and human G6PDH; (**3**) the elucidation of the binding site of steroids to the trypanosomal enzyme, which differed from that propossed for the *Leishmania infantum* and human homologue; and (**4**) the confirmation that G6PDH is predominantly a cytosolic protein targeted by epiandrosterone in epimastigotes of different *T. cruzi* strains.

In summary, this study made important contributions to the molecular characterization of this therapeutic target by allowing the identification of different and distinctive structural features that may be exploited towards the rational design of inhibitors.

INDICE GENERAL

TABLA DE CONTENIDOS

Capítulo 1. INTRODUCCIÓN

Capítulo 2. OBJETIVOS

Capítulo 3. RESULTADOS

LISTA DE ABREVIATURAS

CTC	Ditolil-ciano-cloruro de tetrazolio
DHEA	dehidroepiandrosterona
DTT	ditiotreitol
EA	epiandrosterona
E4P	eritrosa 4-fosfato
F6P	fructosa 6-fosfato
G3P	gliceraldehído 3-fosfato
GK	glicerol kinasa
G6PDH	glucosa 6-fosfato deshidrogenasa
G6P	glucosa 6-fosfato
GSH	glutatión reducido
GSSG	glutatión oxidado
HK	hexoquinasa
NTD	enfermedades tropicales desatendidas
PTS	peroxisomal targeting signal
PEX	*peroxina*
PFK	fosfofructo quinasa
PGK	fosfoglicerol quinasa
PK	piruvato quinasa
PPP	vía de las pentosas fosfato
P5F	pentosa 5-fosfato
RPE	ribulosa 5-fosfato epimerasa
RPI	ribosa 5-fosfato isomerasa
R5P	ribosa-5-fosfato
RU5P	ribulosa 5-fosfato
S7P	sedoheptulosa-7P
TAL	transaldolasa
TKT	transcetolasa
TryR	tripanotión reductasa
T(SH)2	tripanotión reducido
TS2	tripanotión oxidado
TXN	triparredoxina

SEC	cromatografía de exclusión molecular
X5P	xilulosa 5-fosfato
6-AN	6-amoninicotinamida
16-BrEA	16-bromoepiandrosterona
6-PGDH	6-fosfogluconato deshidrogenasa
6-PGL	6-fosfogluconolactonasa
Δ37N	mutante con una deleción de 37 residuos en el N-terminal
Δ57N	mutante con una deleción de 57 residuos en el N-terminal

introducción

Capítulo 1.

INTRODUCCIÓN

1.1 Enfermedades desatendidas

La enfermedad de Chagas, la tripanosomiasis africana y la leishmaniasis son enfermedades causadas por parásitos protozoarios pertenecientes a la clase *Kinetoplastea*, los cuales comparten características bioquímicas y estructurales similares (Stuart et al., 2008). Las dolencias que estos organismos infecciosos causan, afectan a más de 100 millones de personas en el mundo y son consideradas "enfermedades olvidadas" (*neglected tropical diseases*: NTD) dado que tienen por blanco a las poblaciones más vulnerables desde el punto de vista social y económico. Paradójicamente, a pesar que las mismas ocasionan costos de miles de millones de dólares cada año debido a la alta morbilidad y discapacidad que generan en las personas enfermas, las mismas no reciben la atención ni los fondos suficientes por parte de los gobiernos para lograr su erradicación. En los últimos años y gracias a los esfuerzos de la academia y algunas ONGs (ejemplo; DNDi & WHO) se han logrado avances importantes en lo que respecta a la identificación, validación y caracterización de potenciales blancos de fármacos. A su vez se han identificado nuevos candidatos a fármacos y reformulado alguno de los ya establecidos. También se han desarrollado nuevas técnicas y herramientas que son útiles para comprender mejor los mecanismos de la enfermedad, detectar nuevos inhibidores y validar a los nuevos blancos moleculares (El-Sayed et al., 2005; Frearson et al., 2007). Sin embargo, las terapias y tratamientos disponibles a la fecha, distan mucho de lo ideal. A pesar de existir un consenso a nivel mundial acerca de la necesidad de contar con tratamientos/fármacos más efectivos, seguros y accesibles, estas enfermedades continúan siendo de escaso interés para la industria farmacéutica.

1.2 La enfermedad de Chagas y *Trypanosoma cruzi*

La enfermedad de Chagas es una zoonosis causada por *T. cruzi*, la cual es endémica de América del Sur y Central. Si bien fue descrita por primera vez en 1909 por el Dr. Carlos Chagas, existe evidencia que esta enfermedad ha co-existido con el ser humano desde hace más de 9000 años (Aufderheide et al., 2004; Salvatella R, 2009).

El mal de Chagas al igual que el resto de las NTDs, constituye un problema de salud pública importante, con una clara dimensión social, asociada a la pobreza y a la falta de recursos para su prevención y tratamiento. Se estima que alrededor de 7 millones de personas están infectadas, siendo la tasa de mortalidad de 12.000 personas por año (Lee et al., 2013). La morbilidad y

mortalidad son especialmente elevadas en personas que viven en el medio rural y en condiciones de pobreza, donde el tipo de vivienda y dificultades en el acceso a la atención médica facilitan la transmisión vectorial y complican el diagnóstico en etapas tempranas de la infección.

La forma más frecuente de infección se da por transmisión vectorial, y se produce por el contacto de las mucosas o dermis del ser humano con heces de insectos triatominos (familia *Reduviidae*) infectados. Alrededor de 25 millones de personas se encuentran en riesgo de contagio, afortunadamente gracias a los programas para interrumpir la transmisión vectorial, esta cifra se redujo considerablemente en las últimas dos décadas, siendo nuestro país el primero en declararse libre de transmisión vectorial en el año 1997 (Barrios et al., 2015; Rosa et al., 2001). Otras vías de transmisión de la enfermedad son la congénita, la transfusión de sangre o el trasplante de órganos infectados, así como la ingesta de alimentos contaminados con parásitos (Sánchez and Ramírez, 2013; Yoshida, 2009). Las primeras constituyen las principales causas de propagación de la enfermedad a regiones no endémicas, debido a los flujos migratorios de personas infectadas (Conners et al., 2016), ver figura 1.

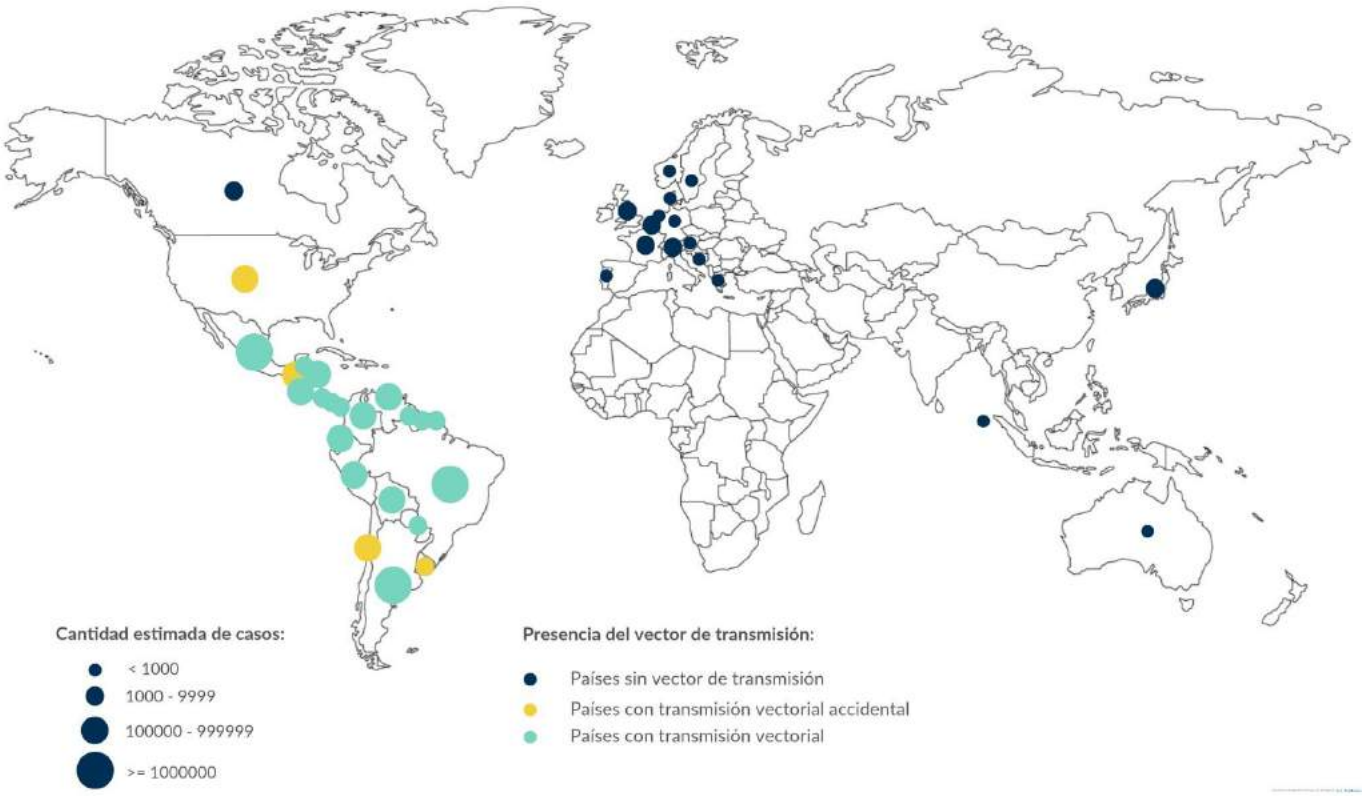

Figura 1. Distribución geográfica de la enfermedad de Chagas.
Presencia del vector de transmisión y cantidad estimada de casos entre los años 2006-2009. Imagen tomada de http://www.bayerpharma.com.

1.2.1 Cuadro clínico

La enfermedad suele presentarse bajo dos formas clínicas: la etapa aguda y la etapa crónica.

La fase aguda muchas veces pasa inadvertida o se la confunde con otras patologías infecciosas comunes ya que en el 90% de los casos es asintomática, la manifestación clínica de la enfermedad es poco específica, salvo en los casos donde se evidencia la presencia de un edema en el sitio de infección conocido como Chagoma. Esta etapa dura de 30-60 días y se caracteriza por una elevada parasitemia e invasión tisular, suele ser mortal para el 5-7% de los casos. Luego de esta fase, el 70% de los infectados pasan por un periodo asintomático que puede durar unos 10 o 30 años y que en la mayoría de los casos deriva en la fase crónica. Esta fase se caracteriza por fallas de tipo cardíaco y visceral, y menos frecuentemente en afectaciones del aparato urinario, glándulas suprarrenales y sistema nervioso (Gonçalves et al., 2010; Barrett et al., 2003; Lewis et al., 2014); la disfunción de los distintos órganos además de afectar la calidad de vida, puede ser letal para los enfermos.

1.2.2 Tratamiento

La cura definitiva del mal de Chagas presenta dos grandes desafíos, por un lado el control de la transmisión del agente infeccioso y por el otro, contar con un tratamiento efectivo para la enfermedad (Lannes-Vieira et al., 2010). El primero involucra el control de la transmisión vectorial, congénita y por transfusiones/transplantes, y se encuentran bajo el ámbito gubernamental y de ONGs como la DNDi y médicos sin fronteras. El segundo, al no ser redituable económicamente para las industrias farmacéuticas, recae casi exclusivamente (salvo algunas excepciones) en los esfuerzos que la academia realiza por encontrar nuevas estrategias terapéuticas y fármacos, y en algunos estados dispuestos a apoyar la producción de estas medicinas.

Lamentablemente, los esfuerzos por generar vacunas no han resultado exitosos ya que si bien varios estudios de inmunización realizados en modelos murinos han mostrado un incremento en la supervivencia de los animales, esta estrategia no logró esterilidad inmunológica frente al parásito (Sanchez-Burgos et al., 2007; Cazorla et al., 2010). Por este motivo, la quimioterapia continúa siendo una opción viable para el tratamiento de esta enfermedad, si bien se reconoce que deben realizarse mejoras sustanciales en los medicamentos disponibles o en desarrollos terapéuticos tendientes a incrementar la eficacia del tratamiento en la fase crónica de la

enfermedad, la cual a la fecha es prácticamente incurable (Tarleton and Zhang, 1999; Rodriguez et al., 2016).

Históricamente se emplean dos fármacos para tratar la enfermedad de Chagas, ambos son nitroheterociclos que fueron descubiertos empíricamente hace más de seis décadas. El Nifurtimox de Bayer, es efectivo para tratar la fase aguda de la enfermedad, ya que muestra un efecto tripanocida, eliminando principalmente a los tripomastigotas circulantes en sangre y otros fluidos. Lamentablemente, este fármaco requiere de tratamientos prolongados y presenta efectos secundarios no deseados que afectan el sistema nervioso y el aparato digestivo, por esta razón, actualmente su uso se encuentra discontinuado en algunos países. Llamativamente, para Uruguay y el Salvador, el nifurtimox es la única opción disponible. Por otro lado, se dispone del benznidazol (Barrett et al., 2003), cuya patente fue cedida por Roche al gobierno brasileño y es producido tanto por Lafepe en Brasil y por el laboratorio privado ELEA en Argentina (Molina et al., 2015). Recientemente, se ha desarrollado una nueva formulación pedíatrica para el benznidazol (Altcheh et al., 2014). Este compuesto presenta como desventajas, elevada toxicidad, limitada eficacia en la fase crónica de la enfermedad y un alto costo para tratamientos prolongados (Cavalli et al., 2009; Irigoín et al., 2008). Por otro lado, para ambos derivados nitroheterocíclicos se ha observado desarrollo de resistencia (Murta and Romanha, 1998; Murta et al., 1998; Sokolova et al., 2010), ver figura 2.

Actualmente se están evaluando algunos candidatos a fármacos que incluyen a los inhibidores de la cruzipaína, como la vinilsulfona, k777, y su análogo que contiene una arginina protonable, el wrr483, siendo ambos eficaces para el tratamiento de la fase aguda de la enfermedad y también activos en modelos murinos de Chagas crónico (McKerrow et al., 2009). Estos compuestos presentan buenas características fisicoquímicas, buena biodisponibilidad oral y ausencia de efectos mutagénicos (Abdulla et al., 2007). Sin embargo, para la versión neutra de k777 se han reportado efectos tóxicos lo cual, sumado al alto costo del escalado de su producción, llevó a que se detuvieran los estudios de fase clínica, ver figura 2.

Los derivados de triazol, originalmente empleados como antifúngicos que inhiben la síntesis del ergosterol, como el posaconazol y el ravuconazol o E1224 (Urbina, 2009; Pinazo et al., 2010; Bernard Pécoul et al., 2009) mostraron buena actividad en el modelo animal de Chagas (Francisco et al., 2015; Taylor et al., 2015). El posaconazol y el E1224 fueron sometidos a ensayos clínicos, los cuales fueron desalentadores en el sentido que si bien ambos mostraron actividad tripanocida su eficiencia fue similar a la del benznidazol (Molina et al., 2014a, 2014b; Salomao et al., 2016), con la desventaja de su elevado costo de producción, ver figura 2.

Finalmente, experimentos realizados en ratones mostraron que tratamientos combinados con posaconazol y aminodrona o dronedarona, disminuyen la parasitemia y prolongan la expectativa de vida de los animales infectados, ya que la co-administración de los últimos compuestos tiene efectos positivos sobre la función cardíaca, la cual, como se mencionó anteriormente se ve afectada por la infección. La combinación con posaconazol presenta un efecto aditivo ya que ambos compuestos son capaces de inhibir la síntesis de esteroles. Además, la aminodrona y dronedarona inducen la liberación de calcio y otros iones desde los acidocalcisomas y de esta manera afectan la homeostasis del calcio que resulta letal para *T. cruzi*; mientras que a nivel del hospedero mejoran el cuadro cardíaco, disminuyendo los episodios de arritmia (Benamin G 2012- Nature), ver figura 2.

Fármacos actuales

NIFURTIMOX

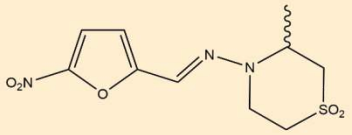

Ciclador redox, genera ROS

BENZNIDAZOL

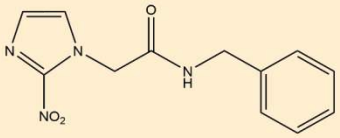

Afecta el metabolismo del tripanotión, genera ROS, depleta tioles libres.

Fármacos en estudio

K777

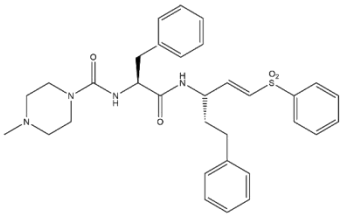

Inhibidor de cruzipaina

WRR483

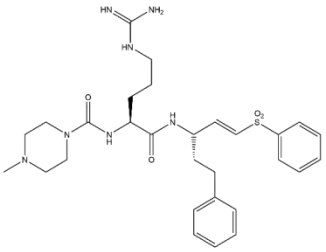

Inhibidor de cruzipaina

POSACONAZOL

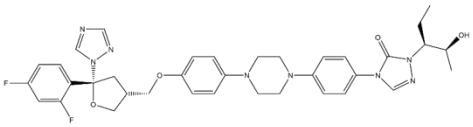

Inhibe síntesis de ergosterol

RUVACONAZOL (E1224)

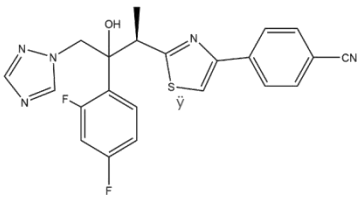

Inhibe síntesis de ergosterol

AMINODRONA

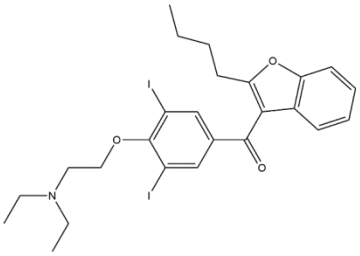

Afecta homeostasis del calcio, inhibe síntesis de esteroles

DRONEDARONA

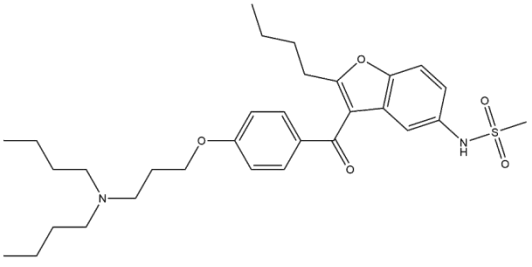

Inhibe síntesis de esteroles

Figura 2. Fármacos empleados en el tratamiento de la enfermedad de Chagas
Estructuras químicas y blanco de acción de los fármacos utilizados para tratar la enfermedad de Chagas. Los fármacos en uso clínico se muestran sobre fondo amarillo. Estructuras realizadas en Chemdraw.

1.2.3 Ciclo de vida de *Trypanosoma cruzi*

Trypanosoma cruzi es un protozoario unicelular flagelado perteneciente al orden *Trypanosomatidae* (Barrett et al., 2003). Este parásito presenta un ciclo de vida complejo que incluye la colonización de un organismo invertebrado (vector) y otro mamífero (huésped). Para adaptarse a los diferentes ambientes que encuentra en el vector y el huésped, el parásito atraviesa cambios morfológicos y metabólicos altamente controlados. Las adaptaciones a nivel estructural implican cambios en las proteínas de superficie, transportadores de nutrientes y en el citoesqueleto, mientras que a nivel metabólico se induce o reprime la expresión de diferentes enzimas del metabolismo energético, todo lo cual resulta clave para su supervivencia (Jimenez, 2014; Noireau et al., 2009). Durante el ciclo de vida de *T. cruzi* se reconocen cuatro estadios: epimastigota, tripomastigota metacíclico, tripomastigota y amastigota, cada uno de ellos con características morfólogicas, ultraestructurales y metabólicas bien definidas. El epimastigota es la forma no infectiva, extracelular y proliferativa que se localiza en el intestino del insecto vector. Presenta una mitocondria desarrollada que se ubica de manera central junto con el kinetoplasto (región de la mitocondria que contiene el ADN mitocondrial). En la parte posterior del intestino del vector, los epimastigotas se diferencian a tripomastigotas metacíclicos. La metaciclogénesis conlleva a importantes cambios en la expresión de marcadores de superficie y a nivel del metabolismo del parásito, que juegan un papel decisivo en la invasión. Los tripomastigotas metacíclicos presentan una mitocondria condensada y su kinetoplasto se localiza en el extremo posterior del parásito, si bien este estadio es altamente infectivo para el huésped mamífero, el mismo no posee capacidad replicativa. Tras la picadura y defecación del insecto, los tripomastigotas metacíclicos logran entrar a la circulación sanguínea de su huésped y son capaces de invadir una amplia gama de células nucleadas (ej. fibroblastos, células epiteliales). En etapas iniciales de la invasión, los macrófagos juegan un rol esencial ya que son la primera línea de defensa contra la infección, pero también los encargados de transportar los parásitos a otros sitios del cuerpo, como el tejido miocárdico y el tubo digestivo principalmente (Barrett et al., 2003). Mediante un proceso de endocitosis que involucra la formación de una vacuola parasitófora, el parásito consigue invadir la célula blanco y en su interior se diferencia a la forma intracelular, infectiva y proliferativa llamada amastigota. Los amastigotas presentan una forma redondeada que carece de flagelo, una pequeña mitocondria con el kinetoplasto altamente condensado que se localiza de manera anterior al núcleo. El amastigota se divide por fisión binaria formando un pseudoquiste dentro de la célula, al cabo de 5 días se diferencian al estadio de tripomastigota (flagelado, replicativo, extracelular e infectivo). El gran contenido de

tripomastigotas intracelulares sumado a su movilidad conlleva al aumento del volumen de la célula huésped y a su posterior lisis. Los parásitos al torrente sanguíneo podrán infectar nuevas células o bien ser ingeridos por el insecto vector, para finalmente volverse a diferenciar a epimastigotes, en el intestino del triatominio, cerrando así el ciclo. (Burleigh and Woolsey, 2002; Tyler and Engman, 2001).

1.3 Metabolismo de la glucosa en trypanosomas

En la mayoría de los organismos la glucosa se metaboliza a través de dos vías: la glicólisis y la vía de las pentosas 5-fosfato (PPP). Ambas vías utilizan a la glucosa 6-fosfato (G6P) como primer sustrato y ambas cumplen funciones diferentes e indispensables para la supervivencia del parásito tal como se discute en las próximas secciones.

1.3.1 Glicosomas: Rol y compartimentalización

Los tripanosomátidos poseen características estructurales que los hacen únicos como por ejemplo el flagelo, el arreglo microtubular que forma su citoesqueleto, el ADN mitocondrial (kinetoplasto), el cual se encuentra empaquetado formando maxi y mini círculos. También se caracterizan por poseer un organelo tipo peroxisoma que carece de actividad catalasa pero contiene la gran mayoría de las enzimas de la vía glicolítica, por lo que se lo ha denominado glicosoma. Los glicosomas fueron originalmente detectados en *T. brucei* y descritos por primera vez en 1977 por Opperdoes y Borst. Son organelos de membrana simple, que comparten características morfológicas con los peroxisomas y que retienen algunas de sus funciones, como por ejemplo la biosíntesis de lípidos. Para la forma sanguínea de *T. brucei* se ha observado que el 90% de las enzimas de la glicólisis se encuentran compartimentalizadas en este organelo. Por otro lado, los glicosomas también alojan enzimas de la vía de las pentosas, del salvataje de purinas y de la gluconeogénesis, entre otras. El número de glicosomas así como su contenido en actividad enzimática varía según la especie y el estadio en que se encuentre el parásito. Se ha demostrado que, la compartimentación es esencial para el parásito (Bakker et al., 2000; Fry et al., 1993; Guerra-Giraldez et al., 2002; Krazy and Michels, 2006; Moyersoen et al., 2003; Verplaetse et al., 2009) y existen varias teorías acerca de cuál podría ser su rol, las cuales se exponen a continuación:

1) Los glicosomas garantizan un elevado flujo glicolítico. Dado que estos organelos representan cerca del 4% del volumen celular total de *T. brucei*, esto implica que las enzimas glicolíticas están confinadas en un volumen pequeño que por otro lado permite alcanzar concentraciones de sustratos/metabolitos sustancialmente elevadas. De esta forma se logra un mejor control y eficiencia de este proceso metabólico (Bakker et al., 1995, 2000).

2) Confinar enzimas en un volumen pequeño, facilita la "canalización" de sustratos de una misma ruta metabólica. Esta teoría es muy discutida desde que el grupo de Aman Ra en 1986 demostró que no hay contribución real por "canalización" de sustratos (Haanstra et al., 2014).

3) La compartimentación es necesaria para un correcto funcionamiento de las enzimas glicolíticas. Esta aseveración se basa en evidencias biológicas que muestran que afectar los mecanismos de importación de proteínas glicosomales es perjudicial para la supervivencia del parásito (Bakker et al., 2000; Furuya et al., 2002; Guerra-Giraldez et al., 2002).

La compartimentalización junto con la plasticidad metabólica, le permiten al parásito adaptarse rápidamente a la demanda energética celular sin necesidad de depender de estrategias de inhibición por producto o sustrato (en parte debido a la alta eficiencia catalítica de esta vía), como se observa en otros organismos que carecen de dicho organelo. Sin embargo, se ha encontrado evidencia que durante el ciclo celular muchas de las proteínas glicosomales presentan patrones variables de fosforilación (dependientes del estadio y del entorno), lo que sugiere que algunas de dichas enzimas podrían estar sometidas a otro tipo de regulación pos-traduccional (Haanstra et al., 2016).

Como ya se ha mencionado anteriormente los diferentes estadios del ciclo celular de los tripanosomátidos están obligados a reprogramar su metabolismo para adaptarse, persistir y proliferar en los diferentes huéspedes que infectan. Por un lado, las formas extracelulares sanguíneas de *T. brucei* y *T. cruzi* encuentran una gran disponibilidad de glucosa en el medio y por lo tanto utilizan la glicólisis para obtener ATP. Mientras que, para las formas que residen en el insecto o intracelularmente (amastigota) la disponibilidad de glucosa es limitada y la fuente de energía se obtiene a partir del catabolismo de aminoácidos, aunque para amastigotes de *T. cruzi* la oxidación de los ácidos grasos, no puede ser del todo excluida (Silber et al., 2009). Esto indica claramente que la capacidad metabólica de cada uno de estos estadios es un reflejo de la disponibilidad de nutrientes de cada ambiente específico.

1.3.2 Importación de proteínas glicosomales

Los glicosomas son organelos que carecen de ADN por lo tanto, las proteínas glicosomales deben ser codificadas por genes nucleares y posteriormente ser transportadas al glicosoma (Opperdoes et al., 1984). La importación de estas proteínas es similar a la de los peroxisomas de mamíferos. Uno de los mecanismos de transporte involucra la presencia de señales de importación, similares a las observadas en los peroxisomas, *peroxisomal targeting signal* (PTS) (Haanstra et al., 2014). Dentro de las PTS presentes en proteínas glicosomales se destacan: i) señal tipo PTS1, que consta de 12 aminoácidos poco conservados entre mamíferos y tripanosomátidos, que se localizan en el extremo C-terminal del polipéptido (Neuberger et al., 2003); ii) señal tipo PTS2, localizada en el extremo N-terminal de la proteína e identificada en la aldolasa de tripanosomátidos (Blattner et al., 1995; Chudzik et al., 2000). También se han identificado señales internas, no conservadas, de reclutamiento glicosomal (I-PTS, del inglés *internal-PTS*) como sucede para la triosafosfato isomerasa (Galland et al., 2007). Para otras proteínas glicosomales no se han logrado identificar PTS canónicas.

Las señales PTS son reconocidas en el citosol por receptores, peroxinas (PEX), que están involucradas en la biogénesis o translocación de proteínas hacia el glicosoma. Hasta el momento se sabe que la internalización de proteínas al glicosoma implica la formación de complejos proteicos que incluyen a las PEX2 (Guerra-Giraldez et al., 2002), PEX5 (de Walque et al., 1999) y PEX14 (Moyersoen et al., 2003). Donde el primer paso es el de reconocimiento de la secuencia señal, PTS1 o PTS2, por los receptores citosólicos PEX5 y PEX7 respectivamente (Blattner et al., 1995). Luego, la proteína de membrana glicosomal PEX14 se encarga de anclar a PEX5 para que finalmente PEX2 lleve a cabo la translocación de los complejos proteína-receptor hacia la matriz glicosomal, dirigiendo posteriormente la salida del receptor hacia el citosol (Schliebs and Kunau, 2006). Experimentos con líneas celulares de parásitos *knockout* condicionales para varias PEX demostraron que es indispensable que las enzimas glicolíticas estén confinadas en los glicosomas para la supervivencia del parásito en presencia de glucosa y/o glicerol (Fry et al., 1993; Guerra-Giraldez et al., 2002; Krazy and Michels, 2006; Moyersoen et al., 2003; Verplaetse et al., 2009). Dado que el metabolismo energético de la forma sanguínea de *T. brucei* es altamente dependiente del consumo de glucosa, las PEX son consideradas como interesantes blancos para el desarrollo de fármacos.

1.3.3 Transporte de metabolitos a través de la membrana glicosomal

El glicosoma posee una membrana poco permeable para la mayoría de los metabolitos, entre ellos el NAD/H, el ATP/ADP, glucosa, G6P, glicerol, fumarato, malato, etc. Si bien se ha reportado la translocación bidireccional de metabolitos, la tasa de la misma es extremadamente lenta en comparación con el flujo glicolítico. Lo que sugiere que el transporte a través de la membrana glicosomal deba realizarse por transportadores (Hannaert et al., 2003). Si bien se han detectado varios candidatos, solo se han logrado caracterizar unos pocos, como por ejemplo los transportadores ABC o GATs 1-3, así como 24 proteínas pertenecientes a la familia de transportadores mitocondriales (MCF) que son capaces de transportar distintos nucléotidos (AMP, ADP, ATP, y NAD); (Haanstra et al., 2014). Para *T. brucei* sanguíneo, se comprobó la existencia de poros glicosomales, similares a los hallados en los peroxisomas de plantas y otros eucariotas que permitirían el pasaje selectivo y eficiente de estos metabolitos (Grunau et al., 2009; Rokka et al., 2009). Justamente, el hecho que varios de estos metabolitos estén confinados en el glicosoma previene el denominado "efecto turbo" causado por una alta tasa glicolítica y que conlleva a una marcada depleción del ATP y acumulación de intermediarios de hexosas fosfato como lo son la G6P y la F6P, y que en su conjunto conducen a la muerte celular (Bakker et al., 2000; Haanstra et al., 2008).

1.3.4 Glicólisis

Los glicosomas no son organelos productores de ATP, en su interior siempre hay balance de ATP, además de equilibrio a nivel del poder reductor de NADH. La producción neta de ATP se dará en el citosol y dependerá si la obtención del mismo es vía glicolisis aeróbica o anaeróbica.

En la glicólisis aeróbica por cada molécula de glucosa consumida se invierten 2 moléculas de ATP (que se recuperan posteriormente), para poner en marcha a la hexoquinasa (HK) y la fosfofructo quinasa (PFK). La ganancia final se da en el citosol, vía la piruvato quinasa (PK) y es de 2 moléculas de ATP por mol de glucosa consumido. Mientras que para la glicólisis anaeróbica la fosfoglicerol quinasa (PGK) y la glicerol kinasa (GK) utilizan cada una 1 ATP, que es recuperado dentro del glicosoma. Esta ruta catabólica rinde 1 sola molécula de ATP y cantidades equimolares de piruvato y glicerol por cada molécula de glucosa consumida. Se puede decir que la glicólisis es una vía autocatalítica, que requiere de la inversión inicial de ATP para poner en marcha sus etapas iniciales, y este mecanismo de retroalimentación positiva se conoce como "efecto turbo" (Teusink et al., 1998). Por lo tanto, puede interpretarse que la esencialidad del glicosoma para la prevención de dicho efecto es más una consecuencia de la

compartimentalización de la glicólisis, que su causa (Gualdron-López et al., 2012; Haanstra et al., 2016).

1.4 Vía de las pentosas fosfato

En la PPP se generan metabolitos importantes para el parásito como: i) el NADPH, cuyo poder reductor es empleado en reacciones de biosíntesis y en la defensa contra especies oxidantes (Barrett, 1997; Igoillo-Esteve and Cazzulo, 2006; Mielniczki-Pereira et al., 2007), ii) la ribosa-5-fosfato (R5P), necesaria para la síntesis de ácidos nucleicos, iii) la eritrosa 4-fosfato (E4P), que es precursora de aminoácidos aromáticos y vitaminas, y iv) la fructosa 6-fosfato (F6P) y gliceraldehído 3-fosfato (G3P), que constituyen importantes intermediarios de la glicólisis. Esta vía se divide en dos ramas, una oxidativa (generadora de poder reductor) y otra no oxidativa (productora de diferentes hidratos de carbono), ver figura 3.

La funcionalidad de la vía completa ha sido demostrada en epimastigotes de *T. cruzi* (Maugeri and Cazzulo, 2004) y en promastigotas de *L. braziliensis* (Keegan et al., 1987) y *L. mexicana* (Maugeri et al., 2003). En esta ruta metabólica participan siete enzimas, todas se expresan en los cuatro estadios del ciclo de vida de *T. cruzi* (Maugeri and Cazzulo, 2004) y en promastigotas de *L. mexicana* (Maugeri et al., 2003), mientras que para *T. brucei* se observó que todos los componentes son expresados por la forma procíclica mientras que únicamente las enzimas de la rama oxidativa son expresadas por la forma sanguínea del parásito (Cronín et al., 1989).

1.4.1 Rama Oxidativa

De la rama oxidativa de la PPP participan la glucosa 6-fosfato deshidrogenasa (G6PDH), la 6-fosfogluconolactonasa (6-PGL) y la 6-fosfogluconato deshidrogenasa (6PGDH). Todas estas enzimas están filogenéticamente relacionadas con sus homólogos de cianobacterias y de plantas, y desempeñan un papel esencial en el metabolismo de los parásitos. La primera reacción es llevada a cabo por la G6PDH, que oxida a la G6P para dar 6-PGL con la concomitante reducción de $NADP^+$ a NADPH. La ∂-6PGL se hidroliza a 6-fosfo gluconato de manera espontánea o catalizada por la 6-PGL, de no ser así se produce un rearreglo intramolecular que da lugar a la formación de Y-G6PL, la cual no puede ser metabolizada y cuya acumulación se vuelve tóxica (Rakitzis and Papandreou, 1998). Paso seguido, el 6-fosfo gluconato es oxidado y decarboxilado por la 6PGDH dando lugar a la formación de ribulosa 5-fosfato (RU5P) siendo el aceptor final de

electrones el $NADP^+$. La RU5P, es posteriormente metabolizada en la fase no oxidativa de esta vía, ver figura 3.

1.4.2 Rama no oxidativa

A diferencia de la fase oxidativa, la rama no oxidativa implica una serie de reacciones reversibles donde participan la ribosa 5-fosfato isomerasa (RPI), la ribulosa 5-fosfato epimerasa (RPE), la transaldolasa (TAL) y la transcetolasa (TKT).

La primera reacción de esta fase consiste en la isomerización de la RU5P a R5P catalizada por la RPI. Eventualmente, la RPE se encarga de convertir la R5P a xilulosa 5-fosfato (X5P) y la TKT puede transferir dos o más unidades carbonadas de la X5P a la R5P generándose así sedoheptulosa-7P (S7P) y G3P. Posteriormente, la TAL emplea a S7P y G3P como sustratos para transformarlos en eritrosa 4-fosfato (E4P) y F6P. Dependiendo de los requerimientos celulares, la TKT puede también catalizar la transferencia de dos unidades carbonadas de la X5P a la E4P para dar G3P y F6P, los cuales pueden ingresar a la vía glicolítica para la producción de energía. En caso que la R5P no sea derivada a la síntesis de nucleótidos, los productos generados por esta via son F6P y G3P. También se ha visto que esta vía también puede actuar en forma reversa y generar R5P y X5P a partir de F6P y G3P que serían provistos por la glicólisis (Kovářová and Barrett, 2016), ver figura3.

La vía de las pentosas no necesariamente funciona como un ciclo, y dependiendo de los requerimientos celulares por los diferentes metabolitos puede mantener operativas o no, las siguientes reacciones enzimáticas (Lubert Stryer, 1999), ver figura 3.

- Si la célula necesita más NADPH que R5P, es el caso de aquellas células que llevan a cabo una síntesis activa de lípidos, la F6P será isomerizada a G6P, por medio de la fosfoglucosa isomerasa, la cual entrará nuevamente en la rama oxidativa de la vía.
- Si la célula necesita más R5P que NADPH, como es el caso de células en activa división, se favorecerá el funcionamiento de la rama no oxidativa en forma reversa, donde F6P y G3P generados durante la glicolisis serán convertidos a R5P por acción de la TAL y TKT.
- Si las necesidades de NADPH y R5P en célula están balanceadas, funcionará la rama oxidativa de la vía para cubrir las necesidades de NADPH, y la RU5P generada será isomerizada a R5P para su posterior utilización (Lubert Stryer, 1999).

Se realizaron experimentos de fraccionamiento celular en epimastigotes de *T.cruzi* para evaluar si las enzimas de la PPP se encuentran compartimentalizadas, pudiéndose determinar que la localización de las mismas es esencialmente citosólica, aunque también se observó la presencia de una pequeña fracción glicosomal para la TAL, RPI, G6PDH, 6PGLD y TKT (Kovářová and Barrett, 2016; Maugeri and Cazzulo, 2004). Estudios similares llevados a cabo en *T. brucei*, indicaron que las enzimas de la PPP presentan localización dual, encontrándose señal tanto en citosol como en glicosoma. Por ejemplo el 85% y 55% de la actividad de 6-PGL y de G6PDH, respectivamente, fue detectada en citosol (Duffieux et al., 2000; Heise and Opperdoes, 1999). Por otra parte, se ha reportado que TKT presenta una secuencia PTS para glicosoma a pesar de encontrarse mayoritariamente en citosol (Stoffel et al., 2011; Veitch et al., 2004). Para el caso de 6PGD, en la forma procíclica de *T. brucei*, su localización aún no está definida, pero todo parece indicar que además de encontrarse en el citosol, una parte estaría confinada también en los glicosomas (Güther et al., 2014; Heise and Opperdoes, 1999). En *Leishmania donovani*, TKT y G6PDH fueron localizadas en la fracción glicosomal (Kovářová and Barrett, 2016).

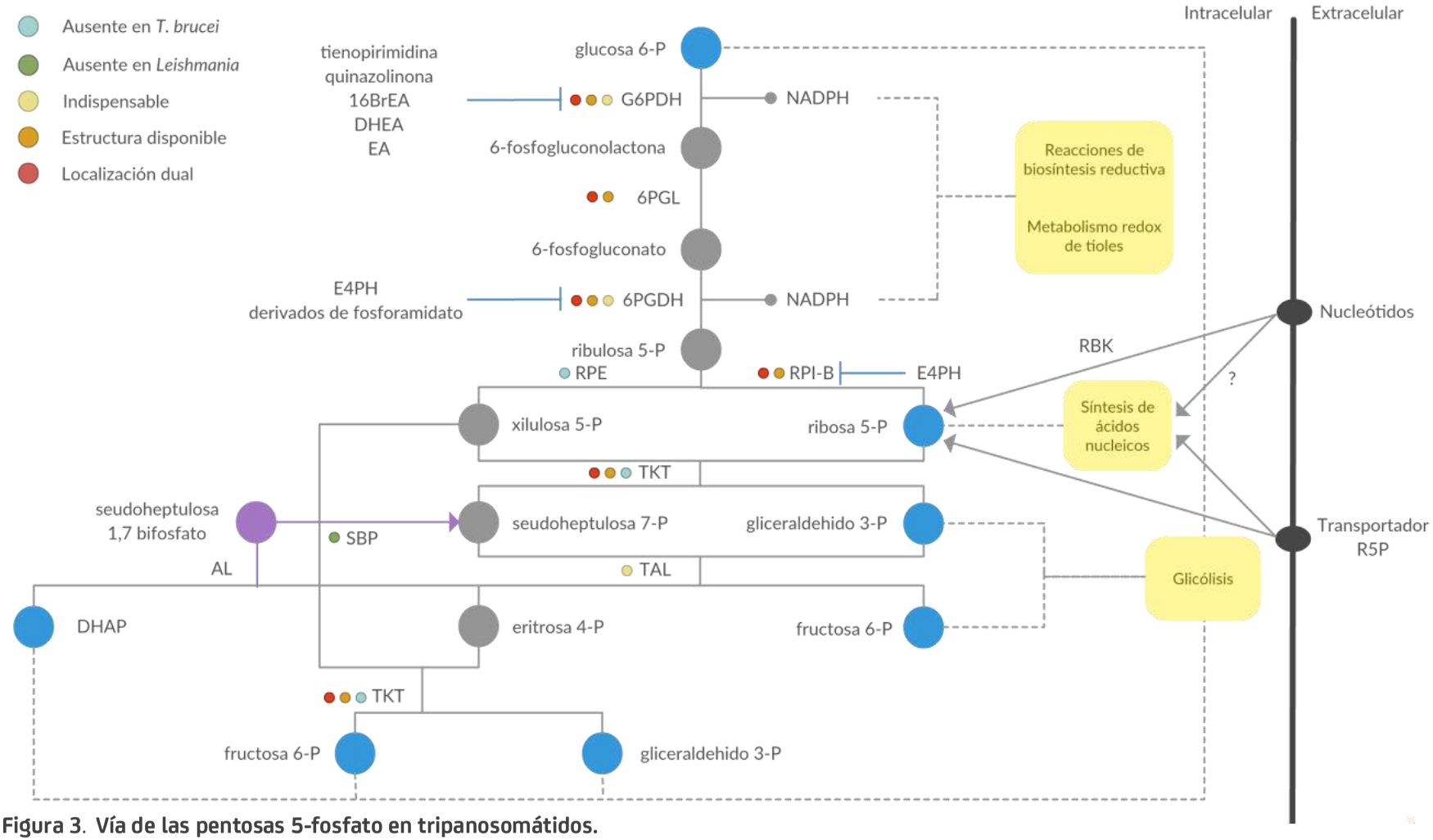

Figura 3. Vía de las pentosas 5-fosfato en tripanosomátidos.

Componentes, relevancia biológica, disponibilidad de estructuras tridimensionales, localización subcelular e inhibidores. Los sustratos y productos de la via de las pentosas compartidos con la ruta glicolítica se muestran en círculos azules. Los componentes de la rama oxidativa de la PPP son la: glucosa 6-fosfato deshidrogenasa (G6PDH), 6-fosfogluconolactonasa (6PGL), 6-fosfoglucono deshidrogenasa (6PGDH), ribosa fosfato isomerasa tipo B (RPI-B), ribosa fosfato epimerasa (RPE), transketolasa (TKT), transaldolasa (TAL), y aldolasa (AL). Las vías de salvataje para R5P incluyen:i) transportadores de membrana para R5P y/o nucleótidos, ii) la fosforilación de ribosa por ribosa quinasa (RBK); Iii) la vía de biogénesis de ribosa mediante la acción de la aldolasa (AL) y la seudoheptulosa bisfosfatasa (SBP); la dihidroxiacetona-fosfato (DHAP) y el gliceraldehído 3- fosfato que son convertidos en seudoheptulosa 7-fosfato.

1.5 Glucosa-6-fosfato deshidrogenasa

La glucosa 6-fosfato deshidrogenasa (G6PDH) es una enzima ubicua, presente en diferentes organismos, desde bacterias al hombre. Como ya se ha mencionado anteriormente su función es catalizar la primera reacción de la fase oxidativa de la PPP, que consiste en la oxidación de glucosa-6-fosfato a 6-fosfogluconato con la concomitante reducción de $NADP^+$ a NADPH.

Si bien en tripanosomátidos existen otras enzimas productoras de NADPH, como lo son la malato deshidrogenasa, la glutamato-deshidrogenasa y la isocitrato-deshidrogenasa, varios estudios sugieren que para *T. cruzi* el principal suministro de NADPH proviene de la vía de las pentosas (Barderi et al., 1998; Leroux et al., 2011a, 2011b). En la mayoría de los organismos la G6PDH presenta una distribución predominantemente citosólica aunque en plantas se la ha localizado tanto en peroxisomas como en cloroplasto (Wendt et al., 2000). En el caso del trypanosoma Africano se ha detectado presencia de actividad G6PDH en las fracciones glicosomales (Heise and Opperdoes, 1999).

La primera estructura cristalina reportada para esta oxidoreductasa corresponde a la enzima del lactobacilo, *Leuconostoc mesenteroides* (Cosgrove et al., 1998; Naylor et al., 2001). Los datos estructurales mostraron una proteína homodimérica, donde cada uno de sus monómeros contenía dos dominios: i) el dominio N-terminal de unión al sustrato nucleotídico (residuos 1-177) y el cual presenta un plegamiento β-α-β tipo Rossmann y ii) un dominio C- terminal con plegamiento β-α (residuos 178-485) donde se encuentran residuos que participan en la unión del glucósido. Es importante resaltar que la forma activa de la proteína requiere de una conformación homodimérica (Rowland et al., 1994).

Años más tarde, el grupo de Adams reportó la estructura cristalina de la G6PDH humana (hG6PDH) con una resolución de 3 Å. La topología de la enzima humana es similar a la de *L. mesenteroides*, identificándose por monómero un total de 15 hélices α y 15 hojas β. A diferencia de la enzima del lactobacilo, la hG6PDH se encuentra en un equilibrio dinámico monómero-dímero-tetrámero, el cual es altamente influenciado por el pH, la fuerza iónica del medio así como la presencia de sustratos y productos. En medio básico y condiciones de elevada fuerza iónica el equilibrio se desplaza hacia la forma dimérica, mientras que a pH<6 y baja fuerza iónica predomina la forma tetramérica. A pesar de que cada subunidad (peso molecular aproximado de 59 kDa) contiene los sitios de unión para el sustrato y cofactor, el monómero es inactivo (Au et al., 2000). El sitio activo de unión a G6P, esta conservado en la mayoría de las deshidrogenasas y presenta como marca distintiva al nonapéptido, RIDHYLGKE (residuos 198-206). El sitio de unión

a $NADP^+$ abarca la región comprendida entre los aminoácidos 38-47 e incluye la secuencia altamente conservada GxxGDLx. La co-cristalización de hG6PDH en presencia de $NADP^+$, puso en evidencia la presencia de un segundo sitio de unión a $NADP^+$ que cumple un rol estructural importante durante la catálisis aunque no participa directamente de la misma (Kotaka et al., 2005; Verma et al., 2016). Finalmente, la interface que forma el dímero presenta una superficie de 2856 $Å^2$, involucra 57 residuos altamente conservados donde 31 de ellos son hidrofóbicos (Au et al., 2000).

1.5.1 DEFICIENCIA DE G6PDH Y RESISTENCIA A PALUDISMO

La deficiencia de G6PDH es la enzimopatía más frecuente en humanos, afectando al 7,5% de la población mundial (Ali et al., 2005; Beutler, 1994). Si bien ésta deficiencia se conoce desde la antigüedad como favismo, donde los portadores desarrollaban anemia hemolítica al consumir habas (Arese and De Flora, 1990; Longo et al., 2002), la misma fue descrita por primera vez recién en 1956. Años más tarde se logró asociarla a mutaciones en el cromosoma X (Alving et al., 1956; Childs et al., 1958). Estudios posteriores (Notaro et al., 2000) permitieron identificar más de 500 variantes de hG6PDH y más de 80 mutaciones responsables de la heterogeneidad fenotípica (Chen et al., 1991). Hoy en día se ha logrado documentar que las manifestaciones clínicas se originan por mutaciones que desestabilizan la proteína, afectan su eficiencia catalítica e interfieren con la formación del dímero o de su plegamiento cuaternario (Beutler, 1994; Wang et al., 2005).

En 1967 se establecieron los criterios para clasificar las distintas variantes de hG6PDH, los cuales tienen en cuenta la actividad enzimática y los síntomas clínicos, y se dividen en: clase I, deficiencia enzimática severa (actividad enzimática menor al 10%, asociada a marcada inestabilidad del dímero); clase II, deficiencia enzimática severa no asociada con hemólisis crónica; clase III, deficiencia enzimática leve a moderada (10-60% de actividad enzimática) y hemólisis solo por exposición a ciertos fármacos y agentes infecciosos; clase IV, leve o sin deficiencia y actividad funcional no modificada, la hG6PDH retiene el 60-100% de su actividad enzimática; clase V, presenta actividad enzimática incrementada (hasta dos veces superior a la normal) (Betke K et al., 1967).

En particular ha llamado la atención la gran prevalencia de ésta enzimopatía en poblaciones que residen en zonas endémicas de malaria (Capellini MD and Fiorelli G 2008). La malaria es una de

las parasitosis de mayor incidencia a nivel mundial, es causada por diferentes especies de *Plasmodium* y se estima que más de medio millón de personas mueren por año debido a esta enfermedad (Preuss J 2012). En su ciclo infeccioso el parásito infecta eritrocitos provocando, entre otros síntomas clínicos, una anemia hemolítica severa debido a que el patógeno utiliza esta célula no nucleada para replicarse masivamente, desencadenando su lisis. Existe evidencia de varios polimorfismos asociados a los genes que codifican para la hemoglobina (HbS, HbC, HbE, talasemias) y la resistencia a la malaria (Kwiatkowski, 2005; Miller, 1994). También se ha propuesto que la deficiencia en G6PDH ha co-evolucionado con la infección por plasmodio (se estima que co-existen desde hace más de 50000-60000 años), este último actuando como un importante agente de presión selectiva. Por ejemplo, se ha observado que el crecimiento del parásito se inhibe en los individuos deficientes en G6PDH (Allison and Clyde, 1961; Motulsky AG, 1961; Oppenheim et al., 1993); de hecho, individuos con genotipo hemicigoto para la variante G6PD A-, presentan un riesgo 50% menor que personas normales de contraer malaria (Friedman et al., 1979; Roth et al., 1983; Ruwende et al., 1995). Por otro lado, estudios de RFLP´s y microsatélites sobre el gen de la G6PDH permitieron estimar la edad de los alelos asociados a deficiencia en G6PDH y resistencia a malaria (por ejemplo las variantes G6PD A- y Mediterráneo), hallándose un desequilibrio de ligamiento en estos alelos que coincide con la propagación de la malaria (Ruwende et al., 1995; Tishkoff et al., 2001).

En resumen, la deficiencia en G6PD no es letal para humanos y probablemente ha evolucionado como un mecanismo de protección contra parásitos hemocíticos (Volkman et al., 2001).

1.5.2 G6PDH de tripanosomátidos

El número de genes que codifican para G6PDH difiere entre los tripanosomátidos, mientras que *T. brucei* y *L. mexicana* poseen un gen de copia única (Duffieux et al., 2000; Hannaert et al., 2003), *T. cruzi* cuenta con cinco secuencias putativas para G6PDH, donde dos corresponden a pseudogenes (Igoillo-Esteve and Cazzulo, 2006). Esta proteína presenta una identidad de secuencia con la hG6PDH que es < 50%. Un análisis preliminar de la secuencia de G6PDH de tripanosomátidos destaca la presencia de una extensión N-terminal, la cual está ausente en la homóloga de mamíferos.

Estudios bioquímicos llevados a cabo con la forma recombinante de la G6PDH de *T. cruzi* mostraron que la forma nativa de la enzima es inactivada por agentes reductores (DTT, glutatión); (Igoillo-Esteve and Cazzulo, 2006) y aunque no fue investigado en detalle, este comportamiento plantea la posibilidad que la actividad de la misma se encuentra regulada por

un mecanismo redox, tal como se ha descrito para las proteínas homólogas de cloroplastos de papas y cianobacterias (Hauschild and von Schaewen, 2003; Née et al., 2009; Wenderoth et al., 1997). En los organismos fotosintéticos, la modulación redox de la actividad de la G6PDH aumenta la eficiencia metabólica durante los ciclos luz/oscuridad, evitando ciclos fútiles de consumo y generación de equivalentes de reducción. En las isoformas plastídicas de la G6PDH los residuos de cisteína que son blanco de regulación redox están distribuidos azarosamente en la secuencia (Née et al., 2009), mientras que para la TcG6PDH se planteó que los grupos tiol responsables de la inactivación redox de la enzima se localizan en la región N-terminal (Igoillo-Esteve and Cazzulo, 2006).

Respecto a la relevancia biológica de la G6PDH para *T. cruzi*, altos niveles de la enzima se han reportado tanto en cepas virulentas (ej. Tulahuen o Tulahuen 2) así como en los estadíos infectivos del parásito (Finzi et al., 2004; Gupta et al., 2011a; Igoillo-Esteve and Cazzulo, 2006; Mancilla and Naquira, 1964; Maugeri and Cazzulo, 2004; Mielniczki-Pereira et al., 2007). También se observó un incremento en la actividad G6PDH luego de exponer los parásitos a agentes (pro)oxidantes (Igoillo-Esteve and Cazzulo, 2006; Maugeri and Cazzulo, 2004). Por otro lado, estudios recientes mostraron niveles elevados de G6PDH en una línea celular de *L. chagasi* resistente a NO así como en *L. donovani* sometida a estrés oxidativo (Ghosh 2015; Alcolea 2016). Incluso la sobreexpresión de G6PDH en *L. donovani* confirió resistencia a este parásito contra 3 fármacos de uso clínico: sales de antimonio, amfotericina B y mitelfosina (Ghosh 2015). Todo esto posiciona a esta enzima como un potencial factor de virulencia en tripanosomátidos.

La indispensabilidad de la G6PDH quedó demostrada en el trypanosoma africano mediante la técnica de silenciamiento pos-transcripcional (ARNi) (Cordeiro et al., 2009). Esta enzima es la primera de una ruta metabólica que genera diversos productos importantes, por lo tanto su esencialidad podría estar determinada por una deficiencia en la síntesis de un metabolito en particular o bien por varios o todos ellos. En ese sentido estudios de genética reversa realizados sobre la RPI de *T. brucei* y *L. infantum* demostraron que la síntesis de R5P es indispensable para la (replicación) sobrevida de los parásitos en el huésped (Faria et al., 2016). Si bien no se cuenta con estudios similares realizados sobre *T. cruzi,* es altamente esperable que la G6PDH de este organismo sea igualmente indispensable, tal como lo indican los experimentos de validación química que se discuten más adelante (Cordeiro and Thiemann, 2010).

1.6 Metabolismo redox de tripanosomas

La mayoría de las células emplean parte del poder reductor generado durante la PPP para sostener la homeostasis redox intracelular a través de diferentes sistemas redox que operan de manera complementaria. Este es otro de los aspectos que distingue a los tripanosomátidos del resto de los organismos vivos. Mientras la mayoría de los organismos utiliza al sistema glutatión/glutatión reductasa y al sistema tiorredoxina/tiorredoxina reductasa como principales medios para vehiculizar electrones hacia distintas proteínas blancos, los Kinetoplastidos carecen de estas dos reductasas principales y emplean un sistema basado en el tripanotión (N^1,N^8-bisglutationil espermidina, $T(SH)_2$) (Krauth-Siegel and Leroux, 2012). Este ditiol es producto de la conjugación de dos moléculas de GSH y una de espermidina catalizada por la enzima tripanotión sintetasa (Fairlamb et al., 1985; Krauth-Siegel et al., 1998). El sistema redox de estos protozoarios se completa con la tripanotión reductasa (TryR), encargada de reducir al tripanotión oxidado a expensas del NADPH, y la triparredoxina (TXN), una oxidoreductasa capaz de transferir los electrones provenientes del tripanotión hacia diferentes blancos moleculares. En particular se destacan como blancos de la TXN, las peroxidasas que participan en la defensa contra diferentes agentes oxidantes y la ribonucleotido reductasa, una enzima indispensable en la síntesis de los precursores ácidos nucleicos. Por lo tanto, el NADPH provisto por la PPP u otra fuente metabólica, es utilizado por este sistema para sostener el balance redox intracelular y la proliferación celular. ver figura 4. (Benítez et al., 2016; Comini et al., 2005, 2007; Dormeyer et al., 2001; Flohé, 2012; Romao et al., 2009),

T. cruzi es un organismo muy heterogéneo que se presenta bajo la forma de distintas cepas que presentan diferentes grados de virulencia e infectividad, tropismo por órganos y tejidos que, por lo tanto, están asociadas a diferentes manifestaciones clínicas. Parte de estas adaptaciones incluyen a los componentes de su sistema de defensa contra oxidantes que le permite lidiar con la respuesta inmune generada por el hospedero. En ese sentido, se ha reportado mayor virulencia en cepas que sobreexpresan algunos de los componentes del sistema redox. Entre ellos se encuentran proteínas claves para la detoxificación de oxidantes como lo son las triparredoxinas, peroxirredoxinas o superóxido dismutasas (SOD). En el caso de la triparredoxina peroxidasa mitocondrial y citosólica, un incremento en su expresión vuelve a los tripomastigostas más resistentes al estrés oxidativo, además de mejorar su capacidad de replicación y de supervivencia en macrófagos (Contreras et al., 1988; Piacenza et al., 2009, 2013; Piñeyro et al., 2008). Estudios de proteómica han revelado un incremento en la expresión de las mismas frente a estrés oxidativo para las formas metacíclicas y epimastigotas (Parodi-

Talice et al., 2007) así como un contenido diferencial de las mismas entre tripanosomas metacíclicos y epimastigotes (Piacenza et al., 2009). Recientemente se ha observado un incremento en la expresión de las mismas para las cepas Colombiana y Silvio que presentan mayor resistencia al tratamiento con oxidantes respecto de una cepa de laboratorio (TCC) (Zago et al., 2016). Tal como se indicó anteriormente, niveles elevados de G6PDH han sido también reportados en las formas infectivas como para algunas cepas virulentas de *T. cruzi* (Finzi et al., 2004; Igoillo-Esteve and Cazzulo, 2006; Mancilla and Naquira, 1964; Maugeri and Cazzulo, 2004; Mielniczki-Pereira et al., 2007), lo cual está relacionado al abastecimiento de poder reductor que realiza esta enzima sobre el sistema redox del parásito. Por otra parte, existe evidencia, aunque limitada, sobre cepas de *T. cruzi* resistentes a benznidazole y nifurtimox que presentan mutaciones en el gen que codifica para la nitrorreductasa 1, responsable de la selectividad de estos fármacos, también se observó que cepas sobreexpresantes de FeSOD presentan resistencia a benznidazol (Piacenza et al., 2013). Estos datos sugieren una asociación entre virulencia y contenido de enzimas antioxidantes, posicionando a los componentes del sistema redox como potenciales candidatos para el desarrollo de fármacos anti-chagásicos.

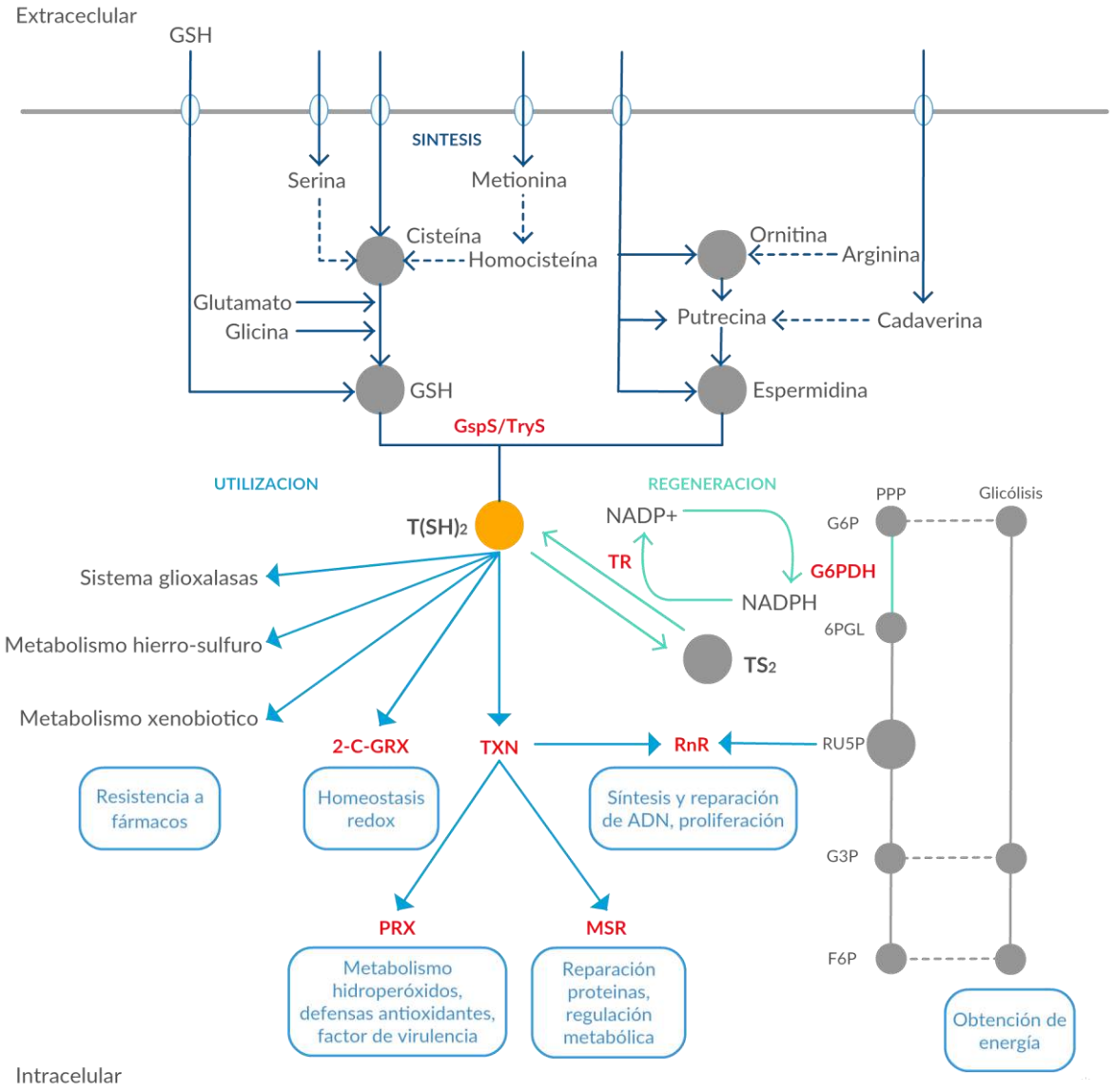

Figura 4. Vías metabólicas implicadas en la síntesis, utilización y regeneración del tripanotión. Esquema que resume el metabolismo redox dependiente de tripanotión en tripanosomátidos. En líneas azules: las vías para llegar a la síntesis del tripanotión (incluyendo la incorporación o síntesis *de novo* de cisteína, la biosíntesis de glutatión, la asimilación o biosíntesis de poliaminas y la biosíntesis del tripanotión, donde en algunas especies pueden estar implicada una segunda enzima, la GspS, además de la TryS); en líneas verde claro: las reacciones involucradas en la regeneración de la forma reducida del tripanotión; y en color azul claro: los diferentes usos del tripanotión por parte de distintas proteínas y procesos celulares. Tripanotión sintetasa (TryS), monoglutationil-espermidina sintetasa (GspS), tripanotión reductasa (TR), tripanotión en estado reducido [$T(SH)_2$], tripanotión oxidado (TS_2), glutatión reducido (GSH), vía de las pentosas 5-fosfato (PPP), glucosa 6-fosfato deshidrogenasa (G6PDH), glicerol 3-fosfato (G3P), fructosa 6-fosfato (F6P), ribulosa 5-fosfato (Ru5P), triparredoxina (TXN), peroxidasa (PRX), ribonucleótido reductasa (RnR), glucosa 6-fosfato (G6P), 6-fosfogluconolactona (6PGL), metionina sulfóxido reductasa (MSR), glutarredoxinas ditiólicas (2-C-GRX). Imagen tomada y adaptada de Comini, 2013 y Manta 2013.

1.7 Inhibidores específicos de la G6PDH

La G6PDH ha sido propuesta como una potencial diana para el desarrollo de fármacos anti-chagásicos (Gupta et al., 2011b, 2011a; Mercaldi et al., 2014; Ortiz et al., 2016). A la fecha, existen reportes de inhibidores de la enzima de *T. cruzi* y de otras especies. Entre ellos encontramos a la 6-aminonicotinamida (Köhler et al., 1970), las galato catequinas (Shin et al., 2008), el bromofenol y otros fenoles de origen vegetal (Mikami et al., 2016), los derivados de benzotiazonas, las pirimidin-trionas y cromo-2-onas capaces de inhibir a la enzima bifuncional de *Plasmodium falciparum* (Preuss et al., 2012a, 2012b), las quinazonlinonas y tieno-pirimidinas que inhiben selectivamente la enzima de *T. cruzi* (Mercaldi et al., 2014) o los derivados esteroideos, como lo son la dehidroepiandrosterona, epiandrosterona y 16-bromo-epiandrosterona (Cordeiro and Thiemann, 2010; Gordon et al., 1995; Gupta et al., 2011b, 2011a; Hamilton et al., 2012; Marks and Banks, 1960; Raineri and Levy, 1970), ver figura 5.

La 6-amoninicotinamida (6AN) es un inhibidor competitivo para $NADP^+$ de la G6PDH de mamiferos, que fue formulada originariamente como potente inhibidor de la rama oxidativa de la PPP para vislumbrar su rol en embriones, tejido mamario y hepático (Köhler et al., 1970). Casi 20 años después este compuesto es retomado y empleado para potenciar el efecto de drogas anti-neoplásicas como la cisplatina o para ser administrado en combinación con la 2-deoxy-D-glucosa para disminuir el crecimiento tumoral en cáncer de pulmón, cáncer oral y glioblastoma, así también como de aumentar la eficacia de la radioterapia en cáncer de mama (Bhardwaj et al., 2012; Budihardjo et al., 2000). Recientemente, se comprobó que la administración de 6AN como complemento quimioterápico para el tratamiento de la leucemia leucocitaria, permitiría reducir las dosis de los otros fármacos, minimizando así sus efectos secundarios (Zhelev et al., 2016). Cabe destacar que este trabajo fue realizado en líneas celulares, lo que no descarta la posibilidad que este compuesto pueda inducir daño nervioso y/o deficiencia en vitamina B en humanos, tal como se observó previamente en ratones (Köhler et al., 1970), ver figura 5.

Las galato catequinas son compuestos naturales obtenidos a partir del té verde que fueron identificadas como inhibidores de la G6PDH de levadura con un IC50 < 7,7 µM. Estudios de SAR determinaron que la presencia del grupo galoil es fundamental para conferir actividad inhibitoria (Shin et al., 2008). Sin embargo, estudios realizados sobre adipocitos no mostraron actividad inhibitoria significativa contra la G6PDH, determinándose que estos compuestos carecen de selectividad al ser capaces de inhibir un amplio espectro de enzimas que utilizan $NADP^+$ como cofactor, como es el caso de la galacto deshidrogenasa, la isocitrato deshidrogenasa, la ácido graso sintasa y la 6PGDH (Shin et al., 2008), ver figura 5.

Los bromofenoles fueron obtenidos a partir de algas marinas (*Rhodomelaceae algae*) y mostraron ser inhibidores no competitivos de la G6PDH de *L. mesenteroides y Saccharomyces cerevisiae* (IC_{50} < 5 µM). Los dímeros simétricos de bromofenoles resultaron ser los más potentes, donde los derivados del dibenzil-eter y los de diaril-metano presentaron mayor selectividad y potencia por la enzima del lactobacilo y la de levadura, respectivamente (Mikami et al., 2013, 2016), ver figura 5.

Campañas de cribado de alto procesamiento (HTS, del inglés *high troughput screening*) contra la G6PDH de *P. falciparum* y humana, permitieron identificar nuevos inhibidores de esta enzima. Para la hG6PDH se identificaron 4 compuestos con IC_{50} menores a 3 µM, es decir 100 a 1000 veces más potentes que 6AN o dehidroepiandrosterona (Preuss et al., 2013). Todos los hits mostraron un mecanismo competitivo frente al sustrato que varío entre mixto a no-competitivo con respecto al $NADP^+$. Uno de estos compuestos (CB83) redujo la viabilidad de una línea celular de cáncer de mama MCF10-AT1 (IC_{50} 25 µM) (Preuss et al., 2012b). Para la G6PDH de plasmodio no se encontraron inhibidores que fueran específicos, entre los más potentes se seleccionaron los pertenecientes a las familias de las pirimidin-trionas y las cromo-2-onas. La actividad de alguno de estos análogos contra los parásitos fue moderada (EC_{50} < 6 µM), probablemente debido a la baja permeabilidad y poca estabilidad de los mismos. Ese mismo año, a partir de una biblioteca de 350.000 compuestos se obtuvieron varios hits contra la G6PDH de plasmodio, la mayoría de los cuales corresponde al *scaffold* de benzotiazonas (Preuss et al., 2012a, 2012b). La optimización de estos compuestos guiada por estudios de SAR, permitió obtener un derivado (ML276) capaz de inhibir selectivamente a la enzima del parásito con una IC_{50} = 889 nM y con buena potencia contra el crecimiento *in vitro* de plasmodio (EC_{50} = 2,6 µM) (Maloney et al., 2010a, 2010b). A diferencia de los compuestos hallados previamente en el HTS (Preuss et al., 2012b), estos nuevos derivados de benzotiazonas presentan buenos criterios de ADME/T, escasa toxicidad, buena solubilidad y estabilidad, ver figura 5.

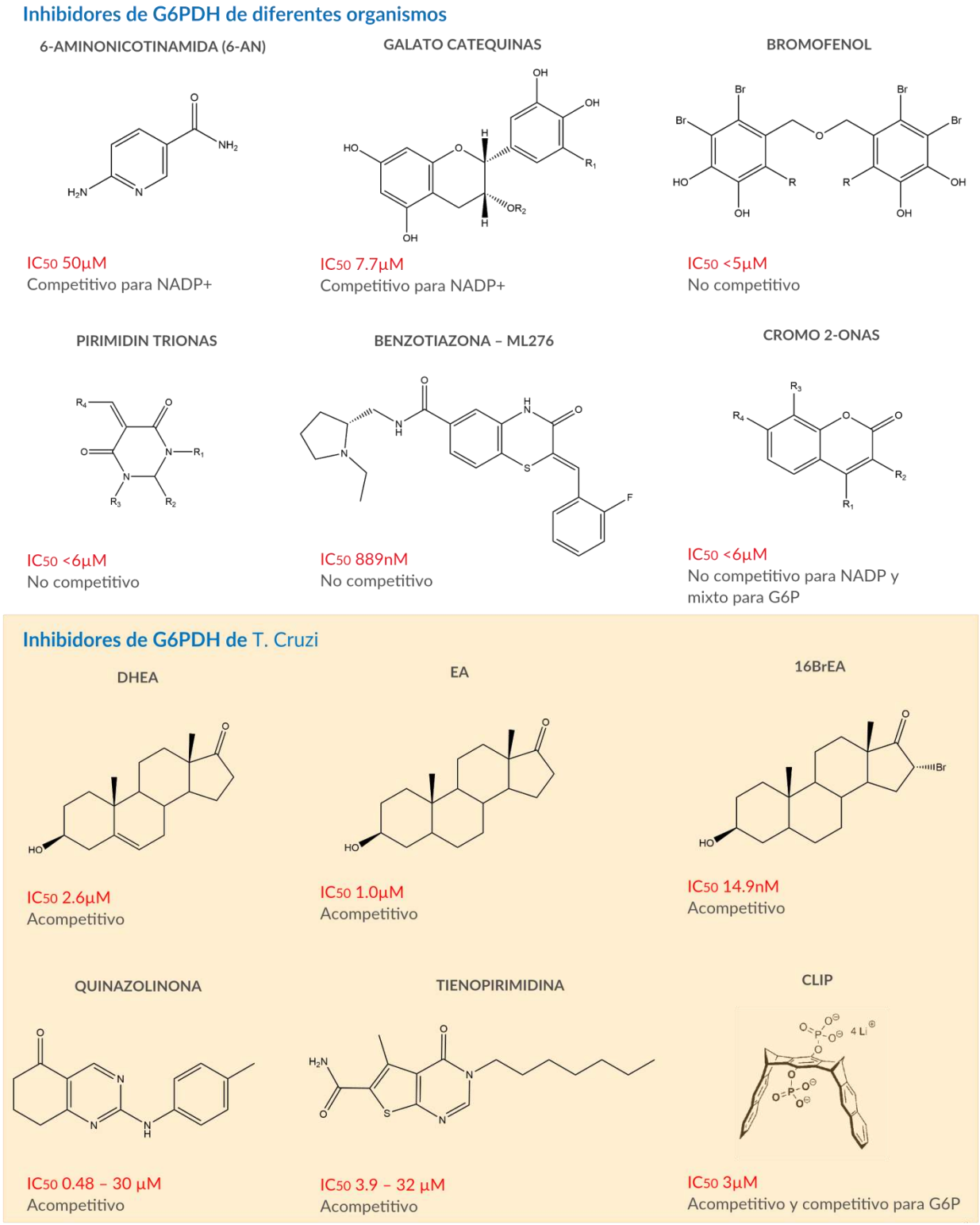

Figura 5. Inhibidores de Glucosa- 6 fosfato deshidrogenasa.
Estructuras químicas, IC_{50s} y tipo de mecanismo de acción para inhibidores de G6PDH de *Trypanosoma cruzi*, en fondo amarillo y para G6PDHs provenientes de otros organismos, sin fondo de color. Estructuras realizadas en Chemdraw.

Por otra parte, el grupo de Schrader diseñó un clip molecular basado en la estructura del antraceno con grupos fosfatos ligados, que es capaz de atrapar al $NADP^+$ por efecto de apilamiento (*stacking*) molecular y en simultáneo ocupar el sitio de unión de la G6P (Kirsch et al., 2009). Con este mecanismo dual se logró obtener selectividad por la G6PDH sobre otras deshidrogenasas. Para la G6PDH de lactobacilo se reportó un IC_{50} = 7 µM (Kirsch et al., 2009). Estudios realizados en nuestro laboratorio demostraron que, el análogo más activo contra la enzima humana fue capaz de inhibir a la forma recombinante de la G6PDH de *T. cruzi* con un valor de IC_{50} de 3 µM. Sin embargo, dicho compuesto no mostró actividad contra epimastigotes del parásito, lo cual puede deberse a su baja permeabilidad y/o a la inestabilidad de los grupos fosfatos, claves para la interacción con el $NADP^+$ (datos no publicados).

Al inicio de esta tesis, los derivados esteroideos mejor caracterizados como inhibidores de la G6PDH eran la epiandrosterona (EA), dehidroepiandrosterona (DHEA) y bromo-epiandrosterona (16-BrEA). Dichos compuestos inhiben de manera acompetitiva a la forma recombinante de G6PDH de distintas especies de tripanosomátidos y presentan efecto anti-proliferativo sobre la forma infectiva de *T. brucei* y no infectiva (epimastigota) de *T. cruzi* (Cordeiro and Thiemann, 2010; Cordeiro et al., 2009). Llamativamente, la G6PDH de *L. mexicana* resultó refractaria a la inhibición por estos esteroides. Este hallazgo fue confirmado mediante ensayos de complementación *in vitro* sobre una línea celular de *T. brucei* deficiente en la G6PDH endógena, y donde la expresión de la enzima de *Leishmania* tornó a estos parásitos resistentes contra DHEA y EA (Cordeiro et al., 2009; Gupta et al., 2011b, 2011a). Estudios posteriores, mostraron que la 16BrEA presenta mayor especificidad contra la G6PDH de tripanosomas, respecto de la enzima humana (Mercaldi et al., 2014). Es importante recalcar que, la mayoría de estos derivados fueron descritos previamente como inhibidores de la proteína humana *(Gordon et al., 1995; Hamilton et al., 2012; Marks and Banks, 1960; Raineri and Levy, 1970).* Sin embargo, esta aparente selectividad obtenida contra la G6PDH de tripanosomas alienta a profundizar la caracterización de esta familia de compuestos con el fin último de poder generar derivados con mayor especificidad y potencia (Hamilton et al., 2012).

En esta línea, pero teniendo como blanco a la proteína humana, el grupo de Hamilton realizó ensayos de SAR sobre derivados de la DHEA, obteniendo análogos con mayor potencia. Si bien esta familia de inhibidores de la G6PDH fue descrita hace más de 60 años, a la fecha de inicio de este trabajo de tesis se desconocía su sitio de unión a la enzima y durante el curso de la misma Zhao y colaboradores intentaron elucidar esta interrogante empleando aproximaciones *in silico* (Zhao et al., 2014). Sin embargo, lo concluido por este estudio discrepa con el modo de

inhibición (acompetitivo) reportado para los esteroides ya que el mismo plantea que DHEA estaría desplazando al cofactor y ocupando su sitio de unión, lo cual tornaría competitivo a este inhibidor.

Finalmente, pocos años atrás se realizó un HTS contra la G6PDH de *T. cruzi* que permitió identificar nuevos inhibidores acompetitvos de tipo no esteroideos y pertenecientes a las familias de tienopirimidinas (IC_{50} 4.9-32 µM) y quinazolinas (IC_{50} 0,48-30 µM). Algo a destacar es que los compuestos: 1a- tienopirimidina y 2a- quinazolinona compiten por el sitio de unión de EA. Se estudió la toxicidad de los mismos, tratando epimastigotes y se pudo observar que las quinazolinonas son las que tienen mayor efecto tripanocida, presentando EC_{50} similares a las obtenidas con benznidazol, mientras que distintos derivados de las tienopirimidinas resultaron inactivos (Mercaldi et al., 2014), ver figura 5.

El diseño racional de inhibidores contra la G6PDH de *T. cruzi* requiere del conocimiento de los aspectos bioquímicos y estructurales que caracterizan a esta enzima en relación con su contraparte humana. Uno de los principales obstáculos que limitaban esos estudios es que al inicio de esta tesis no se contaba con reportes de la estructura de la enzima del patógeno, el cual fue uno de nuestros principales objetivos.

objetivos

Capítulo 2.

OBJETIVOS

La validación de la TcG6PDH como blanco de fármacos antichagásicos requiere de un conocimiento profundo, tanto de sus aspectos bioquímicos y biológicos, así como de su biología estructural.

Es por ello que en esta tesis nos planteamos los siguientes objetivos.

2.1 Objetivos generales

Caracterización bioquímica, estructural y biológica de la glucosa-6-fosfato deshidrogenasa de *Trypanosoma cruzi* para evaluar el potencial de la misma como blanco terapéutico.

2.2 Objetivos específicos

1. Resolución de la estructura tridimensional de la TcG6PDH y análisis detallado de la misma para identificar características diferenciales con respecto a su homólogo humano.

2. Evaluar la relevancia de esas diferencias mediante la generación y caracterización enzimática de mutantes puntuales localizados en regiones específicas y de interés para el desarrollo y optimización de fármacos.

3. Identificar, evaluar y caracterizar el modo de acción y el sitio de unión de nuevos potenciales inhibidores de la TcG6PDH.

4. Confirmar la localización subcelular de la G6PDH en *Trypanosoma cruzi* y el blanco molecular de los inhibidores esteroideos.

resultados

Capítulo 3

RESULTADOS

Drug Targets in Trypanosomal and Leishmanial Pentose Phosphate Pathway.

Comini Marcelo A., **Ortíz Cecilia** and Cazzulo Juan José
Capítulo 16 del Libro: Trypanosomatids diseases, molecular routes to drug discovery.
Editores: T. Jäger, O. Koch, L.Flohé,
Editorial: Wiley-Blackwell. ISBN: 978-3-527-33255-7

3.1 Resumen

Si bien en los últimos años las enzimas que participan de la vía de las pentosas de tripanosomátidos han recibido especial interés, al momento de la escritura de este capítulo, no existía ningún relevamiento comprensivo de los aspectos bioquímicos, estructurales e inhibidores descritos para las proteínas que participan de esta vía. Fue por ello que creímos que se sería de gran utilidad compilar y sistematizar la información reportada hasta ese momento.

La PPP, al igual que la vía glicolítica, es responsable de metabolizar la glucosa que se encuentra disponible para, a partir de ello obtener poder reductor y ribosa 5-fosfato, el cual constituye un bloque indispensable en la síntesis de ácidos nucleicos. La relevancia de la vía de las pentosas y su organización general son similares entre tripanosomátidos y mamíferos. Sin embargo, en este capítulo nos hemos propuesto evaluar a partir de la información disponible, si las enzimas que participan de la vía podrían llegar a calificar como blanco de fármacos.

De las siete enzimas que componen la PPP, la G6PDH y la 6PGDH mostraron ser esenciales para tripanosomátidos. Respecto a la primera de ellas, esta última presenta una menor identidad de secuencia con su contraparte humana. Para ambas se han reportado estructuras cristalinas y se han realizado esfuerzos en la identificación de inhibidores selectivos.

Existen dos isoformas para la RPI, las formas A y B que presentan diferencias importantes entre sí. La isoforma A es característica de mamíferos mientras que la isoforma B predomina en tripanosomátidos. Esta característica junto a los datos cristalográficos disponibles en presencia de diversos inhibidores la posiciona como un blanco de drogas ideal. Sin embargo, a la fecha de elaboración de dicho capítulo no se contaba con pruebas contundentes acerca de su esencialidad, las cuales fueron obtenidas recientemente tanto para *L. infantum* como para *T. brucei* (Faria et al. 2016).

Por el contrario, las demás enzimas de la PPP carecen de interés como blancos moleculares de fármacos ya que varias de ellas no se expresan en los estadios infectivos de determinadas especies o bien se sospecha que carecen de un rol biológico relevante.

Mis contribuciones:

Búsqueda bibliográfica y escritura del capítulo.

16
Drug Targets in Trypanosomal and Leishmanial Pentose Phosphate Pathway

Marcelo A. Comini[*], *Cecilia Ortíz, and Juan José Cazzulo*

Abstract

Trypanosomatids utilize glucose to sustain critical cellular functions. A key metabolic pathway that relies on glucose is the pentose phosphate pathway (PPP), which comprises reactions oxidizing substrates (oxidative phase) and interconversions to phosphorylated saccharides (non-oxidative phase). The products (ribose-5-phosphate), intermediates (glyceraldehyde-3-phosphate, fructose-6-phosphate), and cofactors (NADPH) of this metabolism are used in the synthesis of nucleic acids and lipids, and for the maintenance of redox homeostasis. Enzymes from the oxidative branch (i.e., glucose-6-phosphate dehydrogenase (G6PDH), 6-phosphogluconolactonase (6PGL), and 6-phosphogluconate dehydrogenase (6PGDH)) are phylogenetically related to their cyanobacterial and plant counterparts, and play an essential house-keeping role in the parasites. The components of the non-oxidative branch (i.e., ribose-phosphate isomerase (RPI), ribose-phosphate epimerase (RPE), transketolase (TKT), and transaldolase (TAL)) are more heterogeneous, with a member that has no orthologous sequence in mammals (RPI) and others (RPE and TKT) that are developmentally regulated and species-specific dispensable. Except for 6PGDH, no systematic drug discovery studies have been performed on PPP enzymes. Only few chemical entities have been identified as inhibitors of G6PDH, and there are no investigations addressing this question for 6PGL, RPI, RPE, TKT, and TAL. Thus, the search for inhibitors against PPP enzymes from trypanosomatids does not keep pace with the substantial information available on their biochemical and structural properties. The aim of this chapter to attract attention to PPP enzymes already qualifying as trypanosomatid drug targets.

Pentose Phosphate Pathway in Trypanosomatids: General Considerations and Biological Relevance

Trypanosomiasis and leishmaniasis are life-threatening diseases of mammals for which an effective, safer, and affordable chemotherapy and/or immunoprophylaxis (vaccine) remain major and challenging goals for the scientific and public

* Corresponding Author

Trypanosomatid Diseases: Molecular Routes to Drug Discovery, First edition. Edited by T. Jäger, O. Koch, and L. Flohé.
© 2013 Wiley-VCH Verlag GmbH & Co. KGaA. Published 2013 by Wiley-VCH Verlag GmbH & Co. KGaA.

health domain. Over the last decades, this limitation has prompted the search for suitable drug target candidates – an enterprise that requires a detailed biochemical, biological, and structural analysis of the metabolic pathways and their components [1]. The glucose-based metabolism of trypanosomatids is among those critical pathways that have been investigated thoroughly but not completely. In most organisms glucose is metabolized through two major pathways: the glycolytic, or Embden–Meyerhof, pathway, and the pentose phosphate pathway (PPP). Both pathways start from glucose-6-phosphate (G6P), but have different functions, which all are important for survival. Whereas glycolysis is the chief pathway to catabolize glucose gaining energy in the form of ATP, the PPP is involved in the production of ribose-5-phosphate (R5P), required for nucleotide and nucleic acid synthesis, and for sustaining reducing power in the form of NADPH, which is essential for a number of biosynthetic processes and for the protection of the cell against oxidative stress (see below and Chapter 9 of this volume). The pathway consists of two branches, namely an oxidative branch, involving glucose-6-phosphate dehydrogenase (G6PDH), 6-phosphogluconolactonase (6PGL), and 6-phosphogluconate dehydrogenase (6PGDH), and a non-oxidative, or sugar interconversion, branch, involving ribose-5-phosphate isomerase (RPI), ribulose-5-phosphate epimerase (RPE), transaldolase (TAL), and transketolase (TKT) (Figure 16.1). The PPP has also been known as the pentose phosphate cycle, since, when functioning as a whole, the fructose-6-phosphate (F6P) and glyceraldehyde-3-phosphate (Gly3P) formed can be converted back to G6P, entering the oxidative branch again. However, the PPP does not need to act as a cycle and the different enzymatic reactions will be operative according to the cell needs [2].

As opposed to the glycolytic pathway, which has been thoroughly studied in trypanosomatids over the last three decades, the PPP received much less attention up to the late 1990s. At present, we know that all seven enzymes of the pathway are expressed in the four major stages of the life cycle of *Trypanosoma cruzi* (epimastigote and metacyclic trypomastigote in the insect vector, amastigote and bloodstream trypomastigote in the mammal) [3] and in promastigotes of *Leishmania mexicana* [4], whereas the pathway is developmentally regulated in *T. brucei*, with expression of all components in the procyclic (insect dwelling) form and the oxidative branch enzymes in the bloodstream form [5]. The functionality of the pathway has been demonstrated in *T. cruzi* epimastigotes [3], and in *L. braziliensis* [6] and *L. mexicana* promastigotes [4] by determining the amount of $[^{14}C]CO_2$ released for glucose labeled in C1 or C6. A similar study seems not to have been conducted on *T. brucei*, although several lines of evidence point to the functionality of the pathway in this parasite, at least in the procyclic stage. At this point it is worth noting that trypanosomatids contain an organelle called the glycosome, which has a peroxisomal origin and evolved to host several components or steps of key pathways such as glycolysis, gluconeogenesis, PPP, lipid biosynthesis, purine salvage, and pyrimidine biogenesis ([7] and Chapter 7 of this volume) Accordingly, several enzymes of the PPP are localized in the glycosomes, although not exclusively, as discussed below for each enzymatic entity [8]. Another interesting aspect of the trypanosomatids

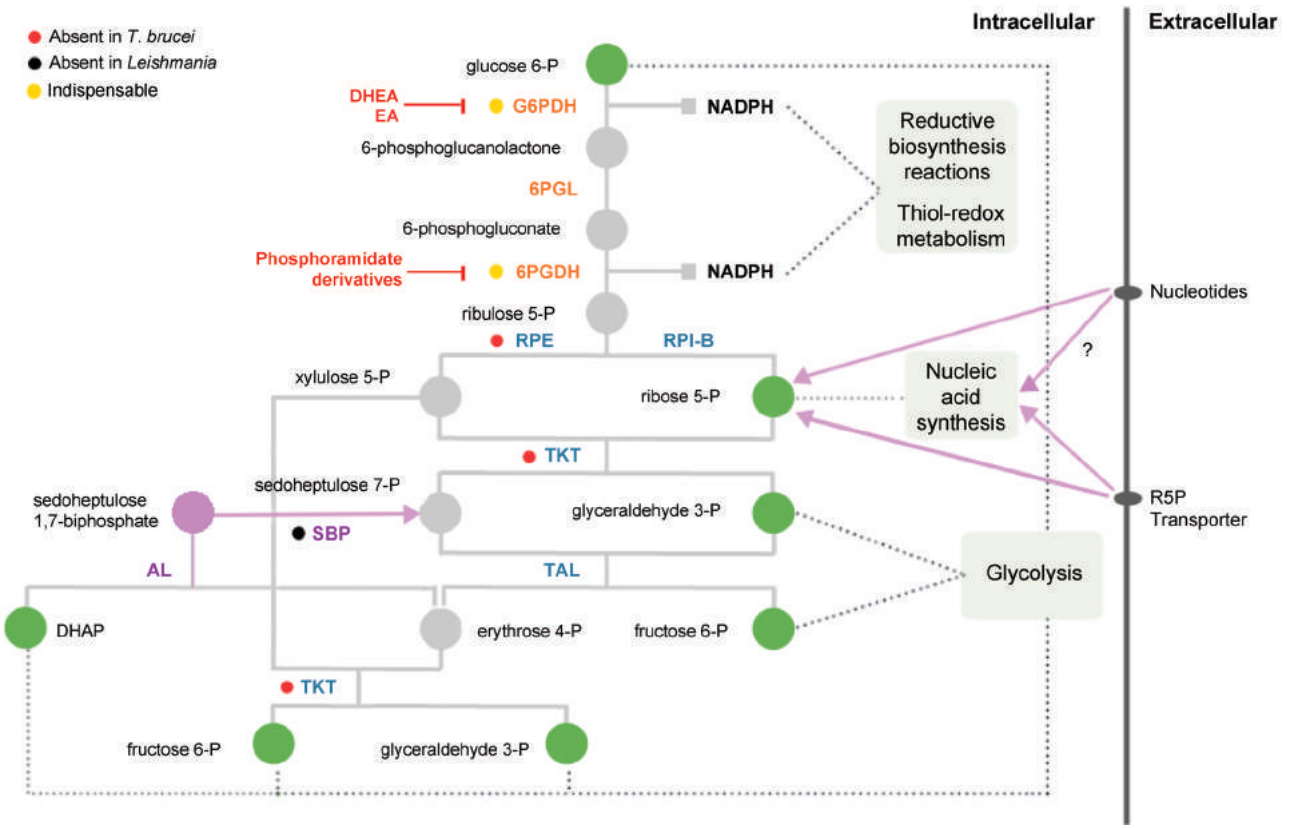

Figure 16.1 Scheme of the PPP in trypanosomatids: components, biological relevance, and inhibitors. The shared substrates and products of the PPP are labeled with a green dot. Characterized enzyme inhibitors are shown in red. The enzymatic components of the oxidative and non-oxidative phase of the PPP are in orange and light blue, respectively: G6PDH, glucose-6-phosphate dehydrogenase; 6PGL, 6-phosphogluconolactonase; 6PGDH, 6-phosphogluconate dehydrogenase; RPI-B, type B ribose phosphate isomerase; RPE, ribose phosphate epimerase; TKT, transketolase; TAL, transaldolase; AL, aldolase. Salvage pathways for R5P are depicted in magenta, and include: (i) membrane transporters for R5P and/or nucleotides, (ii) the phosphorylation of ribose by ribose kinase (RBK), and (iii) the riboneogenesis pathway where by the concerted action of aldolase (AL) and sedohepotulose bisphosphatase (SBP), dihydroxyacetone phosphate (DHAP), and glyceraldehyde-3-phosphate are converted into sedoheptulose-7-phosphate. Enzymes absent in infective *T. brucei* and *Leishmania* spp. are marked with a red and violet dot, respectively. Enzymes of proved indispensability are indicated with blue dot. Promising enzyme inhibitors are shown in red.

enzymes from the oxidative branch (G6PDH, 6PGL, and 6PGDH) is their evolutionary link to cyanobacteria and plant orthologs – a phylogenetic relationship that supports the view of a kinetoplastid photosynthetic plastid being an endosymbiotic ancestor of the glycosome [9,10].

G6PDH, which catalyzes the oxidation of G6P to 6-phosphogluconolactone with the concomitant reduction of NADP to NADPH, is the first and, probably, rate-limiting enzyme of the PPP. The number of genes encoding for G6PDH differs between trypanosomatids, with *T. brucei* and *L. mexicana* harboring a single-copy sequence [11,12], and *T. cruzi* containing five different putative sequences, two of them being pseudogenes [13]. The enzyme is predominantly distributed in the cytosol, with a minor fraction compartmentalized in glycosomes, although a typical peroxisomal targeting sequence (PTS) is absent [3,8,11,14]. The production of NADPH in this organelle likely serves to support the biosynthesis of ether lipid and sterols and antioxidant defense [12,15–19]. The indispensability of G6PDH has been confirmed for the infective form of African trypanosomes by means of RNA interference [20]. The deleterious phenotype observed (growth rate impairment and reduced tolerance to H_2O_2) is likely a consequence of an imbalance in nucleotide and NADPH pools. A critical role of G6PDH in the defense against oxidative stress has also been demonstrated in *T. cruzi* [13]. The enzyme activity increased about 45-fold in trypomastigotes subjected to H_2O_2 challenge and, under non-stress conditions, G6PDH levels were markedly elevated in the infective stages (trypomastigote and amastigote) [13]. Also, other studies revealed that G6PDH is more abundant in *T. cruzi* strains of higher virulence [21,22]. However, chemical validation of G6PDH remains controversial (see below Section 16.3).

6PGL, the second enzyme of the oxidative phase, is responsible for decreasing the lifetime of the highly reactive 6-phosphogluconolactone by hydrolytic cleavage to 6-phosphogluconate [11]. In *T. brucei*, a single-copy gene encodes a putative 6PGL that displays a dual subcellular localization– about 85% being in the cytosol and 15% in the glycosomes [23]. A PTS-1 targets the protein to the glycosomes [11]. In promastigotes of different strains from *L. mexicana*, 6PGL was by far the most prominent enzymatic activity of the PPP [4]. The essentiality of 6PGL has not yet been addressed for any trypanosomatid; however, although the lactone can be spontaneously hydrolyzed, it is tempting to speculate that under certain conditions, (i.e., high NADPH demand) 6-phosphogluconolactone may accumulate to toxic levels that require catalytic elimination. Such function for 6PGL may be critical inside the glycosomes, where a high concentration of the highly electrophilic 6-phosphogluconolactone [24] may lead to the irreversible inactivation of key metabolic enzymes.

6PGDH is the best-studied enzyme of the PPP in *T. brucei*, and, to a lesser extent, in *T. cruzi* and *L. mexicana*. It catalyzes, in the presence of NADP, the third step of the oxidative branch that involves the reversible oxidative decarboxylation of 6-phosphogluconate to ribulose-5-phosphate (Ru5P) with concomitant production of NADPH and carbonic anhydride [25]. 6PGDH activity is predominantly cytosolic, with a small glycosomal component in procyclic *T. brucei* [14]. The biological importance of 6PGD for bloodstream *T. b. rhodesiense* and intracellular

amastigotes of *T. cruzi* amastigotes was first revealed by cytotoxicity studies performed with specific enzyme inhibitors [26] (see Section 16.3). Unpublished work of Barrett *et al*. indicated that the enzyme is indispensable for bloodstream *T. brucei* [27,28]. Taking into account that the infective stage of African trypanosomes depends exclusively on glycolysis for energy production and glucose-6-phosphate isomerase has been shown to be extremely sensitive to 6-phosphogluconate [29], the deleterious phenotype of 6PGDH-depleted *T. brucei* was suggested to be caused by accumulation of phosphorylated gluconate with concomitant inhibition of glycolysis [28]. This effect is likely amplified *in vivo* by an increment in the flux of G6P through the PPP and the consequent increased formation of the phosphorylated intermediate [30]. Whether a shortage in R5P also contributes to this phenotype remains to be investigated.

RPI catalyzes the isomerization of R5P and Ru5P that will proceed in either direction depending on the relative substrate and product concentrations. If R5P is abundant, the phosphorylated sugar will be diverted to the production of precursors for aromatic vitamins (not yet fully documented for trypanosomatids) and glycolytic intermediates, whereas a decline in R5P will stimulate the reverse reaction leading to its synthesis and that of nucleotides and cofactors. According to their distribution among the phylogenetic scale, RPIs are classified into type A (with representatives in all three kingdoms of life) or type B (restricted to some bacteria and protozoa) [31]. Trypanosomatids lack type A RPI but are endowed with type B RPI [32], whose activity was detected in different life stages of *T. brucei* [5], *L. tropica* and *L. major* [33], and *T. cruzi* [34]. Although the essentiality of RPI for trypanosomatids remains to be demonstrated, the adverse phenotype observed in phylogenetically distant organisms, namely *Escherichia coli* [31] and human [35], deficient in this enzyme points to an evolutionary conserved critical function for this protein. The absence of type B RPIs in mammalian genomes and the significant structural divergence between both enzyme classes (see below) have raised trypanosomal RPIs to the level of attractive drug target candidates [34,36].

RPE is responsible for catalyzing the interconversion of R5P and xylulose-5-phosphate (X5P). The genome of the CL Brener clone of *T. cruzi* harbors two genes encoding RPEs with one of them containing a PTS-1 at the C-terminus. The enzyme is expressed in all four biological stages of this parasite and, in contrast to the other PPP enzymes, is not upregulated in metacyclic trypomastigotes. It is present in membrane-bound vesicles [3] – a behavior of unknown biological relevance. The genome of *Leishmania* encodes for two isoenzymes that differ in the presence and absence of a glycosomal targeting sequence [37]. In promastigotes of different strains of *L. mexicana*, the activity of RPE was almost 3-fold higher than that of the competing enzyme, RPI [4]. In *T. brucei*, RPE, and also TKT, activity is detected in the procyclic form, but not in parasites isolated from mice [5], indicating that the non-oxidative segment of the PPP is dispensable for the latter. A possible explanation for this exceptional metabolic adaptation is to constrain sugar metabolization to the production of R5P and NADPH via the oxidative phase of the PPP in order to meet the remarkably high proliferative rate of bloodstream parasites. In summary, RPE does not qualify as potential drug target against African

trypanosomes, but the biological importance of this enzyme for the intracellular parasites *Leishmania* spp. and *T. cruzi* remains to be investigated.

TAL transfers a dihydroxyacetone unit from F6P to erythrose-4-phosphate (E4P) to synthesize sedoheptulose-7-phosphate and, as byproduct, Gly3P. The backward reaction is also catalyzed by the enzyme. TAL activity was detected in the cytosol of bloodstream *T. brucei* [5]. The presence of this enzyme was also identified in the four developmental stages of *T. cruzi* with a 3- to 5-fold higher activity in the highly infective metacyclic trypomastigotes [3]. Unpublished data propose the presence of four TAL isoforms in *T. cruzi* epimastigotes [38]. Promastigotes of *L. mexicana* also display TAL activity [4]. The role of TAL in trypanosomatids has not yet been addressed. In higher eukaryotes the enzyme plays an important function as a regulator of the metabolic fluxes through the PPP [39] – a function that can be shared by the New World trypanosomes (*T. cruzi* and *Leishmania* spp.), which present a fully active PPP, but likely not by *T. brucei*, since the infective form presents a defective non-oxidative branch (see above) and deletion of TKT gene, whose product will synthesize the substrates for TAL, in the procyclic stage went phenotypically unnoticed (see below) [40]. Thus, TAL can be disregarded as drug target candidate for African trypanosomes, and its role in *T. cruzi* and *Leishmania* spp. deserves further research to draw final conclusions in this respect.

TKT is a thiamine diphosphate-dependent enzyme capable of catalyzing two reversible reactions that involve the transfer of 2-carbons from: (i) X5P to R5P to produce sedoheptulose-7-phosphate and Gly3P, and (ii) from X5P to E4P to generate F6P and Gly3P. The four developmental stages of *T. cruzi* express TKT activity that in epimastigotes is distributed among the cytosol (around 80%) and the small granule fraction (around 20%) representing the glycosomes [3]. TKT activity was reported to occur in several species of *Leishmania* [41], and a dual cytosolic and glycosomal localization of the protein has been unambiguously demonstrated in *L. mexicana* promastigotes [42]. In *T. brucei*, TKT is encoded by a single-copy gene containing a PTS-1 [42], which is actively expressed and repressed in the procyclic and bloodstream stage, respectively [5,40]. The biological relevance of TKT has only been addressed for African trypanosomes [40], whereby, at least under *in vitro* growth conditions, TKT-null mutants of the procyclic form did not exhibit any growth or morphologic phenotype despite an alteration in the metabolic profile (i.e., increase in TKT substrates and absence of sedoheptulose-7-phosphate). A role for TKT in *T. cruzi* and *Leishmania* has yet to be determined, but since they harbor a fully operative PPP, the enzyme may function in preventing the accumulation of phosphorylated carbohydrate intermediates of the pathway in the glycosome, some of which are metabolically toxic, and/or modulating NADPH production by redirecting sugar phosphates towards the oxidative branch of the cycle [40].

In other organisms such as yeast, a salvage pathway for the synthesis of R5P from glycolytic intermediates without production of NADPH is operative. This is the so-called riboneogenesis pathway that via the combined action of transketolase and aldolase, glycolytic intermediates are transformed into sedoheptulose-1,7-bisphosphate, which is further hydrolyzed by the enzyme sedoheptulose-1,7-bisphosphatase to sedoheptulose-7-phosphate. This product can be transformed into R5P by TKT

(Figure 16.1). Candidate genes encoding for this protein are present in the genome of *T. brucei* and *T. cruzi*, but are absent in *Leishmania* [37]. Whether riboneogenesis is functional in these parasites and to what extent it contributes to the intracellular pool of R5P should be further investigated.

Biochemical and Structural Hallmarks of Trypanosomatids PPP Enzymes

To assess the possibility of one or more of the PPP enzymes being suitable targets for chemotherapy, a detailed comparison of their structure and properties with those of the corresponding mammalian enzymes is required. The most relevant biochemical and structural features from the components of the trypanosomal and leishmanial PPP that can provide a basis for the development of specific inhibitors are summarized below.

G6PDHs from the TriTryps share about 64–69% amino acid identity between each other and about 50% identity with the human ortholog. The kinetic constants for substrate (K_m for G6P ~60–200 μM) and coenzyme (K_m for NADP ~4–12 μM) reported for G6PDH from *T. cruzi* [13], *T. brucei* [14], and *L. mexicana* [20] were of the same order of magnitude, suggesting an overall conservation of the major catalytic and ligand-binding residues. The k_{cat} reported for *T. brucei* and *L. mexicana* G6PDH is noteworthy (k_{cat} of 16–22 s^{-1} [20]), as it is almost one order of magnitude lower than those observed for the *T. cruzi* and human enzymes (k_{cat} of 130–190 s^{-1}) [13,43], and indicates a lower catalytic efficiency of the former enzymes. Also striking is the significant sensitiveness of *T. cruzi* G6PDH to inhibition by NADPH (K_i for NADPH of 0.76 versus 9 μM for the *T. cruzi* and human enzyme, respectively) [13,44], suggesting a control of the enzyme activity by the NADPH/NADP ratio. Other major molecular and structural features that distinguish the *T. cruzi* enzyme from the human ortholog are: (i) in contrast to the human enzyme, which exists in a rapid equilibrium between monomeric, dimeric, and tetrameric species [45], the trypanosomal protein forms highly stable tetramers ([46]; Ortíz *et al*., unpublished), and (ii) *T. cruzi* G6PDH, but not the enzymes from *T. brucei* and *L. mexicana* and neither the human counterpart, contains an N-terminal extension with non-conserved cysteines, some of them engaged in the formation of disulfide bridges that stabilize a more active conformation of the enzyme ([13]; Ortíz *et al*., unpublished). Crystals of the protein in the apo-state and with bound G6P have recently been obtained, and diffracted at 2.9- and 3.4-Å resolution, respectively [46]. The refined structures are currently being subjected to a thorough comparative analysis with the human ortholog in order to explore molecular differences that can be exploited for the design or optimization of specific drugs.

The *T. brucei* and *T. cruzi* representatives for 6PGL have been expressed in recombinant soluble forms exhibiting a monomeric conformation (Beluardi and Cazzulo, unpublished; [47]) similar to that reported for the enzyme from bovine erythrocytes [48]. Kinetic studies on 6PGL are very difficult, because its substrate is very unstable and must be generated *in situ*. Nevertheless, a K_m value of 50 μM has

been determined for the *T. cruzi* enzyme [38], which is close to one of the values reported for the rat liver enzyme (80 μM) [49]. Despite this limitation, the crystal structure of *T. brucei* 6PGL has recently been solved at about 2 Å in the absence (Protein Data Bank (PDB) ID: 2J0E) [47] and presence of ligands (PDB ID: 3E7F, 3EB9) [23], which facilitates a detailed mechanistic and dynamic characterization of the enzyme [23,50]. The atomic coordinates for the crystal structure of 6PGL from *L. braziliensis* (PDB ID: 3CH7; Arakati and Merrit, unpublished) and *L. guyanensis* (PDB ID: 3CSS; Painter and Merrit, unpublished) have also been deposited. Although the structure of the human ortholog remains to be elucidated, its low amino acid identity with the plastid-like parasite proteins (below 20%) predicts important structural differences.

6PGDH from kinetoplastids exhibits low amino acid sequence identity (below 35%) with its mammalian counterpart that translates into differential affinities for ligands [51]. The reported K_m values for NADP are 1.5, 5.9, and 3–30 μM, for the *T. brucei*, *T. cruzi*, and human enzymes, respectively, and the corresponding values for 6PG are 3.5, 22.2, and 20–32 μM, respectively [30,52,53]. The apparent K_m values for 6PG and NADP for the *L. mexicana* enzyme were 6.9 and 5.2 μM, respectively [54]. The K_i for NADPH and Ru5P was 0.6 and 30 μM, respectively, for the *T. brucei* enzyme. These differences in kinetic parameters originate in subtle structural differences (see below) and are particularly noteworthy for *T. brucei* 6PGDH, since they can, at least in part, explain the greater sensitivity of the enzyme to a number of inhibitors (see Section 16.3).

The three-dimensional structure of *T. brucei* 6PGDH has been determined to a 2.8-Å resolution (PDB ID: 1PGJ [55]) and thoroughly compared with that of a mammalian representative – the sheep liver enzyme [56]. Despite the low protein sequence identity between both enzymes, a high conservation was observed in the overall structure and for residues directly engaged in substrate and coenzyme binding. However, several secondary residues surrounding the substrate binding site (i.e., either making direct contact with the substrate or shaping the active site at the interface between subunits), as well as others bridging the C-terminal tail on the coenzyme binding site, differed significantly in identity or structural disposition and were proposed to account for the different affinities of the enzymes for substrate/coenzyme and inhibitors [56]. The analysis of this structural data [57] has facilitated a more rational design of inhibitors (see Section 16.3). Homology modeling of the *L. mexicana* and *T. cruzi* 6GPDH suggest a limited structural divergence among kinetoplastid proteins, raising the possibility for designing inhibitors equally effective against the enzymes from these species [54]. The structure of human 6PGDH has recently been delivered (PDB ID: 2JKV; Ng *et al.*, unpublished). Comparison with the parasite protein should contribute to the improvement of inhibitor specificity (see Section 16.3).

RPI from trypanosomatids can be considered as an ideal drug target, since it belongs to the B-type RPI group absent in all mammalian genomes and has significant structural divergence from the A-type enzymes. The protein from *T. cruzi*, the only representative from a trypanosomatid that has been characterized, is a homodimer [32,34]. *T. cruzi* RPI presented K_m values in the millimolar range (K_m for R5P and Ru5P of 4 and 1.4 mM, respectively), similar to those reported for

the enzyme from human erythrocytes (e.g., K_m for R5P of 2.2 mM) [58], despite the significant differences at the active-site motif. The three-dimensional structure of *T. cruzi* RPI-B has been determined at 2.2-Å resolution in the apo-form or in complex with D-R5P or the inhibitors 4-phospho-D-erythronohydroxamic acid and D-allose-6-phosphate (PDB ID: 3K7O, 3K7P, 3K7S, 3K8C, and 3M1P) [34]. This study further revealed the occurrence of small conformational changes upon substrate binding, the critical role of a phosphate-binding loop close to the active site, both contributing to substrate and inhibitor binding, and the residues responsible for catalysis.

In the case of *T. cruzi* TKT, the apparent K_m values determined for R5P, E4P, and X5P were 1.34, 0.1, and 0.07 mM, respectively [38]. For the leishmanial enzyme, only the apparent K_m for R5P, 2.75 mM, was determined [42], whereas the homolog from *T. brucei* showed apparent K_m values for R5P and X5P of 0.8 and 0.2 mM, respectively [40]. The K_m values for the recombinant human enzyme, recently reported by Mitschke *et al*. [59], were 0.48 and 0.25 mM for R5P and X5P, respectively. As previously proposed for the *T. brucei* enzyme [40], a regulatory role in the PPP may also be envisaged for *T. cruzi* and *L. mexicana* TKT because of the low R5P concentration in steady-state and the high K_m values of these enzymes for this substrate. The crystal structure of *L. mexicana* TKT has been solved at 2.22 Å (PDB ID: 1R9J), and comparison with the structures of poorly related eukaryote orthologs (i.e., yeast and maize) revealed a high degree of similarity at the active site, cofactor, and ion-binding regions [42]. A high-resolution structure of the human enzyme has been recently determined at 1.75 Å (PDB ID: 3MOS [59]), but not yet compared to the leishmanial protein. At least two residues that are important for cofactor and substrate binding in the mammal enzyme (Gln189 and Lys260 in human TKT) [59] are not conserved in the trypanosomatid's proteins.

Inhibitor Discovery Against PPP Enzymes

Only a handful of compounds have been investigated as potential inhibitors of kinetoplastid G6PDH, most of them previously identified as inhibitors of the human enzyme. The steroids dehydroepiandrosterone (DHEA) and epiandrosterone (EA) inhibited the *T. brucei* enzyme with K_i values about 6-fold lower than those reported for the human enzyme [20]. Strikingly, *L. mexicana* G6PDH was not affected by similar concentrations of the drugs [20]. The same inhibitors also were active against the enzyme from *T. cruzi*, but the K_i values obtained, close to 22 μM for DHEA and to 4.8 μM for EA [60], were higher than those for the human enzyme (8.9–6.2 μM for DHEA and 3–3.4 μM for EA [20]). The 16α-bromated (16Br) derivatives of both drugs were more active than the parental precursors, with IC_{50} values about 5-fold lower for 16BrDHEA and 2.5-fold lower for 16BrEA (Figure 16.2) [60]. All these compounds were uncompetitive inhibitors for both substrates – a very rare mechanism where the inhibitor exerts its activity by binding to the ternary enzyme–coenzyme–substrate complex. The recent elucidation of the *T. cruzi* G6PDH structure may disclose the so far unknown binding site of these drugs. The bromated derivatives were toxic for *T. cruzi* epimastigotes with LD_{50} values ranging from 12 to 20 μM [60], similar to the

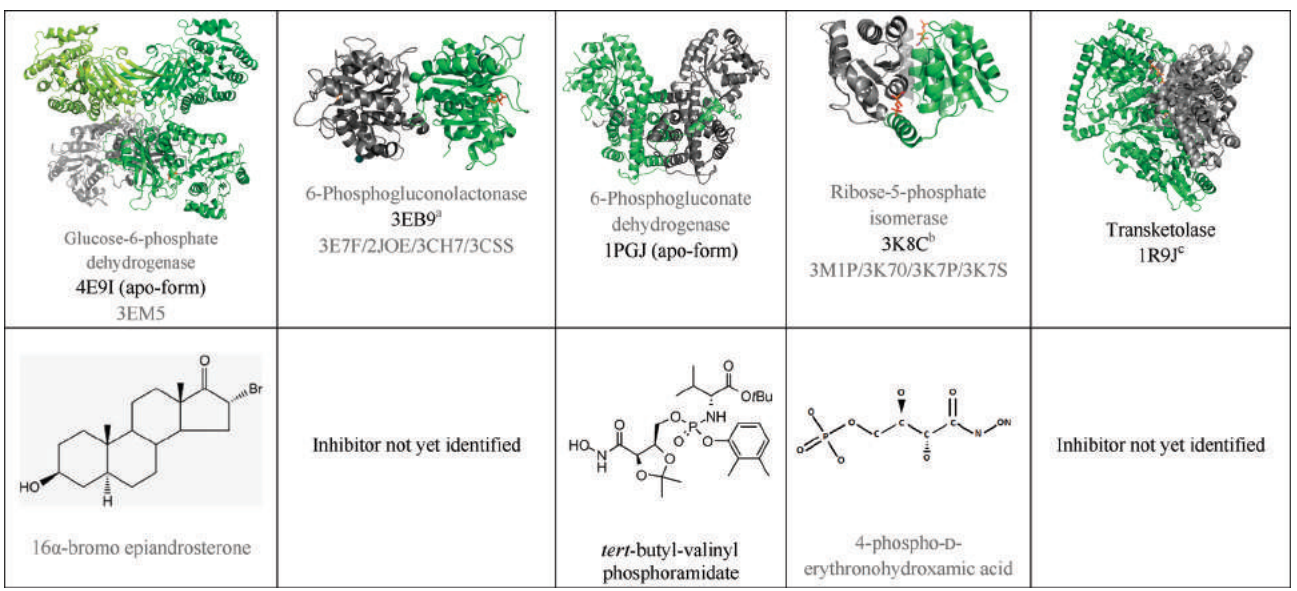

Figure 16.2 Three-dimensional structure and best inhibitors identified for PPP enzymes of trypanosomatids. Bold IDs indicate the PDB ID corresponding to the structure shown. The protein subunits are shown in different colors; dark brown depicts the following ligands: [a]citrate, [b]with 4-deoxy-4-phospho-D-erythronohydroxamic acid, and [c]thiamine diphosphate.

values obtained for DHEA and EA against the bloodstream form of *T. brucei* [20]. For both microorganisms the *in vivo* potency of the steroids was more than 10-fold lower than the inhibitory activity displayed against the recombinant enzymes. On the other hand, metacyclic promastigotes of *L. mexicana* were not affected by similar concentrations of the latter compounds [20]. The specific action of steroids against G6PDH from different trypanosomatids has been confirmed by genetic means [22]. At the *in vivo* level, DHEA administered subcutaneously to male rats infected with *T. cruzi* led to a significant reduction in parasite load, which was associated with enhanced lymphoproliferative (thymocyte and macrophage proliferation) and pro-inflammatory (interleukin-12, nitric oxide production) responses [61,62]. The contribution of trypanosomal G6PDH inhibition by DHEA to the trypanostatic effect exerted by the drug *in vivo* has not yet been addressed. A new class of inhibitors, namely the molecular tweezers or clips, has been recently developed against G6PDH [63]. They consist of two naphthalene or anthracene molecules linked by a benzene moiety with phosphate groups as inorganic substituent. A representative of the benzene–naphthalene family proved to inhibit *T. cruzi* G6PDH with an IC_{50} of 3 μM (Ortíz *et al.*, unpublished), which is 2-fold lower than that reported for the human enzyme (7 μM) [63]. The compound did not exhibit a significant toxicity against *T. cruzi* epimastigotes ($LD_{50} \sim 100$ μM), which may be due to poor drug uptake and/or metabolization (i.e., low permeability and phosphatases).

As part of an ongoing target-based drug discovery program, Barrett *et al.* performed a systematic search for 6PGDH inhibitors of the *T. brucei* enzyme. Large differences between the trypanosomal and sheep enzymes in the affinity of substrate analogs (e.g., the K_i value for 6-P-2-deoxygluconate versus 6-phosphogluconate was 200-fold lower for *T. brucei* 6PGDH than for the sheep enzyme) [30] has prompted the design of substrate-based inhibitors [28]. Several phosphonated monosaccharides showed acceptable selectivity against the parasite enzyme with K_i values in the micro- to submicromolar range [64]. Based on molecular modeling and structural analysis [55,57], new substrate-based analogs were synthesized and tested [65]. One of the first series ((2*R*)-2-methyl-4,5-dideoxy-6-phosphogluconate) and six of the second ((2*R*)-2-methyl-4-deoxy-6-phosphogluconate) were able to inhibit competitively both enzymes, one of them showing some selectivity towards the enzyme from the parasite. Compounds of the third series (2,4-dideoxy-6-phosphogluconate) were completely inactive. The major conclusion arising from this work indicates that substituents at positions 2 and 4, but not at 6 (the phosphate moiety), are critical for effective inhibitor binding. Three of the compounds showed a moderate activity against *T. b. rhodesiense* trypomastigotes (below 12 μM) and two had a moderate toxicity against *T. cruzi* amastigotes (below 10 μM), but none of them had any significant anti-leishmanial activity [65]. Taking into account that suramin, a polysulfonated benzyl-rich drug used to treat African trypanosomiasis, inhibited *T. brucei* 6PGDH, several related triphenylmethane derivatives were assayed [57]. In general, the compounds exhibited a moderate activity and selectivity towards the parasite enzyme that opens the possibility to use the most active molecules as drug scaffolds. Some hydroxamate derivatives of D-erythronic acid, analogs of the high-energy intermediate of the 6PGDH reaction, were potent and selective inhibitors of the

T. brucei enzyme, with K_i values in the nanomolar range [26]. However, the poor drug-like characteristic of these molecules (e.g., low permeability and instability) will hamper their clinical use. In an attempt to improve these features, Ruda *et al.* [66] synthesized a number of phosphate pro-drugs of the inhibitor 4-phospho-D-erythronohydroxamic acid, which was a selective inhibitor of the *T. brucei* enzyme compared with the sheep liver enzyme (K_i values 0.035 and 1.1 μM, respectively). Most of the compounds were toxic for *T. brucei*. More recently Ruda *et al.* [67] have developed new pro-drugs, aryl-phosphoramidates of 2,3-*O*-isopropylidene-4-erythronohydroxamate; the EC_{50} values came down from above 330 μM up to 0.008 μM for the drug and the best pro-drug, respectively (Figure 16.2). Moreover, rational modifications of satellite alkyl groups (i.e., amino acid side-chain, amino acid, and aryl ester groups) entailed a significant increase in the stability of the compounds. So far, no experiment has been conducted on an animal model to scrutinize the potential of the most potent compounds. In the search for novel molecules that may serve as future drug scaffolds, a novel "virtual fragment screening" approach was implemented [68]. In this strategy, the structure of *Lactococcus lactis* 6PGDH was used as docking template because atomic coordinates for ligand binding to the active site were available and this region is almost identical to that of *T. brucei* 6PGDH. The initial selection of compounds was restricted according to their molecular weight (molecules less than 320 Da) and the presence of functional groups resembling phosphate. Nearly 10% of the 64 000 preselected compounds could be docked into the structure and only 71 (0.1%) qualified as promising candidates for testing. Finally, 10 compounds displayed $IC_{50} < 50$ μM against *T. brucei* 6PGDH and encouraging physicochemical and pharmacological properties.

So far, there is no information available on inhibitors of RPI (most of the compounds tested as potential inhibitors of *T. cruzi* type B RPI were inactive or poorly active, with the exception of 4-phospho-D-erythronohydroxamic acid (Figure 16.2), a competitive inhibitor of R5P with a K_i value of 1.2 mM [32,34]), RPE, 6PGL, TAL, and TKT from trypanosomatids. A recent high-throughput screen against human TKT detected a couple of compounds displaying a reasonable IC_{50} (around 4 μM) and a potent growth-inhibitory effect against tumor cells (EC_{50} 0.4–10 μM) [69]. It will be interesting to test the activity of these new molecules towards TKT from trypanosomatids, since a positive hit will convert them in potential scaffolds for further development of more selective versions.

Conclusions

Although the general organization and relevance of the PPP is similar in trypanosomatids and mammals, some of the enzymes present marked differences, either in structure or in kinetics, or in both, which makes them suitable candidates as targets for specific chemotherapy. In this respect, several of the trypanosomal and leishmanial PPP enzymes appear to be ideal, since they fulfill important prerequisites for entering in a fast-track drug discovery program: (i) indispensability for parasite survival or virulence and/or functional/structural divergence with mammal

counterparts, (ii) suitable expression in recombinant active forms, (iii) availability of assays to test enzyme activity, and (iv) availability of structural data. The particular oligomeric arrangement and/or allosteric properties exhibited by the parasite enzymes offer additional chances to be exploited for the design of specific inhibitors.

Acknowledgments

We thank the following: Drs Frank Gerrit and Thomas Schrader (Universität Duisburg-Essen) for providing G6PDH clip inhibitor; Drs Horacio Botti and Alejandro Buschiazzo (Protein Crystallography Unit, Institut Pasteur de Montevideo) for providing PDB codes for *T. cruzi* G6PDH; and The Agencia Nacional de Investigación e Innovación (grant Innova Uruguay, agreement DCI-ALA/2007/19.040 between Uruguay and the European Commission) and Comisión Intersectorial de Investigaciones Científicas, Universidad de la República, Uruguay, for financial support to M.A.C. and C.O.

References

1 Fairlamb, A.H., Ridley, R.G., and Vial, H.J. (2003) *Drugs Against Parasitic Diseases R&D Methodologies and Issues*, WHO, Geneva.
2 Stryer, L. (1999) *Biochemistry*, 4th edn, Freeman, New York, pp. 559–565.
3 Maugeri, D. and Cazzulo, J.J. (2004) The pentose phosphate pathway in *Trypanosoma cruzi*. *FEMS Microbiol. Lett.*, **234**, 117–123.
4 Maugeri, D.A., Cazzulo, J.J., Burchmore, R.J., Barrett, M.P., and Ogbunude, P.O. (2003) Pentose phosphate metabolism in *Leishmania mexicana*. *Mol. Biochem. Parasitol.*, **130**, 117–125.
5 Cronin, C.N., Nolan, D.P., and Voorheis, H.P. (1989) The enzymes of the classical pentose phosphate pathway display differential activities in procyclic and bloodstream forms of *Trypanosoma brucei*. *FEBS Lett.*, **244**, 26–30.
6 Keegan, F.P., Sansone, L., and Blum, J.J. (1987) Oxidation of glucose, ribose, alanine and glutamate by *Leishmania braziliensis panamensis*. *J. Protozool.*, **34**, 174–179.
7 Michels, P.A., Bringaud, F., Herman, M., and Hannaert, V. (2006) Metabolic functions of glycosomes in trypanosomatids. *Biochim. Biophys. Acta.*, **1763**, 1463–1477.
8 Opperdoes, F.R. and Szikora, J.P. (2006) *In silico* prediction of the glycosomal enzymes of *Leishmania major* and trypanosomes. *Mol. Biochem. Parasitol.*, **147**, 193–206.
9 Krepinsky, K., Plaumann, M., Martin, W., and Schnarrenberger, C. (2001) Purification and cloning of chloroplast 6-phosphogluconate dehydrogenase from spinach. Cyanobacterial genes for chloroplast and cytosolic isoenzymes encoded in eukaryotic chromosomes. *Eur. J. Biochem.*, **268**, 2678–2686.
10 Hannaert, V., Bringaud, F., Opperdoes, F.R., and Michels, P.A. (2003) Evolution of energy metabolism and its compartmentation in Kinetoplastida. *J. Mol. Biol.*, **331**, 653–665.
11 Duffieux, F., Van Roy, J., Michels, P.A., and Opperdoes, F.R. (2000) Molecular characterization of the first two enzymes of the pentose phosphate pathway of *Trypanosoma brucei*. *J. Biol. Chem.*, **275**, 27559–27565.
12 Hannaert, V., Saavedra, E., Duffieux, F., Szikora, J.P., Rigden, D.J., Michels, P.A., and Opperdoes, F.R. (2003) Plant-like traits associated with metabolism of *Trypanosoma* parasites. *Proc. Natl. Acad. Sci. USA*, **100**, 1067–1071.

13 Igoillo-Esteve, M. and Cazzulo, J.J. (2006) The glucose-6-phosphate dehydrogenase from *Trypanosoma cruzi*: its role in the defense of the parasite against oxidative stress. *Mol. Biochem. Parasitol.*, **149**, 170–181.

14 Heise, N. and Opperdoes, F.R. (1999) Purification, localization and characterization of glucose-6-phosphate dehydrogenase of *Trypanosoma brucei*. *Mol. Biochem. Parasitol.*, **99**, 21–32.

15 Dufernez, F., Yernaux, C., Gerbod, D., Noël, C., Chauvenet, M., Wintjens, R., Edgcomb, V.P., Capron, M., Opperdoes, F.R., and Viscogliosi, E. (2006) The presence of four iron-containing superoxide dismutase isozymes in trypanosomatidae: characterization, subcellular localization, and phylogenetic origin in *Trypanosoma brucei*. *Free Radic. Biol. Med.*, **40**, 210–225.

16 Wilkinson, S.R., Prathalingam, S.R., Taylor, M.C., Ahmed, A., Horn, D., and Kelly, J.M. (2006) Functional characterisation of the iron superoxide dismutase gene repertoire in *Trypanosoma brucei*. *Free Radic. Biol. Med.*, **40**, 198–209.

17 Plewes, K.A., Barr, S.D., and Gedamu, L. (2003) Iron superoxide dismutases targeted to the glycosomes of *Leishmania chagasi* are important for survival. *Infect. Immun.*, **71**, 5910–5920.

18 Schlecker, T., Schmidt, A., Dirdjaja, N., Voncken, F., Clayton, C., and Krauth-Siegel, R.L. (2005) Substrate specificity, localization, and essential role of the glutathione peroxidase-type tryparedoxin peroxidases in *Trypanosoma brucei*. *J. Biol. Chem.*, **280**, 14385–14389.

19 Colasante, C., Robles, A., Li, C.H., Schwede, A., Benz, C., Voncken, F., Guilbride, D.L., and Clayton, C. (2007) Regulated expression of glycosomal phosphoglycerate kinase in *Trypanosoma brucei*. *Mol. Biochem. Parasitol.*, **151**, 193–204.

20 Cordeiro, A.T., Thiemann, O.H., and Michels, P.A. (2009) Inhibition of *Trypanosoma brucei* glucose-6-phosphate dehydrogenase by human steroids and their effects on the viability of cultured parasites. *Bioorg. Med. Chem.*, **17**, 2483–2489.

21 Mielniczki-Pereira, A.A., Chiavegatto, C.M., López, J.A., Colli, W., Alves, M.J., and Gadelha, F.R. (2006) *Trypanosoma cruzi* strains, Tulahuen 2 and Y, besides the difference in resistance to oxidative stress, display differential glucose-6-phosphate and 6-phosphogluconate dehydrogenases activities. *Acta Trop.*, **101**, 54–60.

22 Gupta, S., Igoillo-Esteve, M., Michels, P.A., and Cordeiro, A.T. (2011) Glucose-6-phosphate dehydrogenase of trypanosomatids: characterization, target validation, and drug discovery. *Mol. Biol. Int.*, **2011**, 135701.

23 Duclert-Savatier, N., Poggi, L., Miclet, E., Lopes, P., Ouazzani, J., Chevalier, N., Nilges, M., Delarue, M., and Stoven, V. (2009) Insights into the enzymatic mechanism of 6-phosphogluconolactonase from *Trypanosoma brucei* using structural data and molecular dynamics simulation. *J. Mol. Biol.*, **388**, 1009–1021.

24 Rakitzis, E.T. and Papandreou, P. (1998) Reactivity of 6-phosphogluconolactone with hydroxylamine: the possible involvement of glucose-6-phosphate dehydrogenase in endogenous glycation reactions. *Chem. Biol. Interact.*, **113**, 205–216.

25 Hanau, S., Montin, K., Cervellati, C., Magnani, M., and Dallocchio, F. (2010) 6-phosphogluconate dehydrogenase mechanism evidence for allosteric modulation by substrate. *J. Biol. Chem.*, **285**, 21366–21371.

26 Dardonville, C., Rinaldi, E., Barrett, M.P., Brun, R., Gilbert, I.H., and Hanau, S. (2004) Selective inhibition of *Trypanosoma brucei* 6-phosphogluconate dehydrogenase by high-energy intermediate and transition-state analogues. *J. Med. Chem.*, **47**, 3427–3437.

27 Barrett, M.P. and Gilbert, I.H. (2002) Perspectives for new drugs against trypanosomiasis and leishmaniasis. *Curr. Top. Med. Chem.*, **2**, 471–482.

28 Hanau, S., Rinaldi, E., Dallocchio, F., Gilbert, I.H., Dardonville, C., Adams, M.J., Gover, S., and Barrett, M.P. (2004) 6-phosphogluconate dehydrogenase: a target for drugs in African trypanosomes. *Curr. Med. Chem.*, **11**, 1345–1359.

29 Marchand, M., Kooystra, U., Wierenga, R.K., Lambeir, A.M., Van Beeumen, J., Opperdoes, F.R., and Michels, P.A. (1989) Glucosephosphate isomerase from *Trypanosoma brucei*. Cloning and characterization of the gene and analysis of the enzyme. *Eur. J. Biochem.*, **184**, 455–464.

30 Hanau, S., Rippa, M., Bertelli, M., Dallocchio, F., and Barrett, M.P. (1996) 6-Phosphogluconate dehydrogenase from *Trypanosoma brucei*. Kinetic analysis and inhibition by trypanocidal drugs. *Eur. J. Biochem.*, **240**, 592–599.

31 Sørensen, K.I. and Hove-Jensen, B. (1996) Ribose catabolism of *Escherichia coli*: characterization of the RpiB gene encoding ribose phosphate isomerase B and of the *rpiR* gene, which is involved in regulation of RpiB expression. *J. Bacteriol.*, **178**, 1003–1011.

32 Stern, A.L., Burgos, E., Salmon, L., and Cazzulo, J.J. (2007) Ribose 5-phosphate type B from *Trypanosoma cruzi*: kinetic properties and site-directed mutagenesis reveal information about the reaction mechanism. *Biochem. J.*, **401**, 279–285.

33 Al-Mulla Hummadi, Y.M., Al-Bashir, N.M., and Najim, R.A. (2006) *Leishmania major* and *Leishmania tropica*: II. Effect of an immunomodulator, S(2) complex on the enzymes of the parasites. *Exp. Parasitol.*, **112**, 85–91.

34 Stern, A.L., Naworyta, A., Cazzulo, J.J., and Mowbray, S.L. (2011) Structures of type B ribose 5-phosphate isomerase from *Trypanosoma cruzi* shed light on the determinants of sugar specificity in the structural family. *FEBS J.*, **278**, 793–808.

35 Huck, J.H., Verhoeven, N.M., Struys, E.A., Salomons, G.S., Jakobs, C., and van der Knaap, M.S. (2004) Ribose-5-phosphate isomerase deficiency: new inborn error in the pentose phosphate pathway associated with a slowly progressive leukoencephalopathy. *Am. J. Hum. Genet.*, **74**, 745–751.

36 Zhang, R.G., Andersson, C.E., Skarina, T., Evdokimova, E., Edwards, A.M., Joachimiak, A., Savchenko, A., and Mowbray, S.L. (2003) The 2.2 A resolution structure of RpiB/AlsB from *Escherichia coli* illustrates a new approach to the ribose-5-phosphate isomerase reaction. *J. Mol. Biol.*, **332**, 1083–1094.

37 Opperdoes, F.R. and Coombs, G.H. (2007) Metabolism of *Leishmania*: proven and predicted. *Trends Parasitol.*, **23**, 149–158.

38 Igoillo-Esteve, M., Maugeri, D., Stern, A.L., Beluardi, P., and Cazzulo, J.J. (2007) The pentose phosphate pathway in *Trypanosoma cruzi*: a potential target for the chemotherapy of Chagas disease. *An. Acad. Bras. Cienc.*, **79**, 649–663.

39 Perl, A. (2007) The pathogenesis of transaldolase deficiency. *IUBMB Life*, **59**, 365–373.

40 Stoffel, S.A., Alibub, V.P., Hubert, J., Ebikeme, C., Portais, J.C., Bringaud, F., Schweingrubere, M.E., and Barrett, M.P. (2011) Transketolase in *Trypanosoma brucei*. *Mol. Biochem. Parasitol.*, **179**, 1–7.

41 Martin, E., Simon, M.W., Schaefer, F.W., and Mukkada, A.J. (1976) Enzymes of carbohydrate metabolism in four human species of *Leishmania*: a comparative study. *J. Protozool.*, **23**, 600–607.

42 Veitch, N.J., Maugeri, D.A., Cazzulo, J.J., Lindqvist, Y., and Barrett, M.P. (2004) Transketolase from *Leishmania mexicana* has a dual subcellular localisation. *Biochem. J.*, **382**, 759–767.

43 Cohen, P. and Rosemeyer, M.A. (1975) Glucose-6-phosphate dehydrogenase from human erythrocytes. *Methods Enzymol.*, **41**, 208–214.

44 Wang, X.T., Au, S.W., Lam, V.M., and Engel, P.C. (2002) Recombinant human glucose-6-phosphate dehydrogenase. Evidence for a rapid-equilibrium random-order mechanism. *Eur. J. Biochem.*, **269**, 3417–3424.

45 Wrigley, N.G., Heather, J.V., Bonsignore, A., and De Flora, A. (1972) Human erythrocyte glucose 6-phosphate dehydrogenase: electron microscope studies on structure and interconversion of tetramers, dimers and monomers. *J. Mol. Biol.*, **68**, 483–499.

46 Ortíz, C., Larrieux, N., Medeiros, A., Botti, H., Comini, M., and Buschiazzo, A. (2011) Expression, crystallization and preliminary X-ray crystallographic analysis of glucose-6-phosphate dehydrogenase from the human pathogen *Trypanosoma cruzi* in complex

with substrate. *Acta. Crystallogr. F*, **67**, 1457–1461.

47 Delarue, M., Duclert-Savatier, N., Miclet, E., Haouz, A., Giganti, D., Ouazzani, J., Lopez, P., Nilges, M., and Stoven, V. (2007) Three dimensional structure and implications for the catalytic mechanism of 6-phosphogluconolactonase from *Trypanosoma brucei*. *J. Mol. Biol.*, **366**, 868–881.

48 Bauer, H.P., Srihari, T., Jochims, J.C., and Hofer, H.W. (1983) 1.6-phosphogluconolactonase. Purification, properties and activities in various tissues. *Eur. J. Biochem.*, **133**, 163–168.

49 Schofield, P.J. and Sols, A. (1976) Rat liver 6-phosphogluconolactonase: a low K_m enzyme. *Biochem. Biophys. Res. Commun.*, **71**, 1313–1318.

50 Calligari, P.A., Salgado, G.F., Pelupessy, P., Lopes, P., Ouazzani, J., Bodenhausen, G., and Abergel, D. (2012) Insights into internal dynamics of 6-phosphogluconolactonase from *Trypanosoma brucei* studied by nuclear magnetic resonance and molecular dynamics. *Proteins*, **80**, 1196–1210.

51 Barrett, M.P. (1997) The pentose phosphate pathway and parasitic protozoa. *Parasitol. Today*, **13**, 11–16.

52 Igoillo-Esteve, M. and Cazzulo, J.J. (2004) The 6-phosphogluconate dehydrogenase from *Trypanosoma cruzi*: the absence of two inter-subunit salt bridges as a reason for enzyme instability. *Mol. Biochem. Parasitol.*, **133**, 197–207.

53 Pearse, B.M. and Rosemeyer, M.A. (1974) Human 6-phosphogluconate dehydrogenase purification of the erythrocyte enzyme and the influence of ions and NADPH on its activity. *Eur. J. Biochem.*, **42**, 213–223.

54 González, D., Pérez, J.L., Serrano, M.L., Igoillo-Esteve, M., Cazzulo, J.J., Barrett, M. P., Bubis, J., and Mendoza-León, A. (2010) The 6-phosphogluconate dehydrogenase of *Leishmania* (*Leishmania Mexicana*): gene characterisation and protein structure prediction. *J. Mol. Microbiol. Biotechnol.*, **19**, 213–223.

55 Phillips, C., Dohnalek, J., Gover, S., Barrett, M.P., and Adams, M.J. (1998) A 2.8 Å resolution structure of 6-phosphogluconate dehydrogenase from the Protozoan parasite *Trypanosoma brucei*: comparison with the sheep enzyme accounts for differences in activity with coenzyme and substrate analogues. *J. Mol. Biol.*, **282**, 667–681.

56 Adams, M.J., Ellis, G.H., Gover, S., Naylor, C.E., and Phillips, C. (1994) Crystallographic study of coenzyme, coenzyme analogue and substrate binding in 6-phosphogluconate dehydrogenase: implications for NADP specificity and the enzyme mechanism. *Structure*, **2**, 651–668.

57 Bertelli, M., El-Bastawissy, E., Knaggs, M. H., Barrett, M.P., Hanau, S., and Gilbert, I. H. (2001) Selective inhibition of 6-phosphogluconate dehydrogenase from *Trypanosoma brucei*. *J. Comput. Aided Mol. Des.*, **15**, 465–475.

58 Moltmann, E.A. (1972) Aldose–ketose isomerases, in *The Enzymes*, 3rd edn (ed. P.D. Boyer), Academic Press, New York, vol. **6**, pp. 271–354.

59 Mitschke, L., Parthier, C., Schroder-Tittmann, K., Coy, J., Ludtke, S., and Tittmann, K. (2010) The crystal structure of human transketolase and new insights into its mode of action. *J. Biol. Chem.*, **285**, 31559–31570.

60 Cordeiro, A.T. and Thiemann, O.H. (2010) 16-bromoepiandrosterone, an activator of the mammalian immune system, inhibits glucose 6-phosphate dehydrogenase from *Trypanosoma cruzi* and is toxic to these parasites grown in culture. *Bioorg. Med. Chem.*, **18**, 4762–4768.

61 Dos Santos, C.D., Toldo, M.P., and do Prado, J.C. (2005) *Trypanosoma cruzi*: The effects of dehydroepiandrosterone (DHEA) treatment during experimental infection. *Acta Trop.*, **95**, 109–115.

62 Filipin, M., del, V., Caetano, L.C., Brazão, V., Santello, F.H., Toldo, M.P., and do Prado, J. (2010) DHEA and testosterone therapies in *Trypanosoma cruzi*-infected rats are associated with thymic changes. *Res. Vet. Sc.*, **89**, 98–103.

63 Kirsch, M., Talbiersky, P., Polkowska, J., Bastkowski, F., Schaller, T., de Groot, H., Klärner, F.G., and Schrader, T. (2009)

A mechanism of efficient G6PD inhibition by a molecular clip. *Angew. Chem. Int. Ed. Engl.*, **48**, 2886–2890.

64 Pasti, C., Rinaldi, E., Cervellati, C., Dallocchio, F., Hardré, R., Salmon, L., and Hanau, S. (2003) Sugar derivatives as new 6-phosphogluconate dehydrogenase inhibitors selective for the parasite *Trypanosoma brucei*. *Bioorg. Med. Chem.*, **11**, 1207–1214.

65 Dardonville, C., Rinaldi, E., Hanau, S., Barrett, M.P., Brun, R., and Gilbert, I.H. (2003) Synthesis and biological evaluation of substrate-based inhibitors of 6-phosphogluconate dehydrogenase as potential drugs against African trypanosomiasis. *Bioorg. Med. Chem.*, **11**, 3205–3214.

66 Ruda, G.F., Alibu, V.P., Mitsos, C., Bidet, O., Kaiser, M., Brun, R., Barrett, M.P., and Gilbert, I.H. (2007) Synthesis and biological evaluation of phosphate prodrugs of 4-phospho-D-erythronohydroxamic acid, an inhibitor of 6-phosphogluconate dehydrogenase. *Chem. Med. Chem.*, **2**, 1169–1180.

67 Ruda, G.F., Wong, P.E., Alibu, V.P., Norval, S., Read, K.D., Barrett, M.P., and Gilbert, I.H. (2010) Aryl phosphoramidates of 5-phospho erythronohydroxamic acid, a new class of potent trypanocidal compounds. *J. Med. Chem.*, **53**, 6071–6078.

68 Ruda, G.F., Campbell, G., Alibu, V.P., Barrett, M.P., Brenk, R., and Gilbert, I.H. (2010) Virtual fragment screening for novel inhibitors of 6-phosphogluconate dehydrogenase. *Bioorg. Med. Chem.*, **18**, 5056–5062.

69 Hammes, H.P., Du, X., Edelstein, D., Taguchi, T., Matsumura, T., Ju, Q., Lin, J., Bierhaus, A., Nawroth, P., Hannak, D., Neumaier, M., Bergfeld, R., Giardino, I., and Brownlee, M. (2003) Benfotiamine blocks three major pathways of hyperglycemic damage and prevents experimental diabetic retinopathy. *Nat. Med.*, **9**, 294–299.

Expression, crystallization and preliminary X-ray crystallographic analysis of glucose-6-phosphate dehydrogenase from the human pathogen *Trypanosoma cruzi* in complex with substrate.

Cecilia Ortız, Nicole Larrieux, Andrea Medeiros, Horacio Botti, Marcelo Comini and Alejandro Buschiazzo.
Acta Crystallographica Section; Structural Biology and Crystallization Communications. F67, 1457-1461.

3.2 Resumen

Para validar a la G6PDH de *T. cruzi* como blanco de fármacos antichagásicos, es necesario tener un conocimiento profundo de su bioquímica y biología estructural.

Al inicio de esta tesis nos encontramos con el primer obstáculo, no existían datos estructurales reportados para ninguna G6PDH proveniente de un organismo patógeno y la información bioquímica disponible sobre la enzima de *T. cruzi* era muy acotada. En ese momento existía un único trabajo publicado para la forma recombinante de la G6PDH de *T. cruzi*, donde los autores habían conseguido expresar satisfactoriamente tanto una versión truncada (carecía de los 37 primeros residuos del N-terminal) como completa (larga) de la proteína, pero con rendimientos tan bajos que la misma debía ser detectada mediante técnica de *Western blot* (Igoillo-Esteve 2006). Los autores también debieron enfrentar el problema de inactivación de la proteína durante la purificación.

En este sentido nos planteamos como objetivo optimizar la expresión de la forma recombinante de ambas versiones de la proteína de manera tal que nos permitiesen llevar adelante estudios tanto estructurales como bioquímicos con la misma. Para obtener proteína recombinante en cantidad y calidad adecuadas, trabajamos arduamente en la selección de la cepa de expresión y en la optimización de las condiciones de expresión que rindieran altos niveles de proteína activa. El problema de inactivación enzimática fue resuelto utilizando un nuevo sistema buffer y acondicionando manualmente la columna de afinidad por metales utilizada en el primer paso cromatográfico. La inclusión de una segunda cromatografía de exclusión molecular permitió obtener una muestra altamente homogénea. Trabajamos con porcentajes de pureza mayores al 95% y pusimos a punto los protocolos de concentración ya que la misma precipitaba y con el tiempo se oxidaba inespecíficamente dando lugar a formas multiméricas que nos impedían llegar a los ensayos de cristalización con una muestra homogénea.

Dado que se obtuvieron mejores resultados con la forma truncada de la proteína es que con esta forma se realizaron los *screenings* de cristalización para la forma apo y holo, en presencia de G6P o $NADP^+$.

Finalmente obtuvimos cristales de forma y tamaño adecuado para difractar, optimizamos manualmente las condiciones de cristalización en presencia y ausencia de sustratos, empleando estrategias de co-cristalización y siembra de micro-cristales. Los cristales obtenidos fueron enviados al sincrotrón de la Universidad de California Davis y la colecta de datos fue realizada vía remota. De esta colecta de datos se obtuvo la información necesaria para resolver la forma

apo y posteriormente utilizando las fases de la forma apo y la estrategia de reemplazo molecular trabajamos en la resolución del complejo G6PDH-G6P.

Seguimos trabajando en los ensayos de cristalización para obtener cristales en presencia de $NADP^+$ y obtuvimos cristales para el mutante C8SG6PDH en presencia de $NADP^+$, los cristales fueron enviados al sincrotrón de Soleil-Paris, pero la difracción de los mismos no fue exitosa.

A su vez conseguimos cristalizar la forma larga de la proteína, realizamos la colecta en el difractor de rayos x de nuestro instituto y resolvimos su estructura (datos no mostrados). Lamentablemente la región N-terminal no se pudo resolver, ya que los mapas de densidad electrónica presentaron muy baja resolución, evidenciando la naturaleza flexible de esta región, que nos impidió observar las cisteínas N-terminales.

El objetivo principal de este trabajo consistió en obtener material suficiente y de elevada pureza para la generación de cristales de buena calidad que permitirán resolver por primera vez la estructura de la G6PDH proveniente de un organismo patógeno, en nuestro caso particular de *Trypanosoma cruzi*.
Se expresó y purificó la versión N- terminal truncada de la enzima G6PDH de *Trypanosoma cruzi* que carece de los primeros 37 residuos. En solución, la proteína presentó un peso molecular de 260 kDa, lo que es consistente con que la misma presenta una estructura tetramérica (siendo el peso molecular teórico para la forma monomérica de 61 kDa). Con esta proteína en su forma apo o en presencia de G6P se realizaron *screnningsrobóticos* que permitieron identificar condiciones que promovían la formación de cristales. Estas condiciones fueron optimizadas manualmente, testeándose diferentes concentraciones de proteína, aditivos, pH, precipitantes y fuerza iónica. También se realizó la siembra de microcristales con el objetivo de mejorar la calidad y el tamaño de los cristales. Para la colecta de datos se seleccionaron condiciones óptimas de crioprotección y se realizó la colecta de datos remota, obteniéndose grupos de datos de difracción que se correspondieron con resoluciones atómicas de 2,85 Å y 3,35 Å para la forma apo y en complejo con G6P, respectivamente. La estructura tridimensional de la proteína cristalizada en ambas condiciones se resolvió de manera preliminar empleando la estrategia de reemplazo molecular utilizando como modelo el monómero de la estructura de la G6PDH humana (PDB: 1QKI, cadena A) para la forma apo, mientras que para la resolución de la forma holo se emplearon además los datos de fases y mapas diferenciales de densidad electrónica de Fourier obtenidos para la forma apo de esta enzima. Se observaron cristales isomorfos que presentaron un grupo de espacio P21 con 4 o 5 moléculas por unidad asimétrica y mostraron

simetría no cristalográfica. Los mapas de función de auto-rotación fueron consistentes con el grupo 222, donde se identificaron tres ejes ortogonales de simetría no cristalográfica (SNC), lo que evidencia una conformación tetramérica organizada como dímero de dímeros. El pico 1 de SNC se corresponde al eje de simetría del dímero, que implica el dímero de dímeros, donde la interface inter-monómeros del dímero muestra mayor número de interacciones proteína-proteína en comparación con los picos observados para los contactos entre dímeros. Mientras que los picos 2 y 3 corresponden a los ejes que relacionan un monómero con el otro y entre dímeros, respectivamente.

Para el complejo enzima-sustrato, la densidad electrónica para la G6P fue buena y confirmó la presencia del sustrato en todas las subunidades del tetrámero, esta información nos permitirá, una vez resuelta y refinada la estructura, analizar los cambios producidos en la simetría interna del cristal en presencia o ausencia de sustrato.

Finalmente, se depositaron las estructuras cristalográficas resueltas tanto para la proteína en su forma apo como en presencia de ligando, en la base de datos PDB: 4E9I y 4EM5, respectivamente.

Mis contribuciones:

Optimización de la expresión y purificación de la versión N- terminal truncada de la enzima G6PDH de *Trypanosoma cruzi*.

Screening inicial de condiciones de cristalización, optimización manual de las mismas y posterior búsqueda de condiciones de crio-protección.

Participación en la resolución de la estructura en presencia de sustrato

Escritura del artículo.

Acta Crystallographica Section F
Structural Biology and Crystallization Communications
ISSN 1744-3091

Cecilia Ortíz,[a] Nicole Larrieux,[b] Andrea Medeiros,[a,c] Horacio Botti,[b] Marcelo Comini[a]* and Alejandro Buschiazzo[b,d]*

[a]Redox Biology of Trypanosomes Laboratory, Institut Pasteur de Montevideo, Mataojo 2020, 11400 Montevideo, Uruguay, [b]Unit of Protein Crystallography, Institut Pasteur de Montevideo, Mataojo 2020, 11400 Montevideo, Uruguay, [c]Biochemistry Department, Universidad de la República, Avenida General Flores 2125, 11800 Montevideo, Uruguay, and [d]Department of Structural Biology and Chemistry, Institut Pasteur, 25 Rue du Dr Roux, 75015 Paris, France

Correspondence e-mail: mcomini@pasteur.edu.uy, alebus@pasteur.edu.uy

Received 26 July 2011
Accepted 16 September 2011

© 2011 International Union of Crystallography
All rights reserved

Expression, crystallization and preliminary X-ray crystallographic analysis of glucose-6-phosphate dehydrogenase from the human pathogen *Trypanosoma cruzi* in complex with substrate

An N-terminally truncated version of the enzyme glucose-6-phosphate dehydrogenase from *Trypanosoma cruzi* lacking the first 37 residues was crystallized both in its apo form and in a binary complex with glucose 6-phosphate. The crystals both belonged to space group $P2_1$ and diffracted to 2.85 and 3.35 Å resolution, respectively. Self-rotation function maps were consistent with point group 222. The structure was solved by molecular replacement, confirming a tetrameric quaternary structure.

1. Introduction

The protozoan organisms of the family Trypanosomatidae encompass parasitic species that cause highly disabling and fatal diseases in humans and animals. *Trypanosoma cruzi* is a human pathogen that is responsible for Chagas disease, which has a prevalence of approximately 12–16 million cases in Latin America (Dias, 2009). New therapeutic approaches are urgently needed, given that the available treatments rely on drugs with severe side effects and typically low efficacy in the chronic stage of the disease. In this scenario, the identification and detailed characterization of essential biomolecules for the survival and/or virulence of the parasites, particularly those that are substantially different or even absent in the mammalian host, may contribute to improving the current situation. Several enzymes of the trypanosomatid pentose-phosphate pathway (PPP) have received increasing attention owing to their potential as drug targets (Igoillo-Esteve *et al.*, 2007). The first branch of the PPP involves the stepwise oxidation of glucose 6-phosphate (G6P) to ribulose 5-phosphate, with the concomitant generation of two NADPH molecules. The first reaction

$$\mathrm{NADP^+ + G6P \rightarrow 6\text{-phosphogluconolactone + NADPH}}$$

is catalyzed by glucose-6-phosphate dehydrogenase (G6PDH). The reducing power resulting from this reaction fuels anabolic pathways (lipid and nucleotide biosyntheses) and contributes to cellular redox homeostasis. In *T. cruzi*, G6PDH is encoded by three different sequences that share >97% amino-acid identity (Igoillo-Esteve & Cazzulo, 2006). Levels of G6PDH have been reported to be elevated in virulent strains and infective stages of the parasite, as well as in response to oxidative insult (Mancilla & Naquira, 1964; Igoillo-Esteve & Cazzulo, 2006; Mielniczki-Pereira *et al.*, 2007). This led to consideration of the enzyme as a virulence factor that plays an important role within the antioxidant defence systems of the parasite (Igoillo-Esteve & Cazzulo, 2006). More recently, the orthologue from *T. brucei brucei* (the causative agent of the cattle disease nagana) has been shown to be essential for the growth of infective parasites (Cordeiro *et al.*, 2009). Despite the high conservation of catalytic residues and substrate-binding motifs between the *T. cruzi* and human enzymes, they display only 46% overall amino-acid identity (Fig. 1). A detailed atomic study of the parasite protein is deemed to be essential to reveal regions that might be targets for selective inhibition. Although the three-dimensional structures of several PPP enzymes from trypanosomatids have been elucidated (Phillips *et al.*, 1998; Veitch *et al.*, 2004; Delarue *et al.*, 2007), to date no structural information is available for G6PDH from a protist. With the final aim of performing a thorough structural characterization of *T. cruzi*

G6PDH, we report the heterologous expression, crystallization and X-ray diffraction data collection of an N-terminally truncated form of G6PDH from *T. cruzi*, which retains full catalytic activity, in both apo and G6P-bound forms.

2. Materials and methods

2.1. Expression and purification of His-tagged Δ37N G6PDH from *T. cruzi*

All of the chemicals and reagents used were of analytical grade and were purchased from Sigma unless stated otherwise. Attempts to obtain the recombinant full-length form of *T. cruzi* G6PDH (accession No. Q4E0B2) from vector pET28a (Igoillo-Esteve & Cazzulo, 2006) resulted in low yields and unstable enzyme, precluding its use in crystallization screening. Instead, a truncated form of TcG6PDH lacking the first 37 amino acids (TcG6PDHΔ37N; referred to in the following as Δ37N; Fig. 1) but displaying enzyme activity and kinetic parameters similar to those of the full-length form (Igoillo-Esteve & Cazzulo, 2006) was selected. In addition, Δ37N retains 94% of the overall sequence and overlaps the full length of the human enzyme, making it a suitable model for future structural studies (Fig. 1). Δ37N was expressed as an N-terminally 6×His-tagged protein using vector pET28a (the expression construct was a kind gift from Professor Cazzulo, Universidad de San Martín, Argentina; Igoillo-Esteve & Cazzulo, 2006) and *Escherichia coli* Tuner DE3 as a heterologous expression host. The transformed bacteria were grown in Terrific Broth medium with 10 g l^{-1} glucose and 50 mg l^{-1} kanamycin at 310 K and 200 rev min^{-1} agitation. When the optical density at 600 nm reached 0.8, the cultures were incubated at 277 K without shaking. After 30 min, 0.5 m*M* isopropyl *β*-D-1-thiogalactopyranoside (Euromedex) was added to induce recombinant protein expression and growth of the culture was immediately resumed at 298 K and 180 rev min^{-1} for ∼16 h. The cells were harvested by centrifugation at 5000*g* for 10 min at 277 K. The pellets were suspended at a ratio of 1 g wet weight per 5 ml cold buffer *A* (50 m*M* Tris pH 8.0, 500 m*M* NaCl, 5 m*M* $MgCl_2$) with 0.3 g l^{-1} lysozyme, 150 n*M* pepstatin, 4 n*M* cystatin, 1 m*M* phenylmethanesulfonylfluoride and then incubated on ice for 60 min. Complete cell lysis was achieved by three cycles of sonication (30 pulses per minute at 55% power) using a microtip and a Digital Sonifier 450 (Branson). The cell lysate was centrifuged at 12 000*g* (15 min, 277 K) and the supernatant was further cleared of debris by centrifugation at 18 000*g* (45 min, 277 K) and filtration through a 0.7 µm cellulose acetate/cellulose nitrate mixed-ester filter (Sigma). This sample was applied onto a 1 ml HisTrap column (GE Healthcare) pre-equilibrated in buffer *A*. The column was washed with 20 ml buffer *A* followed by 20 ml buffer *A* containing 80 m*M* imidazole and the protein was eluted with buffer *A* containing 500 m*M* imidazole. The purification was performed at 277 K using a flow rate of 1.0 ml min^{-1}. The elution fractions containing active enzyme (see below) were pooled, concentrated by centrifugation on an Amicon Ultra-15 30K NMWL filter (Millipore; 4000*g*, 277 K) and purified by gel-filtration chromatography on Superdex G200 (Tricorn 10/300 column, GE Healthcare) equilibrated in buffer *A*. The chromatography was performed at room temperature using an ÄKTA-purifier system (GE Healthcare) and a flow rate of 0.5–0.7 ml min^{-1}. Elution samples showing the highest purity of Δ37N, as assessed by Coomassie Blue-stained SDS–PAGE gels, were pooled, tested for enzyme specific activity and stored at 277 K until further use. The enzyme activity was measured spectrophotometrically at 340 nm and 298 K in 50 m*M* Tris pH 7.5, 5 m*M* $MgCl_2$ buffer using 500 µ*M* NADP and 1 m*M* glucose 6-phosphate (G6P). The protein concentration was determined using the bicinchoninic acid assay (Sigma). The final yield of pure recombinant protein was estimated to be ∼1.7 mg per litre of culture medium.

2.2. Crystallization

Prior to crystallization, buffer-exchange of purified Δ37N was performed using an Amicon Ultra-15 30K NMWL filter (Millipore). Briefly, 0.5 ml protein solution was diluted to 5 ml with 20 m*M* Tris–HCl pH 8.0 and reconcentrated three times by centrifugation at 4000*g* and 277 K. To obtain sample containing substrate, the final concentration step was performed in the presence of 20 m*M* Tris–HCl pH 8.0 supplemented with 5 m*M* G6P. The proteins were concentrated by centrifugation (15 000*g* and 277 K) with a 10 kDa cutoff IVSS Vivaspin 500 filter device (Sigma). Initial crystallization screenings were performed by the sitting-drop vapour-diffusion method with Crystal Screen and Crystal Screen 2 (Hampton Research) using a robotic pipetting station (Honeybee 963, Digilab). Drops consisting

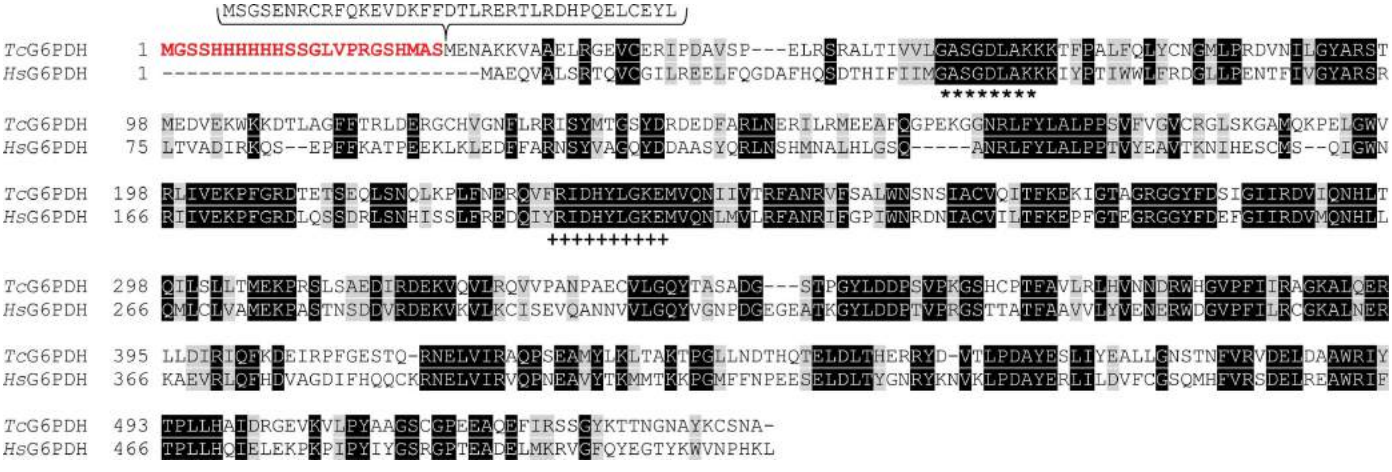

Figure 1
Amino-acid sequence of the G6PDH from *T. cruzi* (*Tc*G6PDH, accession No. Q4E0B2) used for crystallization. The N-terminal extension, which is absent in the truncated mutant Δ37N, is shown as an insertion fragment at the top of the figure. The N-terminal stretch incorporated as a fusion from the expression vector is indicated in bold red. Identical residues with respect to the human enzyme (accession No. P11413) are shown on a black background, while conservative substitutions are highlighted with a grey background. The cofactor-binding and substrate-binding sites are indicated by asterisks and crosses, respectively.

Table 1
Data-collection statistics for Δ37N G6PDH.

Values in parentheses are for the highest resolution shell.

	Apoprotein	G6P–protein complex
No. of crystals	1	1
Crystal dimensions (μm)	50 × 50 × 200	50 × 50 × 100
Beamline	ALS 5.0.2	ALS 5.0.2
Wavelength (Å)	1.00	1.00
Detector	ADSC Quantum 315	ADSC Quantum 315
Crystal-to-detector distance (mm)	390	385
Rotation range per image (°)	0.5	0.5
Total rotation range (°)	170.5	167.5
Exposure time per image (s)	0.5	0.5
Resolution range (Å)	30.00–2.85 (3.00–2.85)	67.36–3.35 (3.53–3.35)
Space group	$P2_1$	$P2_1$
Unit-cell parameters (Å, °)	a = 96.6, b = 133.0, c = 107.8, β = 100.1	a = 96.8, b = 133.0, c = 107.7, β = 100.3
Mosaicity (°)	0.94	0.88
Measured reflections	214946	134881
Unique reflections	62028	38508
Multiplicity	3.5 (3.4)	3.5 (3.6)
Mean $I/\sigma(I)$	7.1 (2.3)	5.5 (2.9)
Completeness (%)	99.1 (99.2)	99.5 (99.9)
$R_{\rm merge}$† (%)	0.138 (0.501)	0.209 (0.450)
$R_{\rm meas}$† (%)	0.163 (0.594)	0.246 (0.530)
Matthews coefficient‡ (Å^3 Da^{-1})	2.79	2.80
Solvent content‡ (%)	56.0	56.1

† $R_{\rm merge} = \sum_{hkl}\sum_i |I_i(hkl) - \langle I(hkl)\rangle| / \sum_{hkl}\sum_i I_i(hkl)$ and $R_{\rm meas} = \sum_{hkl}[N/(N-1)]^{1/2} \times \sum_i |I_i(hkl) - \langle I(hkl)\rangle| / \sum_{hkl}\sum_i I_i(hkl)$, where $\langle I(hkl)\rangle$ is the average of symmetry-related (or Friedel-related) observations of a unique reflection. ‡ These figures correspond to the inclusion of four molecules in the asymmetric unit. In principle, a Matthews coefficient of 2.24 Å^3 Da^{-1} (45% solvent) would be compatible with five protomers. Structure determination confirmed that a tetramer is the correct choice (see text).

of 0.4 μl protein solution mixed with 0.4 μl reservoir solution were dispensed into the wells of a CrystalQuick 96-well plate (plate model No. 609820, Greiner) containing 90 μl reservoir solution. After 4 d, crystals developed under Crystal Screen condition No. 39. Crystallization conditions were optimized manually using a hanging-drop vapour-diffusion setup, testing the following variables: protein and precipitant concentration, pH, additives and seeding. Optimal crystallization of the apo form (20 mg ml^{-1}) was achieved in the presence of 6% PEG 400, 1.6 *M* ammonium sulfate, 0.1 *M* Na HEPES pH 7.5. In the presence of 5 m*M* G6P, the crystallization conditions were adjusted to 33 mg ml^{-1} protein, 4% PEG 400, 1.8 *M* ammonium sulfate, 0.1 *M* Na HEPES pH 7.5. Optimizations were carried out using 4 μl drops (2 μl protein with or without substrate plus 2 μl reservoir solution) in VDX 24-well crystallization plates (Hampton Research) filled with 1 ml reservoir solution per well. All crystallization assays were performed at 293 K.

2.3. X-ray diffraction data collection and processing and structure determination

The crystals were mounted in nylon loops of 0.1–0.3 μm and flash-cooled in liquid nitrogen after addition of 22%(*v*/*v*) glycerol to the mother liquor. In the case of the G6P complex the PEG 400 concentration was raised to 6% during cryopreservation. Data collection was performed remotely using the robotic facilities at beamline 5.0.2 of the Advanced Light Source synchrotron (Lawrence Berkeley National Laboratory). Diffraction data were indexed and integrated with *MOSFLM* v.7.0.7/*iMOSFLM* v.1.0.5 (Battye *et al.*, 2011) and then scaled and reduced with *SCALA*/*TRUNCATE* within the *CCP*4 suite (Winn *et al.*, 2011; see Table 1 for full statistics). A monomer of human G6PDH (PDB entry 1qki) was used as a search probe for molecular replacement with the program *AMoRe* (Navaza, 1994).

3. Results and discussion

A truncated mutant of *T. cruzi* G6PDH lacking the nonconserved N-terminal end (the first 37 residues), which had previously been subjected to biochemical characterization (Igoillo-Esteve & Cazzulo, 2006), was expressed in a soluble form in *E. coli* and purified to homogeneity using immobilized metal-affinity and size-exclusion chromatography. The active enzyme displayed a molecular weight of ∼260 kDa in solution, which is consistent with the protein being a tetramer (protomer molecular weight of 61 kDa; Fig. 2). Screening of 96 crystallogenesis conditions using recombinant protein alone or attempting cocrystallization in complex with the substrate G6P yielded positive hits that were further optimized. Crystallization was manually optimized using the hanging-drop vapour-diffusion method. X-ray diffraction analysis was performed on Δ37N single crystals, which grew in a few days under the following conditions: (i) 6% PEG 400, 1.6 *M* ammonium sulfate, 0.1 *M* Na HEPES pH 7.50 and (ii) 4% PEG 400, 1.8 *M* ammonium sulfate, 0.1 *M* Na HEPES pH 7.5, 5 m*M* G6P (Fig. 3). Data sets for these crystals were collected to 2.85 and 3.35 Å resolution, respectively, using synchrotron radiation (Fig. 4*a*). The crystals both belonged to space group $P2_1$; they proved to be isomorphous and appeared to contain four or five molecules in the asymmetric unit (Table 1). A self-rotation function (SRF) was calculated using the scaled amplitudes (Fig. 4*b*), allowing the identification of three orthogonal twofold noncrystallographic (NCS) axes, compatible with a tetramer possessing 222 (*D*2) point-group symmetry. The NCS dyad located at $(\theta, \varphi, \chi) = (54, 180, 180°)$ in polar coordinates (peak 1 in Fig. 4*b*) is stronger than the other two peaks, probably because it is perpendicular to the unique crystallographic axis, which doubles the number of Patterson vectors contributing to the peak. The two weaker peaks (peaks 2 and 3) are both orthogonal to the first peak. None of the three NCS axes are parallel to the monoclinic dyad, which is consistent with the absence of peaks on the

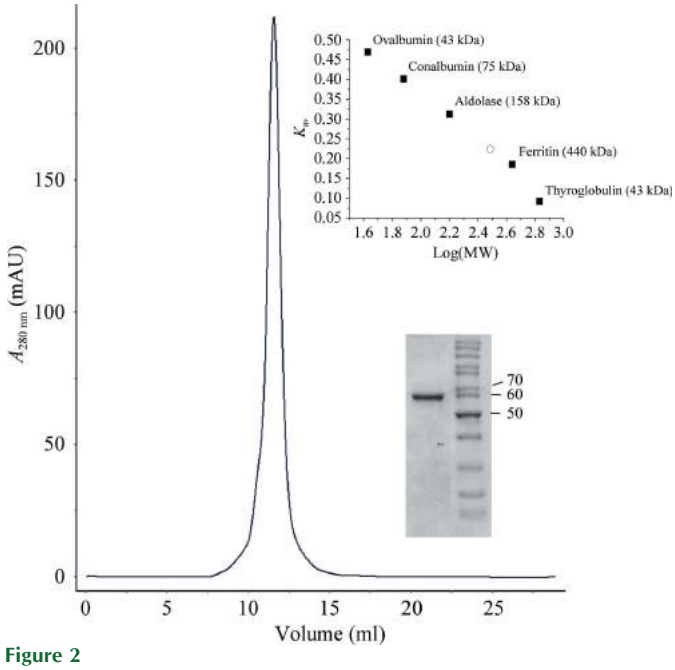

Figure 2
Purification and oligomeric state analysis of *T. cruzi* Δ37N G6PDH. Isocratic elution chromatogram of the recombinant protein separated by size-exclusion chromatography (SEC) on a Superdex G200 column. Bottom inset, 12% SDS–PAGE of the SEC peak fraction stained with Coomassie Blue; the right lane contains molecular-weight markers labelled in kDa. Top inset, plot employed to determine the apparent molecular mass of Δ37N (filled squares, molecular-weight standards; circle, recombinant TcG6PDHΔ37N).

v = 0.5 section of the native Patterson map. There is nevertheless a non-origin peak in these Patterson maps (u = 0.13, v = 0, w = 0.13) displaying ∼20% of the origin peak signal. Typically, such a peak may reveal pseudo-translational symmetry, *e.g.* derived from near-perfect alignment of different protomers in the asymmetric unit. However, in this case it is very likely to be the consequence of a crystal-packing defect (see below), with no simple interpretation, and to be related in some way to the almost continuous streak of twofold peaks that connect NCS peak 1 with the crystallographic y-axis poles in the SRF section (Fig. 4*b*). Different crystals showed variable heights of these streaking peaks, which sometimes even became undetectable over the noise. The crystals that we report here represent the best crystals in terms of the resolution limit and were hence selected for further work. In order to confirm the preliminary analyses, we solved the structures by molecular replacement (Navaza, 1994), initially using the apo data set with one monomer of the human orthologue (PDB entry 1qki, chain *A*) as the search probe (the solution of the isomorphous G6P complex data set was straightforward starting from the apo crystal phases and difference Fourier electron-density maps). Although refinements are still in progress, with an $R_{\rm free}$ of ∼25% we can already safely confirm the space-group assignment, the presence of four monomers in the asymmetric unit and the correctness of the essential features of the SRF analysis presented above. In particular, NCS peak 1 corresponds to the axis that relates one dimer to the

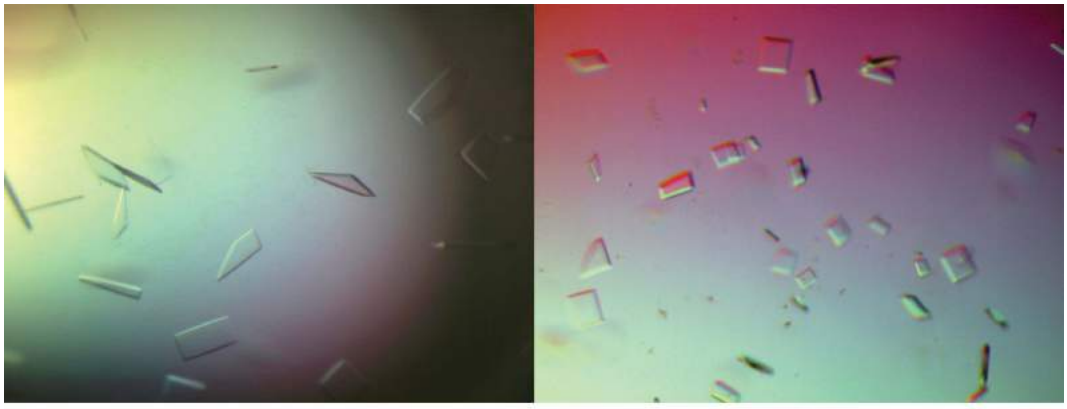

Figure 3
Crystals of *T. cruzi* Δ37N G6PDH: (*a*) apo form, (*b*) cocrystallized in the presence of G6P.

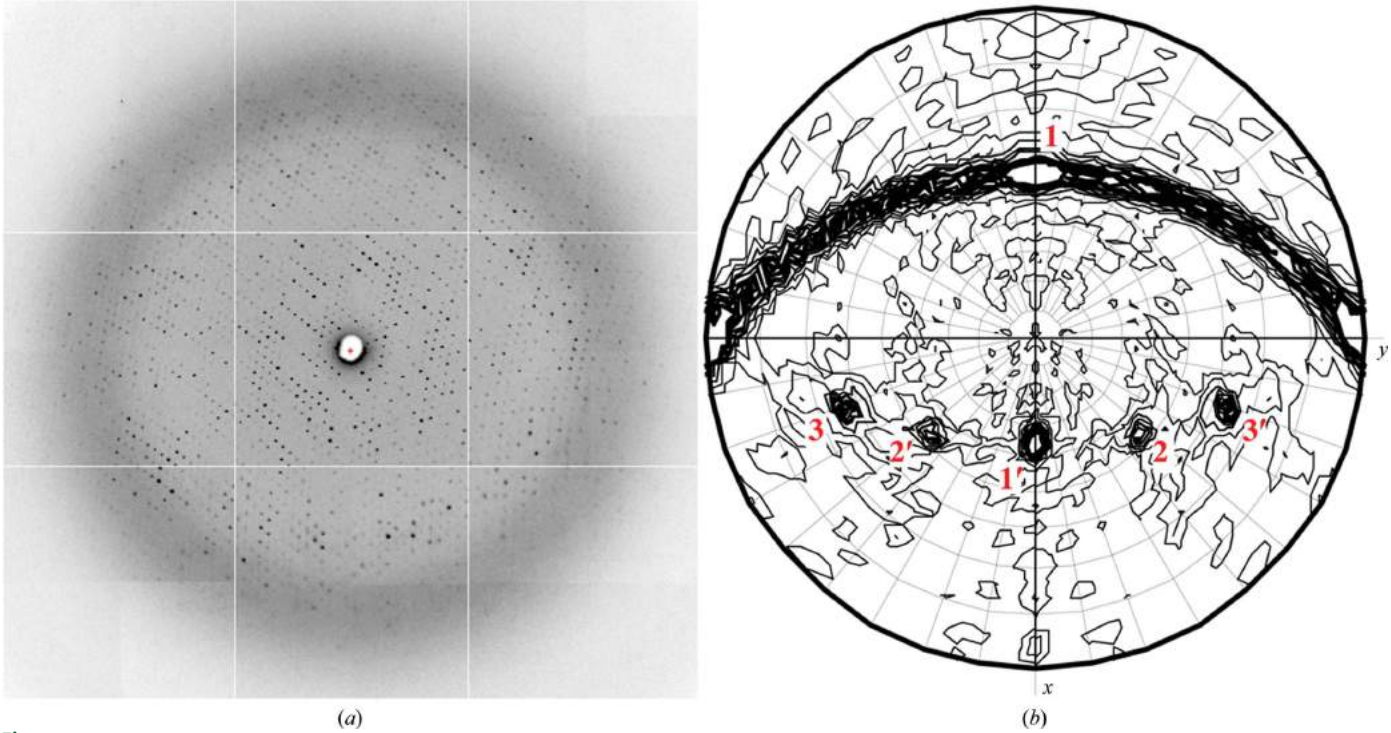

Figure 4
X-ray diffraction of *T. cruzi* Δ37N G6PDH apo-form crystals. (*a*) A typical frame picked out from the data set, showing diffraction to 2.85 Å resolution. (*b*) χ = 180° section of the self-rotation function calculated with observed structure-factor amplitudes using *MOLREP* (Vagin & Teplyakov, 2010). The unique crystallographic axis is parallel to y [$I/\sigma(I)$ = 31.8]. The major [$I/\sigma(I)$ = 26.9] noncrystallographic symmetry (NCS) twofold axis [marked as peak 1 in the stereographic projection, polar coordinates (53.8, 180, 180°)], corresponds to the proper 180° rotation that relates one dimer to the other in the asymmetric unit. This axis is orthogonal to the crystallographic axis, as well as to the weaker NCS dyads marked as peaks 2 [(47.2, 47.3, 180°), $I/\sigma(I)$ = 7.7] and 3 [(64.1, 290.7, 180°), $I/\sigma(I)$ = 7.5] which relate one monomer to the other within each dimer and to the non-equivalent monomer of the other dimer, respectively. 1′, 2′ and 3′ correspond to the symmetrically equivalent NCS axes. Note the streak of twofold peaks observed connecting 1 to the y-axis poles.

other, with an architecture that is similar overall to that seen in the human 'dimer of dimers' tetramer (Au *et al.*, 2000), in which each dimer has much larger inter-monomeric protein–protein interactions compared with the fewer contacts between dimers. NCS peaks 2 and 3 correspond to the axes relating one monomer to the other within and between dimers, respectively. Recomputation of the SRF with the calculated amplitudes results in clearer sections (no signals from the streak of NCS dyads) and elimination of the non-origin peak in the native Patterson maps.

Clear electron density for bound glucose 6-phosphate in the second crystal constitutes further strong evidence in support of the determined structure solution. Full refinement of the structures reported here will ultimately allow full analysis of the quaternary-structure features and the potential effects of bound ligands in terms of internal symmetry.

The Unit of Recombinant Proteins at the Institut Pasteur de Montevideo is acknowledged for their production and purification facilities. Dr Felipe Trajtenberg (Unit of Protein Crystallography, Institut Pasteur de Montevideo) and Dr Peter Zwart (Berkeley Center for Structural Biology, LBNL, Berkeley, USA) are gratefully acknowledged for their assistance during data collection. We would like to thank Jorge Navaza and one of the manuscript reviewers for useful discussions in the analyses of the self-rotation functions and Patterson maps. This work was supported by Agencia Nacional de Investigación e Innovación (Innova Uruguay, Agreement No. DCI–ALA/2007/19.040 between Uruguay and the European Commission) and CeBEM (Centro de Biologia Estructural del Mercosur).

References

Au, S. W., Gover, S., Lam, V. M. & Adams, M. J. (2000). *Structure*, **8**, 293–303.
Battye, T. G. G., Kontogiannis, L., Johnson, O., Powell, H. R. & Leslie, A. G. W. (2011). *Acta Cryst.* D**67**, 271–281.
Cordeiro, A. T., Thiemann, O. H. & Michels, P. A. (2009). *Bioorg. Med. Chem.* **17**, 2483–2489.
Delarue, M., Duclert-Savatier, N., Miclet, E., Haouz, A., Giganti, D., Ouazzani, J., Lopez, P., Nilges, M. & Stoven, V. (2007). *J. Mol. Biol.* **366**, 868–881.
Dias, J. C. P. (2009). *Mem. Inst. Oswaldo Cruz*, **104**, Suppl. 1, 41–45.
Igoillo-Esteve, M. & Cazzulo, J. J. (2006). *Mol. Biochem. Parasitol.* **149**, 170–181.
Igoillo-Esteve, M., Maugeri, D., Stern, A. L., Beluardi, P. & Cazzulo, J. J. (2007). *Ann. Acad. Bras. Cienc.* **79**, 649–663.
Mancilla, R. & Naquira, C. (1964). *J. Protozool.* **11**, 509–513.
Mielniczki-Pereira, A. A., Chiavegatto, C. M., López, J. A., Colli, W., Alves, M. J. & Gadelha, F. R. (2007). *Acta Trop.* **101**, 54–60.
Navaza, J. (1994). *Acta Cryst.* A**50**, 157–163.
Phillips, C., Dohnalek, J., Gover, S., Barrett, M. P. & Adams, M. J. (1998). *J. Mol. Biol.* **282**, 667–681.
Vagin, A. & Teplyakov, A. (2010). *Acta Cryst.* D**66**, 22–25.
Veitch, N. J., Maugeri, D. A., Cazzulo, J. J., Lindqvist, Y. & Barrett, M. P. (2004). *Biochem. J.* **382**, 759–767.
Winn, M. D. *et al.* (2011). *Acta Cryst.* D**67**, 235–242.

Binding mode and selectivity of steroids towards glucose-6-phosphate dehydrogenase from the pathogen *Trypanosoma cruzi.*

Cecilia Ortiz, Francesca Moraca, Andrea Medeiros, Maurizio Botta, Niall Hamilton and Marcelo A. Comini.
Molecules, 2016. V. 21, p 368-381

3.3 Resumen

Distintos derivados de compuestos conteniendo el núcleo estructural del androsteno han sido reportados como inhibidores acompetitivos de la G6PDH. El sitio de unión de estos compuestos a la G6PDH es desconocido, aunque una aproximación al mismo fue provista por un estudio *in silico* realizado tomando como modelo a la G6PDH humana. Sin embargo, el modelo de unión propuesto por estos investigadores no es compatible con el mecanismo de inhibición enzimático, ya que los esteroides ocuparían parcialmente el sito de unión a $NADP^+$.
Por otro lado, el diseño racional de fármacos especie-específicos contra G6PDH, requiere del conocimiento de la forma en que el inhibidor interactúa con la enzima, incluyendo esto en lo posible, detalles moleculares precisos de las regiones y residuos que participan en la interacción proteína-ligando.

Motivados entonces por la necesidad imperiosa de identificar el sitio de unión de compuestos esteroides a la TcG6PDH y de análogos que presenten selectividad contra esta enzima, así como también de resolver la discrepancia planteada arriba para la enzima humana, es que en este estudio nos propusimos investigar dichos interrogantes.

En este sentido trabajamos en la obtención de cristales de la TcG6PDH en complejo con los inhibidores. Visto que los esfuerzos puestos en la optimización de cristales de TcG6PD en complejo con inhibidor con buena difracción no fueron satisfactorios, debimos dar por culminada esa actividad. Lo que nos condujo al empleo de técnicas de dinámica molecular y *docking* que explotan los datos cristalográficos que nuestro grupo obtuvo para esta enzima (PDB 4EM5). De manera complementaria, se llevaron a cabo estudios de caracterización bioquímica (ensayos cinéticos) para mutantes puntuales de la enzima y de relación estructura-actividad para diferentes análogos de epiandrosterona. Esto tuvo como finalidad validar los modelos de unión ligando-proteína obtenidos *in silico*.

Los estudios de dinámica molecular y *docking* fueron realizados en colaboración con el Dr. Maurizio Botta y la Dra. Francesca Moracca de la Universidad de Siena, Italia, mientras que el Dr. Niall Hamilton (Universidad de Manchester, Inglaterra) nos facilitó varios derivados de la epiandrosterona para los estudios de inhibición.

Los modelos de unión esteroide-TcG6PDH obtenidos *in silico* para las diferentes moléculas que fueron objeto de estudio fueron totalmente compatibles con el modo de inhibición acompetitivo y con los datos obtenidos en los ensayos bioquímicos. Por primera vez se reportó un modelo de unión de esteroides a G6PDH, el cual presenta gran potencial para investigar otras familias de

inhibidores acompetitivos de la TcG6PDH para los cuales se ha reportado que compiten con la unión de epiandrosterona a la enzima. Nuestro estudio también permitió entender las bases moleculares de la gran potencia y selectividad mostrada por la 16-Br epiandrosterona contra TcG6PDH, así como identificar nuevos derivados con selectividad contra la proteína del parásito.

La obtención de la estructura molecular de la G6PDH de *T. cruzi* en presencia de G6P y en su forma apo, nos permitió realizar estudios de dinámica molecular y *docking* con epiandrosterona (EA) y derivados. Los mismos revelaron que EA se une a un bolsillo molecular próximo al sitio activo de la enzima, y que esta unión no afecta la unión de G6P ni de $NADP^+$ pero si interfiriere estéricamente con la interacción entre ambos sustratos a nivel del sitio catalítico, impidiendo de esta manera que se produzca la catálisis. Según lo observado, el anillo de 5 carbonos de la EA estaría desestabilizando e impidiendo que el $NADP^+$ se oriente adecuadamente para recibir el hidrogenión de la G6P. Dichos resultados fueron validados con la generación de mutantes puntuales para los residuos L80, K83 y K84, los cuales, según las predicciones *in silico*, participarían dinámicamente en la estabilización de la hélice-1 de la enzima, la cual es importante para dar forma al sitio catalítico y orientar correctamente a la G6P.

Asimismo, se evaluó la relación actividad-estructura de algunos análogos de EA, generándose modelos de *docking* que permitieron identificar sustituciones en posiciones claves para la inhibición selectiva de la enzima del patógeno respecto a la homóloga humana. Se observó que las sustituciones por grupos polares y voluminosos en la posición 3 de EA mejoran la inhibición selectiva de TcG6PDH. También se pudo determinar que la inclusión de un átomo de bromo en la posición 16 mejora significativamente la selectividad y actividad inhibitoria del compuesto contra la enzima de *T. cruzi*, incrementándola 65 veces con respecto a su contraparte humana. Esto se explica por una unión más fuerte del inhibidor al sitio activo de la enzima a través de un enlace halógeno con el átomo de Br. Por otro lado confirmamos que la sustitución con grupos polares en la posición 17 o la presencia del grupo etilurea en la posición 3 disminuyen la afinidad de la enzima del parásito por el compuesto, y por lo tanto la potencia inhbitoria de los mismos. Por el contrario, dichos cambios estuvieron asociados a una mejora significativa en la actividad inhibitoria contra la enzima humana.

En resumen, considerando los resultados obtenidos y los recopilados en la bibliografía para la enzima humana podemos sugerir una unión diferencial para estos derivados esteroideos en la enzima del patógeno y la humana. Según lo observado, serían los residuos secundarios no conservados y que dan forma al sitio activo los responsables de este comportamiento especie-

específico, lo que abre la posibilidad de desarrollar inhibidores más selectivos contra la enzima del patógeno.

Mis contribuciones:

Generación y caracterización de mutantes puntuales
Ensayos cinéticos con inhibidores
Análisis estructural
Escritura del artículo

molecules

MDPI

Article

Binding Mode and Selectivity of Steroids towards Glucose-6-phosphate Dehydrogenase from the Pathogen *Trypanosoma cruzi*

Cecilia Ortiz [1,†], Francesca Moraca [2,3,†], Andrea Medeiros [1,4], Maurizio Botta [2], Niall Hamilton [5] and Marcelo A. Comini [1,*]

1 Redox Biology of Trypanosomes, Institut Pasteur de Montevideo, Mataojo 2020, Montevideo 11400, Uruguay; cortiz@pasteur.edu.uy (C.O.); amedeiros@pasteur.edu.uy (A.M.)
2 Dipartimento di Biotecnologie, Chimica e Farmacia, Università degli Studi di Siena, Via Aldo Moro 2, Siena 53100, Italy; francesca.moraca@gmail.com (F.M.); botta.maurizio@gmail.com (M.B.)
3 Sbarro Institute for Cancer Research and Molecular Medicine, Center for Biotechnology, College of Science and Technology, Temple University, BioLife Science Building, Suite 333, 1900 N 12th Street, Philadelphia, PA 19122, USA
4 Departamento de Bioquímica, Facultad de Medicina, Universidad de la República, Av. Gral. Flores 2125, Montevideo 11800, Uruguay
5 Drug Discovery Unit, Cancer Research, UK Manchester Institute, Wilmslow Road, Manchester M204BX, UK; Niall.Hamilton@cruk.manchester.ac.uk
* Correspondence: mcomini@pasteur.edu.uy; Tel.: +598-2522-09-10
† These authors contributed equally to this work.

Academic Editor: Thomas J. Schmidt
Received: 5 February 2016 ; Accepted: 11 March 2016 ; Published: 17 March 2016

Abstract: Glucose-6-phosphate dehydrogenase (G6PDH) plays a housekeeping role in cell metabolism by generating reducing power (NADPH) and fueling the production of nucleotide precursors (ribose-5-phosphate). Based on its indispensability for pathogenic parasites from the genus *Trypanosoma*, G6PDH is considered a drug target candidate. Several steroid-like scaffolds were previously reported to target the activity of G6PDH. Epiandrosterone (EA) is an uncompetitive inhibitor of trypanosomal G6PDH for which its binding site to the enzyme remains unknown. Molecular simulation studies with the structure of *Trypanosoma cruzi* G6PDH revealed that EA binds in a pocket close to the G6P binding-site and protrudes into the active site blocking the interaction between substrates and hence catalysis. Site directed mutagenesis revealed the important steroid-stabilizing effect of residues (L80, K83 and K84) located on helix α-1 of *T. cruzi* G6PDH. The higher affinity and potency of 16α-Br EA by *T. cruzi* G6PDH is explained by the formation of a halogen bond with the hydrogen from the terminal amide of the NADP+-nicotinamide. At variance with the human enzyme, the inclusion of a 21-hydroxypregnane-20-one moiety to a 3β-substituted steroid is detrimental for *T. cruzi* G6PDH inhibition. The species-specificity of certain steroid derivatives towards the parasite G6PDH and the corresponding biochemically validated binding models disclosed in this work may prove valuable for the development of selective inhibitors against the pathogen's enzyme.

Keywords: epiandrosterone; pentose phosphate pathway; Chagas disease; *Leishmania*; inhibition by steroids; structure activity relationship

1. Introduction

The genera *Trypanosoma* and *Leishmania* encompass parasite species causing severe and, if left untreated, fatal diseases in animals and humans [1]. So far, vaccine development against

trypanosomiasis and leishmaniasis appears unattainable due to the capacity of the parasites to evade the host immune response. Thus, the discovery of new chemotherapeutic approaches remains the most reliable strategy to combat these pathogens [2].

Several studies indicate that the glucose-based metabolism of trypanosomatids offers the possibility for selective pharmacological intervention, because of the biochemical and structural differences of some of its components with their human counterparts [3,4]. Like most organisms, trypanosomatids metabolize glucose via the glycolytic or Embden-Meyerhof pathway, and the pentose phosphate pathway (PPP) [5,6]. The first reaction of the PPP is catalyzed by glucose-6-phosphate dehydrogenase (G6PDH) that oxidizes G6P to 6-phosphogluconolactone with concomitant reduction of $NADP^+$ to NADPH, which fuels several biosynthetic reactions and antioxidant systems. In *T. cruzi*, G6PDH appears to play an important role during infection since its content was significantly higher in the infective stages and its activity was increased about 45-fold in infective trypomastigotes challenged with H_2O_2 [7]. Epigenetic interference with G6PDH expression in the bloodstream form of African trypanosomes demonstrated that the enzyme is essential for parasite survival [8].

The steroids dehydroepiandrosterone (DHEA) and epiandrosterone (EA), first discovered as inhibitors of the human G6PDH [9], were later reported to target the trypanosomal but not the leishmanial enzyme [10]. In agreement with these results, both compounds were cytotoxic towards *T. brucei* and *T. cruzi* but not against *L. mexicana* [8,10,11]. Moreover, African trypanosomes deficient in the endogenous G6PDH but expressing an ectopic copy of *L. mexicana* G6PDH were resistant to EA [11], thus confirming the refractoriness of the leishmanial enzyme to steroids. *In vitro*, G6PDH from *T. brucei* was about 6-fold more sensitive towards inhibition by steroids (Ki value of 1.7 and 0.5 μM for DHEA and EA, respectively) [8] than the *T. cruzi* (Ki value of 2.6–25 μM and 1–5.6 μM for DHEA and EA, respectively) [10,12] and the human homologue (Ki value of 6–9 μM and 3 μM for DHEA and EA) [13]. Recently, a drug screening campaign with a large commercial library of wide chemical diversity led to the identification of new uncompetitive inhibitors of *T. cruzi* G6PDH (*Tc*G6PDH) that belonged to the thienopyrimidine and quinazoline families [12].

In an effort to obtain information about the binding of steroidal inhibitors to G6PDH, Zhao *et al.* performed *in silico* studies with DHEA and derivatives using the structure of human G6PDH with bound G6P as molecular target [14]. The work proposes that H-bonds and non-polar interactions with residues close to the enzyme active site stabilize and orient the inhibitor in the binding site. However, the binding model is not compatible with the uncompetitive inhibition mechanism described for steroids against G6PDH from different species [8,10,13], since the inhibitors partially occupy the nicotinamide nucleotide binding region.

*Tc*G6PDH in its apo- and substrate-bound form has been recently crystallized by our group and the corresponding structures solved (PDB 4E9I and PDB 4EM5, respectively) [15]. Here we exploit the structural information available for *Tc*G6PDH to address the binding mode of steroids to the enzyme. Structural models of steroids bound to *Tc*G6PDH were generated *in silico* and subjected to validation with enzyme point mutants and SAR analysis with different novel steroids [16]. Our study discloses the region and residues of *Tc*G6PDH involved in steroid binding and paves the way for the further challenging design of derivatives targeting selectively the pathogen's enzyme.

2. Results and Discussion

2.1. EA Binding to the T. cruzi G6PDH-G6P-$NADP^+$ Ternary Complex

The crystal structure of apo- (PDB 4E9I) and G6P-bound *Tc*G6PDH (PDB 4EM5) have recently been obtained [15] and a full structural characterization will be reported elsewhere. *Tc*G6PDH is a tetrameric protein with each subunit composed of an N-terminal domain with a typical Rossmann-fold involved in $NADP^+$ binding and a C-terminal domain that contains the G6P binding site and residues engaged in subunit interactions [15]. The catalytic site of G6PDH localizes at the interface between the N- and C-terminal domains and far from regions participating in protein dimerization and tetramerization [17–19].

As a first approach to identify potential binding sites for steroids in *Tc*G6PDH, we have used the Fpocket algorithm that is based on Voronoi tessellation to detect protein cavities geometrically suitable and accessible to ligands [20]. Inspection of the coordinates for G6P-bound *Tc*G6PDH (PDB 4EM5) with Fpocket revealed a total of 21 pockets with seven of them presenting a score >20, indicating that they can be investigated as putative binding sites for inhibitors. Most of these cavities correspond to regions encompassing or close to the substrates binding sites (*i.e.*, pockets 1, 2, 3, 6 and 7; Figure 1).

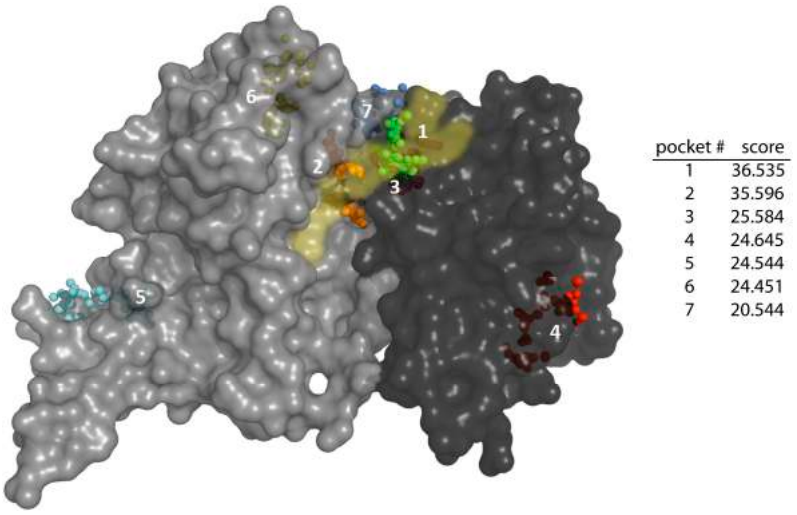

Figure 1. Pocket detection on G6P-*Tc*G6PDH using Fpocket algorithm. Top-7 pockets on the holo-*Tc*G6PDH (PDB 4EM5). *Tc*G6PDH surface representation in grey color (dark and light grey denote the N-terminal and C-terminal protein domains, respectively) with substrates binding sites highlighted in yellow transparent. The alpha sphere centres corresponding to the different cavities are depicted as small colored spheres and the pockets labeled according to their score ranking shown in the table on the right.

Among them, the pockets presenting the highest score localized next to the $NADP^+$ binding site (pocket 1, score = 36.535), between the G6P and $NADP^+$ binding sites (pocket 2, score = 35.596) or within the $NADP^+$ binding site (pocket 3, score = 25.584). In contrast to pockets 2 and 3, and despite its high score, cavity 1 appears more buried in the protein structure and is unlikely to be accessible to the bulky structure of steroids. Nonetheless, ligand binding to any of these sites is expected to influence substrate binding and/or catalysis. Two additional pockets (4 and 5) with relatively good score (score = 24.6) localize in regions far from the active site (Figure 1). Pocket 4 is located on a solvent-exposed area of the Rossmann fold domain, distal from the active site and shaped by residues located in loops from structural elements contributing to $NADP^+$ binding. Pocket 5 is located in a non-structured region of the C-terminal domain that is involved in contacts between protein subunits. Because of the likely dynamic nature of the elements involved in forming pockets 4 and 5, the lack of evidence demonstrating steroids affect $NADP^+$-binding ([8–10,13] and this work) and the oligomeric structure of G6PDH (not shown), these sites were ruled out as potential cavities for EA binding. Instead, the results obtained for the top-three pockets surrounding the catalytic site guided the docking and molecular dynamics studies.

Taking into account that steroids are uncompetitive inhibitors of G6PDH [8–10,13] and such inhibition mechanism implies the binding of the inhibitor to the enzyme-substrate(s) complex, a model of the *Tc*G6PDH ternary complex was first generated. Analysis of the crystal structure of apo- or G6P-bound *Tc*G6PDH shows that non-structured elements from the Rossmann-fold, which are critical for anchoring the adenine-phosphate nucleotide moiety of $NADP^+$, present conformations not compatible with co-substrate binding (Figure S1). Thus, first $NADP^+$ was docked to the structure of *Tc*G6PDH with bound G6P (PDB 4EM5) using the induced fit algorithm of the Schrödinger suite.

Nineteen models were obtained and those showing an orientation of substrates consistent with the catalytic mechanism of G6PDH [21,22] were chosen for further docking of EA and analogues thereof. Docking of EA in the newly generated *Tc*G6PDH/G6P/NADP$^+$ complex has been performed by means of Glide, using the Standard Precision (SP) scoring function [23]. The resulting binding mode of EA, with the steroid occupying a cavity between G6P and NADP$^+$ (*i.e.*, pocket 2 according to Fpocket detection) is consistent with its uncompetitive mode of inhibition. In particular, EA shows an H-bond between its hydroxyl group and R408, being mostly stabilized by hydrophobic contacts with both the protein and G6P. The stability of the *Tc*G6PDH/G6P/NADP$^+$/EA complex was checked by means of 80 ns MD simulation. Surprisingly, during the simulation G6P loses the H-bonds with the two catalytic His residues (H247 and H309) [18,19] and, consequently, is displaced from the catalytic site, which precludes electron exchange between G6P and NADP$^+$.

In the molecular dynamic model, G6P shows H-bonds with R408 (total occupancy = 99.4%), K251 (total occupancy = 60.9%), H247 (total occupancy = 12.2%) and H309 (total occupancy = 0.19%). On the other hand, EA shows H-bonds only with E216 with a significant occupancy over the 80 ns MD simulation (total occupancy = 31.5%). At the end of the 80 ns, EA loses its contacts with the protein exiting its binding site (Figure S2). The NADP$^+$ cofactor, remains in its binding site over the whole simulation. Indeed, as can be seen from the RMSF plots (Figure S3), residues from the catalytic site (D246, H247 and H309), and other residues involved in stabilizing G6P- (R408) or EA-binding (L80, K83 and K84) to the protein, present considerable fluctuations, while residues from the NADP$^+$ binding site remain more stable throughout the simulation. Taken together, the MD simulation results support a steric effect of the inhibitor in the proximity of the catalytic site that hampers catalysis.

Considering that the success rate of Fpocket to identify sites of protein-ligand interaction has been reported to be over 90% for the best three pockets [20], the docking grid of EA was centered on G6P with an inner and outer box of 20 and 40 cubic Å, respectively, which comprises the area of the top-3 ligand-binding sites previously identified with Fpocket. The stability of the G6PDH/G6P/NADP$^+$ ternary complex together with EA was checked by means of molecular dynamics (MD) simulation, previously validated on the 4EM5 complex. Analysis of the top-ten docking poses (Table S1) shows that the inhibitor occupies a cavity at the G6P-binding pocket that extends to the catalytic site and is sandwiched between G6P and residues D^{79}LAKKK^{84} from helix α1 (Figure 2 and Figure S4).

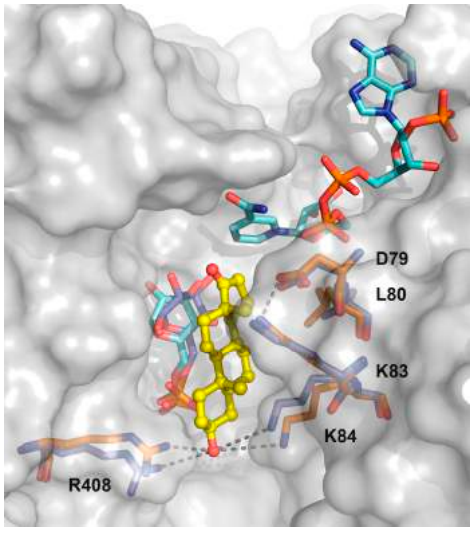

Figure 2. Binding mode of EA to the ternary complex of *Tc*G6PDH. Superimposition of the crystal structure of *Tc*G6PDH with bound G6P (PDB 4EM5, residues shown as violet sticks) with the molecular model of the corresponding energy minimized quaternary complex of the enzyme (protein surface is colored in grey, residues and substrates are shown as bright orange and cyan sticks, respectively, and EA is depicted as yellow balls and sticks). The dashed lines denote the interactions described in the text. The RMSD value for the backbone of both structures is 0.719 Å.

In the most represented (five out of 10) poses (see a representative pose in Figure 2), EA shows the following conformation and interactions: (i) the 10β- and 13β-methyl groups face helix α1; (ii) the 3β-hydroxyl group is oriented outside the catalytic site, pointing towards a positively charged region formed by K84 and R408, residues that participate in binding the phosphate group of G6P; (iii) the oxygen of the 3β-OH group is at a distance for H-bonds with the NH_2 from the side chain of R408 and K84, whereas the H from the 3β-OH group may establish weak polar interactions with the phosphate of G6P; (iv) the 5-membered D-ring of EA is placed close to the nicotinamide, where the non-polar side chain of L80 provides an hydrophobic environment to stabilize it. Furthermore, electrostatic interaction between K83 and D79 contributes to stabilize the N-terminal region of helix α1 and the position of L80.

It is worth noting, the docking model shows that EA does not affect substrates binding but instead interferes with catalysis by positioning them into non-catalytically competent orientations. In this respect, the binding of nicotinamide to G6PDH is destabilized by the 5-membered D-ring of EA that hinders the interaction between both substrates. In addition, the planar and rigid conformation of the EA ring system and its angular methyl groups, which intercalate between structural elements and residues important for catalysis, provide additional structural restraints in the catalytic site of the protein. In summary, this binding model of EA to *Tc*G6PDH is compatible with the uncompetitive inhibition mechanism reported for steroids.

2.2. Biochemical Validation of EA Binding to TcG6PDH

To further validate the *in silico* model of the holo-*Tc*G6PDH-EA complex, point mutations of residues key for stabilizing steroid binding were generated and kinetically characterized (Table 1).

Table 1. Kinetic parameters of wildtype and point mutants of recombinant *Tc*G6PDH with substrates [a] and the inhibitor epiandrosterone (EA).

G6PDH	K_M G6P (μM)	*kcat* (s^{-1})	*kcat*/K_M G6P ($s^{-1} \cdot \mu M^{-1}$)	K_M $NADP^+$ (μM)	*kcat* (s^{-1})	*kcat*/K_M $NADP^+$ ($s^{-1} \cdot \mu M^{-1}$)	K_i EA [b] (μM)
WT	77 ± 20	62 ± 3	0.8	16 ± 3	52 ± 2	3.2	2.5 [c]
L80G	74 ± 17	2.0 ± 0.1	0.027	75 ± 9	2.7 ± 0.1	0.036	31 [d]
K83A	537 ± 99	2.8 ± 0.2	0.005	21 ± 3	3.0 ± 0.1	0.14	11 [e]
K84A	618 ± 78	24.6 ± 0.9	0.04	17 ± 4	58 ± 2	3.4	8 [f]
R408A	168 ± 7	15.0 ± 0.3	0.089	17 ± 3	19 ± 1	1.1	3 [g]

[a] The apparent kinetic parameters were determined from non-linear regression plots of velocity *vs.* [substrate] from triplicate experimental determinations; [b] The Ki for EA was calculated using the equation: $Ki = IC_{50}/(K_M/[S] + 1)$; If $S >> K_M$, $Ki \approx IC_{50}$ and the corresponding associated errors for each mutant are: [c] 12%; [d] 3.2%; [e] 22%; [f] 13% and [g] 21%.

As pointed out above, L80 is at the N-terminus of a helix that contains residues key for G6P-binding, and provides a hydrophobic environment suitable for binding the nicotinamide ring of $NADP^+$ and the 5-membered D-ring of EA. This residue was replaced by a glycine, which presents a significantly less bulky and hydrophobic side chain. As expected, the L80G mutation did not affect the apparent K_M for G6P (K_M = 74 μM) but increased 4.7-fold the apparent K_M for $NADP^+$ (K_M for $NADP^+$ = 75 μM) when compared to the parameters exhibited by the WT enzyme (K_M for G6P = 77 μM and K_M for $NADP^+$ = 16 μM). Interestingly, the *kcat* value of the L80G mutant decreased by 20 to 30-fold (2.7–2.0 s^{-1}) with respect to that of WT *Tc*G6PDH (*kcat* ~ 52–62 s^{-1}), suggesting that this residue plays an important role during catalysis. In agreement with the changes observed in the kinetic parameters and the docking model, the inhibition constant (Ki) of the mutant L80G for EA was one order of magnitude higher (Ki EA = 31 μM) than that corresponding to WT *Tc*G6PDH (Ki EA = 2.5 μM), indicating a significant destabilization of inhibitor binding in the absence of Leu.

According to the docking model, the side chains of the lysine residues at position 83 and 84 are engaged in polar interactions with D79 and the 3β-OH of EA, respectively (Figure 2). In addition,

the model of the (catalytic) ternary complex shows that both residues interact with the phosphate group of G6P (not shown). In support of the *in silico* models, the replacement of K83 or K84 by alanine produced an almost 7- to 8-fold increase in the apparent K_M for G6P (K_M for G6P = 537 μM and 618 μM for K83A and K84A, respectively) and, a negligible change in the apparent K_M for $NADP^+$ (K_M for $NADP^+$ = 21 and 17 μM, for K83A and K84A, respectively), with respect to the reference parameters of the wildtype enzyme (K_M for G6P = 77 μM and K_M for $NADP^+$ = 16 μM; Table 1). Similarly to the mutant L80G, replacement of K83 entailed a marked decrease (~20-fold) in the *kcat* that affected negatively enzyme turnover with both substrates and rendered $kcat/K_M$ values 20 to 160-fold lower than those corresponding to the WT enzyme (Table 1). In contrast, catalysis was not significantly affected in the mutant K84A, where the 2-fold lower *kcat* obtained at varying concentrations of G6P is explained by the increased apparent K_M (618 μM) for this substrate and the not fully saturating concentration (5 mM G6P) used during the kinetic characterization of the mutant. As described above, the docking model of EA shows that both residues are directly (K84) or indirectly (K83) involved in EA-binding to *Tc*G6PDH, which was confirmed by the 3- to 4-fold increase in the Ki for EA determined for K83A (Ki = 11 μM) and K84A (Ki = 8 μM), respectively. Taking together, the biochemical and structural data led us to propose that K83 fulfils an important structural role by providing helix 1 with the right orientation to bind G6P (in a catalytically competent mode) or EA and demonstrate that K84 is engaged in G6P- and EA-binding.

As mentioned in the previous section, the 3β-OH group of EA is also at distance to establish an H-bond with the side chain of R408 and contributes to G6P binding during catalysis. In addition, the catalytic model shows that R408 is not exclusively involved in G6P binding but also engaged in a polar contact with a negatively charged residue, namely E285, from a loop close to the catalytic site (Figure S1). In order to determine the real contribution of R408 to inhibitor binding, this residue was exchanged by an alanine. Compared to the WT enzyme, the R408A mutant displayed an almost identical apparent K_M for $NADP^+$ (17 μM), a ~2-fold higher K_M for G6P (168 μM) and a >3-fold decrease in the *kcat*. Thus, the kinetic behavior of this mutant is fully compatible with the stabilizing role assigned to R408 in G6P-binding during catalysis. Because the Ki for EA of the mutant R408A was almost identical (Ki EA = 3 μM) to that of the WT enzyme, it can be concluded that R408 is not a major determinant for steroid binding.

2.3. Activity and Binding Mode to TcG6PDH of Novel EA Derivatives

The activity and binding mode of a series of EA derivatives (Figure 3) to *Tc*G6PDH were studied. The compounds were selected for containing substitutions in positions that, according to the docking model for EA, are key for steroid binding and *Tc*G6PDH inhibition.

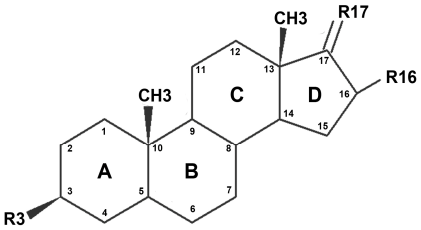

EA	16-BrEA	Compound 1
R3 = β-OH	R3 = β-OH	R3 = β-NHCONHEt
R6 = H2	R6 = H2	R6 = H2
R16 = H2	R16 = Br	R16 = H2
R17 = O	R17 = O	R17 = O
Compound 2	**Compound 3**	**Compound 4**
R3 = β-NHSO2NH2	R3 = β-NHSO2NH2	R3 = β-OH
R6 = H2	R6 = H2	R6 = H2
R16 = H2	R16 = H2	R16 = H2
R17 = O	R17 = α-H, β-COCH2OH	R17 = α-H, β-COCH2OH

Figure 3. Chemical structure of epiandrosterone (EA) and derivatives analyzed in this study. EA, epiandrosterone; 16-BrEA, 16-bromo epiandrosterone; **1**, 3β-ethylurea analogue of EA; **2**, 3β-sulfamide analogue of EA; **3**, 21-hydroxypregnan-20-one analogue of **2**; **4**, 21-hydroxypregnan-20-one analogue of EA.

The EA analogues subjected to biochemical (Table 2) and/or *in silico* analysis (Table S1) are: 16-bromo epiandrosterone (16-BrEA), a derivative with a 3β-ethylurea (compound **1**) or a 3β-sulfamide (compound **2**), and a 21-hydroxypregan-20-one with a 3β-sulfamide (compound **3**) or a 3β-alcohol (compound **4**).

Table 2. Inhibition of *Tc*G6PDH by steroids.

Compound	Substituent				IC_{50} (μM) [a]	G6PDH Activity [%] ± SD at 30 μM Compound [b]
	3-α	3-β	17-	16-α		
EA	H	OH	O	H	3.0 ± 0.4 [c]	12 ± 2
16Br-EA	H	OH	O	Br	0.015 (13.3 to 16.6) [d]	ND [e]
1	H	NHCONHEt	O	H	1.5 (1.0 to 2.0) [f]	7 ± 1
2	H	$NHSO_2NH_2$	O	H	2.2 (1.8 to 2.9) [f]	9 ± 1
3	H	$NHSO_2NH_2$	α-H, β-$COCH_2OH$	H	ND [e]	30 ± 2
4	H	OH	α-H, β-$COCH_2OH$	H	ND [e]	43 ± 2

[a] The IC_{50} was determined from dose/response curves with 7 point concentrations tested in triplicate; [b] The values are expressed as the mean % G6PDH activity with respect to the control without inhibitor from triplicate experimental determinations; [c] The value is expressed as mean ± standard deviation; [d] Value reported by [12] with confidence interval provided within brackets; [e] ND, not determined; [f] IC_{50} values with corresponding confidence intervals.

Overall, docking of steroids **1** and **2** to the *Tc*G6PDH ternary complex shows that the corresponding 3β-substituents determine two possible orientations of the androstane moiety in the binding site. Binding of **1** to helix α1 is dictated by H-bonds between the 3β-urea and the NHε of K84 (Figure 4A, Figure S5 image A). This binding conformation together with the rigid structure of the androstane determines that the 5-membered D-ring protrudes towards the space between both substrates at the catalytic site (Figure 4A, Figure S5A). In contrast, an H-bond between the 3β-urea oxygen and the side chain of R408 favors binding of **1** parallel to the substrate and with its D-ring occupying only a minor volume of the catalytic pocket (Figure 4B, Figure S5B).

Binding of compound **2** to *Tc*G6PDH occurs in the same pocket used by EA and **1**. In several conformers, the inhibitor is anchored to helix α1 through an H-bond between one sulfamide oxygen and the NHδ of K84 (Figure 4C and Figure S5C). In an alternative and more stable binding conformation ($\Delta G \approx -14.37$ kcal/mol), the sulfamide moiety of the inhibitor establishes H-bonds with the side chains of K84 and R408 (Figure 4D and Figure S5D). Independently of the conformation adopted by compound **2**, the angular methyl groups point towards the solvent and the 17-ketone group, although located slightly further from the active site, is able to provide steric hindrance at the catalytic site.

Compared to the parental scaffold, the inclusion of polar substitutions at position 3β of EA (compound **1** and **2**) increased by ~10-fold the inhibition of human G6PDH [16] but only moderately (⩽2-fold) their potency towards the parasite enzyme (Table 2). This suggests a species-specific binding mode of steroids to G6PDH.

If the binding models obtained for EA and the 3β derivatives **1** and **2** are correct, then the addition of bulky groups at position 16 or 17 may be beneficial or detrimental for inhibition depending on the nature and size of the substituent. To test this, derivatives of EA with a bromide atom at position 16 (16-Br EA) or a 21-hydroxypregan-20-one group at position 17 with a 3β-sulfamide (compound **3**) or a 3β-alcohol (compound **4**) were assayed against the recombinant enzyme and/or their potential binding modes simulated *in silico*.

In 7 out of 10 docking poses, the binding mode of 16α-Br EA to *Tc*G6PDH resembled that of EA. In the most stable protein-ligand complex (ΔG −12.07 kcal/mol), the steroid makes a full occupancy of the catalytic site and fixes the substrates in conformations not suitable for catalysis

(Figure 4E and Figure S5E). The major interactions between the enzyme-substrate complex and the inhibitor are: an H-bond between the 3β-OH and the NHδ of K84 and an halogen bond between the bromide and the hydrogen from the terminal amide of nicotinamide (Figure 4E). Although weaker in strength with respect to hydrogen bonds, this Br···H-N bond contributes to increase the affinity of the inhibitor for bound $NADP^+$ while restraining the mobility of the nicotinamide ring to approach G6P. This likely explains the 65- and 115-fold higher potency of the 16-halogenated congeners of EA and DHEA, respectively, towards *Tc*G6PDH [10] (Table 2). Notably, this derivative is almost two orders of magnitude less active against the human G6PDH [12,16,24].

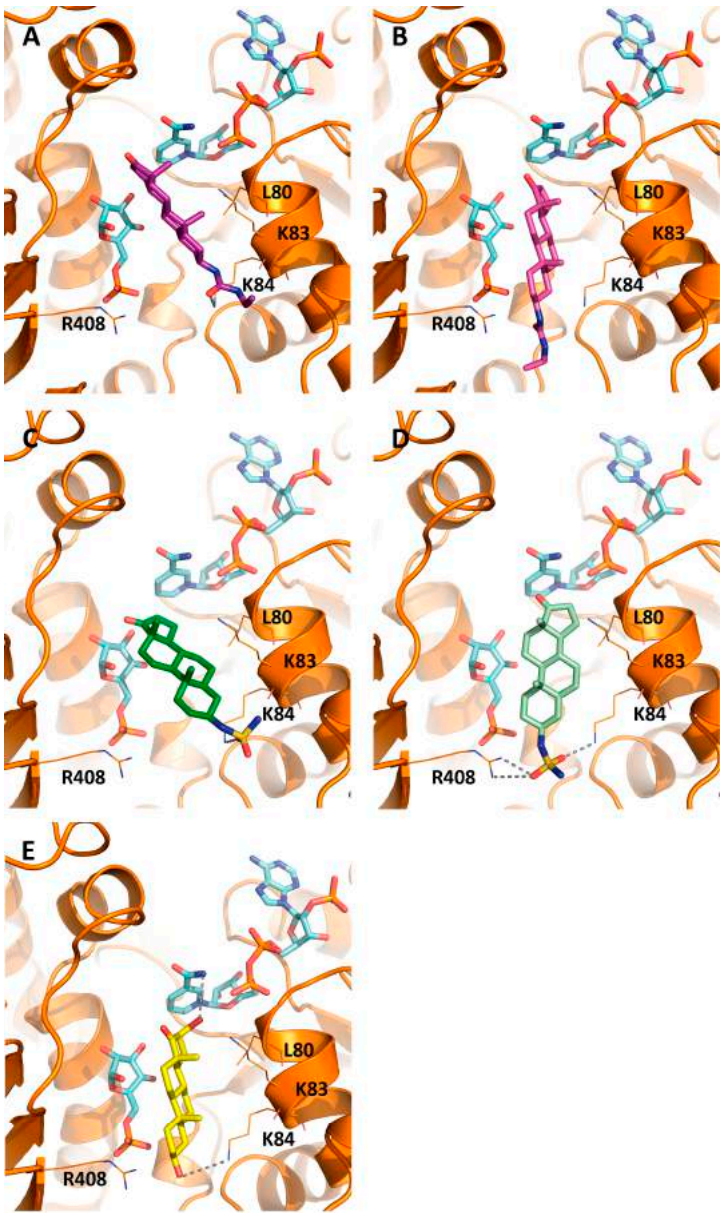

Figure 4. Binding modes of 3β- and 16β-substituted androstanes to the catalytic complex of *T. cruzi* G6PDH. *Tc*G6PDH structure and residues relevant for inhibitor binding are shown in orange cartoon and lines. The substrates are depicted in sky blue sticks and the H-bonds with grey dashed lines. The figures show the most stable pose for (**A**) **1** (dark purple sticks) and (**D**) **2** (pale green sticks) and alternative binding conformations for (**B**) **1** (purple sticks) and (**C**) **2** (dark green); (**E**) Best docking pose for 16Br-EA, showing the 5-membered D-ring group occupying the active site and the bromide atom establishing a halogen bond with the amide of $NADP^+$.

Molecular docking of steroids **3** and **4** shows that both compounds occupy the steroid binding site of *Tc*G6PDH with orientations determined by polar interactions of the 3β-sulfamide (**3**) and 21-hydroxypregnan-20-one (**4**) groups with K84 and R408 (Figure 5).

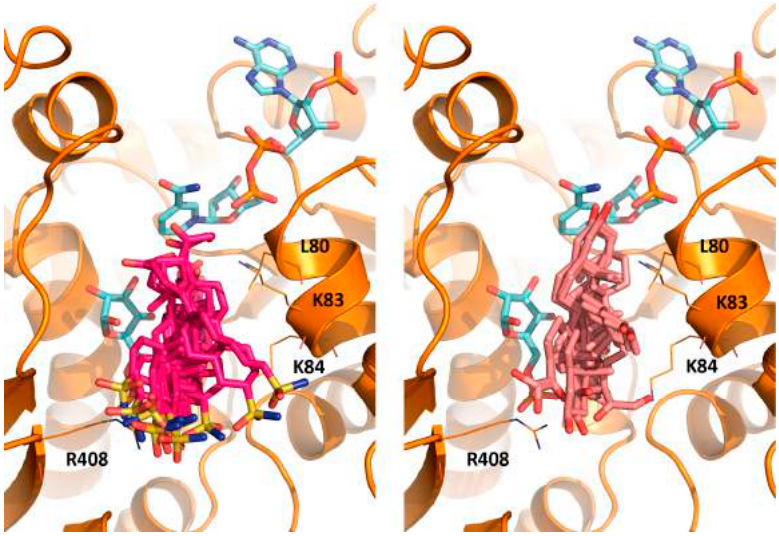

Figure 5. Binding of **3** and **4** to *Tc*G6PDH in complex with G6P and $NADP^+$. *Tc*G6PDH structure is shown as orange cartoon and residues participating in interactions are shown in lines with substrates depicted in sky blue sticks. The different poses obtained during the docking studies are shown for **3** (dark pink sticks) and **4** (pink sticks).

However, the occupancy of the cavity by **3** and **4** is not full and, for all poses, the D-ring localizes distant from the catalytic site, which agrees with their lower inhibitory activity (60%–70% inhibition at 30 μM compound; Table 2). This behavior contrasted with the enhanced anti-human G6PDH activity reported for these compounds (IC_{50} ~ 2 μM) but is not surprising since compounds reported to target *Tc*G6PDH do not inhibit well the human enzyme [16].

In order to confirm the binding preference of steroids suggested by the docking models, the activity of EA analogues was tested towards *Tc*G6PDH mutants using saturating concentrations of substrates and compounds at a final concentration of 30 μM (Figure 6). As previously observed for EA (Table 1), only mutations in L80, K83 and K84 but not in R408 affected significantly and negatively the inhibitory activity of compounds **1** to **4** (Figure 6), pointing to an important stabilizing effect of these residues in steroid binding as suggested by the docking models (Figures 2 and 4).

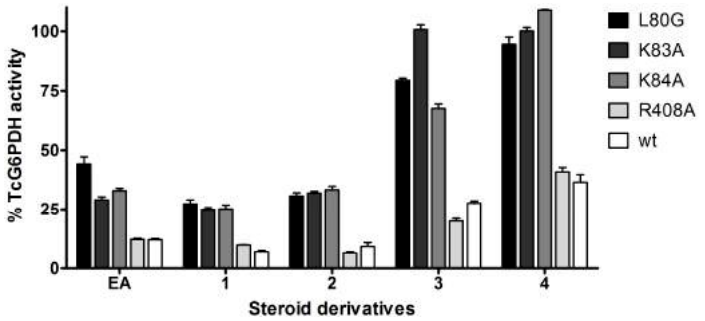

Figure 6. Inhibitory activity of steroids toward *Tc*G6PDH WT and mutants. The inhibitory activity of EA and derivatives thereof was tested against the wildtype and mutants L80G, K83A, K84A or R408A of *Tc*G6PDH, as described in Section 3.4. of the Experimental Section. The activity is shown as a percentage relative to the corresponding non-treated enzyme controls and compounds were tested at a fixed concentration of 30 μM.

A recent *in silico* study proposes a binding region for steroids in human G6PDH [14] that differs from the one elucidated here for the *T. cruzi* enzyme. Although this may explain the species-specificity observed for certain steroids, such an assumption must be taken with care because the docking models obtained for the human enzyme show a partial occupancy of the nicotinamide binding site by the inhibitors, which is not compatible with the uncompetitive inhibition mechanism exerted by steroids. This inconsistency probably stems from the use of the binary (human G6PDH-G6P) and not the ternary enzyme-substrate complex as a template for the dockings.

3. Experimental Section

3.1. Plasmids

The expression vector for N-terminally His-tagged full-length (pET28a (+)-*Tc*G6PDH$_L$; Accession Nr. ABD72517.1) was a kind gift of Juan José Cazzulo (Universidad de San Martín, CONICET, Buenos Aires, Argentina) [7]. The single Lys84Ala, Leu80Gly, Arg408Ala and Arg408Lys mutants of *Tc*G6PDH were generated with the Quick Change site-directed mutagenesis kit (Stratagene, La Jolla, CA, USA) using the parental plasmid as template and the primer pairs K83A Fwd 5′ CTCGGTGCA AGCGGGGACTTGGCCAAAGCGAAGACCTTTCCGGCG 3′/K83A Rev 5′ CGCCGGAAAGGTCTT CGCTTTGGCCAAGTCCCCGCTTGCACCGAG 3′ K84A Fwd 5′ GGGGACTTGGCCAAAAAGGCG ACCTTTCCGGCGCTTTTT 3′/K84A Rev 5′ AAAAAGCGCCGGAAAGGTCGCCTTTTTGGCCAAG TCCCC 3′, and L80G Fwd 5′ CTCGGTGCAAGCGGGGACTCCGCCAAAAAGAAGACC 3′/L80G Rev 5′ GGTCTT CTTTTTGGCGGAGTCCCCGCTTGCACCGAG 3′, R408A Fwd 5′ CCGGAAAGGCACTC GAAGAGGCTCTGCTTGATATCCGTATTCAGTTCAAGGAC 3′/R408A Rev 5′ GTCCT TGAACTG AATACGGATATCAAGCAGAGCCTCTTCGAGTGCCTTTCCGGC 3′ (underlined are indicated the mutated bases), respectively. The PCR were performed in a total reaction volume of 50 µL according to the instructions of the supplier. One Shot® MAX Efficiency® DH5α™-T1R cells were transformed with the mutagenesis reaction. The correctness of the targeted mutations was confirmed in at least three independent plasmids from each construct by DNA sequencing (Molecular Biology Unit, Institut Pasteur de Montevideo, Montevideo, Uruguay).

3.2. Expression and Purification of Recombinant Proteins

The wild-type (WT) form and mutants (K83A, K84A, L80G and R408A) of *Tc*G6PDH$_L$ were expressed in *Escherichia coli* BL21 (DE3) grown in ZYM-5052 auto-induction medium. Briefly, an overnight culture of transformed bacteria grown in LB was inoculated at a ratio 1:100 in ZYM-5052 containing 50 µg/L kanamycin, and incubated for 48 h at 25 °C and 200 rpm. Cells were harvested by centrifugation (5000× *g*, 10 min, 4 °C) and resuspended in 50 mM Tris, pH 8.0, 500 mM NaCl, 5 mM $MgCl_2$ (buffer A) containing 1 mM PMSF, 40 µg/mL TLCK, 150 nM pepstatin, 4 nM cystatin and 1 mg/mL lysozyme. After incubating for 45 min at 4 °C, the cell lysate was subjected to three cycles of sonication (30 pulses per minute at 55% amplitude with a macrotip) in a Digital Sonifier 450 (Branson, Danbury, CT, USA) and then cleared by centrifugation at 27,000× *g* (45 min, 4 °C) followed by filtration in a 0.45 µm nitrocellulose filter (Millipore, Billerica, MA, USA). The cleared lysate was loaded onto a HisTrap column (GE-HealthCare, Little Chalfont, UK) pre-equilibrated with buffer A and unbound proteins were removed with 5 column volumes of buffer A. After washing the column with buffer A containing 5 mM imidazole, the His-tagged proteins were eluted with 500 mM imidazole in buffer A and concentrated by diafiltration (Ultra-15 30K NMWL filter, 4 °C, 7000× *g* Amicon, Darmstadt, Germany). The final purification was performed in an AKTA Purifier system, using a Superdex 200 10/300 GL column (GE-HealthCare) pre-equilibrated with buffer A. Enzyme purity and concentration was assessed by Coomasie blue stained SDS-PAGE gels and the bicinchoninic acid assay (Bicinchoninic Acid Protein Assay Kit, Sigma, St. Louis, MO, USA), respectively. G6PDH activity was determined as described below. The protein was concentrated to 0.5 mg/mL and stored at 4 °C.

3.3. Kinetic Assays

G6PDH activity was determined at ~25 °C by monitoring NADPH (ε340 = 6220 $M^{-1} \cdot cm^{-1}$) formation at 340 nm. All assays were performed in buffer B (50 mM Tris pH 7.5, 5 mM $MgCl_2$) in a final reaction volume of 150 µL and started by addition of glucose-6-phosphate (G6P). For WT *Tc*G6PDH, the Michaelis' constants (K_M) and the maximum initial velocity (Vmax) were determined varying reciprocally the substrate (10, 50, 200, 1000 and 5000 µM G6P) and coenzyme (5, 10, 50, 250 and 625 µM $NADP^+$) concentrations. For the mutants, the kinetic characterization was performed at a fixed saturating concentration of the corresponding co-substrate (*i.e.*, 6 mM G6P and 700 µM $NADP^+$) and varying concentrations of the substrate (25, 50, 70, 100, 250, 350, 500 and 700 µM $NADP^+$, and 0.005, 0.025, 0.05, 0.25, 0.65, 1, 2.5 and 5 mM G6P). The concentration of enzyme in the assay was of 9.7, 970, 534, 316 and 100 nM for WT, K83A, K84A, L80G and R408A respectively. The first 30 s of the reaction were used to calculate initial velocities that were normalized by the corresponding enzyme concentration in the assay. All measurements were performed in triplicate using a Cary 50 Bio spectrophotometer (Agilent Technologies, Santa Clara, CA, USA). The initial rates were determined with the Origin Pro 8.0 software (OriginLab Corporation, Northampton, MA, USA), and the apparent kinetic constants were calculated by nonlinear regression using the GraphPad Prism 5.0 software (GraphPad Inc., San Diego, CA, USA). The data were fitted to the Cleland or Michaelis-Menten equation to obtain the corresponding kinetic parameters.

3.4. Inhibitor Assays with Wildtype or Mutants of TcG6PDH

For all inhibition assays with wildtype or mutants of *Tc*$G6PDH_L$, initial reaction rates under saturating conditions of both substrates ($NADP^+$ 0.7 mM and G6P 6 mM) and different concentrations of steroidal compounds were measured at 340 nm with a Cary 50 Bio spectrophotometer. Stock and working solutions of compounds were prepared in 100% (*v*/*v*) DMSO. The reactions were performed in a quartz cuvette containing 5 µL of inhibitor solution and 245 µL buffer B added of 1.4 mM $NADP^+$ and 12 mM G6P and started by addition of 250 µL of an enzyme solution in Buffer B. The final concentration of enzyme in the assay was: 698 nM for *Tc*G6PDH K83A, 495 nM for *Tc*G6PDH K84A, 380 nM for *Tc*G6PDH L80G, 40 nM for *Tc*G6PDH R408A, and 48 nM (for assays with EA) or 13 nM (for assays with steroid derivatives) for *Tc*G6PDH wildtype. A reaction control with 1% (*v*/*v*) DMSO was run for each enzyme species. The activity of the steroid derivatives EA and **1** to **4** was initially assayed at 30 µM against wildtype and mutants of *Tc*G6PDH. To obtain IC_{50} values for EA and the most potent derivatives, the activity of the compounds was tested at concentrations of 0.5, 5, 10, 25, 50, 100, 250 µM, and 0.5, 1.5, 3.0, 7.5, 15, 30 µM, respectively. The IC_{50} was estimated from non-linear regression fitting of initial velocity *vs.* [compound] plot using the program GraphPad prism 5.0. The Ki was calculated with the equation [25]:

$$Ki = IC_{50}/(K_M/[S] + 1)$$

3.5. Generation of TcG6PDH/G6P/$NADP^+$ Ternary Complex and Steroids Docking

The crystal structure of a truncated form of *Tc*G6PDH lacking the first 37 amino acids and co-crystallized in presence of its physiological substrate G6P (PDB ID: 4EM5; resolution 3.35 Å) [15] was pretreated by means of the Protein Preparation Wizard tool of the Maestro suite 9.2 [26] at default settings, adding hydrogen atoms, deleting water molecules, fill in missing amino acids side chains and eventual missing loop using Prime [27], generating ionization states of the co-crystallized ligand at pH 7 ± 3.0 using Epik [28] and checking amino acid protonation state using Propka, always at physiological pH [29]. $NADP^+$, EA and all the other steroid structures discussed here were modeled with LigPrep [30] at default settings. In order to obtain a complete protein model, the missing $NADP^+$ was docked in the pretreated chain C of the tetramer *Tc*G6PDH by means of induced fit docking (Maestro suite 9.2) [31]. The induced fit algorithm is designed to reproduce conformational changes in the protein binding site upon ligand binding, using both Glide and Prime. In order to generate

a diverse ensemble of ligand poses, the procedure uses reduced Van der Waals radii and an increased Coulomb-vdw cutoff, and can temporarily remove highly flexible side chains during the docking step. For each pose, a Prime structure prediction is then used to accommodate the ligand by reorienting nearby side chains. These residues and the ligand are then minimized. Finally, each ligand is re-docked into its corresponding low energy protein structures and the resulting complexes are ranked according to the GlideScore. Based on the inhibition mechanism exerted by EA on *Tc*G6PDH, the ligand and the other steroid inhibitors were docked in the catalytic site of the *Tc*G6PDH/G6P/$NADP^+$ complex. The docking grid was centered on G6P with an inner box size of 20 × 20 × 20 Å and an outer box size of 40 × 40 × 40 Å. Docking runs were performed using the Glide Standard Precision (SP) scoring function, choosing the best 50 structures undergoing the post-docking energy minimization, saving the very best 10 poses showing a threshold energy lower than 0.50 kcal· mol^{-1}. The 10 final poses were then rescored by means of SZYBKI 1.8.0.1 [23], using the Poisson-Boltzmann solvation model [32]. Model images were generated and analyzed using PyMol 1.7.1.3 [33].

3.6. MD Simulation of TcG6PDH/G6P/$NADP^+$/EA Complex

The MD simulation of the *Tc*G6PDH/G6P/$NADP^+$/EA complex has been performed by means of NAMD 2.10 [34] using the CHARMM 36 force field [35]. For the system set up, a first minimization in vacuum (only H atoms and then the whole system for a total of 2000 minimization steps) has been performed, followed by solvation of the minimized complex in a TIP3P water box 10 Å longer than the protein in all six directions. Six neutralizing Na^+ ions were added. During production MD, temperature was kept constant at 310 K by coupling all non-hydrogen atoms to a Langevin thermostat with a friction coefficient of 5 ps^{-1}. Non-bonded interactions were cut off above 10 Å and smoothed to zero beginning from 9 Å. PME long range electrostatic with a grid spacing of 2 Å was used, and all bonds involving hydrogen atoms were constrained using RATTLE [36]. Production runs have been performed at constant pressure (NPT ensemble), for a total of 80 ns with a time step of 2 fs.

4. Conclusions

Our study discloses the putative site binding of steroids to the ternary complex of *Tc*G6PDH, which involves a groove that runs alongside the G6P-binding site and helix α1 with its aliphatic (K83 and K84) and hydrophobic (L80) residues that provide stabilizing interactions. Such a binding mode of EA does not affect substrate binding but directly interferes with catalysis because: (i) it affects the dynamic of helix α1—a structural element that shapes the catalytic site and participates in $NADP^+$ and G6P binding; (ii) provides steric hindrance for the interaction of the nicotinamide group of $NADP^+$ with G6P via its D-ring group that protrudes into the catalytic site; and (iii) delays the exit of G6P or, eventually, its product (6-phosphogluconolactone) from the active site.

Furthermore, SAR analysis of EA analogues supported by docking models provides clues towards the determinants for the selective inhibition of the pathogen enzyme by steroids: (i) polar substitutions at position 3β of EA were well tolerated and rendered congeners that increased moderately the activity against *Tc*G6PDH; (ii) a bromide atom at position 16 of EA favors the formation of an halogen bond with $NADP^+$, which increases the affinity for the inhibitor and the steric effect on the catalytic site of *Tc*G6PDH; (iii) in contrast to the human enzyme, polarizable groups at position 17β of EA or compound **1** have a destabilizing effect on inhibitor binding to *Tc*G6PDH, with the steroids exploring different binding conformations that are less suited to interfere with catalysis. Taking together, these data also suggest the presence of different binding orientation or sites for steroids in the host and pathogen enzyme.

The structural information obtained from this study may prove valuable to investigate the binding mode of the recently discovered new uncompetitive inhibitors of *T. cruzi* G6PDH [12] as well as for the challenging design of more potent and selective inhibitors targeting the pathogen enzyme.

Supplementary Materials: Supplementary materials can be accessed at: http://www.mdpi.com/1420-3049/21/3/368/s1.

Acknowledgments: CO acknowledges support from ANII (Agencia Nacional de Investigación e Innovación, Uruguay; doctoral fellowship POS_NAC_2012_1_8803) and CSIC (Comisión Sectorial de Investigaciones Científicas, Universidad de la República Uruguay). CSIC and the Coimbra Group is acknowledged, the last for supporting a research traineeship at the Università degli Studi di Siena, is acknowledged by AM. MAC acknowledges the financial support of FOCEM (MERCOSUR Structural Convergence Fund) COF 03/11 and grant INNOVA Uruguay (agreement No. DCI-ALA/2007/19.040 between Uruguay and the European Commision). We acknowledge Cameron F. Abrams (Drexel University, Philadelphia, PA, USA) for the computational resources and help.

Author Contributions: Marcelo A. Comini, Cecilia Ortiz and Francesca Moraca conceived and designed the experiments; Cecilia Ortiz, Francesca Moraca and Andrea Medeiros performed the experiments; Marcelo A. Comini and Cecilia Ortiz analyzed the data; Marcelo A. Comini, Maurizio Botta, Niall Hamilton contributed reagents/materials/analysis tools; Marcelo A. Comini and Cecilia Ortiz wrote the paper.

Conflicts of Interest: The authors declare no conflict of interest. The founding sponsors had no role in the design of the study; in the collection, analyses, or interpretation of data; in the writing of the manuscript, and in the decision to publish the results.

References

1. Hotez, P.J.; Bottazzi, M.E.; Franco-Paredes, C.; Ault, S.K.; Periago, M.R. The neglected tropical diseases of Latin America and the Caribbean: A review of disease burden and distribution and a roadmap for control and elimination. *PLoS Negl. Trop. Dis.* **2008**, *2*, e300. [CrossRef] [PubMed]
2. Barrett, M.P.; Gilbert, I.H. Perspectives for new drugs against trypanosomiasis and leishmaniasis. *Curr. Top. Med. Chem.* **2002**, *2*, 471–482. [CrossRef] [PubMed]
3. Opperdoes, F.R.; Michels, P.A. Enzymes of carbohydrate metabolism as potential drug targets. *Int. J. Parasitol.* **2001**, *31*, 482–490. [CrossRef]
4. Comini, M.A.; Ortíz, C.; Cazzulo, J.J. Drug targets in trypanosomal and leishmanial pentose phosphate pathway. In *Trypanosomatid Diseases: Molecular Routes to Drug Discovery*; Jäger, T., Koch, O., Flohé, L., Eds.; Wiley-VCH Verlag GmbH & Co. KgaA: Weinheim, Germany, 2013; pp. 297–313.
5. Maugeri, D.A.; Cazzulo, J.J. The pentose phosphate pathway in *Trypanosoma cruzi*. *FEMS Microbiol. Lett.* **2004**, *234*, 117–123. [CrossRef] [PubMed]
6. Maugeri, D.A.; Cannata, J.J.; Cazzulo, J.J. Glucose metabolism in *Trypanosoma cruzi*. *Essays Biochem.* **2011**, *51*, 15–30. [CrossRef] [PubMed]
7. Igoillo-Esteve, M.; Cazzulo, J.J. The glucose-6-phosphate dehydrogenase from *Trypanosoma cruzi*: Its role in the defense of the parasite against oxidative stress. *Mol. Biochem. Parasitol.* **2006**, *149*, 170–181. [CrossRef] [PubMed]
8. Cordeiro, A.T.; Thiemann, O.H.; Michels, P.A. Inhibition of *Trypanosoma brucei* glucose-6-phosphate dehydrogenase by human steroids and their effects on the viability of cultured parasites. *Bioorg. Med. Chem.* **2009**, *17*, 2483–2489. [CrossRef] [PubMed]
9. Marks, P.A.; Banks, J. Inhibition of mammalian glucose-6-phosphate dehydrogenase by steroids. *Proc. Natl. Acad. Sci. USA* **1960**, *46*, 447–452. [CrossRef] [PubMed]
10. Cordeiro, A.T.; Thiemann, O.H. 16-Bromoepiandrosterone, an activator of the mammalian immune system, inhibits glucose 6-phosphate dehydrogenase from *Trypanosoma cruzi* and is toxic to these parasites grown in culture. *Bioorg. Med. Chem.* **2010**, *18*, 4762–4768. [CrossRef] [PubMed]
11. Gupta, S.; Cordeiro, A.T.; Michels, P.A. Glucose-6-phosphate dehydrogenase is the target for the trypanocidal action of human steroids. *Mol. Biochem. Parasitol.* **2011**, *176*, 112–115. [CrossRef] [PubMed]
12. Mercaldi, G.F.; Ranzani, A.T.; Cordeiro, A.T. Discovery of new uncompetitive inhibitors of glucose-6-phosphate dehydrogenase. *J. Biomol. Screen* **2014**, *19*, 1362–1371. [CrossRef] [PubMed]
13. Gordon, G.; Mackow, M.C.; Levy, H.R. On the mechanism of interaction of steroids with human glucose 6-phosphate dehydrogenase. *Arch. Biochem. Biophys.* **1995**, *318*, 25–29. [CrossRef] [PubMed]
14. Zhao, Z.B.; Liu, Y.; Yao, Y. Computational determination of binding structures and free energies of glucose 6-phosphate dehydrogenase with novel steroid inhibitors. *J. Mol. Graph. Model.* **2014**, *51*, 168–172. [CrossRef] [PubMed]
15. Ortiz, C.; Larrieux, N.; Medeiros, A.; Botti, H.; Comini, M.; Buschiazzo, A. Expression, crystallization and preliminary X-ray crystallographic analysis of glucose-6-phosphate dehydrogenase from the human pathogen *Trypanosoma cruzi* in complex with substrate. *Acta Cryst. Sect. F* **2011**, *67*, 1457–1461. [CrossRef] [PubMed]

16. Hamilton, N.M.; Dawson, M.; Fairweather, E.E.; Hamilton, N.S.; Hitchin, J.R.; James, D.I.; Jones, S.D.; Jordan, A.M.; Lyons, A.J.; Small, H.F.; *et al*. Novel steroid inhibitors of glucose 6-phosphate dehydrogenase. *J. Med. Chem.* **2012**, *55*, 4431–4445. [CrossRef] [PubMed]
17. Au, S.W.; Gover, S.; Lam, V.M.; Adams, M.J. Human glucose-6-phosphate dehydrogenase: The crystal structure reveals a structural $NADP^+$ molecule and provides insights into enzyme deficiency. *Structure* **2000**, *8*, 293–303. [CrossRef]
18. Rowland, P.; Basak, A.K.; Gover, S.; Levy, H.R.; Adams, M.J. The three-dimensional structure of glucose 6-phosphate dehydrogenase from Leuconostoc mesenteroides refined at 2.0 Å resolution. *Structure* **1994**, *2*, 1073–1087. [CrossRef]
19. Kotaka, M.; Gover, S.; Vandeputte-Rutten, L.; Au, S.W.; Lam, V.M.; Adams, M.J. Structural studies of glucose-6-phosphate and $NADP^+$ binding to human glucose-6-phosphate dehydrogenase. *Acta Crystallogr. D Biol. Crystallogr.* **2005**, *61*, 495–504. [CrossRef] [PubMed]
20. Le Guilloux, V.; Schmidtke, P.; Tuffery, P. Fpocket: An open source platform for ligand pocket detection. *BMC Bioinform.* **2009**, *10*. [CrossRef] [PubMed]
21. Wang, X.-T.; Au, S.W.; Lam, V.M.; Engel, P.C. Recombinant human glucose-6-phosphate dehydrogenase. *Eur. J. Biochem.* **2002**, *269*, 3417–3424. [CrossRef] [PubMed]
22. Cardi, M.; Chibani, K.; Castiglia, D.; Cafasso, D.; Pizzo, E.; Rouhier, N.; Jacquot, J.P.; Esposito, S. Overexpression, purification and enzymatic characterization of a recombinant plastidial glucose-6-phosphate dehydrogenase from barley (*Hordeum vulgare cv.* Nure) roots. *Plant Physiol. Biochem.* **2013**, *73*, 266–273. [CrossRef] [PubMed]
23. *Glide*; Version 6.5; Schrödinger, L.L.C.: New York, NY, USA, 2014.
24. Raineri, R.R.; Levy, H.R. Specificity of steroid interaction with mammary glucose 6-phosphate dehydrogenase. *Biochemistry* **1970**, *9*, 2233–2243. [CrossRef] [PubMed]
25. Cer, R.Z.; Mudunuri, U.; Stephens, R.; Lebeda, F.J. IC_{50}-to-Ki: A web-based tool for converting IC_{50} to Ki values for inhibitors of enzyme activity and ligand binding. *Nucleic Acids Res.* **2009**, *37*, 441–445. [CrossRef] [PubMed]
26. *Protein Preparation Wizard*; Schrödinger, L.L.C.: New York, NY, USA, 2014.
27. *Prime*; Version 3.8; Schrödinger, L.L.C.: New York, NY, USA, 2014.
28. *Epik*; Version 3.0; Schrödinger, L.L.C.: New York, NY, USA, 2014.
29. Olsson, M.H.M.; Søndergard, C.R.; Rostkowski, M.; Jensen, J.H. PROPKA3: Consistent treatment of internal and surface residues in Empirical pKa predictions. *J. Chem. Theory Comput.* **2011**, *7*, 525–537. [CrossRef] [PubMed]
30. *LigPrep*; Version 3.2; Schrödinger, L.L.C.: New York, NY, USA, 2014.
31. *Maestro*; Version 9.2; Schrödinger, L.L.C.: New York, NY, USA, 2011.
32. Wlodek, S.; Skillman, A.G.; Nicholls, A.J. Ligand entropy in gas-phase, upon solvation and protein complexation. Fast estimation with Quasi-Newton Hessian. *J. Chem. Theory Comput.* **2010**, *6*, 2140–2152. [CrossRef] [PubMed]
33. *The PyMOL Molecular Graphics System*; Version 1.7.1.3; Schrödinger, L.L.C.: New York, NY, USA, 2014.
34. Phillips, J.C.; Braun, R.; Wang, W.; Gumbart, J.; Tajkhorshid, E.; Villa, E.; Chipot, C.; Skeel, R.D.; Kale, L.; Schulten, K. Scalable molecular dynamics with NAMD. *J. Comput. Chem.* **2005**, *2*, 1781–1802. [CrossRef] [PubMed]
35. MacKerell, A.D.; Bashford, D.; Bellott, M.; Dunbrack, R.L.; Evanseck, J.D.; Field, M.J.; Fischer, S.; Gao, J.; Guo, H.; Ha, S.; *et al*. All-atom empirical potential for molecular modeling and dynamics studies of proteins. *J. Phys. Chem.* **1998**, *102*, 3586–3616. [CrossRef] [PubMed]
36. Andersen, H.C. Rattle: A velocity version of the shake algorithm for molecular-dynamics calculations. *J. Comput. Phys.* **1983**, *52*, 24–34. [CrossRef]

Sample Availability: Samples of the compounds **1**, **2**, **3** and **4** are available from the authors.

© 2016 by the authors; licensee MDPI, Basel, Switzerland. This article is an open access article distributed under the terms and conditions of the Creative Commons by Attribution (CC-BY) license (http://creativecommons.org/licenses/by/4.0/).

Supplementary Materials: Binding Mode and Selectivity of Steroids towards Glucose-6-Phosphate Dehydrogenase from the Pathogen *Trypanosoma cruzi*

Cecilia Ortiz, Francesca Moraca, Andrea Medeiros, Maurizio Botta, Niall Hamilton and Marcelo A. Comini

Table S1. Binding ΔG values (kcal/mol) for different binding poses obtained for the respective inhibitors on the energy minimized ternary complex of *Tc*G6PDH. In bold are highlighted the poses for the corresponding compounds shown in Figures 2, 4 and 5.

	ΔG (kcal/mol)					
Docking Pose	**EA**	**16Br-EA** [a]	**1**	**2**	**3**	**4**
1	**−11.458**	−6.509	−11.717	**−11.096**	**−11.325**	−10.595
2	−9.824	−10.750	−10.236	−7.661	−9.467	−12.191
3	−6.471	0.480	**−13.307**	−9.205	−6.108	−11.690
4	−7.420	**−12.069**	**−10.058**	**−14.368**	−11.700	**−11.344**
5	−7.670	−9.013	−9.641	−9.727	−8.224	−5.725
6	−7.767	−8.954	−3.826	−10.398	−9.268	**−14.421**
7	−8.476	−10.423	−8.357	−7.805	−9.980	−11.010
8	−11.323	−0.652	−2.281	−8.161	**−13.918**	−4.379
9	−10.838	−-3.979	−6.088	−4.704	−9.925	−5.400
10	−9.768	−6.391	−9.500	−4.586	−11.675	−10.757

[a] For 16Br-EA was investigated the R-enantiomer.

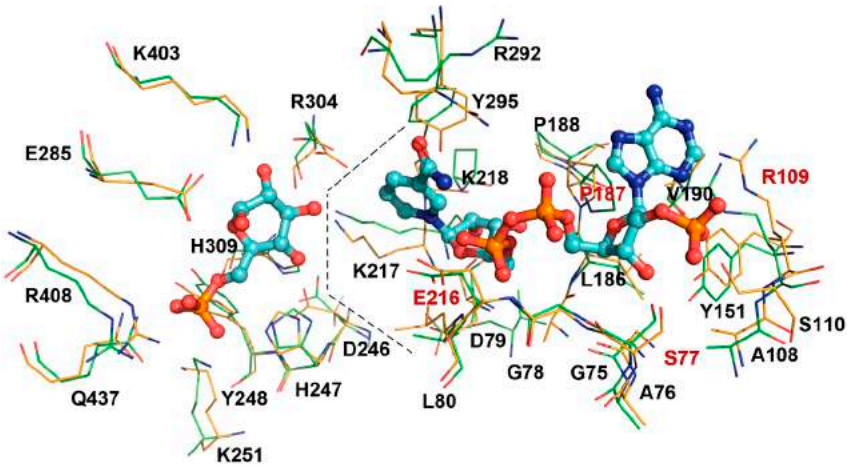

Figure S1. Comparison of the substrate binding sites for the crystal structure of *T. cruzi* G6PDH with bound G6P and the corresponding molecular model of the catalytic complex. The residues involved in substrate binding are shown for *Tc*G6PDH with bound G6P (PDB 4EM5, green lines) and for the model of the ternary complex enzyme-G6P-$NADP^+$ (bright orange lines). The dashed line denotes the separation between the N- (right side) and C-terminal (left side) domain of G6PDH. Residues from PDB 4EM5 interfering with $NADP^+$ binding are labeled with red fonts (S77, R109, P187 and E216): the OH group from S77 (β1-loop-α1) clashes with an oxygen from the phosphate bound at C2′ in the nucleotide-adenine moiety, the side chain of R109 (β2-loop-α3) clashes with the adenine ring from $NADP^+$, P187 (β4-loop-α6) clashes with the adenine ring, and the CO from E216 (β5-loop-α7) clashes with the OH group from the C2′ of $NADP^+$. During MD studies, these residues underwent conformational changes that allowed binding of $NADP^+$.

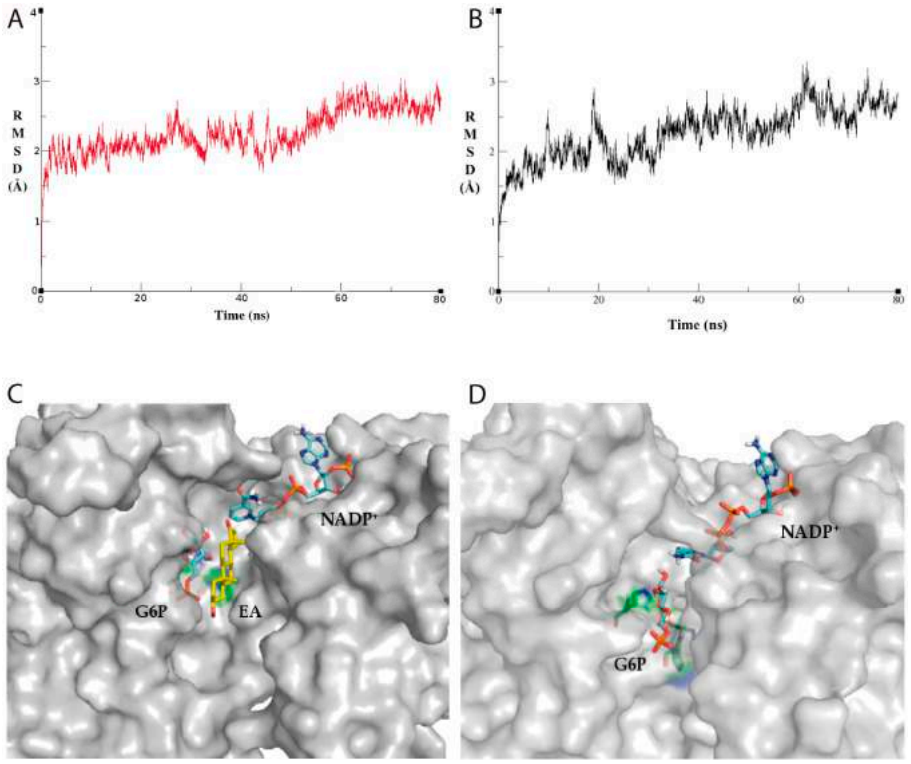

Figure S2. Molecular dynamics analysis of *Tc*G6PDH in complex with ligands. Root mean square deviation plot over 80 ns MD simulation for (**A**) the protein-G6P complex and (**B**) the protein-G6P-$NADP^+$-EA complex, where the deviation from the equilibrium observed after 50 ns correspond to the exit of EA from its binding site; (**C**) EA docking binding pose (yellow stick) in the ternary complex *Tc*G6PDH/G6P/$NADP^+$ (protein surface is depicted in gray and substrates with cyan sticks); (**D**) Conformational change of the docking complex after 80 ns MD simulation, where EA exits the complex and G6P adopts an orientation not favorable for electron exchange with $NADP^+$.

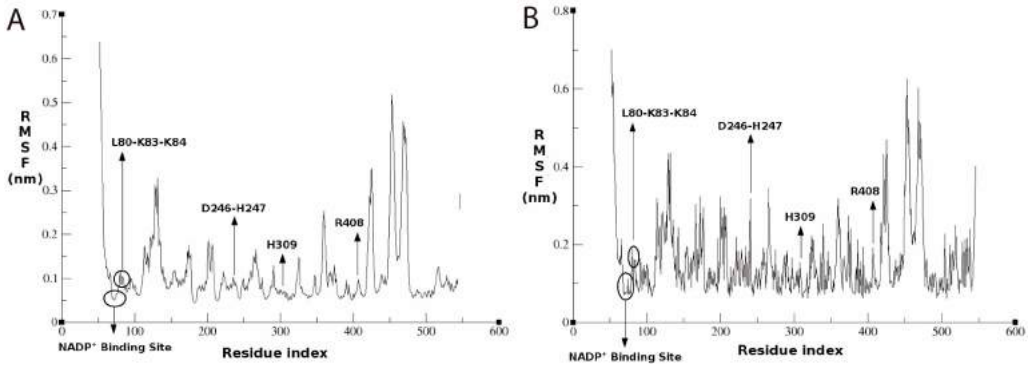

Figure S3. RMSF plots for backbone and side chains of the *Tc*G6PDH/G6P/$NADP^+$/EA complex. The computed root mean square fluctuation plots were obtained for the protein backbone (**A**) and side chains (**B**) of the holo-*Tc*G6PDH with bound EA. The high peaks (RMSF >0.1 nm for plot A or >0.17 nm for plot B) between residues 110 to 140 and residues 420 to 470 correspond to (loop rich) protein regions not engaged in ligand-binding but exposed to the solvent and participating in subunit interactions, respectively. The fluctuations encompassing the last region will be smoothed if running a simulation of the protein tetramer rather than of a single subunit (in our case chain C), but they are not expected to affect the final results since it is located far enough from the substrates- and inhibitor-binding sites. In the plots are highlighted the positions of the main residues responsible for EA binding and/or involved in catalysis (for details see text).

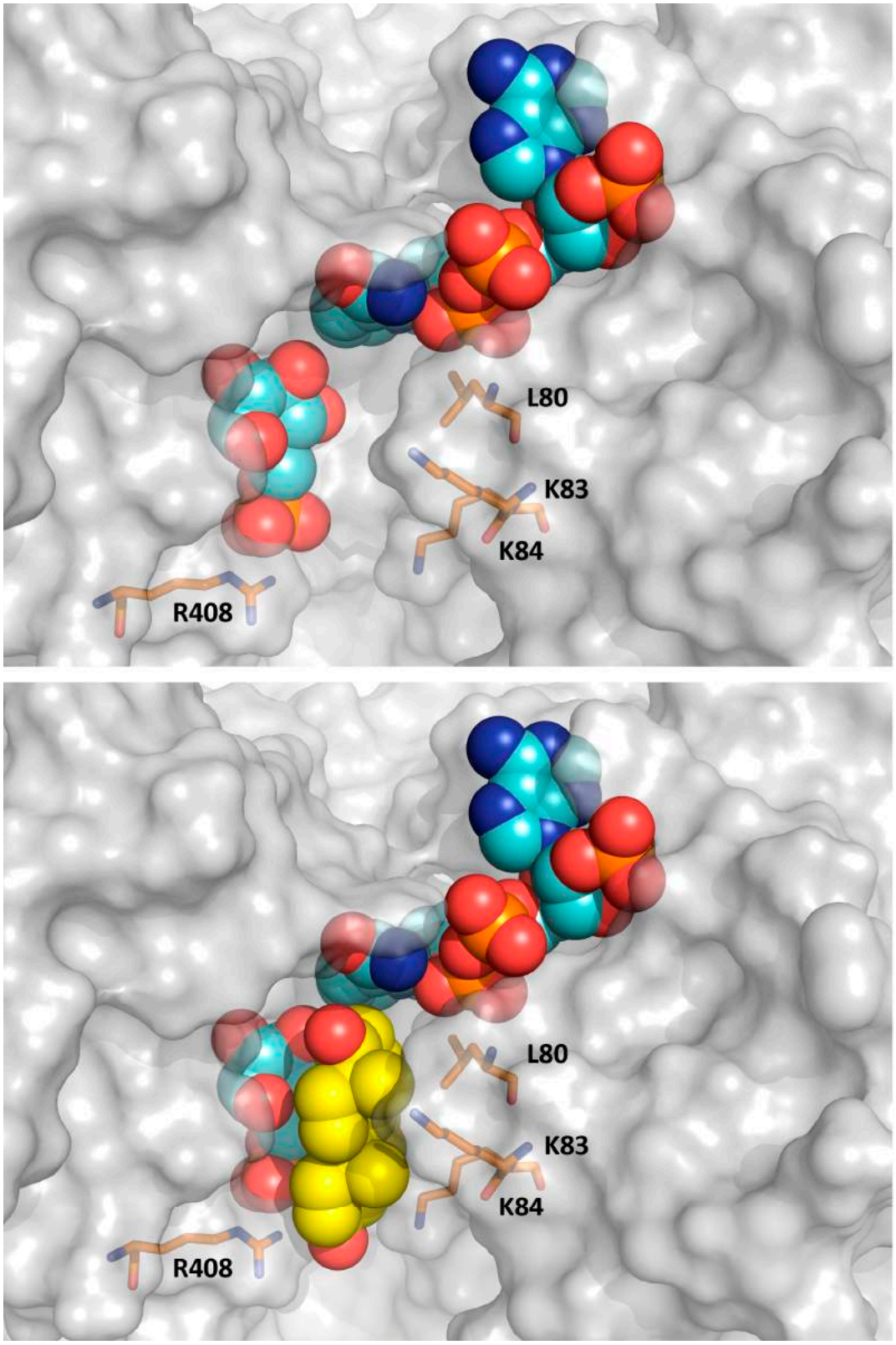

Figure S4. Binding pocket for EA in *Tc*G6PDH. Molecular model of the corresponding energy minimized quaternary complex of the enzyme (grey surface) with residues shown as bright orange sticks and substrates depicted as cyan spheres. Model without (**A**) and with docked EA (**B**), which is shown with yellow spheres.

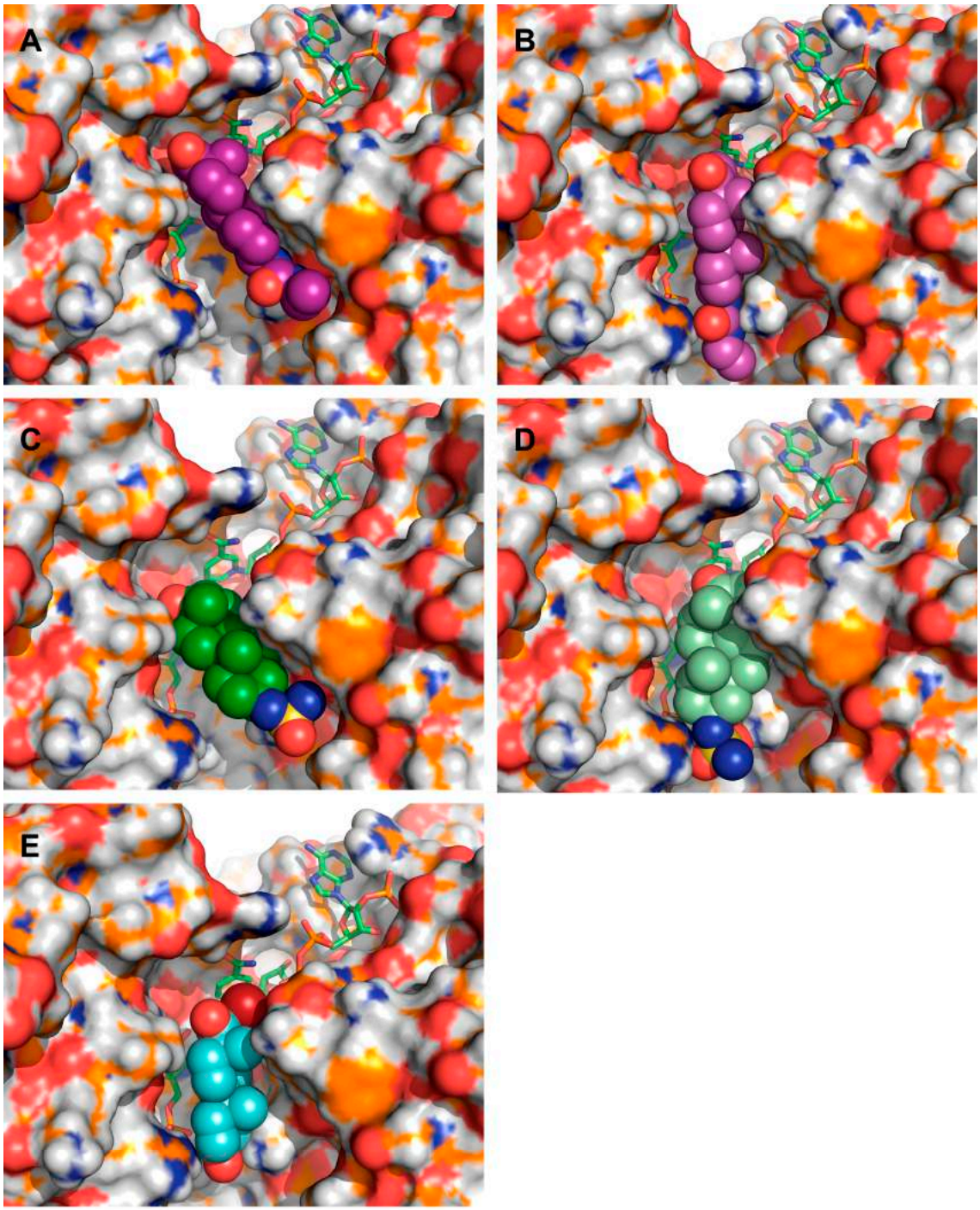

Figure S5. Binding of 3β-, 16β- and 17β-substituted androstanes to the catalytic complex of *T. cruzi* G6PDH. This figure is a replica of Figure 4 with *Tc*G6PDH shown as surface, the substrates as light green sticks and the compounds (lacking hydrogen atoms) as colored spheres. The most stable and alternative poses are shown for (**A**) **1** (dark purple) and (**D**) **2** (pale green) and alternative binding conformations for (**B**) **1** (pale purple) and (**C**) **2** (dark green); (**E**) Best docking pose for 16Br-EA, shown as light blue sphere.

Glucose-6-phosphate dehydrogenase from the human pathogen *Trypanosoma cruzi* evolved unique structural features to support efficient product formation.

Cecilia Ortiz, Horacio Botti, Laverriere Marc, Alejandro Buschiazzo, Marcelo A. Comini
A ser remitido a Journal Molecular Biology

3.4 Resumen

Al inicio de este estudio se desconocían los detalles estructurales que distinguían a la G6PDH de *T. cruzi* de la contraparte humana. En este trabajo nos propusimos indagar sobre la caracterización estructural de la proteína de *T. cruzi* complementando la validación de los hallazgos con el análisis de mutantes puntuales de la misma.

El abordaje de estas interrogantes requirió la resolución de la estructura tridimensional de la proteína ya que los datos de disposición atómica nos permitirán identificar y comprender el rol de los residuos y elementos responsables del comportamiento bioquímico de esta proteína.

La resolución de la estructura de la TcG6PDH significó un gran reto, ya que nos adentrábamos en el área de la biología estructural, en aquel momento un área ajena a nuestro laboratorio. Por este motivo recurrimos a la asistencia de la Unidad de Cristalización de Proteínas del Institut Pasteur de Montevideo, donde recibí entrenamiento práctico el cual complementé a través de mi participación en cursos específicos.

A su vez buscamos proporcionar una visión más amplia acerca de los elementos reguladores y / o estructurales identificados en la estructura para evaluar su potencial como blancos estructurales para el diseño selectivo de fármacos. Para ello recurrimos al estudio bioquímico y cinético de mutantes de sitio activo, de interfase de tetramerización y de regulación redox. Los mismos fueron realizados en nuestro laboratorio y parte en La Universidad de Heidelberg (Alemania) en el marco de una pasantía.

A nivel biológico decidimos explorar la localización subcelular de la proteína en el estadío no infectivo del patógeno mediante técnica de inmunofluorescencia. Además, con el fin de contar con un ensayo que posibilite determinar la actividad de G6PDH a nivel intracelular, el cual podría ser empleado para el cribado o caracterización de compuestos inhibidores de la TcG6PDH es que trabajamos en la puesta a punto de un ensayo citoquímico previamente desarrollado para células de mamífero. Este ensayo lo validamos empleando como a la EA como inhibidor control.

En este trabajo se presenta la resolución de las estructuras 3D de G6PDH de *T. cruzi* tanto para su forma apo como en presencia de G6P. El abordaje estructural y bioquímico empleado en este trabajo nos permitió realizar una comparación exhaustiva y detallada con su contraparte humana. Dicha comparación evidenció la existencia de características estructurales y funcionales distintivas entre ambas enzimas que en un futuro podrían ser explotadas en el diseño racional de inhibidores selectivos.

La G6PDH es una enzima alostérica cuya funcionalidad requiere como unidad mínima, la formación del dímero. En el caso particular de la enzima de *T. cruzi* pudimos comprobar que la misma forma tetrámeros, a partir de la unión no covalente de dos dímeros, muy estables. Esto la distingue de la proteína humana, cuya estructura cuaternaria se haya en un equilibrio dinámico entre especies mono-, di- y tetraméricas. Demostramos que gran parte de la estabilidad que presenta la conformación tetramérica de la TcG6PDH radica en la presencia de un residuo de arginina (R323) que forma puentes salinos con D332 y E333 de una subunidad opuesta. Este residuo positivo se haya sustituido por una alanina en la proteína humana. También demostramos que dicho arreglo cuaternario mejora la eficiencia catalítica y afinidad por sustrato de la TcG6PDH respecto de su forma dimérica, y propusimos que esto se debe a que el puente salino entre dímeros estabiliza la región E285-R318, contigua a R323, la cual contiene residuos involucrados en la unión de G6P y en la catálisis.

En su forma dimérica, la proteína humana estabiliza su conformación activa mediante la unión de $NADP^+$ a un segundo sitio unión que difiere del catalítico. El mismo se localiza en el dominio C-terminal y actúa de manera alostérica, estabilizando los residuos que interactúan con G6P y que participan de la catálisis. De los 11 residuos que participan de la unión de este $NADP^+$ alostérico, solo 8 se encuentran conservados en la proteína de *T. cruzi*. Probamos que, la reconstrucción parcial del mismo en TcG6PDH induce una leve mejoría de los parámetros cinéticos del dímero pero no es suficiente para restaurar completamente los mismos a los valores observados en la forma tetramérica de la proteína. Esto nos llevó a plantear que la enzima del parásito puede prescindir de dicho sitio alostérico debido a la estabilidad funcional que le confiere su conformación tetramérica. Por otro lado, el alto grado de conservación de residuos básicos ocupando el equivalente a la posición 323 de TcG6PDH y la ausencia de sitios completos de unión a $NADP^+$ estructural en las G6PDH de la mayoría de los kinetoplastos, de alguna manera destaca el carácter evolutivo común de esta característica en este linaje de organismos.

Adicionalmente, pudimos identificar al menos uno de los grupos tiol que participa en la regulación redox de la TcG6PDH, la cisteína 8. Este residuo se encuentra en una extensión N-terminal muy dinámica y exclusiva de la enzima de *T. cruzi*, y su oxidación conlleva la formación de un disulfuro intermolecular capaz de modular favorablemente la unión de sustrato y la catálisis en condiciones oxidantes.

Con respecto a la localización subcelular de la proteína, nuestros datos indican que en la forma no infectiva del parásito la proteína presenta una localización predominantemente citosólica. Por otro lado, logramos establecer un ensayo citoquímico para evaluar la actividad de la enzima a nivel intracelular.

A partir de los resultados obtenidos podemos decir que a diferencia de la G6PDH de su hospedero, la enzima de *T. cruzi* eludió los problemas de estabilidad que conlleva la conformación dimérica introduciendo una arginina en la interfase dímero-dímero consiguiendo así una conformación tetramerica altamente estable y funcional. Por otro lado, la presencia de una región N-terminal que modula la actividad de la enzima frente al estado redox intracelular ciertamente le ha conferido ventajas adaptativas al parásito para hacer frente a la producción de poder reductor cuando las condiciones ambientales resultaran adversas (respuesta inmune del huesped) o bien existiera una alta demanda metabólica (proliferación) por el mismo.

Mis contribuciones:

Realización de experimentos
Aanálisis de resultados
Escritura del artículo

Glucose-6-phosphate dehydrogenase from the human pathogen *Trypanosoma cruzi* evolved unique structural features to support efficient product formation.

Cecilia Ortíz[1], Horacio Botti[2], Laverriere Marc[3], Alejandro Buschiazzo[2], Marcelo A. Comini[1]

[1] Laboratory Redox Biology of Trypanosomes and [2] Protein Crystallography Unit, Institut Pasteur de Montevideo, Mataojo 2020, 11400-Montevideo, Uruguay. [3] Instituto de Investigaciones Biotecnológicas IIB-INTECH, Universidad Nacional de San Martín - CONICET, Buenos Aires, Argentina.

Running title: *Trypanosoma cruzi* G6PDH

Corresponding author: Dr. Marcelo A. Comini, Laboratory Redox Biology of Trypanosomes, Institut Pasteur de Montevideo, 11400-Montevideo, Uruguay. Telephone: 00598-25220910 extension 164; FAX: 00598-2522 4185; E-mail: mcomini@pasteur.edu.uy

Articles 40 pages, with no more than 10 figures and 4 tables.

ABSTRACT

Glucose-6-phosphate dehydrogenase (G6PDH) is the metabolic gateway to produce reducing power (NADPH) and ribose-5-phosphate from glucose. G6PDH has been rated as an indispensable virulence factor for pathogenic trypanosomatids. Here we investigated the biochemical and structural features that distinguish G6PDH of the pathogen *Trypanosoma cruzi* (*Tc*G6PDH) from its human homologue. As judged by size exclusion chromatography run under different (bio)chemical conditions, *Tc*G6PDH, at variance with human G6PDH, presents a highly stable tetrameric conformation. Site directed mutagenesis revealed that a Kinetoplastid-specific arginine (position 323 in *Tc*G6PDH) localized in the dimer-dimer interface contributes with two additional salt bridges per subunit to stabilize the tetramer. In contrast to human G6PDH, dimerization of *Tc*G6PDH affected negatively enzyme activity, which was, to some extent, abrogated by partial reconstruction of an allosteric NADP-binding site in the C-terminal domain of the protein. A fraction of the dimer subunits were linked by disulfide bridges between a cysteine from the parasite-specific N-terminal extension (C8) and a second putative thiol group. Kinetic analysis performed with the wildtype protein under reducing conditions and the C8S mutant confirmed the regulatory role played by this residue and region on enzyme activity. Analysis of a biochemically validated model of the ternary complex suggests that the N-terminal and active site of *Tc*G6PDH are highly dynamic regions. Cell-based assays revealed that G6PDH is predominantly a cytosolic protein in the non-infective form of *T. cruzi* targeted by the inhibitor epiandrosterone. *Tc*G6PDH evolved unique structural and functional features that may be exploited for the design of specific inhibitors.

HIGHLIGHTS (max. 85 characters per bullet point including spaces); only the core results of the paper should be covered.

● A structure-function study for *T. cruzi* G6PDH was missing

● *Tc*G6PDH is a highly stable tetramer linked by electrostatic interactions

● Oxidative activation of *Tc*G6PDH implies formation of an intersubunit disulfide

● Residues involved in allosteric regulation of *Tc*G6PDH activity were identified

● Selective drug design should exploit the peculiar structural features of *Tc*G6PDH

KEYWORDS: NADP, pentose phosphate, virulence, Chagas disease, steroid

ABBREVIATIONS

G6P, glucose 6-phosphate; G6PDH, glucose 6-phosphate dehydrogenase; *T.* cruzi, *Trypanosoma cruzi*; *Tc*, *Trypanosoma cruzi*; Δ37N, deletion mutant lacking the first 37 N-terminal residues; Δ57N, deletion mutant lacking the first 57 N-terminal residues; SEC, size exclusion chromatography; CTC, mM cyano-ditolyl-tetrazolium chloride; DTT, dithiotreitol; PPP, pentose phosphate pathway;

INTRODUCTION

Parasitic diseases caused by the genus *Trypanosoma* and *Leishmania* are among the most prevalent and devastating zoonotic infections in tropical and subtropical regions of the world. In America, *Trypanosoma cruzi* is responsible for Chagas´ disease, a disease that invariably develops into a highly disabling chronic stage characterized by the progressive compromise of vital organs (e.g. heart, digestive tract). The infective form of the parasite must withstand the action of harmful reactive oxygen and nitrogen species produced by the host immune system. Inside the host, the parasite invades distinct cell types, where it differentiates to the proliferative amastigote form. Both, protection against radicals and oxidants as well as cell proliferation require the supply of reducing power in the form of NADPH (1,2). To fulfill this demand, the pathogen is endowed with several $NADP^+$-linked dehydrogenases that are developmentally regulated (3–8). Among them, glucose-6-phosphate dehydrogenase (G6PDH) plays a housekeeping role in the generation of NADPH in trypanosomes (9). G6PDH is the first enzyme from the oxidative branch of the pentose phosphate pathway (PPP), a pathway that also provides essential nucleotide precursors and phosphorylated sugar intermediates (10). Initial investigations on carbohydrate metabolism demonstrated that the PPP is operative in all life stages of *T. cruzi* (4,11,12). So far, the subcellular localization of G6PDH was reported only for *T. brucei* (13)(Heise et al. 1998…es del 99 no del 98). Cell-fractionation and digitonin titration of non-infective parasites revealed an almost homogenous distribution of the enzyme between cytosol and glycosomes (parasite-specific organelles hosting several glycolytic enzymes among other metabolic pathways). Several works highlighted a relationship between higher glucose consumption *via* the PPP and increased levels of G6PDH with strain virulence and parasite infectivity (4,8,12,14–16). For *T. cruzi* has been reported an increased G6PDH activity upon oxidative insult and a higher content of the enzyme in the clinically relevant stages of the parasite (8). G6PDH has been validated as indispensable for the *in vitro* survival of *T. brucei* (17) and, more recently, it has been been shown to confer *Leishmania* with protection

towards reactive oxygen species and resistance against several drugs in clinical use (sodium antimony gluconate, amphotericin-B and miltefosine) (16). These overwhelming biological evidences rate G6PDH as an interesting drug target candidate. In this regard, chemical validation of the parasite enzyme in rats infected with *T. cruzi* and treated with steroid precursors (18), some of which are known G6PDH's inhibitors (19–21), remains controversial (22,23).

G6PDH from different trypanosomatids have been shown to share kinetic constants for substrates of the same order of magnitude (8,13,19,24), which indicates an overall conservation of the major catalytic and ligand-binding residues. Interestingly, the *T. cruzi* enzyme is sensitive to inhibition by product (NADPH) and is inactivated by reducing agents (8), though the mechanistic details of this redox-based regulation are unknown. We have reported the crystallization of a truncated form of *Tc*G6PDH lacking the non-conserved N-terminal tail (Δ37N-*Tc*G6PDH) in its apo and substrate-bond form (25). Based on these structural coordinates, recently, the crystal structure of an even shorter deletion mutant of *Tc*G6PDH (Δ57N mutant) in complex with G6P and NADPH was described (26). In solution and crystalline forms, both truncated proteins displayed a tetrameric conformation. This differs from the prevalent dimeric conformation reported previously for *Tc*G6PDH (8) and protein homologues of different species (27–29).

In the present study we performed a comparative analysis of the G6PDH structure from the parasite and human host, and provide functional evidence of unique molecular features evolved by the pathogen enzyme through the biochemical characterization of point mutants. Models for allosteric regulation of *Tc*G6PDH are proposed. In addition, the subcellular localization and *in situ* inhibition of trypanosomal G6PDH by epiandrosterone is also presented.

RESULTS AND DISCUSSION

3D structure of Δ37N-*Tc*G6PDH, general comments

Attempts to obtain good quality crystals for the full-length form of *Tc*G6PDH (*Tc*G6PDH$_L$) failed, likely because the 37-mer N-terminal extension is highly flexible. In contrast, truncated Δ37N-*Tc*G6PDH was crystallized in its apo- and glucose-6-phosphate bound form (25), and the corresponding structures determined by X-ray diffraction at 2.85 Å (Protein Data Bank [PDB] entry 4E9I) and 3.35 Å (PDB 3EM5) resolution, respectively. In both cases the asymmetric units contained four molecules in a tetrameric arrangement of dimer of dimers in a back-to-back orientation (Fig. 1A).

The noncrystallographic symmetry of the Δ37N-*Tc*G6PDH tetramer is 222 and identical to that of the human enzyme (*Hs*G6PDH; (30)). The arrangement of the dimers in the tetramer differs between both structures, with *T. cruzi* and human G6PDH having a dimer-dimer dyad axis angle of 150° and 160°, respectively (31). Nonetheless, superimposition of Δ37N-*Tc*G6PDH and *Hs*G6PDH dimers does not reveal major differences in the backbone structures (Fig 1B), indicating that tetramerization of the trypanosomal protein does not entail neither demand large structural changes at subunit level. For *Tc*G6PDH, the interface monomer-monomer occupies a surface area of 2531 Å^2 per subunit (11.2% of the total surface of the dimer) and, similar to the human protein, the interactions between subunits involve mainly hydrophobic contacts (nearly 30 hydrophobic interactions *vs.* 8 salt bridges). In contrast, the dimer-dimer interface buries a smaller surface area (672 Å^2, 3% of the total surface area) and the protein contacts are predominantly of electrostatic nature (8 salt bridges and 9 hydrogen bonds). The monomeric subunit of *Tc*G6PDH possesses two distinct domains: an N-terminal or coenzyme-binding domain (residues 1–246) and a C-terminal or dimerization domain (residues 251–555) connected by a short α-turn (residues 247-250) (Fig. 2). The coenzyme domain present the typical nucleotide binding fold (β-α-β Rossmann fold) consisting of a β-sheet formed by 6 β-

strands (β1-β6, starting at residue 66) and surrounded by 6 α-helices (α1-α6). The dimerization domain is larger than the N-terminal domain and adopts a half-barrel conformation that comprises 9 antiparallel β-strands, connected by, mainly, loops and 10 α-helices (Fig. 1C). The C-terminal domain also contains residues participating in G6P binding (Fig. 1C and Fig. 2). All subunits from the different crystals lack continuous electron density for residues from the N-terminus (e.g. amino acid positions 38–52), which indicates that this region of the protein is not ordered or highly flexible. Attempts to improve electron density maps and data resolution were unsuccessful. Superposition of the monomer structures shows little difference between the apo- and substrate-bound forms of Δ37N-*Tc*G6PDH, with an overall root mean square difference in Cα coordinates of 0.78 Å over all 332 residues that are part of secondary structures. The largest local differences are in solvated loop regions and areas involved in crystal packing.

*Tc*G6PDH$_L$ forms highly stable tetramers in solution

Human G6PDH has been shown to exist in a dynamic equilibrium between monomer (inactive), dimer (active) and tetramer (active), which is influenced by the physicochemical conditions of the media and by ligands (32,33). The oligomeric conformation adopted by the active form of *Tc*G6PDH remains controversial with a study proposing that full-length and Δ37N-*Tc*G6PDH are dimeric proteins (8) and others showing that different truncated forms of *Tc*G6PDH are tetrameric either in solution and crystalline forms (25,26). This controversy prompted us to revisit this question by subjecting *Tc*G6PDH$_L$ to gel filtration analysis and by investigating the structural basis for protein oligomerization. Taking into account that $NADP^+$ and G6P have been shown to stabilize the dimeric and monomeric forms, respectively, of human G6PDH (34–36), *Tc*G6PDH$_L$ was subjected to size exclusion chromatography (SEC) at saturating concentrations (5 mM) of these ligands (kinetic parameters of *Tc*G6PDH$_L$ reported in Table 1). None of the substrates modified significantly the SEC profile of *Tc*G6PDH$_L$, which

eluted from the column with retention volumes (11.3 mL ≅ 230 kDa for $NADP^+$ and 10.8 mL ≅ 286 kDa for G6P) similar to that of the tetrameric apo-protein (11.2 mL ≅ 240 kDa; Fig. 3 A). Neither the inhibitor DHEA altered the migration of *Tc*G6PDH$_L$ during gel filtration (retention volume of 11.2 mL). For *Hs*G6PDH, a high ionic strength or the removal of Mg^{++} ions from the medium led to protein dimerization (37). The tetrameric conformation of *Tc*G6PDH$_L$ was also refractory to high ionic strength and to the absence of Mg^{++} in the medium, since SEC performed in the presence of 1 mM NaCl or in a buffer lacking the divalent cation rendered retention volumes (11.2 mL and 10.8 mL ≅ 286 kDa, respectively) that resembled that of the untreated sample (11.2 mL, Fig. 3B).

*Tc*G6PDH$_L$ harbors 11 cysteine residues (four more than *Hs*G6PDH) with only one (C244 in *Tc*G6PDH) sharing a conserved position in the human protein (Fig. 2). Only seven cysteine residues are recognized in the structure of Δ37N-*Tc*G6PDH and none of them is engaged in inter-subunit disulphide bonds neither are at distances suitable for their formation (Fig. S1). The remaining four cysteines are placed in highly flexible terminal regions of the protein (C8, C34 and C53 at the N-terminal region, and C552 near the C-termini) for which a conformation is difficult to predict and, hence, may eventually take part in covalent interactions as suggested by inactivation of *Tc*G6PDH$_L$, but not of the Δ37N truncated mutant, by treatment with reducing agents (8). Thus, a potential role of cysteine residues in *Tc*G6PDH$_L$ tetramerization was investigated. Interestingly, SDS-PAGE analysis of *Tc*G6PDH$_L$ shows that under reducing conditions the protein migrates as a single band of ~60 kDa whereas under non-reducing conditions it separates into a heterogeneous population of species linked by intermolecular disulfide bridges with a predominant band of ~120 kDa that correspond to a dimer of G6PDH (Fig. 3C). An identical analysis performed with Δ37N-*Tc*G6PDH showed that independently of its redox state the protein migrates as a single band of ~55 kDa, in full agreement with the estimated molecular weight of the monomer (58 kDa). This result clearly shows that at least C8

and/or C34 participates in disulfide bond formation. Gel filtration of *Tc*G6PDH$_L$ under reducing conditions (DTT 5 mM) confirmed that the tetrameric assemble of the enzyme in solution does not rely on the formation of disulfide bonds between dimers (Fig. 3B). Altogether this suggests that the covalent link involving the N-terminal extension of *Tc*G6PDH$_L$ occurs between subunits of the dimer (addressed later).

Finally, while exposure of *Tc*G6PDH$_L$ to the ionic detergent SDS (3.5 mM) did not entail changes in the migration pattern of the protein during gel filtration (retention volume of 10.8 mL ≅ 286 kDa), SEC in the presence of the non-ionic detergent Triton X-100 (0.1 % v/v) was accompanied by the disappearance of high molecular weight oligomers (> 300 kDa for retention volumes <10.8 mL) and a widening of the protein peak towards retention volumes corresponding to species with apparent molecular masses lower than that of the tetramer (Fig. 3B).

Taken together, this set of confirms that, at variance with the human enzyme, *Tc*G6PDH$_L$ forms highly stable tetramers in solution that are linked by non-covalent interactions.

R323 of *Tc*G6PDH is a structural determinant of protein tetramerization

Structural inspection of the dimer-dimer interface of *Tc*G6PDH reveals that the following residues participate in the formation of inter-subunit salt bridges (e.g. between chain A and chain B): R265 (with D390´), K321 (with D390´), R323 (with E332´ and E333´), D332, E333 and D390, providing thus a total of 8 electrostatic contacts of this kind (Fig. 4). With the exception of R323 (replaced by Ala in *Hs*G6PDH), residues with identical electrostatic nature occupy equivalent positions in the human enzyme (Fig. 2) but only four of them are engaged in the formation of 4 salt bridges (i.e. K275 with E347´ and E287 with K290´; (33,38). R323 is located at the carboxi termini of a loop connecting α13 with α14 in *Tc*G6PDH where it interacts with D332 and E333 located in α14 from the opposite subunit, providing two additional electrostatic bonds per subunit that contribute to stabilize the tetrameric conformation of the trypanosomal

protein. For *Tc*G6PDH, the remaining two salt bridges are provided by the pairs R265/D390´ and D390/R265´. First, in order to verify the electrostatic nature of the forces involved in dimer-dimer interactions, *Tc*G6PDH$_L$ was gel filtrated at pH 5.5, which resulted in the protein eluting with a higher retention volume (11.8 mL) and a lower apparent molecular mass (168 kDa) with respect to the sample run at physiological pH (retention volume of 11.2 mL ≅ 240 kDa; Fig. 3D). In principle, this data suggest a partial dissociation of the *Tc*G6PDH tetramer. Next, to investigate the role of R323 in the tetrameric conformation of the protein, this residue was replaced by a glycine, which increased the retention volume of *Tc*G6PDH$_L$ to a value (12.5 mL) fully compatible with that of a dimeric species (estimated apparent mass of 135 kDa *vs.* theoretical mass of 127 kDa for the His-tagged *Tc*G6PDH$_L$ dimer). Because the elution pattern of R323G *Tc*G6PDH$_L$ in SEC did not change significantly under reducing conditions (DTT 5 mM; retention volume of 12.7 mL or 124 kDa), this demonstrates that the intermolecular disulfide previously identified occurs within and not between dimers.

Taking the sequence of *Tc*G6PDH as reference, database search and analysis of homologues from Kinetoplastids showed the strict conservation of a positively charged residue (R >> K) at position 323 and of the pair D332/E333 in the majority of the species (36 out of 40) with the exception of *L. enrietti*, *C. fasciculata* and *Leptomonas* spp. that presented Q/S/N substitutions at position 323 (Fig. S2). Interestingly, all these species are not pathogenic to humans. The absence of positively charged residues occupying a similar position in protein homologues from other lineages (Fig. 2) strongly suggests that this is a unique feature evolved by most Kinetoplastid G6PDH. Furthermore, modeling of G6PDH from *T. brucei* and *L. mexicana* confirmed that all electrostatic contacts described for the *T. cruzi* enzyme are conserved (not shown), which led us to propose that Kinetoplastids G6PDH containing the triad R or K, D/E will form stable tetramers.

Allosteric role of R323 on *Tc*G6PDH activity

As mentioned before, human G6PDH exhibits higher activity in its dimeric form (39). In order to stabilize this conformation, *Hs*G6PDH evolved an allosteric binding site for $NADP^+$ on the C-terminal part of the dimerization domain (30,36). Although the overall backbone structure of this $NADP^+$-binding site as well as several key residues for the interaction with the cofactor are conserved between the human and *T. cruzi* enzyme (26), *Tc*G6PDH lacks three residues key for binding the adenine-phosphate moiety of the cofactor (Y503, K366 and R487 for *Hs*G6PDH replaced by T544, L409 and C528 in *Tc*G6PDH, respectively) (38). This possess the question whether dimeric *Tc*G6PDH can equally sustain an efficient catalytic activity. Compared to *Tc*G6PDH$_L$ (99 U/mg) the specific activity of the R323G dimeric mutant was 68% lower (32 U/mg), and a similar decrease in activity was obtained for the wildtype form of the protein in an assay performed at pH 5.5 (25 U/mg), a condition that disrupt the tetrameric assembly of *Tc*G6PDH$_L$ (Fig. 3C). A more detailed kinetic analysis of R323G *Tc*G6PDH$_L$ revealed K_M values of 1421 µM and 27 µM for G6P and $NADP^+$, respectively, which compared to the values obtained for the wild-type protein (K_M^{G6P} 77 µM and K_M^{NADP+} 16 µM) were significantly higher for G6P (18-fold) than for $NADP^+$ (1.7-fold). In addition, the catalytic efficiency of the R323G mutant for the substrates was markedly lower for G6P (k_{cat}/K_M 0.0352 μM^{-1} s^{-1}) than for $NADP^+$ (k_{cat}/K_M 0.52 μM^{-1} s^{-1}) and, compared to the wildtype enzyme, this represent a 23- and 6-fold, respectively, lower capacity to process the substrates (Table 1). These results indicate that loss of the tetrameric conformation affects not only G6P binding but also catalysis in *Tc*G6PDH. Interestingly, clinical mutants of human G6PDH (R393G or R393H mutants) with an impaired binding of allosteric $NADP^+$ presented a similar increase in the K_M^{G6P} (2.5- to 13-fold) and minor (1.3-fold increase) or no changes in the K_M^{NADP+} compared to wildtype *Hs*G6PDH (36,40). Thus, it is tempting to speculate that the lack of a second binding site for $NADP^+$ in *Tc*G6PDH may account for the lower activity displayed by the dimeric enzyme. As discussed before, G6PDH from four non-pathogenic Kinetoplastids have replaced R323 by residues not capable to form

salt bridges. Strikingly, the G6PDH from these organisms have several residues of the allosteric $NADP^+$ site (i.e. R487 and W509 of *Hs*G6PDH), which suggests these proteins have retained the capacity to bind $NADP^+$ at the C-terminal domain. In an attempt to verify this hypothesis, the structural $NADP^+$-binding site of *Tc*G6PDH was partially reconstituted in the R323G mutant by replacing C528 by an arginine (C528R), a basic residue shown to be critical for $NADP^+$ binding in the human enzyme (R487 for *Hs*G6PDH; (30,38)). According to SEC, the double R323G-C528R mutation did not alter the dimeric conformation of the protein, which eluted with a hydrodynamic radius similar to that of wildtype *Tc*G6PDH$_L$ (not shown). Compared to the single R323G mutant, R323G-C528R *Tc*G6PDH$_L$ displayed improved kinetic parameters (Table 1), in particular for $NADP^+$ (K_M^{NADP+} 21 µM and $NADP^+$ k_{cat}/K_M 1.91 μM^{-1} s^{-1}), which approached those calculated for the wildtype enzyme. However, the affinity and catalytic efficiency for G6P (K_M^{G6P} 1025 µM and G6P k_{cat}/K_M 0.083 μM^{-1} s^{-1}) was not fully restored.

In this regard, structural analysis of *Tc*G6PDH$_L$ provided a plausible explanation for an allosteric role of R323 in the G6P-binding and catalytic site. R323 is located in a loop contiguous to several upstream elements, from α13 to the C-terminus of β7 (residues R323 to E285), that harbor several residues that interacts with G6P or participate in catalysis (Fig. 2 and 5). In fact, replacing H309 for a glycine (H309G) in *Tc*G6PDH$_L$ lowered by 2-fold the affinity of the enzyme for G6P (K_M^{G6P} 185 µM) but left unaffected its capacity to bind $NADP^+$ (K_M^{NADP+} 18 µM), and, more remarkably, it lowered 2 orders of magnitude the k_{cat} (Table 1). Thus, we hypothesize that the salt bridges between R323 and D332/E333 stabilize the loop containing this arginine and, hence, the adjacent structural elements in the sequence. Exemplified by the mutant R323G, the loss of these interactions, together with other conformational changes that probably accompany protein dimerization, would free the loop containing R323, which will translate into a loosen conformation of the adjacent regions involved in G6P binding (i.e. E285 in the β7-α12 loop and D304 in α12) and catalysis (i.e. H309 in α13). Thus, although R323G *Tc*G6PDH can still bind G6P, it probably does it in a conformation or distance not suitable for catalysis. In addition, a

catalytically competent positioning of H309 may not be reached in this dimeric protein. On the other hand, several residues that participates in binding the structural $NADP^+$ in the human enzyme (i.e. K238, K366 and R393 for *Hs*G6PDH, or K284, L409 and R435, respectively, for *Tc*G6PDH) are adjacent to amino acids interacting with G6P (i.e. E239, R365 and Q395 for *Hs*G6PDH, or E285, R408 and Q437, respectively, for *Tc*G6PDH). Thus, $NADP^+$ binding to this allosteric site will stabilize the interaction of these residues with G6P while restricting conformational changes of the segment E239-A277, which is the region of *Hs*G6PDH equivalent to E285-R323 of *Tc*G6PDH that host the catalytic H263 (or H309 in *Tc*G6PDH) and D258, which interacts with G6P (or D304 in *Tc*G6PDH). Altogether, this reinforces our proposal that the stable tetrameric conformation of *Tc*G6PDH surrogates the stabilizing role of the second $NADP^+$-binding site.

The N-terminal C8 is a key player in redox regulation of *Tc*G6PDH activity

Tc$G6PDH_L$ and Δ37N-*Tc*G6PDH displayed opposite sensitivities towards different reducing agents, with the wildtype enzyme being inhibited or almost fully inactivated (i.e. DTT 25 mM for 30 min) and the truncated form showing activation that was maximal in the presence of glutathione (GSH) 15 mM for 30 min (8). As shown in Fig. 3C, the N-terminal stretch of *Tc*G6PDH (residues 1-37) contains cysteine residues (C8 and C34) that participate in the formation of inter-subunit disulphide bridge(s). However, it remains elusive whether one or both residues are required for disulphide formation as well as the identity of the thiol partner from a second subunit. Based on the presence of an additional Cys (C552) in the non-structured C-terminal region of *Tc*$G6PDH_L$, C552 also emerged as a thiol partner candidate. As a first approach to identify which of these residues take part of the covalent bound and may eventually participate in the redox modulation of *Tc*G6PDH, single Cys→Ser mutants were generated (C8S, C34S and C552S) and characterized biochemically. SEC analysis confirmed that none of these mutations affected the oligomeric state of *Tc*$G6PDH_L$ (not shown) and SDS-PAGE

showed that formation of the covalent dimer was abolished for the mutant C8S but not for C34S and C552S (Fig. 7). Activity measurements revealed that while C34S (90 U/mg) and C552S (96 U/mg) retained specific activities similar to that of the wildtype enzyme (99 U/mg), the activity of the C8S mutant (65 U/mg) decreased to a value close to that determined for ∆37N-*Tc*G6PDH (73 U/mg; Table 1). Further kinetic characterization of C8S provided a clue on the protein regions that are affected by the loss of this covalent bound. The C8S mutant presented a k_{cat} similar to *Tc*G6PDH$_L$ but K_M for both substrates (K_M^{G6P} 128 µM and K_M^{NADP+} 37 µM) that were 50-70% higher than the corresponding values obtained for the wildtype protein (Table 1). Comparison of the substrates k_{cat}/K_M values for the C8S mutant (k_{cat}/K_M for G6P 0.48 μM^{-1} s^{-1} and k_{cat}/K_M for $NADP^+$ 1.54 μM^{-1} s^{-1}) *vs.* the wildtype protein (k_{cat}/K_M for G6P 0.80 μM^{-1} s^{-1} and k_{cat}/K_M for $NADP^+$ 3.25 μM^{-1} s^{-1}) highlighted a ~2-fold lower catalytic efficiency of the mutant to use $NADP^+$ and G6P (Table 1). Interestingly, for assays performed under reducing conditions also wildtype *Tc*G6PDH$_L$ presented kinetic parameters (K_M^{G6P} 318 µM and K_M^{NADP+} 82 µM and k_{cat}/K_M for G6P 0.42 μM^{-1} s^{-1} and k_{cat}/K_M for $NADP^+$ 0.64 μM^{-1} s^{-1}) similar to those of the C8S mutant, which points that except for the disulphide between C8 and a second thiol group, there is no other disulphide bridge in *Tc*G6PDH$_L$ contributing to regulation of enzyme activity. In this respect, it is important to note that the disulphide C53-C135 observed in ∆37N-*Tc*G6PDH (Fig. 6) is probably and artefact originated from the lack of a full-length N-terminal sequence since also the structure of a *Tc*G6PDH mutant lacking the first 57 residues shows a disulphide between C135 and the spatially vicinal C94 (PDB 5AQ1; (26)). Supporting this assumption, the activity of *L. mexicana* G6PDH, which lacks C8 and C34 but present conserved Cys (C56, C97 and C138, respectively) at positions equivalents to 53, 94 and 135 of *Tc*G6PDH, has been shown to be refractory to inactivation by reducing agents (8). Taking together, we can conclude that the reported activation of ∆37N-*Tc*G6PDH induced by reducing agents (8) is probably

consequence of the reduction of the C53-C135 disulphide, while the inter-subunit disulphide coordinated by C8 is critical for redox regulation of the native form of the protein.

A catalytic model of Δ37N-*Tc*G6PDH supports a dynamic conformation of the enzyme N-terminal region and active site

The lack of structural information for the N-terminal stretch of *Tc*G6PDH$_L$ hampers the elucidation of the molecular mechanism involved in the redox-mediated regulation of enzyme activity. As a preliminary approach to get a structural insight whether the N-terminal region of *Tc*G6PDH is prone to undergo conformational changes that may provide a mechanistic explanation for the redox-based regulation of enzyme activity, we compared the crystal structures of N-terminal truncated *Tc*G6PDH with bound substrates (PDB 4EM5 and 5AQ1) with a catalytic model of the enzyme obtained by molecular dynamics (41) and characterized amino acids relevant for catalysis.

The N-terminal region of G6PDH is connected to the strictly-conserved dinucleotide-binding motif G^{75}ASGDL^{80} (Fig. 2, (26)) that precedes two basic residues recently shown to engage in G6P-binding (K84) and in shaping the catalytic site of the trypanosomal enzyme (K83; (41); Fig. 6). As expected, slight deviations in the conformation and backbone structure of Δ37N- (with G6P bound) and Δ57N- (G6P + NADPH complex) *Tc*G6PDH were confined to regions directly involved in dinucleotide binding (loops: β1-α2, β2-α4, β3-α6) and in the region comprising D131-H136. The different conformations adopted by the latter region are determined by the formation of an intramolecular disulphide between C135 and C53 for Δ37N-*Tc*G6PDH or C94 for Δ57N-*Tc*G6PDH. In Δ57N-*Tc*G6PDH, the C94-C135 disulphide unwinds one turn the C-term of α6 (Fig. 6). Even in human G6PDH, which lacks disulphide bonds in this region, the segment α5-α6 appears to be highly dynamic since large changes in its secondary structure are

observed depending on the substrate bound, with $NADP^+$ stabilizing the formation of secondary structures (Fig. S3). As suggested by our biochemical data, the disulphide bridges observed in the crystals of the trypanosomal G6PDH appear to be artefacts originating from the lack of the N-terminal extension or by crystal packing. In line with this, molecular dynamics simulation of the catalytic complex for Δ37N-*Tc*G6PDH required omission of the C53-C135 bond in order to attain an energy minimized system (41). The catalytic model shows that acquisition of a catalytically competent conformation by *Tc*G6PDH does not entail major changes in the backbone structure of the N-terminal domain (except for the appearance of a short α-turn in the loop α5-α6) but is accompanied by movements of most elements listed above (i.e. loop β1-α2, α2, loop β2-α4 and α4-α6; Fig. 8). Taking together, this suggests that the N-terminal region of the protein presents some intrinsic dynamic, which may be modulated by substrate binding or disulphide bond formation, in the case of the trypanosomal protein.

Although for the dynamic model the binding coordinates of the substrates to most side chain residues were conserved with respect to those present in the crystal structures of *Tc*G6PDH, both ligands were positioned differently with $NADP^+$ moving about 3Å towards the catalytic site and G6P being anchored almost orthogonally and deeper in the structure core (Fig. 8). The less solvent exposed conformation observed for G6P in the simulation is facilitated by relaxation of the α-turn connecting β6-α9 (or the linker between the N- and the C-terminal protein domains), which hosts a residue, namely H247, that interacts with the phosphate groups of the substrate. The new conformation adopted by H247 pulls the sugar moiety of G6P down in the binding pocket without compromising the network of interactions required for its binding. Yet, this model, but not structural data from the crystalline forms of *Tc*G6PDH, disclosed several residues from α2 and the preceding loop (i.e. L80, K83 and K84) that proved relevant for G6P and $NADP^+$ binding (41). Another residue that in the catalytic model undergoes conformational changes is K217. This lysine is located contiguous to a proline residue (P218) that in all

subunits of apo or holo *Tc*G6PDH is invariably in *cis* conformation. This differ with data reported for human and *L. mesenteroides* where the residue has been shown to shuttle from a *trans* to a *cis* conformation upon substrate binding (38,42–45). In the *cis* conformation the ζ-NH_2 group of K217 is able to establish hydrogen bonds with G6P O1 and O2 as well as with the O1 carboxylate of D304 (Fig. 9A). According to the simulation, during catalysis a rotation in the Cβ-Cγ angle of this residue leads to loss of the interaction with D304 and to an optimal alignment of its terminal amino group for hydrogen bonding with G6P O1, the oxygen ether of the ribose bound to nicotinamide and the carboxylate of E216 (Fig. 9B). Interestingly, E216 and Y183 forms a hydrogen network that may modulate proton dissociation from K217 and, hence, a role of this residue as secondary catalytic base for hydride transfer to $NADP^+$ (Fig. 9B). Y183 is located at the C-term of β4, an element that has multiple backbone contacts with β1, which, as pointed above, is connected to the mobile N-terminal extension of the protein. Thus, subtle changes in the conformation of β1 may, at distance, affect the physicochemical properties of active site residues. The almost exclusive role of the cis-Pro in catalysis was verified by an increase in two orders of magnitude in the k_{cat} and k_{cat}/K_M for both substrates exhibited by a P218V mutant (Table 1). The impossibility of Val to adopt a *cis* conformation affects negatively the required dynamic of this region that *via* K217 contributes to the rapprochement of both substrates during catalysis. This may also explain the 1.6-fold increase in the K_M^{G6P} (123 µM) observed for P218V. Mutation of K217 to isoleucine (K217I) resulted in a <11-fold decrease in the k_{cat}, which supports a minor role of this residue in catalysis compared to P218 (Table 1). As predicted by the catalytic model, replacement of a positive charge in this position increased (3-folds) the K_M^{G6P} (226 µM) compared to the wildtype enzyme. Surprisingly, the inclusion of a hydrophobic residue in this region (P218V or K217I) had the opposite effect on the K_M^{NADP+}, which decreased 1.8-fold (K_M^{NADP+} = 9 µM) with respect to that of wildtype *Tc*G6PDH$_L$. Although this may be ascribed to a release of a structural tension imposed by the *cis*-Pro in this region, it is probably the more hydrophobic environment provided by valine or isoleucine what favours a

better anchoring of the nicotinamide ring, as shown by the loss of affinity for $NADP^+$ in a *Tc*G6PDH$_L$ lacking the vicinal L80 (41).

*Tc*G6PDH is predominantly a cytosolic protein targeted by epiandosterone

The subcellular localization of G6PDH has not been reported in *T. cruzi* neither confirmed whether the protein is the molecular target of steroids *in situ*. Western blot and immunofluorescence analysis with specific polyclonal antibodies raised against *Tc*G6PDH$_L$ failed to detect endogenous G6PDH in the non-infective form of different *T. cruzi* strains (see representative W. blot in Fig. 10A). Based on the sensitivity of the antibodies (28 ng *Tc*G6PDH), the amount of wildtype parasites required to prepare the cell extract (10 million) and the cell volume reported for *T. cruzi* epimastigotes (30 fL; (46)), we estimated that the intracellular concentration of G6PDH in this stage is lower than 2 µM. To overcome this limitation, the wildtype form of the protein was overexpressed in *T. cruzi* using a tet-inducible system ((47); Fig. 10A). Immunofluorescence performed on G6PDH-overexpressing parasites showed a predominantly cytosolic localization of the protein with a punctuated pattern (Fig. 10B and D) and no signal overlap with other compartments such as nucleus and mitochondrion (Fig. 10C and E). Furthermore, intracellular detection of G6PDH was addressed in different strains of wildtype *T. cruzi* using a modified cytochemical assay where reduction of cyano-ditolyl-tetrazolium chloride (CTC) at expense of the NADPH generated by G6PDH leads to formation of fluorescent formazan salts that accumulates at the site of activity (48). Parasites not treated with epiandrosterone (a G6PDH inhibitor) presented discrete fluorescence signals, confined to a few dots of cytoplasmic localization (Fig. 11 for strain DM28c and Fig. S4 for strain CL-Brener). These cells also presented a very weak and more homogenous CTC signal that stained the whole cytoplasm but excluded the nucleus and mitochondrion (Fig. S5). The CTC-staining pattern was similar for parasites overexpressing G6PDH (Fig. S6), except that they showed a

higher number of dots with respect to wildtype cells (Fig. 11 and Fig. S5). Treatment of the parasites for 24 h with 25 and 100 µM epiandrosterone decreased and fully inhibited, respectively, the development of CTC signal (Fig. 11 and Fig. S4), suggesting inhibition of G6PDH activity. Parallel determinations of G6PDH specific activity in cell extracts of these samples confirmed a concentration dependent reduction of enzyme activity with respect to the un-treated control for both parasite strains (Fig. 11 and Fig. S4). This further confirmed the specificity of the signal observed in the cytochemical assay. Rather than a specific subcellular compartmentalization of G6PDH in the parasites (e.g. glycosomes), the accumulation of CTC signal appears to be an artifact of the technique since also a similar dotted pattern was reported for the G6PDH activity of a sarcoma cell line from rat (48).

In summary, we confirmed a cytosolic distribution of G6PDH in the epimastigote form of different strains from *T. cruzi* as well as its *in situ* inhibition by epiandrosterone.

CONCLUSIONS

The strong evidences supporting an important biological role of the enzyme in the redox homeostasis and drug resistance mechanisms of the parasite (8,16,20) have led to rate this enzyme as an appealing drug target candidate to fight trypanosomatid diseases. The recent elucidation of the 3D structure of G6PDH from *T. cruzi* (25,26,41) allows for a thorough structural comparison with the human counterpart in order to disclose exclusive structural features of the pathogen enzyme that may be exploited for the design of selective inhibitors. In this regard, our study revealed that *Tc*G6PDH presents several exclusive structural and functional features. For instance, in contrast to the highly dynamic oligomeric conformation of the human enzyme (49), *Tc*G6PDH forms stable tetramers. A single residue (R323) has been identified as major determinant for the interaction dimer-dimer in the trypanosomal protein. Importantly, conversion of *Tc*G6PDH into a dimeric species was detrimental for enzyme activity.

In this regard, our data suggests that the protein-protein contacts established *via* the R323 salt bridge are important to stabilize the loop containing this residue and, hence, the upstream elements (segment E285-T318) that contain amino acids engaged in G6P binding or catalysis. In the human protein, the structure and activity of the dimer is stabilized by the presence of a second binding site for $NADP^+$ located in the antiparallel β-sheet of the C-terminal domain. Several residues interacting with this allosteric $NADP^+$ are next to others that interact with G6P, which explains the stabilizing role of the dinucleotide cofactor in catalysis (30). *Tc*G6PDH shares with the human enzyme 8 out of the 11 residues forming the allosteric-$NADP^+$ binding site (38) and partial reconstruction of this site in the dimeric form of the trypanosomal protein improved, to some extent, its kinetic parameters. The inability of the R323G/C528R mutant to completely restore the altered kinetic parameters of the dimer suggests that the conformational changes induced by protein dimerization at the ligand and active site are large enough to be compensated only by the allosteric mechanism evolved by the human enzyme. Interestingly, R323 (and the corresponding negatively charged residues needed for the inter-subunit salt bridge, D332 and E333) is highly conserved in G6PDH from most Kinetoplastid and absent in several representatives from different Phyla. Thus, it is tempting to propose that G6PDH from most Kinetoplastids circumvented the stability problems that a dimeric conformation may entail by introducing a single mutation in a region of the dimer-dimer interface, which will confer the protein a highly stable oligomeric conformation and activity. In line with this, a stable tetramer of *Hs*G6PDH engineered by introducing covalent links (Cys residues) at the dimer-dimer interface yielded a more active enzyme (33).

The stable tetrameric conformation evolved by the trypanosomal protein, which contrast with that of the human counterpart, raises interesting questions about the evolutionary scenario leading to these divergent peculiarities. Several lines of evidence support that G6PDH-deficiency in humans coevolved with Malaria parasitism to destabilize enzyme activity in order

to prevent red blood cell colonization by Plasmodium (50). Indeed, some of the most severe clinical manifestations associated to this enzymopathy originate from mutations of residues from the structural-$NADP^+$ binding site (51–53). In contrast, *T. cruzi* evolved a highly stable and redox-inducible tetrameric G6PDH to support the metabolic needs of it challenging life cycle. Strikingly, a few non-pathogenic species of Kinetoplastids (*Leptomona* spp., *Leishmania enrietti* and *Crithidia fascitulata*) lack a basic residue at the position of R323 but present a higher degree of conservation at the structural $NADP^+$ binding site (9 out 11 residues). Future studies should address whether these proteins display a biochemical behaviour similar to that of the human enzyme and, if so, whether the tetrameric conformation of trypanosomatids´ G6PDH along with loss of binding the structural-$NADP^+$ can be associated to the acquisition of a parasitic life style.

The *T. cruzi* enzyme also developed an additional regulatory mechanism to warrant the production of reducing power under oxidative stress. Under reducing conditions *Tc*G6PDH$_L$ shows K_M for both substrates that are 2- to 4-fold higher than those displayed under non-reducing conditions. Interestingly the catalytic capacity (k_{cat}) of the enzyme under these redox conditions varied less than 2-fold and followed the opposite trend to the changes in K_M, indicating that upon oxidative activation *Tc*G6PDH$_L$ attains to increase substrate affinity over catalysis. C8 was identified as the thiol group from the N-terminal extension of *Tc*G6PDH$_L$ that participates in the formation of an intermolecular disulphide between subunits of the dimer and, hence, in the redox regulation of enzyme activity. In fact, elimination of this residue increased the K_M and lowered the catalytic efficiency of the enzyme for both substrates to values close to those obtained for the wildtype protein under reducing conditions. Also the altered kinetic parameters displayed by the truncated mutant Δ37N-*Tc*G6PDH highlighted the potential role of the N-terminal extension in modulating substrate binding and catalysis. The N-terminal domain of host and pathogen G6PDH appears to be a dynamic region of the protein that host several

residues involved in ligand binding and catalysis, and whose conformation may be modulated by formation of intra- (e.g. Δ37N- and Δ57N-*Tc*G6PDH) or inter-molecular disulfides (C8 in *Tc*G6PDH$_L$) and ligand binding (e.g. *Hs*G6PDH). The activity of plastidic isoform of G6PDH from plants and cyanobacteria has been shown to be subject to redox control that respond to the needs of reducing power in the Calvin cycle for carbon fixation (54–56). The cysteine residues responsible for this regulation are not conserved for these organisms neither with *Tc*G6PDH, which rules out a plastidic origin for the trypanosomal protein, as proposed for several other important metabolic proteins (Hannaer et al 2003). The precise molecular events behind the redox-dependent regulation of *Tc*G6PDH$_L$ activity are unknown. However analysis of structural models and the kinetics of point mutants led us to propose that reduction of the disulphide bridge between C8 and a second putative Cys from other subunit will distort the conformation of the mobile N-terminal extension of *Tc*G6PDH$_L$, which may translate into changes in the structural dynamic properties of the contiguous elements involved in ligand binding and/or in modulating accessibility of the substrates to their corresponding binding sites.

An important secondary conclusion from this study is that although the truncated forms of *Tc*G6PDH retain activity, the structural conformation adopted by some elements from the N-terminal domain may not fully reflect the spatial disposition they will present in the full-length protein. This claim is supported by the subtle but different kinetic parameters displayed by these proteins, the appearance of non-specific intramolecular disulphides and the conformational changes that substrates and several structural elements underwent in a validated molecular dynamics model of the ternary complex.

As described previously (25,26), human and *T. cruzi* G6PDH shares a highly conserved backbone structure and except for the molecular features presented in this and a prior study with inhibitors (41), there appear not to be additional and exclusive structural hallmarks in the parasite protein. Although rational drug design against G6PDH from trypanosomatids deems

challenging, our study provide insight into the several regulatory and/or structural elements that may be selectively targeted in the pathogen enzyme.

EXPERIMENTAL PROCEDURES

Reagents

Molecular biology reagents were purchased from Fermentas (Thermo-Fisher Scientific), New England Biolab, Stratagene and Invitrogen. Chemical reagents were of analytical or higher grade and obtained from Sigma-Aldrich or AppliChem. Antibiotics were purchased from Invitrogen and Sigma-Aldrich. Oligonucleotides were synthesized by IDT. The kits for DNA purification were from Sigma-Aldrich and Invitrogen. All protein purification resins and columns were from General Electric Healthcare Life-Sciences (GE). The brain heart infusion (BHI) broth and additives from the cell culture medium were purchased from Sigma-Aldrich, and tetracycline-free certified fetal calf serum was from PAA Laboratories.

Plasmids

The constructs for the expression of N-terminally His-tagged full-length (*Tc*G6PDH$_L$; Accession Nr. ABD72517.1) and truncated mutant lacking the first 37 amino acids (Δ37N-*Tc*G6PDH) of *T. cruzi* G6PDH were kindly provided by Dr. J. J. Cazzulo (Universidad Nacional de San Martín-CONICET, Argentina; (8)). The single Cys^{8}Ser, Cys^{34}Ser, Lys^{217}Iso, Pro^{218}Val, His^{309}Gly, Arg^{323}Gly and Cys^{552}Ser mutants were generated by using the Quick Change site-directed mutagenesis kit (Stratagene, La Jolla, CA, USA) and the construct pET28a(+)-*Tc*G6PDH$_L$ as template with the primer pairs **Cys^{8}Ser Fwd** 5´ GGA TCG GAG AAT CGC TCC CGC TTC CAA AAG GAG 3´/ **Cys^{8}Ser Rev** 5´ CTC CTT TTG GAA GCG GGA GCG ATT CTC CGA TCC 3', **Cys^{34}Ser Fwd** 5´G GAC CAC CCG CAA GAA TTA TCT GAA TAT TTA ATG G 3´/ **Cys^{34}Ser Rev** 5´C CAT TAA ATA TTC AGA TAA TTC TTG CGG GTG GTC C 3',

Lys^{217}IsoFwd 5´GTC CGT CTC ATT GTT GAG ATT CCC TTT GGC CGG GAC ACG 3´/ **Lys^{217}IsoRe**v 5´CGT GTC CCG GCC AAA GGG TAA CTC AAC AAT GAG ACG GAC 3´, **Pro^{218}ValFwd** 5' CTC ATT GTT GAG AAG GTC TTT GGC CGG GAC ACG 3'/ **Pro^{218}ValRev** 5' CGT GTC CCG GCC AAA GAC CTT CTC AAC AAT GAG 3', or **His^{309}GlyFwd** 5' C GTG ATC CAG AAC GGC CTC ACA CAG ATT C 3' / **His^{309}GlyRev** 5' G AAT CTG TGT GAG GCC GTT CTG GAT CAC G 3', **Arg^{323}GlyFwd** 5´ ACG ATG GAA AAG CCG TGT TCA CTC AGT GCT GAG 3´/ **Arg^{323}GlyRev** 5´ CTC AGC ACT GAG TGA ACA CGG CTT TTC CAT CGT 3´, **Cys^{552}SerFwd** 5´ GGC AAC GCA TAT AAG AGC TCA AAC GCG 3´, **Cys^{552}SerRev** 5´ CGC GTT TGA GCT CTT ATA TGC GTT GCC 3´ (underlined are indicated the mutated bases), respectively. The PCR were performed in a total reaction volume of 50 µL according to the instructions of the supplier. One Shot® MAX Efficiency® DH5α™-T1Rcellsweretransformed with the mutagenesis reaction. The correctness of the targeted mutations was confirmed in at least three independent plasmids from each construct by DNA sequencing (Molecular Biology Unit, Institut Pasteur de Montevideo, Montevideo, Uruguay). The double mutant R323G/C528R was generated using as template the plasmid containing the R323G mutation (construct pET28a(+)-R323G*Tc*G6PDH$_L$), the primers **Cys^{528}ArgFwd** 5´ CCC TAC GCG GCG GGT TCG CGC GGG CCA GAG GAA GCC 3´/ **Cys^{528}ArgRev** 5´ GGC TTC CTC TGG CCC GCG CGA ACC CGC CGC GTA GGG 3´, and the Quick Change site-directed mutagenesis kit as indicated above.

The construct for the inducible expression of *Tc*G6PDH$_L$ in *T. cruzi* was prepared by inserting the sequence of interest into the plasmid p*Tc*INDEX (47). The sequence encoding for *Tc*G6PDH$_L$ was amplified by PCR reaction using the primers *Tc*G6PDHlongFwd 5' ATG AGT GGA TCG GAG AAT CGC 3' and *Tc*G6PDHRev 5' ATT CGC GTT TGA GCA CTT ATA TGC G 3' and subcloned into a pGEM®-T easy vector (Promega). The PCR reaction consisted of 100 ng pET28a(+)-*Tc*G6PDH$_L$ as template, 24 pM of each primer, 0.4 mM dNTPs and 2.5 U Pfu DNA Polymerase (Fermentas, Thermo Scientific) in a total volume of 50 µL. The PCR program

consisted of the following steps: 95°C for 5 min; 35 cycles at 95°C for 45 sec, 55°C for 45 sec and 68°C for 2 min; 68°C for 10 min. The amplicon was purified from an agarose gel (QIAQuick PCR purification Kit, Qiagen), digested with *Not*I and ligated into *Not*I digested and dephosphorylated p*Tc*INDEX.

All constructs were subjected to DNA sequencing (Macrogen, Korea) of the complementary chains to verify the correctness of the sequences.

Expression and purification of recombinant proteins

E. coli Tuner (DE3) cells were transformed with the pET28a(+) constructs encoding for N-terminally hexa histidine-tagged Δ37N-*Tc*G6PDH, *Tc*G6PDH$_L$ and the different single and double mutants of *Tc*G6PDH$_L$. An overnight culture of transformed bacteria in LB medium with 50 µg/L kanamycin was inoculated at a ratio 1:100 in ZYM-5052 auto-induction medium added of 50 µg/L kanamycin and cell grow extended for 48 h at 25°C and 200 rpm. Cells were harvested by centrifugation (5000 rpm, 10 min, 4°C), and resuspended in 50 mM Tris, pH 8.0, 500 mM NaCl, 5 mM $MgCl_2$ (buffer A) plus 1 mM PMSF, 40 µg/ml TLCK, 150 nM pepstatin, 4 nM cystatin, and 1 mg/ml of lysozyme (lysis buffer). After disruption by three cycles of sonication (30 pulses per minute at 70% amplitude) using a macrotip in a Digital Sonifier 450 (Branson), the cell lysate was centrifuged at 5000 *g* (15 min, 4°C) and the supernatant was further cleared of debris by centrifugation at 20000 *g* (30 min, 4°C) and filtration through a 0.45 µm filter (Millipore). The cleared lysate was loaded onto a HisTrap column (GE) pre-equilibrated with buffer A. The column was washed with 10 and 5 column volume of buffer A and 5 mM imidazol in buffer A, respectively, and the protein eluted with 500 mM imidazol in buffer A. The fractions containing the recombinant protein were collected, concentrated via ultrafiltration (30-kDa filter cutoff), and run on a Superdex 200 10/300 GL column (GE) pre-equilibrated with buffer A. Fractions containing the protein of interest, as assessed by Coomasie blue stained SDS-PAGE

gels, were collected, tested for enzyme specific activity (see below), concentrated to 0.5 mg/mL and stored at 4°C. Protein concentration was determined by the bicinchoninic acid assay.

Analytical size exclusion chromatography and mass spectrometry analysis

The oligomeric state of the different recombinant proteins characterized in this work was studied by analytical gel-filtration chromatography on a Superdex 200 10/300 GL column (GE) coupled to an AKTA FPLC system (both from GE-Health Care) with online UV–visible detection. All chromatography experiments were performed at room temperature (RT) in Tris 50 mM, pH 7.5, NaCl 0.5 M and $MgCl_2$ 5 mM (reaction buffer) and at a constant flow of 0.5 mL/min. The column was calibrated under identical running conditions with molecular weight standards (ovalbumin, conalbumin, aldolase, ferritin and tyroglobulin, ranging 43–660 kDa). To test the effect of different ligands on protein oligomerization, between 50-150 µg/mL recombinant enzyme were incubated for 30 min at 4°C in reaction buffer added of 5 mM NADP, 5 mM G6P or 100 µM DHEA, and then resolved by gel filtration in reaction buffer containing the corresponding additives at identical concentrations. Similar amounts of protein were also subjected to gel filtration under different physicochemical conditions that involved the presence of a reducing agent (5 mM DTT), high ionic strength (1 M NaCl), and non-ionic (0.1 % (v/v) Triton X-100) and ionic (0.1 % (w/v) SDS) detergent. The effect of the pH in protein oligomeric structure was study using buffer MES 50 mM at pH 5.5 or 6.5 with NaCl 0.5 M and $MgCl_2$ 5 mM. Protein elution was monitored online at 280 nm. The peaks of interest were subjected to enzymatic tests (see below) and denaturing polyacrylamide gel electrophoresis (SDS 10% PAGE) under reducing (5% (v/v) ß-mercaptoethanol) and non-reducing conditions.

Crystallization and Data collection

The crystallization conditions and X-ray diffraction data collection for recombinant ∆37N-*Tc*G6PDH in its apo-form and bound to glucose-6-phosphate were previously described in Ortiz et al. (2011).

Structure determination

The structure of Δ37N-*Tc*G6PDH in its apo form was solved by molecular replacement using the human G6PDH (PDB 1qki) atomic coordinates as template model. The refinement included alternate cycles of model building using the program Coot (57) and reciprocal space refinement with the program REFMAC5 (58). Solvent molecules were added using ARP/wARP (59) and its stereochemistry and stability were checked during refinement. The model was validated with MolProbidity (60) and PROCHECK (61). The model and structural factors were deposited in the Protein Data Bank with accession number 4E9I for the apo form. The structure of the substrate-bond form of Δ37N-*Tc*G6PDH was solved using molecular replacement with the atomic coordinates and phases obtained previously for the apo-form of the protein. The reliability of the G6P model was checked with Fourier [2mFo-DFc], [mFo-DFc] and omit maps. The atomic coordinates for the model of TcG6PDH in complex with G6P were deposited in the Protein Data Bank with accession number 4EM5.

Protein assays

Protein concentration was determined by the BCA method [20; Bicinchoninic Acid Protein Assay Kit, Sigma] using bovine serum albumin (BSA) as standard. G6PDH activity was determined at ~ 25°C by monitoring NADPH (ε_{340} (NADPH) = 6,220 M^{-1} cm^{-1}) formation at 340 nm. All reactions were performed in 50 mM Tris (pH 7.5), 5 mM $MgCl_2$, in a final volume of 150 µL and started by addition of G6P. For standard assays, $NADP^+$ and G6P were used at fixed concentrations of 500 µM and 1 mM, respectively, and with variable protein concentrations (10-50 nM). For determination of the apparent Michaelis constants (K_m) and maximum initial velocities (V_{max}), each substrate was tested at five different concentrations (15 to 1000 µM for G6P and 1 to 500 µM for $NADP^+$) under fixed concentration of the co-substrate involved (1 mM for G6P and 500 µM for NADP) and at protein concentrations of 15 nM, 16 nM, 63 nM, 160 nM, 150 nM, 138 nM, 43 nM and 34 nM for *Tc*G6PDH$_L$, Δ37N-*Tc*G6PDH, C8S-*Tc*G6PDH$_L$, H309G-

*Tc*G6PDH$_L$, K217I-*Tc*G6PDH$_{L,}$ P218V-*Tc*G6PDH$_L$, R323R-*Tc*G6PDH$_{L,}$ R323R/C528R-*Tc*G6PDH$_{L,}$ respectively. The initial velocities were calculated from the first 30 sec of the reaction and normalized to the corresponding enzyme concentration in assay. All measurements were performed in triplicate using a Cary 50 Bio spectrophotometer (Agilent Technologies, Santa Clara, CA, USA at RT. The initial rates were determined with the Origin Pro 8.0 software (OriginLab Corporation, Northampton, MA, USA), and the apparent kinetic constants were calculated by nonlinear regression using the GraphPad Prism 5.0 software (GraphPad Inc., San Diego, CA, USA). The data were fitted to the Cleland or Michaelis-Menten equation to obtain the corresponding kinetic parameters. Michaelis-Menten equation

$$v = \frac{Vmax\ [S]}{Km + [S]}$$

where V_{max} is the maximum reaction rate, K_m is the Michaelis constant and [*S*] is the substrate concentration.

Trypanosoma cruzi growth and transformation

Epimastigotes of *Trypanosoma cruzi* strains Adriana (Urban et al. 2011), DM28-c and CL-Brener were grown axenically at 28°C in brain-heart tryptose medium (BHT; (62)), supplemented with 2 g/L glucose, streptomycin (100 µg/mL), penicillin (100 IU/mL), haemin (20 µg/mL), and 10% (v/v) heat-inactivated tetracycline-free foetal bovine serum (FBS; PAA, USA).

For inducible expression of *Tc*G6PDH$_L$ in *T. cruzi* strain Adriana, we first generated a cell line expressing the T7 RNA polymerase and tetracycline repressor genes by transforming non-infective parasites with the plasmid pLew13 (63). Epimastigotes in the mid-log phase were washed with and resuspended in BHT medium at a final concentration of 5x10^8 parasites/mL. Aliquots of 0.35 mL were dispensed into disposable 0.4-mm cuvettes (Bio-Rad Laboratories,

Hercules, CA, USA) containing 10 µg of plasmid DNA and electroporated using a Bio-Rad gene pulser at 335 V and 1400 mF, with two consecutive pulses. After 5 min on ice, the parasites were diluted 10-fold with BHT containing 10% FBS and allowed to recover for 24 h at 28°C before adding 200 µg/mL of Geneticin (G418; Life Technologies, Carlsbad, CA, USA). Cells stably transfected with pLew13 were then electroporated with the p*Tc*INDEX-*Tc*G6PDH$_L$ construct and transgenic parasites (named *T. cruzi* G6PDH$_L^{Ti}$) were obtained after 3 weeks of selection with 200 µg/mL G418 and 200 µg/mL hygromycin B (Calbiochem) (47). The expression of the ectopic copy of *Tc*G6PDH$_L$ was induced by growing the parasites in culture medium containing 10 µg/mL oxytetracycline (Laboratorios Microsules, Uruguay).

Western blot

Anti-*Tc*G6PDH$_L$ serum was raised in mice (strain Balbc/J) against the purified recombinant *Tc*G6PDH$_L$ using a standard immunization protocol approved by the Animal Use and Ethic Committee (CEUA) of the Institut Pasteur Montevideo (Protocol n° 005-14) and animals from the in-house *specific pathogen free* animal facility (Transgenic and Experimental Animal Unit, Institut Pasteur de Montevideo). Ten to two-hundred million epimastigotes from different *T. cruzi* strains a late exponential phase culture were harvested by centrifugation at 2000 *g* for 10 min at RT and washed twice with phosphate-buffered saline (PBS, pH 7.4), incubated 15 minutes in 10 mM Tris-HCl, 1 mM EDTA, 0.5 % (v/v) Triton X-100 at 4 °C, then centrifuged at 13000 *g* during 30 min at 4°C, and SDS-PAGE loading buffer (30 mM Tris-HCl pH 6.6, 1 % (w/v) SDS and 5 % (v/v) glycerol) was added to the supernatant followed by two freezing-thawing steps (64). Proteins from total cell extracts of tet-induced and non-induced parasites and different amounts (7, 28 and 70 ng) of recombinant *Tc*G6PDH$_L$ were separated by SDS-10% PAGE under reducing conditions and transferred to a polyvinylidene fluoride (PVDF) membrane (GE-Healthcare). The membrane was blocked with PBS-0.2 % (v/v) Tween-20 (PBS-T) added of 5 % (w/v) non-fat dry milk overnight at 4°C, washed with PBS-T and

incubated with polyclonal mouse serum anti-*Tc*G6PDH$_L$ diluted 1:1000 in PBS-T at RT for 2 h. After three washing steps with PBS-T for 5 min each, the membrane was incubated for 1 h at RT with the corresponding horseradish peroxidase-conjugated goat anti-mouse IgG (Amersham Biosciences, Buckinghamshire, England) as secondary antibody at a 1:10,000 in PBS-T. The membrane was extensively washed in PBS-T prior to chemoluminiscent detection of reactive bands with the Amersham ECL™ Western Blotting Detection Reagents (GE Healthcare) and according to the manufacturer's instructions. Finally, films (Amersham hyperfilm ECL, GE Healthcare) were exposed to the membranes during different times (1, 5 and 10 minutes) and revealed manually for 1 min in developing solution (Sigma).

Indirect immunofluorescence

Five millions *T. cruzi* G6PDH$_L^{Ti}$ epimastigotes (strain Adriana) from the late exponential growth phase grew for 24 h with or without 10 µg/mL oxytetracycline were pelleted at 2000 *g* for 10 min at RT and washed twice with PBS. For fixation, the cells were resuspended in PBS with 4% (w/v) paraformaldehyde, incubated for 18 min at RT, washed twice with PBS and resuspended in PBS at ~ 1x10^5 parasites/µL. Drops containing about 50 µL of this cell suspension were added to a polilysine treated glass slide (StarFrost, Knittel Glass, Germany) and incubated overnight at 4°C. The cells were then permeabilized with 0.2% (v/v) Triton X-100 in PBS for 20 min and washed twice with PBS. The slides were incubated at 4°C overnight and 1 h with purified mouse polyclonal anti-*Tc*G6PDH (1:1000), anti-LipDH (1/200) and rabbit anti-*Tc*TR (1:500), respectively, prepared in PBS added of 0.5% (w/v) gelatin. Then, the slides were washed with PBS and incubated for 1 h with the secondary antibody Alexa Fluor® 488-labeled goat anti-mouse IgG and Alexa Fluor® 594-labeled goat anti-rabbit IgG, respectively, both added at a final dilution of 1:1000. Nucleic acids were stained with Hoechst 3342 (Invitrogen) and cell membranes with CellMask Red (Thermofisher). The parasites were visualized with a

Leica TCS SP5 spectral confocal microscope (Cell Biology Unit, Institut Pasteur de Montevideo) and the merge images generated with the program Adobe Photoshop.

Cytochemical assay for G6PDH

The inhibition of G6PDH by epiandrosterone (EA) was addressed using non-infective epimastigotes from *T. cruzi* strain CL-Brener and DM-28c, and an optimized protocol previously described for cytochemical detection of G6PDH activity in mammalian cells (48). About 5×10^6 cells from a late exponential phase culture were treated with 0, 25 and 100 μM EA for 24 h, then pelleted at 1800 *g* for 10 min at RT and washed three times with PBS. The cell suspension was then incubated with 20 mM $NADP^+$ in buffer B (Tris 50 mM pH 7.5, 5 mM $MgCl_2$) during 20 min at 4°C. The cells were fixed in 4% (w/v) paraformaldehyde for 30 min at RT, washed twice with 0.2 % (v/v) Triton X-100 in PBS and twice with PBS. After each washing step the cells were pelleted by centrifugation at 1800 *g* during 5 min at RT. The permeabilized cells were resuspended in 100 µl of buffer B, added of 600 µL reaction buffer (10 mM G6P, 800 µM $NADP^+$, 0.3 mM phenylmethanesulfonyl fluoride, 5 mM sodium azide, 5 mM cyano-ditolyl-tetrazolium chloride and 6% (w/v) of polyvinyl alcohol, all prepared in buffer B) and incubated for 30 min at RT. The reaction was stopped with 1 mL PBS, followed by three washes in PBS and centrifugation at 1000 *g* for 3 min at RT. The parasites were resuspended in PBS at a density of 1×10^5 cells/mL and 50 µL of this suspension was added to a polylysine coated microscope slide (StarFrost, Knittel Glass, Germany), followed by incubation overnight at 4°C. Nucleic acids were stained with DAPI (Fluoroshield Histology Mounting Media, Sigma). Cell images (bright field and fluorescence) were obtained with a confocal microscope Leica TCS SP5 and further analyzed and prepared with the program ICy (65) and Adobe Photoshop CS5.

ACCESION NUMBERS

*Tc*G6PDH ID: Q1WBU6; PDB: 4E9I, 4EM5, 5AQ1; *Hs*G6PDH ID: P11413; PDB: 1QKI, 2BHL, 2BH9; *St*G6PDH ID: Q8ZNW2; c*St*G6PDH ID: Q43839; c*At* ID: Q43727, *Pf*G6PDH ID: Q8IKU0; *Li*G6PDH ID: A2CIJ8; *Lm*G6PDH ID: P11411; *Tb*G6PDH ID: Q38BZ6.

ACKNOWLEDGEMENTS

This work was supported by a grant from the Agencia Nacional de Investigación e Innovación (ANII; Innova Uruguay, Agreement No. DCI-ALA/2007/19.040 between Uruguay and the European Commission) to MAC. CO and MAC acknowledge the financial support from ANII (POS_NAC_2012_1_8803 and Comisión Académica de Posgrados, Universidad de la Repúpliba, Uruguay) and PEDECIBA. Andrea Medeiros (Lab. Redox Biology of Trypanosomes) and Gabriel Fernández (Transgenic and Animal Experimentation Unit, Institut Pasteur de Montevideo), and Soledad Astrada (Cell Biology Unit, Institut Pasteur de Montevideo) are gratefully acknowledged for technical assistance during production of *Tc*G6PDH antiserum and confocal microscopy, respectively. Dr. Martyn Taylor and Dr. John Kelly (London School of Hygiene and Tropical Medicine, UK) are acknowledged for providing the pTc-INDEX vector.

Conflict of interest: The authors declare that they have no conflicts of interest with the contents of this article.

Author contributions: CO conducted most experiments, analyzed the results, contributed to paper writing. HB contributed to structure refinement and analyzed data. ML prepared active site protein mutant and transgenic cell line from *T. cruzi*. AB contributed to structure refinement, analyzed data. MAC conceived the idea for the project, performed the experimental designs, analyzed data and wrote most of the paper.

REFERENCES

1. Krauth-Siegel RL, Comini MA. Redox control in trypanosomatids, parasitic protozoa with trypanothione-based thiol metabolism. Biochim Biophys Acta. 2008 Nov;1780(11):1236–48.

2. Irigoín F, Cibils L, Comini MA, Wilkinson SR, Flohé L, Radi R. Insights into the redox biology of Trypanosoma cruzi: Trypanothione metabolism and oxidant detoxification. Free Radic Biol Med. 2008 Sep 15;45(6):733–42.

3. Barderi P, Campetella O, Frasch AC, Santomé JA, Hellman U, Pettersson U, et al. The NADP+-linked glutamate dehydrogenase from Trypanosoma cruzi: sequence, genomic organization and expression. Biochem J. 1998 Mar 1;330 (Pt 2):951–8.

4. Maugeri DA, Cazzulo JJ. The pentose phosphate pathway in Trypanosoma cruzi. FEMS Microbiol Lett. 2004 May 1;234(1):117–23.

5. Leroux AE, Maugeri DA, Cazzulo JJ, Nowicki C. Functional characterization of NADP-dependent isocitrate dehydrogenase isozymes from Trypanosoma cruzi. Mol Biochem Parasitol. 2011 May;177(1):61–4.

6. Leroux AE, Maugeri DA, Opperdoes FR, Cazzulo JJ, Nowicki C. Comparative studies on the biochemical properties of the malic enzymes from Trypanosoma cruzi and Trypanosoma brucei. FEMS Microbiol Lett. 2011 Jan;314(1):25–33.

7. Esteve MI, Cazzulo JJ. The 6-phosphogluconate dehydrogenase from Trypanosoma cruzi: the absence of two inter-subunit salt bridges as a reason for enzyme instability. Mol Biochem Parasitol. 2004 Feb;133(2):197–207.

8. Igoillo-Esteve M, Cazzulo JJ. The glucose-6-phosphate dehydrogenase from Trypanosoma cruzi: its role in the defense of the parasite against oxidative stress. Mol Biochem Parasitol. 2006 Oct;149(2):170–81.

9. Comini MA, Ortíz C, Cazzulo JJ. Drug Targets in Trypanosomal and Leishmanial Pentose Phosphate Pathway. In: Jäger T, Koch O, Flohé med h c L, editors. Trypanosomatid Diseases [Internet]. Wiley-VCH Verlag GmbH & Co. KGaA; 2013. p. 297–313. Available from: http://onlinelibrary.wiley.com/doi/10.1002/9783527670383.ch16/summary

10. Kovářová J, Barrett MP. The Pentose Phosphate Pathway in Parasitic Trypanosomatids. Trends Parasitol. 2016 Aug;32(8):622–34.

11. Bowman JE, Smith SM. Theoretical evidence for an autosomal modifying gene pair in glucose-6-phosphate dehydro-genase-deficient families. Ann Hum Genet. 1963 Feb;26:213–8.

12. Mancilla R, Naquira C. COMPARATIVE METABOLISM OF C14-GLUCOSE IN TWO STRAINS OF TRYPANOSOMA CRUZI. J Protozool. 1964 Nov;11:509–13.

13. Heise N, Opperdoes FR. Purification, localisation and characterisation of glucose-6-phosphate dehydrogenase of Trypanosoma brucei. Mol Biochem Parasitol. 1999 Mar 15;99(1):21–32.

14. Finzi JK, Chiavegatto CWM, Corat KF, Lopez JA, Cabrera OG, Mielniczki-Pereira AA, et al. Trypanosoma cruzi response to the oxidative stress generated by hydrogen peroxide. Mol Biochem Parasitol. 2004 Jan;133(1):37–43.

15. Mielniczki-Pereira AA, Chiavegatto CM, López JA, Colli W, Alves MJM, Gadelha FR. Trypanosoma cruzi strains, Tulahuen 2 and Y, besides the difference in resistance to oxidative stress, display differential glucose-6-phosphate and 6-phosphogluconate dehydrogenases activities. Acta Trop. 2007 Jan;101(1):54–60.

16. Ghosh AK, Sardar AH, Mandal A, Saini S, Abhishek K, Kumar A, et al. Metabolic reconfiguration of the central glucose metabolism: a crucial strategy of Leishmania donovani for its survival during oxidative stress. FASEB J Off Publ Fed Am Soc Exp Biol. 2015 May;29(5):2081–98.

17. Gupta S, Cordeiro AT, Michels PAM. Glucose-6-phosphate dehydrogenase is the target for the trypanocidal action of human steroids. Mol Biochem Parasitol. 2011 Apr;176(2):112–5.

18. dos Santos CD, Toldo MPA, do Prado Júnior JC. Trypanosoma cruzi: the effects of dehydroepiandrosterone (DHEA) treatment during experimental infection. Acta Trop. 2005 Aug;95(2):109–15.

19. Cordeiro AT, Thiemann OH, Michels PAM. Inhibition of Trypanosoma brucei glucose-6-phosphate dehydrogenase by human steroids and their effects on the viability of cultured parasites. Bioorg Med Chem. 2009 Mar 15;17(6):2483–9.

20. Gupta S, Igoillo-Esteve M, Michels PAM, Cordeiro AT. Glucose-6-phosphate dehydrogenase of trypanosomatids: characterization, target validation, and drug discovery. Mol Biol Int. 2011;2011:135701.

21. Gordon G, Mackow MC, Levy HR. On the mechanism of interaction of steroids with human glucose 6-phosphate dehydrogenase. Arch Biochem Biophys. 1995 Apr 1;318(1):25–9.

22. Santos CD, Toldo MPA, Santello FH, Filipin MDV, Brazão V, do Prado Júnior JC. Dehydroepiandrosterone increases resistance to experimental infection by Trypanosoma cruzi. Vet Parasitol. 2008 May 31;153(3–4):238–43.

23. Filipin MDV, Caetano LC, Brazão V, Santello FH, Toldo MPA, do Prado JC. DHEA and testosterone therapies in Trypanosoma cruzi-infected rats are associated with thymic changes. Res Vet Sci. 2010 Aug;89(1):98–103.

24. Funayama S, Funayama S, Ito IY, Veiga LA. Trypanosoma cruzi: kinetic properties of glucose-6-phosphate dehydrogenase. Exp Parasitol. 1977 Dec;43(2):376–81.

25. Ortíz C, Larrieux N, Medeiros A, Botti H, Comini M, Buschiazzo A. Expression, crystallization and preliminary X-ray crystallographic analysis of glucose-6-phosphate dehydrogenase from the human pathogen Trypanosoma cruzi in complex with substrate. Acta Crystallograph Sect F Struct Biol Cryst Commun. 2011 Nov 1;67(Pt 11):1457–61.

26. Mercaldi GF, Dawson A, Hunter WN, Cordeiro AT. The structure of a Trypanosoma cruzi glucose-6-phosphate dehydrogenase reveals differences from the mammalian enzyme. FEBS Lett. 2016 Aug;590(16):2776–86.

27. Comakli V, Akkemik E, Ciftci M, Kufrevioglu OI. Purification and characterization of glucose 6-phosphate dehydrogenase enzyme from rainbow trout (Oncorhynchus mykiss) liver and investigation of the effects of some metal ions on enzyme activity. Toxicol Ind Health. 2015 May 1;31(5):403–11.

28. Shreve DS, Levy HR. On the molecular weight of human glucose 6-phosphate dehydrogenase. Biochem Biophys Res Commun. 1977 Oct 24;78(4):1369–75.

29. Adem S, Ciftci M. Purification of rat kidney glucose 6-phosphate dehydrogenase, 6-phosphogluconate dehydrogenase, and glutathione reductase enzymes using 2',5'-ADP Sepharose 4B affinity in a single chromatography step. Protein Expr Purif. 2012 Jan;81(1):1–4.

30. Au SW, Gover S, Lam VM, Adams MJ. Human glucose-6-phosphate dehydrogenase: the crystal structure reveals a structural NADP(+) molecule and provides insights into enzyme deficiency. Struct Lond Engl 1993. 2000 Mar 15;8(3):293–303.

31. Au SW, Naylor CE, Gover S, Vandeputte-Rutten L, Scopes DA, Mason PJ, et al. Solution of the structure of tetrameric human glucose 6-phosphate dehydrogenase by molecular replacement. Acta Crystallogr D Biol Crystallogr. 1999 Apr;55(Pt 4):826–34.

32. Cohen P, Rosemeyer MA. Glucose-6-phosphate dehydrogenase from human erythrocytes. Methods Enzymol. 1975;41:208–14.

33. Ranzani AT, Cordeiro AT. Mutations in the tetramer interface of human glucose-6-phosphate dehydrogenase reveals kinetic differences between oligomeric states. FEBS Lett. 2017 Mar 30;

34. Bonsignore A, Cancedda R, Nicolini A, Damiani G, De Flora A. Metabolism of human erythrocyte glucose-6-phosphate dehydrogenase. VI. Interconversion of multiple molecular forms. Arch Biochem Biophys. 1971 Dec;147(2):493–501.

35. Bonsignore A, Lorenzoni I, Cancedda R, De Flora A. Distinctive patterns of NADP binding to dimeric and tetrameric glucose 6-phosphate dehydrogenase from human red cells. Biochem Biophys Res Commun. 1970 Apr 8;39(1):142–8.

36. Wang X-T, Engel PC. An optimised system for refolding of human glucose 6-phosphate dehydrogenase. BMC Biotechnol. 2009 Mar 11;9:19.

37. Bonsignore A, Lorenzoni I, Cancedda R, Cosulich ME, De Flora A. Effect of divalent cations on the structure of human erythrocyte glucose 6-P dehydrogenase. Biochem Biophys Res Commun. 1971 Jan 22;42(2):159–65.

38. Kotaka M, Gover S, Vandeputte-Rutten L, Au SWN, Lam VMS, Adams MJ. Structural studies of glucose-6-phosphate and NADP+ binding to human glucose-6-phosphate dehydrogenase. Acta Crystallogr D Biol Crystallogr. 2005 May;61(Pt 5):495–504.

39. Babalola AO, Beetlestone JG, Luzzatto L. Genetic variants of human erythrocyte glucose-6-phosphate dehydrogenase. Kinetic and thermodynamic parameters of variants A, B, and A- in relation to quaternary structure. J Biol Chem. 1976 May 25;251(10):2993–3002.

40. Filosa S, Calabrò V, Vallone D, Poggi V, Mason P, Pagnini D, et al. Molecular basis of chronic non-spherocytic haemolytic anaemia: a new G6PD variant (393 Arg----His) with abnormal KmG6P and marked in vivo instability. Br J Haematol. 1992 Jan;80(1):111–6.

41. Ortiz C, Moraca F, Medeiros A, Botta M, Hamilton N, Comini MA. Binding Mode and Selectivity of Steroids towards Glucose-6-phosphate Dehydrogenase from the Pathogen Trypanosoma cruzi. Mol Basel Switz. 2016 Mar 17;21(3):368.

42. Cosgrove MS, Naylor C, Paludan S, Adams MJ, Levy HR. On the mechanism of the reaction catalyzed by glucose 6-phosphate dehydrogenase. Biochemistry (Mosc). 1998 Mar 3;37(9):2759–67.

43. Cosgrove MS, Gover S, Naylor CE, Vandeputte-Rutten L, Adams MJ, Levy HR. An examination of the role of asp-177 in the His-Asp catalytic dyad of Leuconostoc mesenteroides glucose 6-phosphate dehydrogenase: X-ray structure and pH dependence of kinetic parameters of the D177N mutant enzyme. Biochemistry (Mosc). 2000 Dec 12;39(49):15002–11.

44. Naylor CE, Gover S, Basak AK, Cosgrove MS, Levy HR, Adams MJ. NADP+ and NAD+ binding to the dual coenzyme specific enzyme Leuconostoc mesenteroides glucose 6-phosphate dehydrogenase: different interdomain hinge angles are seen in different binary and ternary complexes. Acta Crystallogr D Biol Crystallogr. 2001 May;57(Pt 5):635–48.

45. Rowland P, Basak AK, Gover S, Levy HR, Adams MJ. The three-dimensional structure of glucose 6-phosphate dehydrogenase from Leuconostoc mesenteroides refined at 2.0 A resolution. Struct Lond Engl 1993. 1994 Nov 15;2(11):1073–87.

46. Rangel-Aldao R, Comach G, Mendoza A. In vitro translation of Trypanosoma cruzi antigens recognized by human chagasic sera. J Parasitol. 1987 Aug;73(4):855–7.

47. Taylor MC, Kelly JM. pTcINDEX: a stable tetracycline-regulated expression vector for Trypanosoma cruzi. BMC Biotechnol. 2006 Jul 6;6:32.

48. Frederiks WM, van Marle J, van Oven C, Comin-Anduix B, Cascante M. Improved localization of glucose-6-phosphate dehydrogenase activity in cells with 5-cyano-2,3-ditolyl-tetrazolium chloride as fluorescent redox dye reveals its cell cycle-dependent regulation. J Histochem Cytochem Off J Histochem Soc. 2006 Jan;54(1):47–52.

49. Cohen P, Rosemeyer MA. Subunit Interactions of Glucose-6-Phosphate Dehydrogenase from Human Erythrocytes. Eur J Biochem. 1969 Mar 1;8(1):8–15.

50. Saunders MA, Hammer MF, Nachman MW. Nucleotide variability at G6pd and the signature of malarial selection in humans. Genetics. 2002 Dec;162(4):1849–61.

51. Gómez-Manzo S, Terrón-Hernández J, De la Mora-De la Mora I, González-Valdez A, Marcial-Quino J, García-Torres I, et al. The Stability of G6PD Is Affected by Mutations with Different Clinical Phenotypes. Int J Mol Sci. 2014 Nov 17;15(11):21179–201.

52. Wang X-T, Chan TF, Lam VMS, Engel PC. What is the role of the second “structural” NADP+-binding site in human glucose 6-phosphate dehydrogenase? Protein Sci Publ Protein Soc. 2008 Aug;17(8):1403–11.

53. Wang X-T, Engel PC. Clinical mutants of human glucose 6-phosphate dehydrogenase: impairment of NADP(+) binding affects both folding and stability. Biochim Biophys Acta. 2009 Aug;1792(8):804–9.

54. Wenderoth I, Scheibe R, von Schaewen A. Identification of the cysteine residues involved in redox modification of plant plastidic glucose-6-phosphate dehydrogenase. J Biol Chem. 1997 Oct 24;272(43):26985–90.

55. Wendt UK, Hauschild R, Lange C, Pietersma M, Wenderoth I, von Schaewen A. Evidence for functional convergence of redox regulation in G6PDH isoforms of cyanobacteria and higher plants. Plant Mol Biol. 1999 Jun;40(3):487–94.

56. Hauschild R, von Schaewen A. Differential regulation of glucose-6-phosphate dehydrogenase isoenzyme activities in potato. Plant Physiol. 2003 Sep;133(1):47–62.

57. Emsley P, Cowtan K. Coot: model-building tools for molecular graphics. Acta Crystallogr D Biol Crystallogr. 2004 Dec;60(Pt 12 Pt 1):2126–32.

58. Murshudov GN, Vagin AA, Dodson EJ. Refinement of macromolecular structures by the maximum-likelihood method. Acta Crystallogr D Biol Crystallogr. 1997 May 1;53(Pt 3):240–55.

59. Langer G, Cohen SX, Lamzin VS, Perrakis A. Automated macromolecular model building for X-ray crystallography using ARP/wARP version 7. Nat Protoc. 2008;3(7):1171–9.

60. Chen VB, Arendall WB, Headd JJ, Keedy DA, Immormino RM, Kapral GJ, et al. MolProbity: all-atom structure validation for macromolecular crystallography. Acta Crystallogr D Biol Crystallogr. 2010 Jan 1;66(Pt 1):12–21.

61. Laskowski RA, MacArthur MW, Moss DS, Thornton JM. PROCHECK: a program to check the stereochemical quality of protein structures. J Appl Crystallogr. 1993 Apr 1;26(2):283–91.

62. Cazzulo JJ, Franke de Cazzulo BM, Engel JC, Cannata JJ. End products and enzyme levels of aerobic glucose fermentation in trypanosomatids. Mol Biochem Parasitol. 1985 Sep;16(3):329–43.

63. Wirtz E, Leal S, Ochatt C, Cross GA. A tightly regulated inducible expression system for conditional gene knock-outs and dominant-negative genetics in Trypanosoma brucei. Mol Biochem Parasitol. 1999 Mar 15;99(1):89–101.

64. Piacenza L, Peluffo G, Alvarez MN, Kelly JM, Wilkinson SR, Radi R. Peroxiredoxins play a major role in protecting Trypanosoma cruzi against macrophage- and endogenously-derived peroxynitrite. Biochem J. 2008 Mar 1;410(2):359–68.

65. de Chaumont F, Dallongeville S, Chenouard N, Hervé N, Pop S, Provoost T, et al. Icy: an open bioimage informatics platform for extended reproducible research. Nat Methods. 2012 Jun 28;9(7):690–6.

Table 1. Kinetic parameters for different versions of recombinant form *Tc*G6PDH.

	G6P				NADP			
***Tc*G6PDH**[a]	K_M (μM)	V_{max} (μM.min^{-1})	k_{cat} (s^{-1})	k_{cat}/K_M (μM^{-1}.s^{-1})	K_M (μM)	V_{max} (μM.min^{-1})	k_{cat} (s^{-1})	k_{cat}/K_M (μM^{-1}.s^{-1})
WT	77±20	58±4	62±3	0.81	16±3	49±2	52±2	3.25
WT + DTT	318±49	254±9	108±4	0.34	39±6	191±6	82±3	2.1
Δ37N	275±115	139±14	154±16	0.56	18±5	109±6	121±6	6.70
C8S	128±16	229±6	61±2	0.48	24±6	139±7	37±2	1.54
R323G	1421±91	130±3	50±1	0.04	27±3	36±1	14,1±0,3	0.52
R323G/C528R	1025±80	173±5	85±2	0.08	21±5	81±3	40±2	1.91
P218V	123±16	46 ±1	0.35 ±0.01	0.003	9±1	30±1	0.23±0,01	0.03
H309G	185±33	28 ±2	0.19 ±0.01	0.001	18±5	22±1	0.15±0,01	0.01
K217	226±34	63±3	6.5±0.3	0.029	9±1	42±1	4.4±0,1	0.49

[a] The different forms of TcG6PDH evaluated correspond to: WT, *Tc*G6PDH$_L$; WT + DTT, *Tc*G6PDH$_L$ assayed in the presence of DTT (5 mM); Δ37N, N-terminal truncated mutant of *Tc*G6PDH; C8S, R323G, R323G/C528R, P218V, H309G and K217I are point mutants of *Tc*G6PDH$_L$.

Figure Legends

Figure 1. Tridimensional structure and oligomeric organization of G6P-bound Δ37N-G6PDH from *T. cruzi*. Cartoon representation of Δ37N-*Tc*G6PDH **A)** tetramer, **B)** dimer superimposed to human G6PDH (PDB 2BHL) and **C)** monomer with bound G6P. The N-terminal Rossman-fold domain is colored black or dark grey, whereas the C-terminal domain is shown with different colors according to the subunit (red: chain A, green: chain B, orange: chain C, and blue: chain D). G6P atoms are depicted as spheres without hydrogens (sea-blue: carbon, red: oxygen and orange: phosphate). The subunits of human G6PDH are shown in pale green (chain A) and dark yellow (chain B). The elements conforming the secondary structure of *Tc*G6PDH are numbered accordingly and the short α-turn connecting both domains is depicted in yellow.

Figure 2. Multiple sequence alignment of selected glucose-6-phosphate dehydrogenases from different Phyla. The amino acid sequences for G6PDH shown correspond to *Trypanosoma cruzi* (Tc, Q1WBU6), *Trypanosoma brucei* (Tb, Q38BZ6), *Leishmania infantum* (Li, A2CIJ8), *Homo sapiens* (Hs, P11413), *Salmonella typhimurium* (St, Q8ZNW2), chloroplastic *Solanum tuberosum* (cSt, Q43839), chloroplastic *Arabidopsis thailiana* (cAt, Q43727) *Plasmodium falciparum* (Pf, Q8IKU0) and *Leuconostoc mesenteroides* (Lm, P11411). Residues strictly conserved in all sequences are shown indicated in white letters with black background while those conserved in at least 7 out of 9 sequences are shown in black and bold letters. The secondary structure elements of Δ37N-*Tc*G6PDH with bound G6P (PDB 4EM5) are displayed above the sequence alignment. The black and grey lines highlight the N-terminal V52-K84 and E285-R323 regions that may contribute with allosteric control of *Tc*G6PDH activity. At the bottom of the alignment, the black circle, the empty circle, the asterisk and the arrow indicate residues involved in ionic interactions to stabilize the dimer-dimer contacts, mutated in this study, residues interacting with G6P and the position of R323, respectively.

Figure 3. Size exclusion chromatography analysis of recombinant *Tc*G6PDH$_L$. The full-length form of *Tc*G6PDH (0.8-2.4 µM) was treated and gel filtrated on a Superdex G200 resin (10/300 column) pre-equilibrated in reaction buffer (Tris 50 mM, pH 7.5, NaCl 0.5 M and $MgCl_2$ 5 mM) containing saturating concentrations of different ligands: **A)** DHEA 100 µM (dotted line), NADP 5 mM (dot and dash line), or G6P 5 mM (black line), or under different physicochemical conditions: **B)** reaction buffer lacking magnesium (dotted line), DTT 5 mM (black line), NaCl 1 M (black dashed line), SDS 3.5 mM (grey dashed line), or Triton X-100 0.1 % (v/v) (grey line). For both plots, the head arrow indicate the position at which the peak of the non-treated *Tc*G6PDH$_L$ elutes in reaction buffer (control). **C)** SDS- 15% PAGE for full-length (WT) and ∆37N- (∆37N) *Tc*G6PDH run under reducing (DTT +) and non-reducing (DTT -) conditions. The bands corresponding to monomeric and dimeric species are indicated with arrows while the covalent multimeric species are marked with a bracket. **D)** *Tc*G6PDH$_L$ was gel filtrated on a Superdex G200 (10/300 column) equilibrated at pH 7.5 (dotted line) and pH 5.5 (black line). The R323G *Tc*G6PDH$_L$ mutant was separated in the same column equilibrated in reaction buffer without (dash and dot line) and with DTT 5 mM (grey line). The arrows indicate the position of the peaks corresponding to the molecular weight standards used for column calibration (thyroglobulin Mr 669 kDa, aldolase Mr 158 kDa and albumin 75 kDa). α_4 and α_2 denote the theoretical positions at which the tetrameric and dimeric species, respectively, of TcG6PDH$_L$ are expected to elute.

Figure 4. Tetramer interface of *Tc*G6PDH. Critical residues involve in formation of salt bridges between dimers of *Tc*G6PDH (PDB 4EM5) are shown in green (chain A with transparent surface and backbone shown as cartoon with N- and C-terminal domains colored in black and red, respectively) and blue (chain C shown as surface with N and C-terminal domain colored in grey and pale green, respectively) sticks. Residues non-conserved in *Hs*G6PDH are labeled in red (R323 and D390). The inset shows the saline bridges formed between R323 and D332 and E333 from subunit A and B (green cartoon backbone).

Figure 5. Ligand binging and catalytic elements connected to R323 of *Tc*G6PDH. Surface representation of *Tc*G6PDH (PDB 4EM5, chain A) with backbone elements of the segment E285-R323 displayed as green cartoon. Residues key for interaction with G6P (D304 and E285) and catalysis (H309) are shown as sticks. R323 and the corresponding negatively charged residues from chain B involved in electrostatic interactions (D332 and E333, blue sticks) are also shown.

Figure 6. Dynamic of the N-terminal region of *Tc*G6PDH and influence on the active site. **A**) Surface representation of ∆37N-*Tc*G6PDH (chain D, PDB 4EM5) with the N-terminal and C-terminal domain colored in dark and light grey, respectively. Structural elements corresponding to the region V52-K84 of the crystallographic (deep teal cartoon representation) and catalytic model (deep olive cartoon representation) of ∆37N-*Tc*G6PDH are shown. NADPH (sticks colored in cyan: carbon, red: oxygen, blue: nitrogen and orange: phosphate) and residues involved in substrate binding (G75, S77, D79, L80 and K83) and N-terminal cysteines forming or (C53"-C135" for PDB 4EM5) not an intramolecular disulfide are shown as sticks. **B**) Cartoon representation of the N-terminal segment of ∆37N-*Tc*G6PDH (V52-K84) with bound G6P (deep teal color; chain D, PDB 4EM5) and catalytic model (deep olive color), ∆57N-*Tc*G6PDH (P62-K84: blue color; chain A, PDB 5AQ1) and from *Hs*G6PDH (V27-K47: violet color; chain A, PDB 2BH9). Residues participating in substrate binding are shown as sticks for the catalytic model, and N-terminal cysteines of *Tc*G6PDH engaged (C53-C135 for ∆37N-mutant, C94*-C135* for ∆57N-mutant) or not (C53", C94" and C135" for catalytic model) in intramolecular disulfides are shown as sticks. The structural coordinates for G6P and NADPH, shown as sticks, correspond to those of the catalytic model of ∆37N-*Tc*G6PDH$_L$.

Figure 7. C8 is responsible for the formation of inter-subunit disulfides in *Tc*G6PDH$_L$. SDS- 15% PAGE for full-length (WT) and different Cys to Ser mutants (C8S, C34S and C552S)

of *Tc*G6PDH run under reducing (+) and non-reducing (-) conditions. The bands corresponding to monomeric and dimeric species are indicated with arrows.

Figure 8. Catalytic model of *Tc*G6PDH and conformational changes in elements from N-terminal domain involved in ligand binding. Superimposition of the protein backbone corresponding to the catalytic (yellow cartoon, (41)) and crystallographic (blue cartoon; chain A PDB 5AQ1) model of *Tc*G6PDH with bound substrates. The secondary structure elements displaying shifts in their conformation are labeled (i.e. α2, 3, 4, 5 and 6, and β1 and 2). G6P and $NADP^+(H)$ are shown as sticks with carbon atoms colored according to the backbone color selected for each structure.

Figure 9. Catalytic site of *Tc*G6PDH. Molecular dynamics (**A** and **B**; Ortíz et al. 2016) and crystallographic (**C** and **D**; chain A, PDB 5AQ1) model of the catalytic site of N-terminally truncated *Tc*G6PDH. Residues important for substrate binding and catalysis are shown with lines and labeled. Histidine 247 is shown with sticks to highlight the different conformations it adopts in the catalytic and crystallographic models, which determine also a different localization of G6P (show as sticks). H-bond interactions discussed in the text are depicted with dashed lines.

Figure 10. Subcellular distribution of G6PDH in *T. cruzi*. The content and subcellular localization of G6PDH overexpressed in *T. cruzi* epimastigotes (strain Adriana) was investigated by Western blot (**A**) and confocal microscopy (**B**-**E**). **A**) Cell extracts corresponding to $1x10^6$ parasites induced (5 or 10 µg/mL) and to $1x10^7$ cells non-induced (0 µg/mL) with oxitetracycline (Oxitet), and different amounts of recombinant *Tc*G6PDH (7, 10, 28, 50, 70 and 100 ng) were loaded per lane. **B** and **D**) Indirect immunofluorescence using anti-$TcG6PDH_L$ and secondary anti-mouse serum conjugated to Alexa 488 (green signal) or Alexa 594 (red signal), respectively. **C**) Mitochondrial (K) and nuclear (N) DNA was stained with DAPI (blue signal) and

E) detection of lipoamide dehydrogenase with anti-LipDH serum (and anti-rabbit serum conjugated to Alexa 488) was used to localize the mitochondrion of the parasite (green signal).

Figure 11. *In situ* detection of G6PDH activity in *T. cruzi*. Epimastigotes from *T. cruzi* strain CL-Brener were incubated for 24 h in the absence (no treated) or presence of 25 and 100 µM epiandrosterone (EA). G6PDH activity was measured in cell extracts using the standard enzyme assay (specific activity expressed as U/mg) and detected at intracellular level using a cytochemical assay based on the reduction of 5-cyano-2,3-ditolyl-tetrazolium chloride (CTC; red color). Hoechst 3342 stain (green color) was used to mark nuclear (N) and mitochondrial (K, kinetoplast) DNA. Bright field and merged images are also shown with the white bar indicating a length of 10 µm. A zoom image of the cell with white frame is shown in Fig. S5.

Supplemental information

Figure Legends

Figure S1. Cysteine residues observed in the structure of Δ37N-*Tc*G6PDH. Cartoon representation of the backbone structure of Δ37N-*Tc*G6PDH with bound G6P (PDB 4EM5; A, B, C and D subunits are colored in blue, green, orange and red) and cysteine residues shown as spheres.

Figure S2. Multiple sequence alignment of G6PDH from Kinetoplastid parasites lacking conserved R323. Amino acid sequence alignment for putative G6PDH from *Leptomona seymouri* (Ls), *Leptomona pyrrhocoris* (Lp), *Crithidia fasciculata* (Cf), *Leishmania enrietti* (Le), and of characterized G6PDH from *T. cruzi* and (Tc) and *Homo sapiens* (Hs). Strictly conserved or highly similar residues are shown on black background. Residues that in human G6PDH anchor the allosteric $NADP^+$ are highlighted in blue with those not conserved in the *T. cruzi* enzyme marked with yellow. Residues that in *T. cruzi* G6PDH form salt bridges that stabilize the tetramer are highlighted in green.

Figure S3. Dynamic N-term of human G6PDH. Superimposition of the protein backbone corresponding of human G6PDH with bound G6P (pale cyan color; chain B, PDB 2BHL) or NADP+ (violet purple color; PDB 2BH9) that shows different conformations for elements from the N-terminal region.

Figure S4. *In situ* detection of G6PDH activity in *T. cruzi* strain DM28c. Epimastigotes from *T. cruzi* strain DM28c were incubated for 24 h in the absence (no treated) or presence of 25 and 100 µM epiandrosterone (EA). G6PDH activity was measured in cell extracts using the standard enzyme assay (specific activity expressed as U/mg) and detected at intracellular level using a couple cytochemical assay based on the reduction of 5-cyano-2,3-ditolyl-tetrazolium chloride (CTC; red color). Hoechst 3342 stain (green color) was used to mark nuclear and mitochondrial

DNA. Bright field and merged images are also shown with the white bar indicating a length of 10 µm.

Figure S5. Zoom image of *T. cruzi* cell displaying G6PDH activity. Cell framed in Fig. 11 and corresponding to an epimastigote from *T. cruzi* strain CL-Brener no treated with epiandrosterone and with G6PDH activity assayed with CTC (red signal) and nuclear and mitochondrial DNA stained with Hoechst 3342 (green signal).

Figure S6. *In situ* detection of G6PDH activity in *T. cruzi* strain Adriana overexpressing G6PDH. Epimastigotes from *T. cruzi* strain Adriana grown for 24 h in the presence of 10 µg/mL oxytetracycline to induce overexpression of *Tc*G6PDH$_L$ (Western blot shown in Fig. 10A). G6PDH activity was detected at intracellular level using a cytochemical assay based on the reduction of 5-cyano-2,3-ditolyl-tetrazolium chloride (CTC; green color color). **A**) Bright field image with light dense intracellular particles corresponding to precipitated formazan salt. **B**) CTC signal. **C**) Cell membranes stained with CellMask. **D**) Merge image of CTC and CellMask signals.

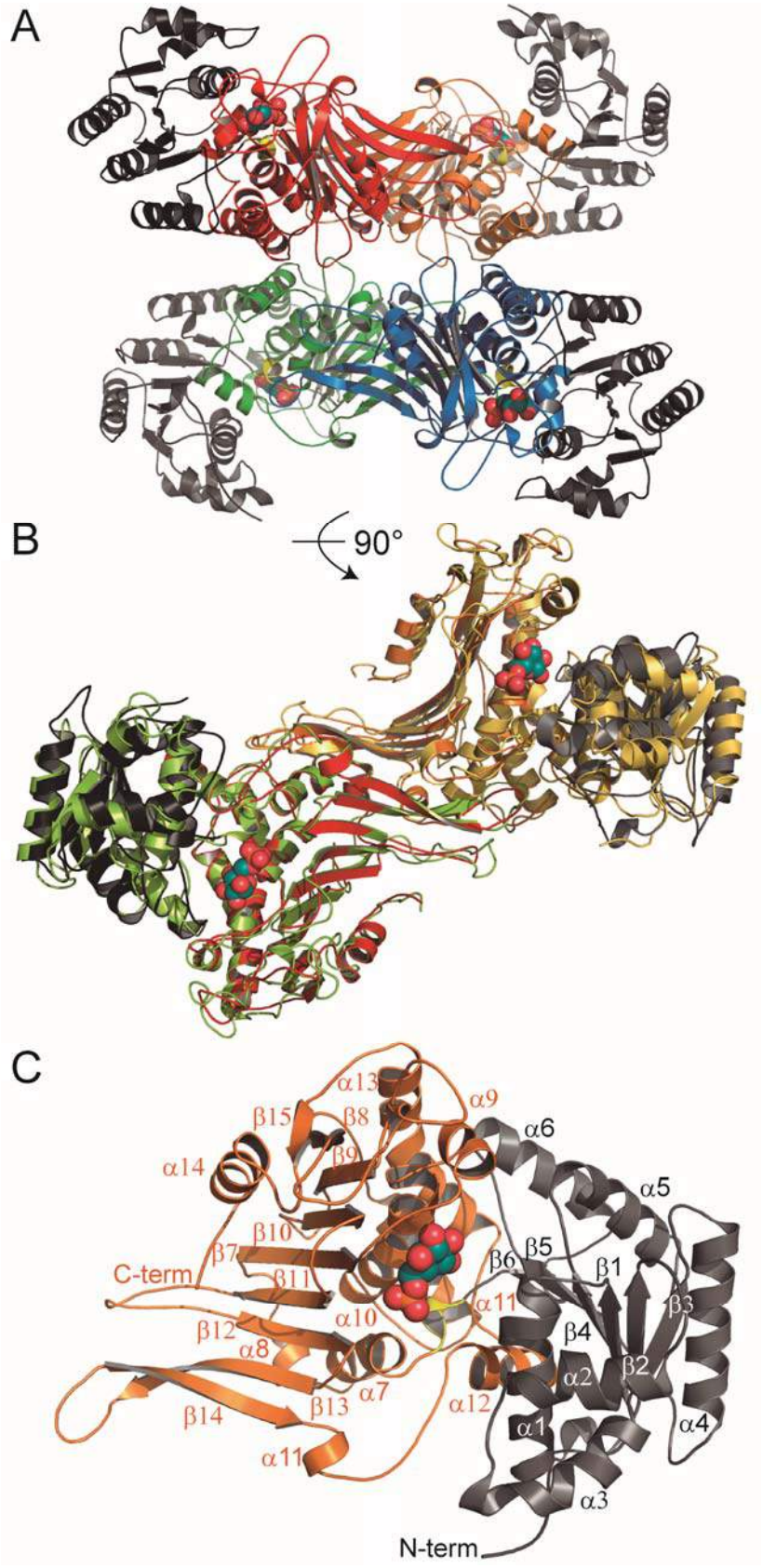
A
B
90°
C
α13
α9
β15
β8
α6
β9
α14
α5
β10
β5
β7
β6
β1
C-term
β11
α11
β3
α10
β12
β4
α8
α2
β2
α7
α12
β14
β13
α1
α4
α11
α3
N-term

Figure 1

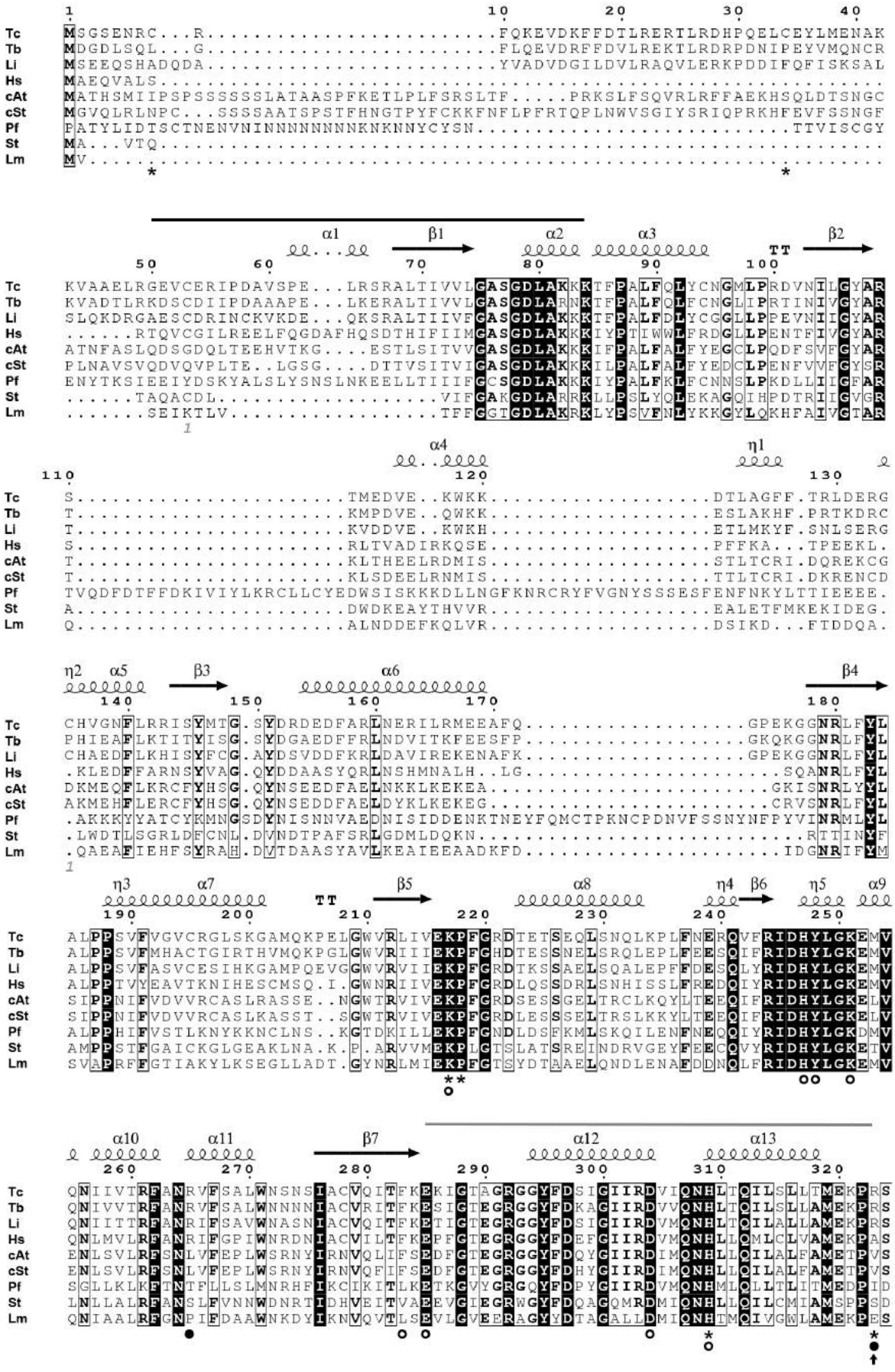
Tc
Tb
Li
Hs
cAt
cSt
Pf
St
Lm

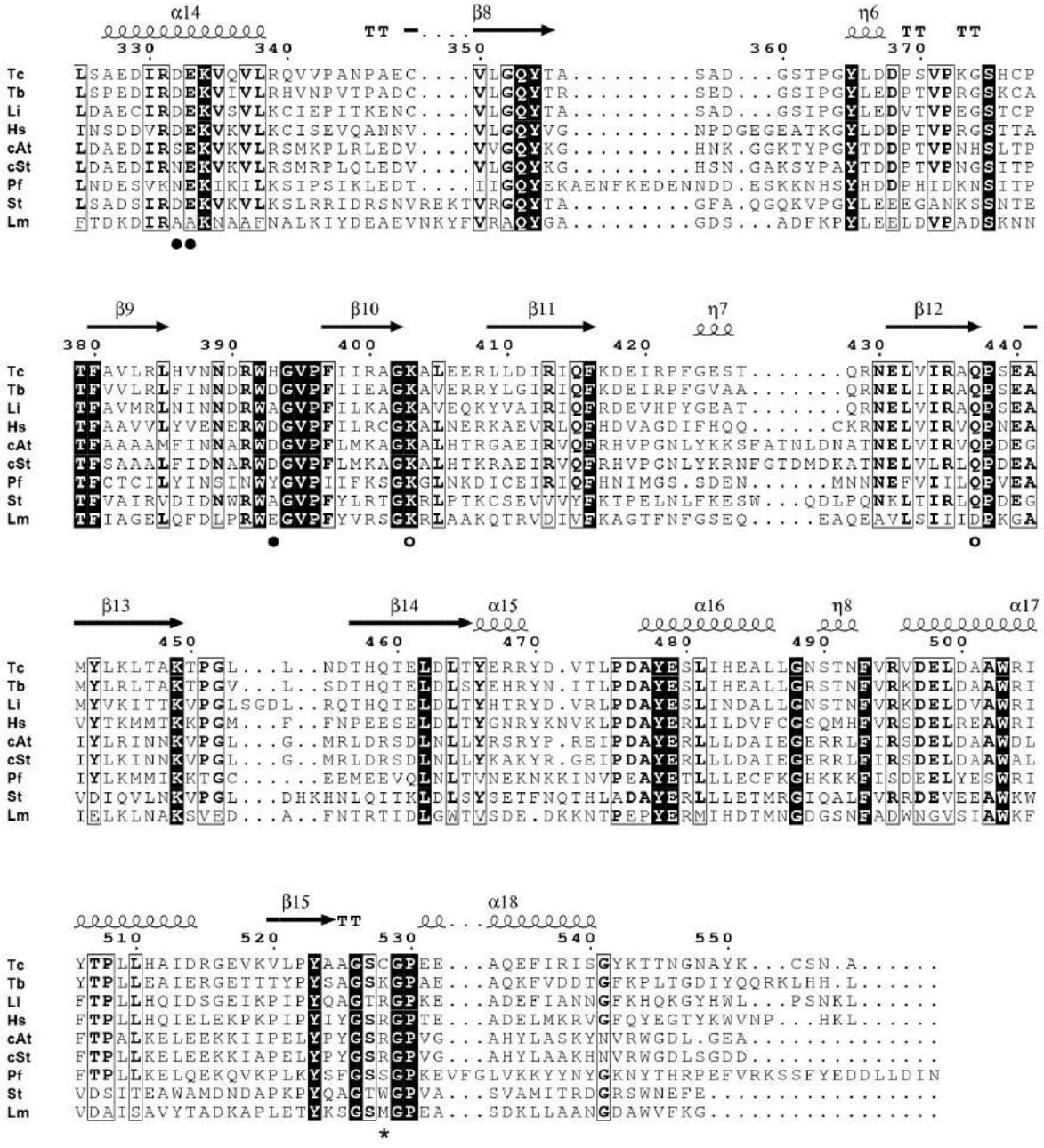
α14
β8
η6
TT
TT
TT
330
340
350
360
370
Tc LSAEDIRDEKVQVLRQVVPANPAEC....VLGQYTA.....SAD...GSTPGYLDDPSVPKGSHCP
Tb LSPEDIRDEKVIVLRHVNPVTPADC....VLGQYTR.....SED...GSIPGYLEDPTVPRGSKCA
Li LDAECIRDEKVSVLKCIEPITKENC....VLGQYTA.....SAD...GSIPGYLEDVTVPEGSTCP
Hs TNSDDVRDEKVKVLKCISEVQANNV....VLGQYVG.....NPDGEGEATKGYLDDPTVPRGSTTA
cAt LDAEDIRSEKVKVLRSMKPLRLEDV....VVGQYKG.....HNK.GGKTYPGYTDDPTVPNHSLTP
cSt LDAEDIRNEKVKVLRSMRPLQLEDV....VLGQYKG.....HSN.GAKSYPAYTDDPTVPNGSITP
Pf LNDESVKNEKIKILKSIPSIKLEDT....IIGQYEKAENFKEDENNDD.ESKKNHSYHDDPHIDKNSITP
St LSADSIRDEKVKVLKSLRRIDRSNVREKTVRGQYTA.....GFA.QGQKVPGYLEEEGANKSSNTE
Lm FTDKDIRAAKNAAFNALKIYDEAEVNKYFVRAQYGA.....GDS...ADFKPYLEELDVPADSKNN
β9
β10
β11
η7
β12
380
390
400
410
420
430
440
Tc TFAVLRLHVNNDRWHGVPFIIRAGKALEERLLDIRIQFKDEIRPFGEST.....QRNELVIRAQPSEA
Tb TFVVLRLFINNDRWDGVPFIIEAGKAVERRYLGIRIQFKDEIRPFGVAA.....QRNELIIRAQPSEA
Li TFAVMRLNINNDRWAGVPFILKAGKAVEQKYVAIRIQFRDEVHPYGEAT.....QRNELVIRAQPSEA
Hs TFAAVVLYVENERWDGVPFILRCGKALNERKAEVRLQFHDVAGDIFHQQ.....CKRNELVIRVQPNEA
cAt TFAAAAMFINNARWDGVPFLMKAGKALHTRGAEIRVQFRHVPGNLYKKSFATNLDNATNELVIRVQPDEG
cSt TFSAAALFIDNARWDGVPFLMKAGKALHTKRAEIRVQFRHVPGNLYKRNFGTDMDKATNELVLRLQPDEA
Pf TFCTCILYINSINWYGVPIIFKSGKGLNKDICEIRIQFHNIMGS.SDEN.....MNNNEFVIILQPVEA
St TFVAIRVDIDNWRWAGVPFYLRTGKRLPTKCSEVVVYFKTPELNLFKESW...QDLPQNKLTIRLQPDEG
Lm TFIAGELQFDLPRWEGVPFYVRSGKRLAAKQTRVDIVFKAGTFNFGSEQ.....EAQEAVLSIIIDPKGA
β13
β14
α15
α16
η8
α17
450
460
470
480
490
500
Tc MYLKLTAKTPGL...L..NDTHQTELDLTYERRYD.VTLPDAYESLIHEALLGNSTNFVRVDELDAAWRI
Tb MYLRLTAKTPGV...L..SDTHQTELDLSYEHRYN.ITLPDAYESLIHEALLGRSTNFVRKDELDAAWRI
Li MYVKITTKVPGLSGDL..RQTHQTELDLTYHTRYD.VRLPDAYESLINDALLGNSTNFVRKDELDVAWRI
Hs VYTKMMTKKPGM...F..FNPEESELDLTYGNRYKNVKLPDAYERLILDVFCGSQMHFVRSDELREAWRI
cAt IYLRINNKVPGL...G..MRLDRSDLNLLYRSRYP.REIPDAYERLLLDAIEGERRLFIRSDELDAAWDL
cSt IYLKINNKVPGL...G..MRLDRSDLNLLYKAKYR.GEIPDAYERLLLDAIEGERRLFIRSDELDAAWAL
Pf IYLKMMIKKTGC.....EEMEEVQLNLTVNEKNKKINVPEAYETLLLECFKGHKKKFISDEELYESWRI
St VDIQVLNKVPGL...DHKHNLQITKLDLSYSETFNQTHLADAYERLLLETMRGIQALFVRRDEVEEAWKW
Lm IELKLNAKSVED...A..FNTRTIDLGWTVSDE.DKKNTPEPYERMIHDTMNGDGSNFADWNGVSIAWKF
β15
α18
510
520
530
540
550
Tc YTPLLHAIDRGEVKVLPYAAGSCGPEE...AQEFIRISGYKTTNGNAYK...CSN.A.....
Tb YTPLLEAIERGETTTYPYSAGSKGPAE...AQKFVDDTGFKPLTGDIYQQRKLHH.L.....
Li FTPLLHQIDSGEIKPIPYQAGTRGPKE...ADEFIANNGFKHQKGYHWL...PSNKL.....
Hs FTPLLHQIELEKPKPIPYIYGSRGPTE...ADELMKRVGFQYEGTYKWVNP...HKL.....
cAt FTPALKELEEKKIIPELYPYGSRGPVG...AHYLASKYNVRWGDL.GEA.............
cSt FTPLLKELEEKKIAPELYPYGSRGPVG...AHYLAAKHNVRWGDLSGDD.............
Pf FTPLLKELQEKQVKPLKYSFGSSGPKEVFGLVKKYYNYGKNYTHRPEFVRKSSFYEDDLLDIN
St VDSITEAWAMDNDAPKPYQAGTWGPVA...SVAMITRDGRSWNEFE.................
Lm VDAISAVYTADKAPLETYKSGSMGPEA...SDKLLAANGDAWVFKG.................

Figure 2

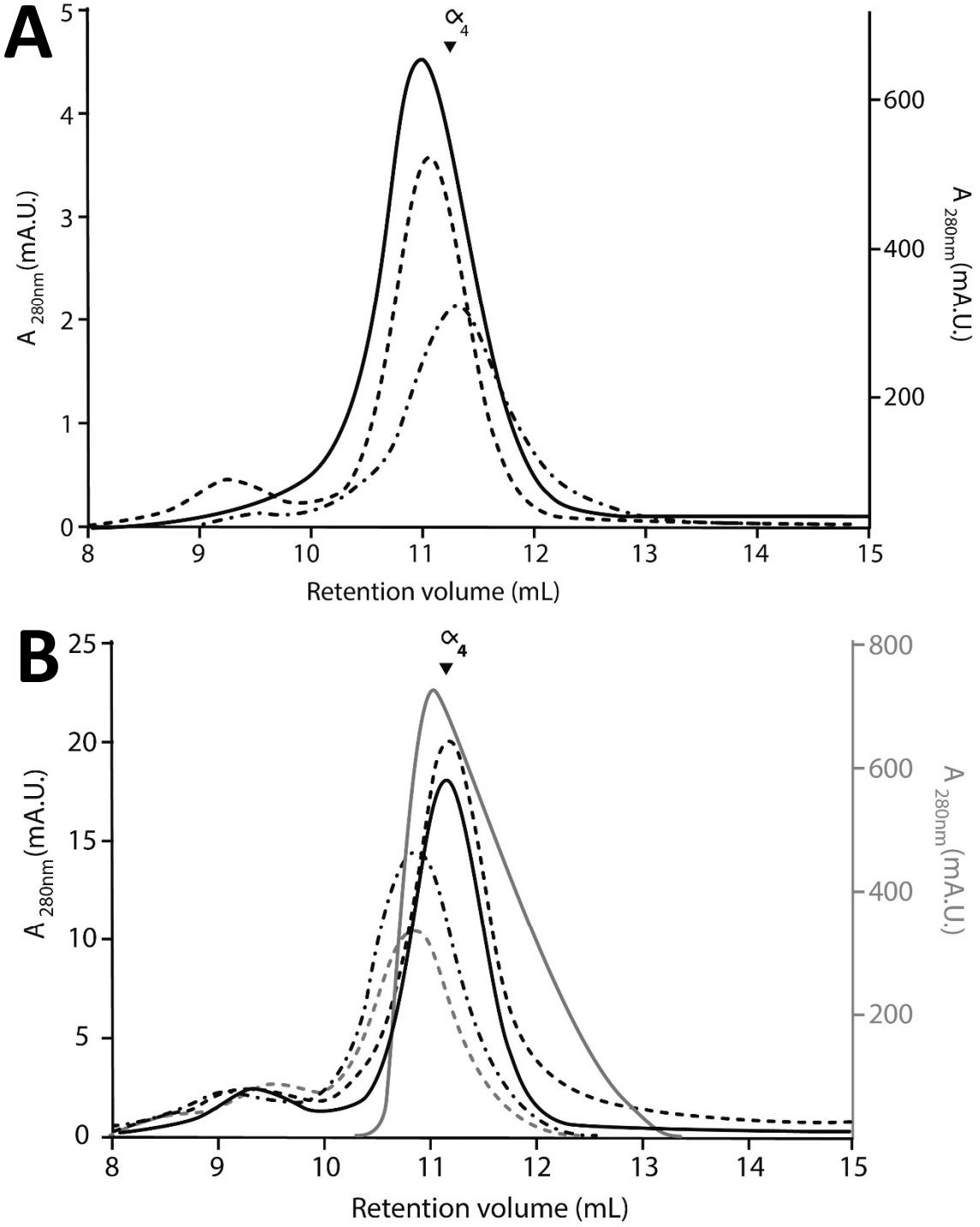
A
α_4
A_{280nm}(mA.U.)
A_{280nm}(mA.U.)
Retention volume (mL)
B
α_4
A_{280nm}(mA.U.)
A_{280nm}(mA.U.)
Retention volume (mL)

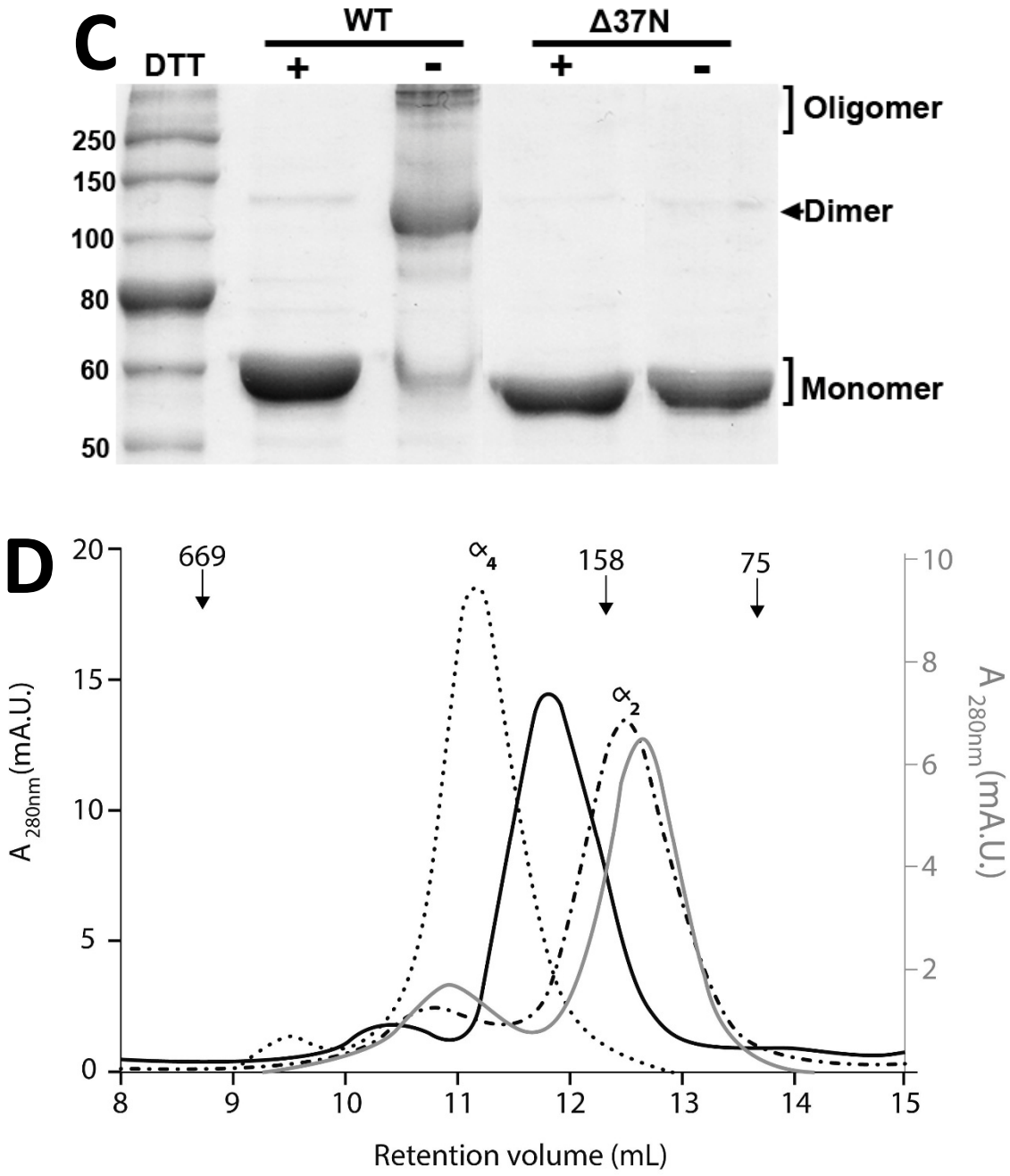
C
DTT
WT
Δ37N
+
-
+
-
250
150
100
80
60
50
Oligomer
Dimer
Monomer
D
669
158
75
α_4
α_2
A_{280nm}(mA.U.)
A_{280nm}(mA.U.)
Retention volume (mL)

Figure 3

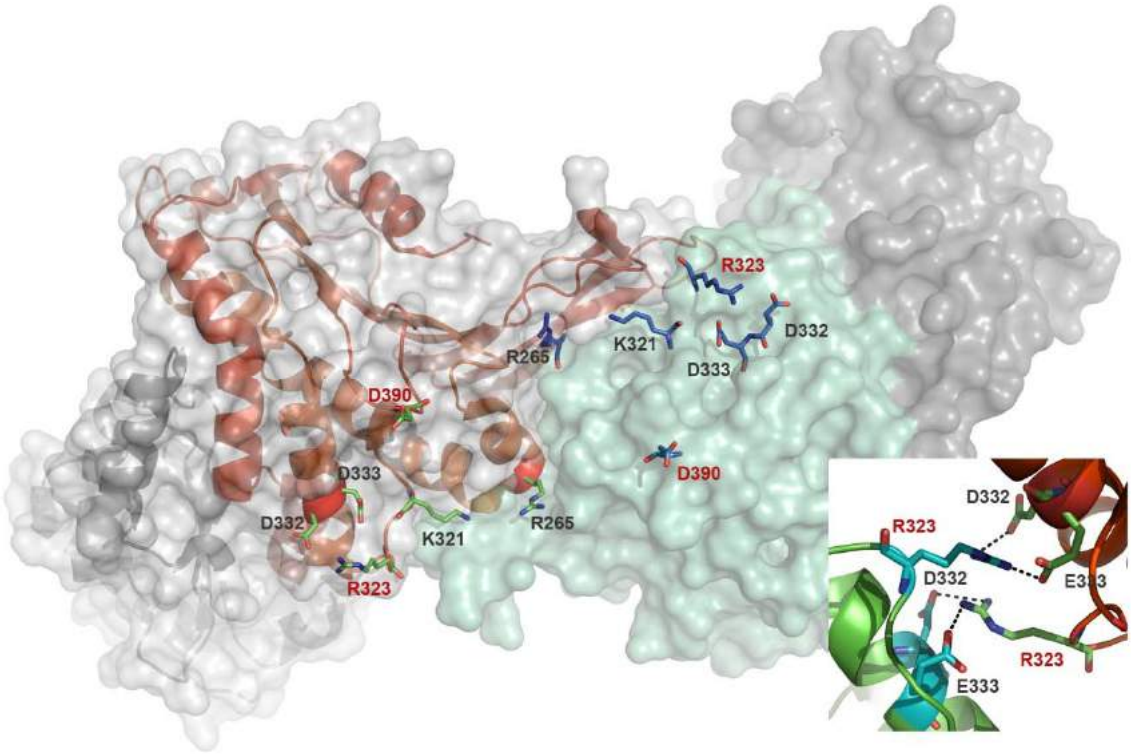
R323
D332
K321
D333
R265
D390
D390
D333
D332
K321
R265
R323
D332
R323
D332
E333
R323
E333

Figure 4

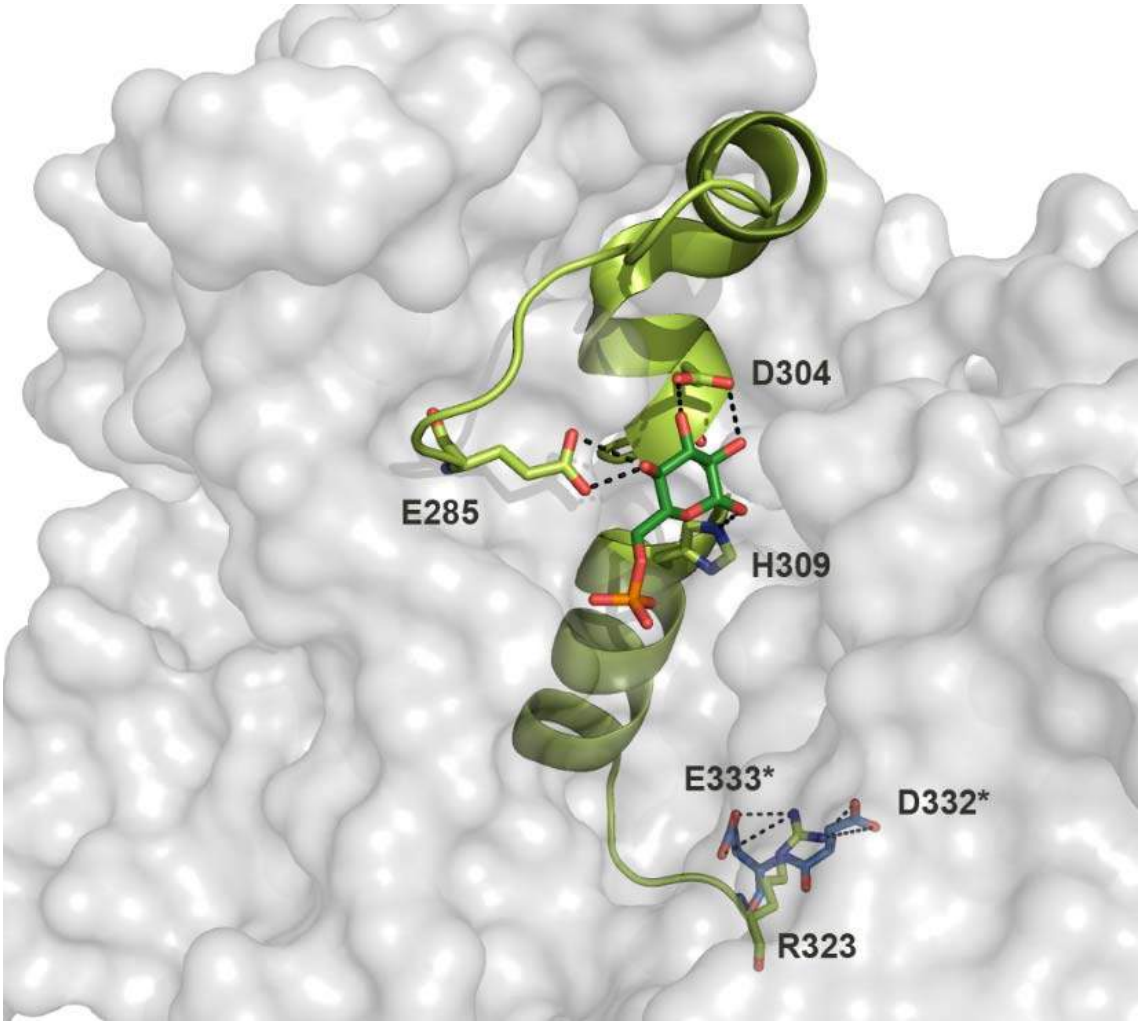

Figure 5

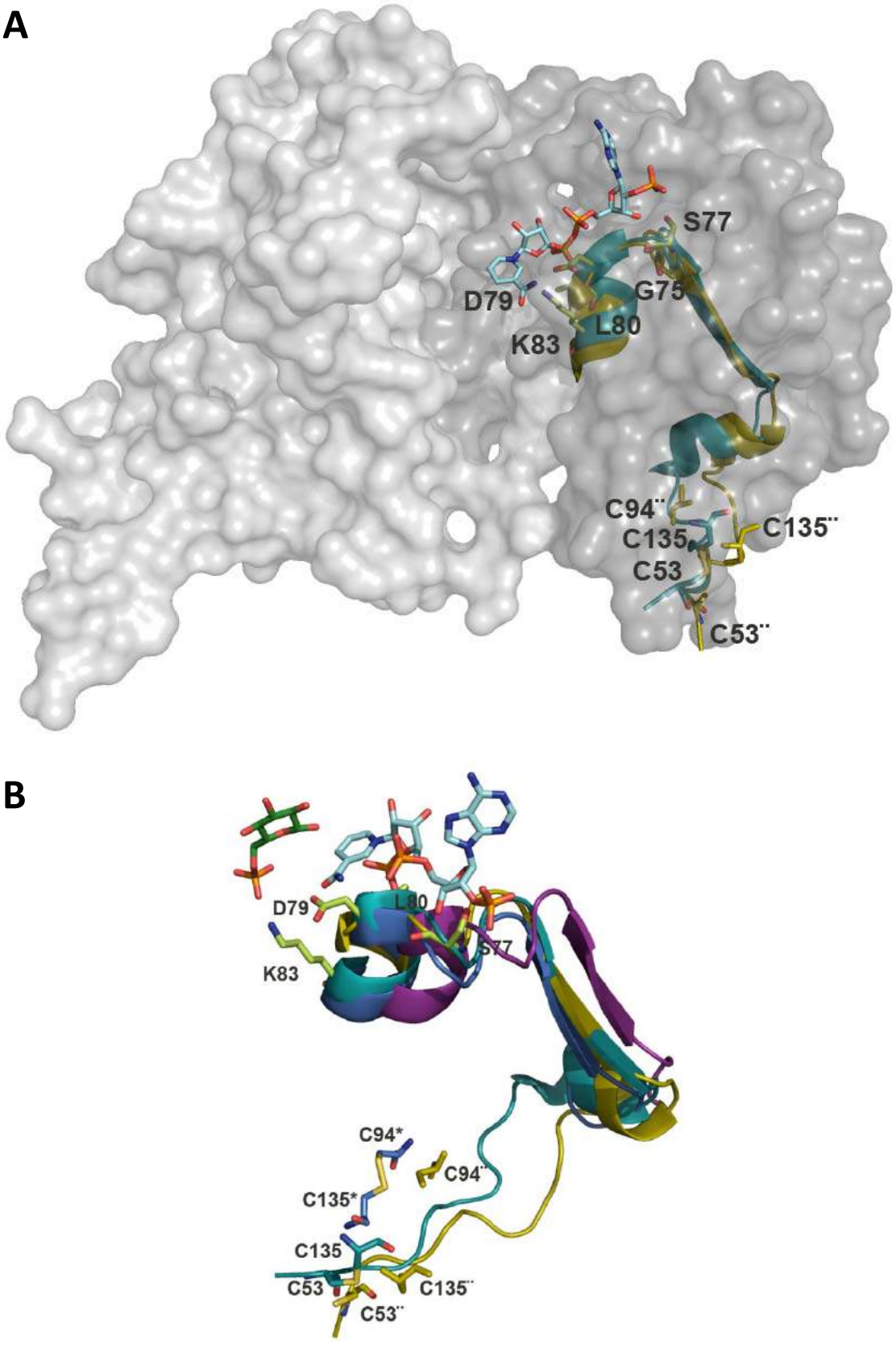
A
S77
D79
G75
L80
K83
C94¨
C135
C135¨
C53
C53¨
B
D79
L80
S77
K83
C94*
C94¨
C135*
C135
C53
C135¨
C53¨

Figure 6

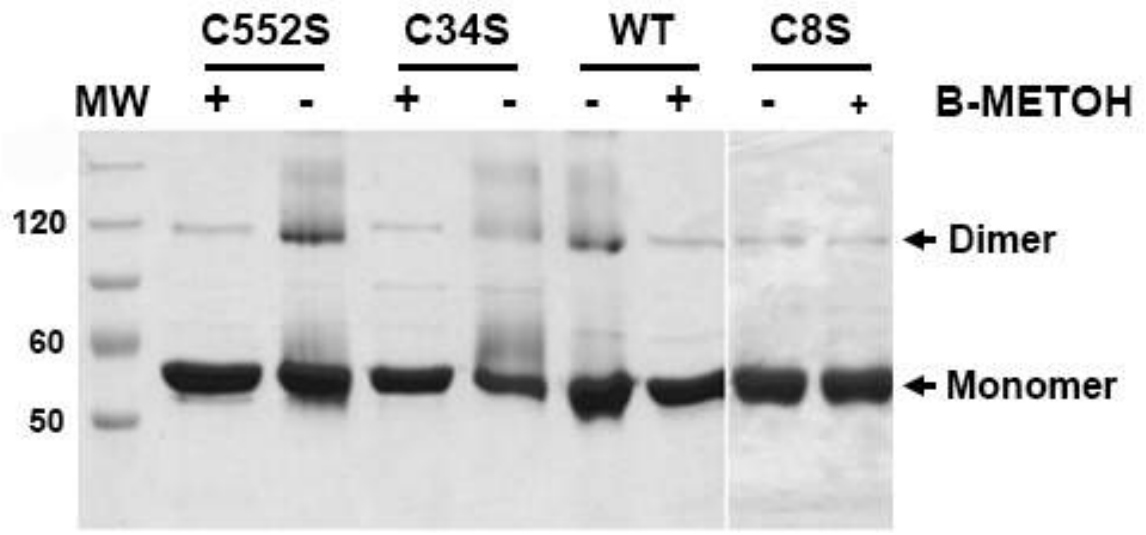

Figure 7

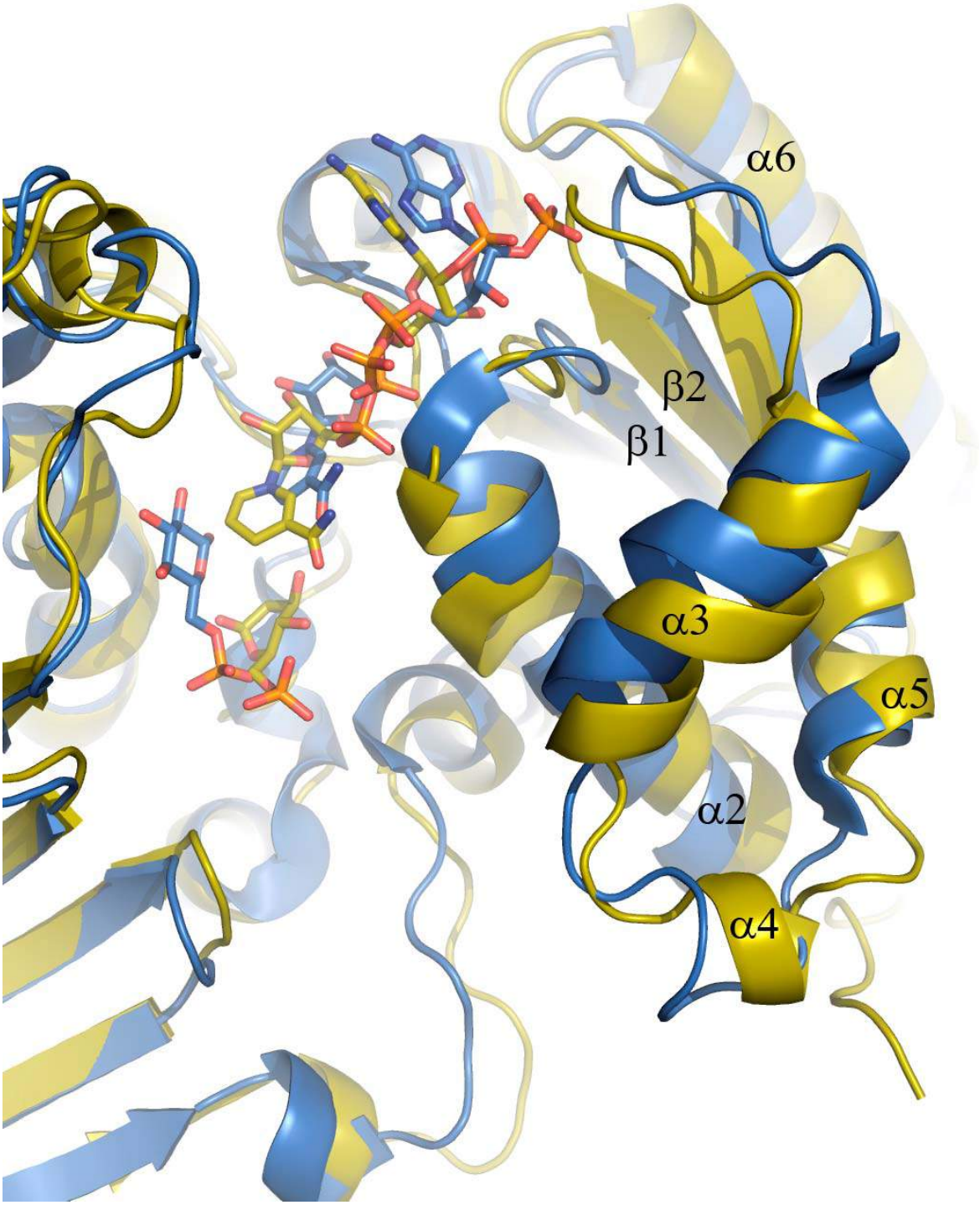

Figure 8

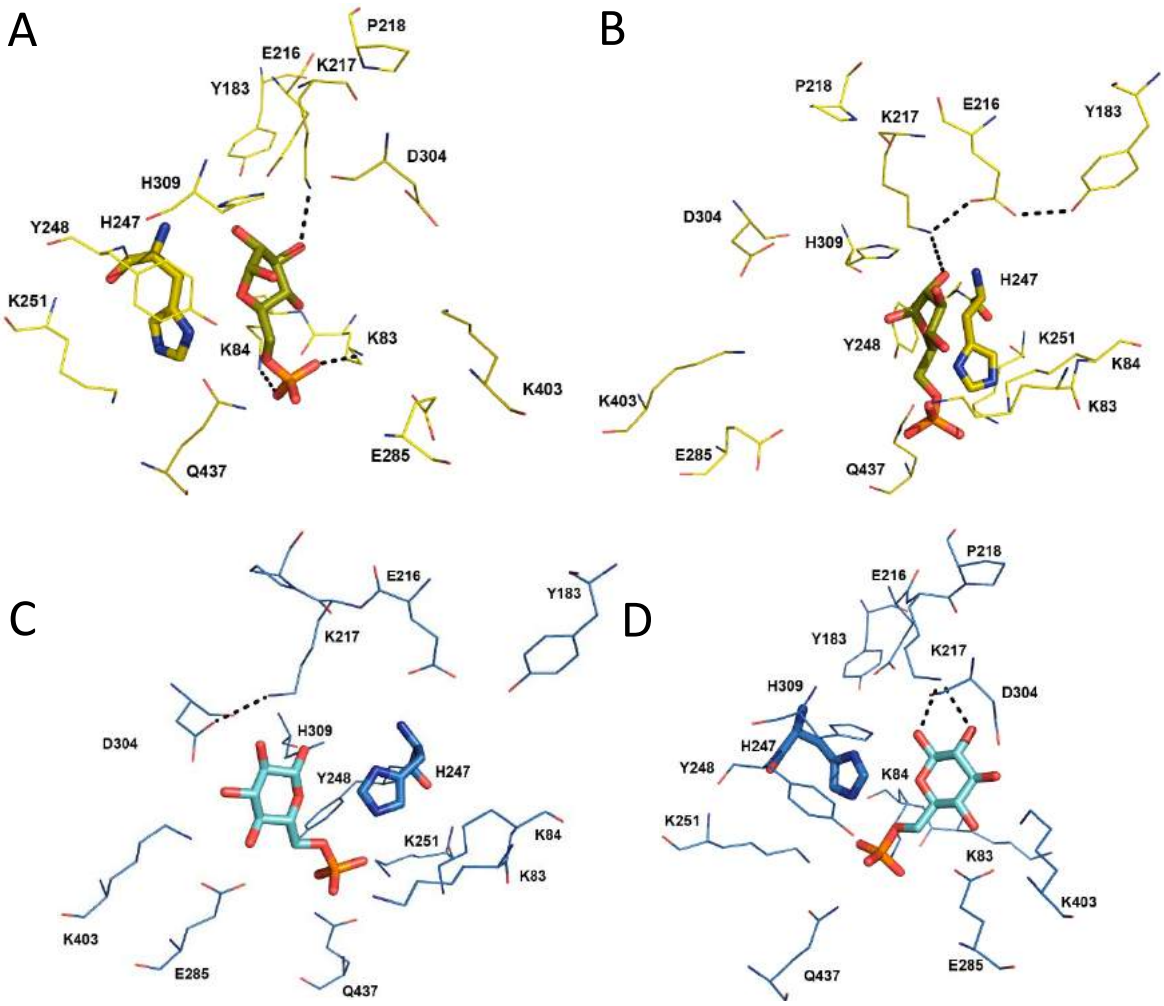
A
P218
E216
K217
Y183
D304
H309
Y248
H247
K251
K84
K83
K403
E285
Q437
B
P218
K217
E216
Y183
D304
H309
H247
Y248
K251
K84
K83
K403
E285
Q437
C
E216
Y183
K217
D304
H309
Y248
H247
K251
K84
K83
K403
E285
Q437
D
P218
E216
Y183
K217
H309
D304
H247
Y248
K84
K251
K83
K403
Q437
E285

Figure 9

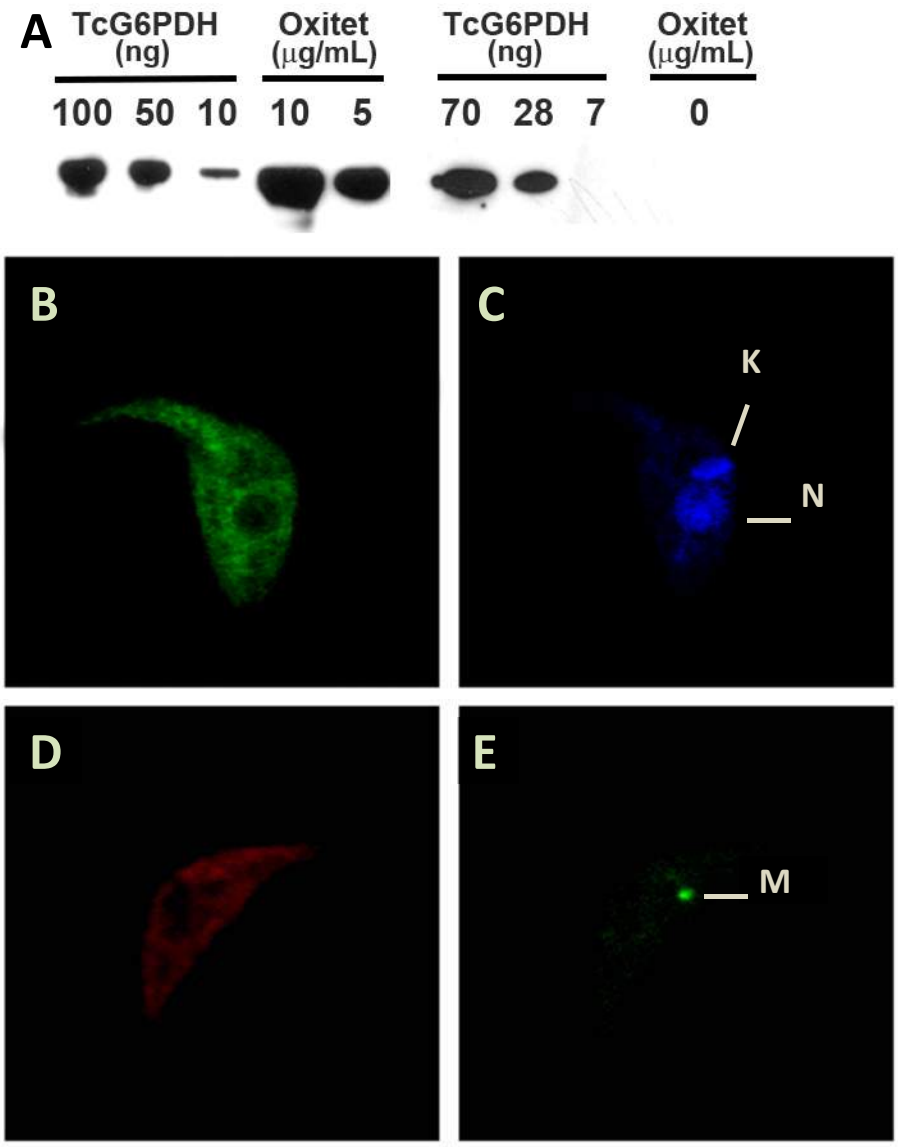
A
TcG6PDH (ng)
Oxitet (μg/mL)
TcG6PDH (ng)
Oxitet (μg/mL)
100 50 10
10 5
70 28 7
0
B
C
K
N
D
E
M

Figure 10

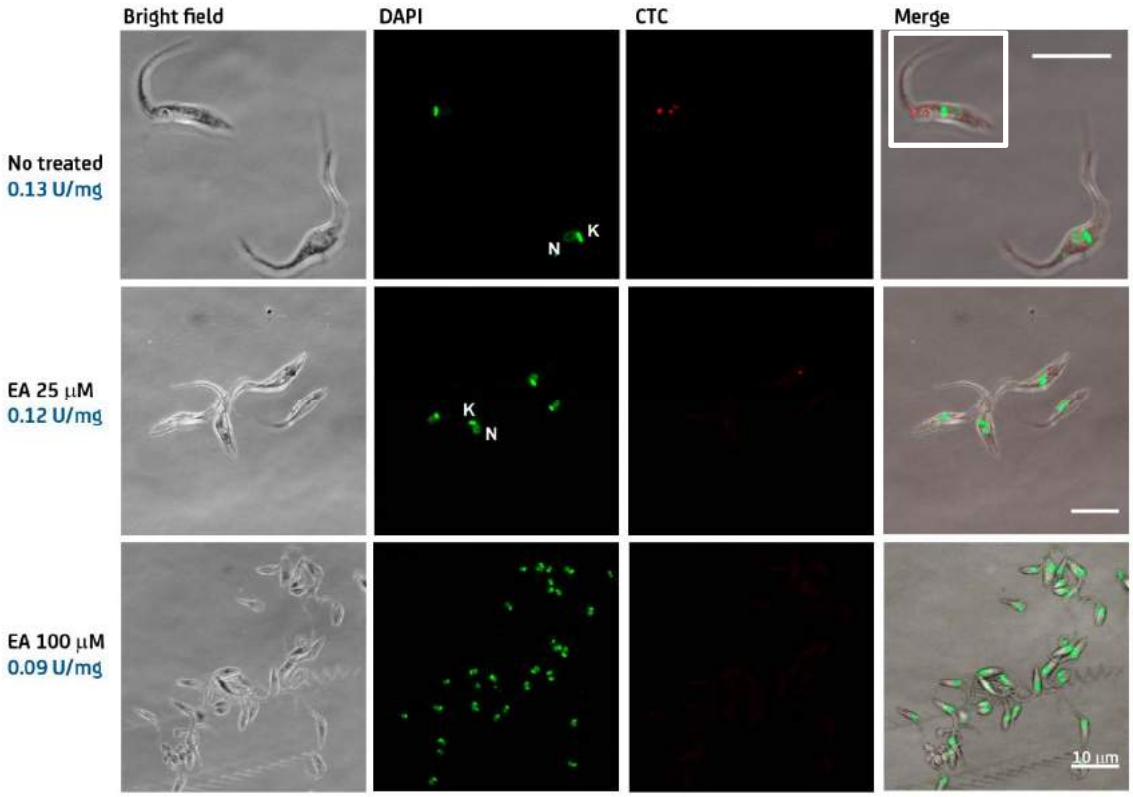
Bright field
DAPI
CTC
Merge
No treated
0.13 U/mg
N
K
EA 25 μM
0.12 U/mg
K
N
EA 100 μM
0.09 U/mg
10 μm

Figure 11

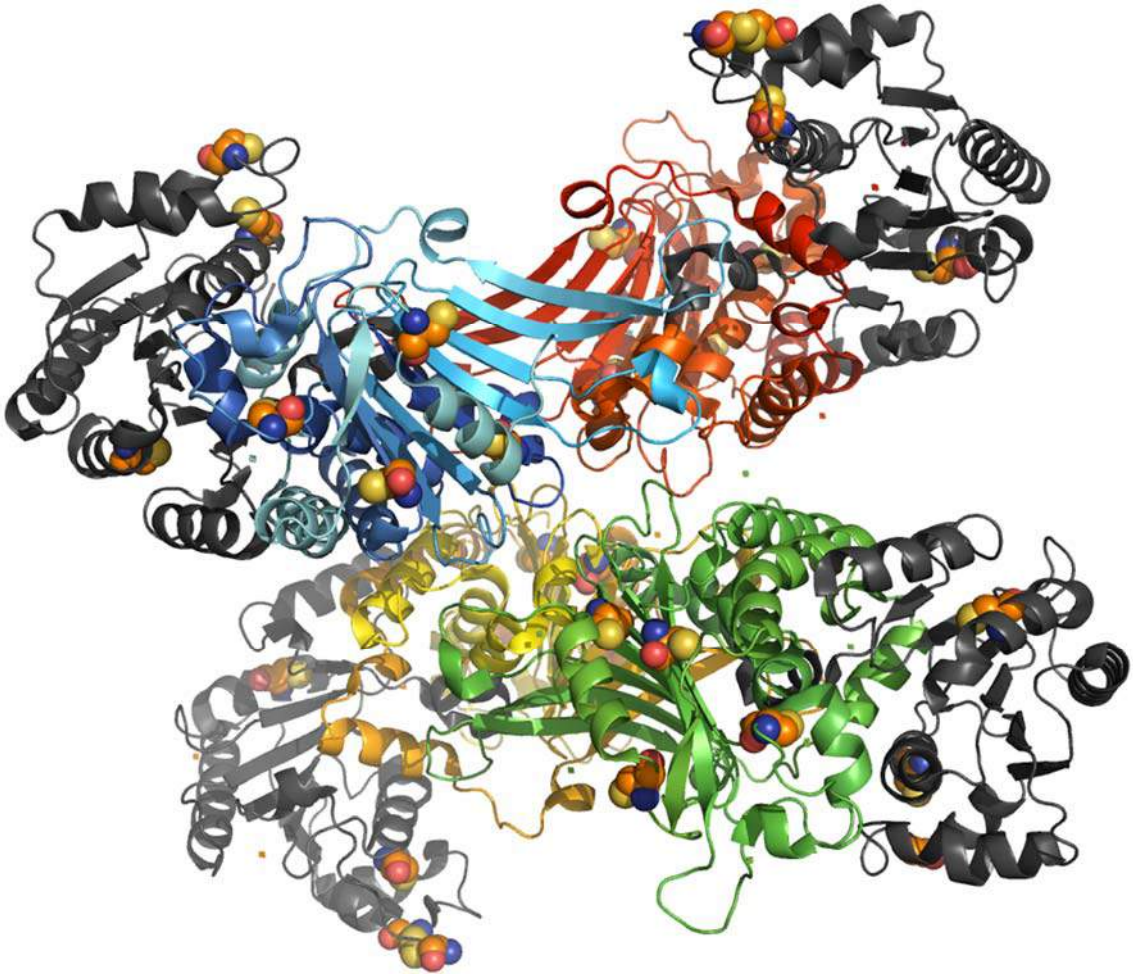

Figure S1

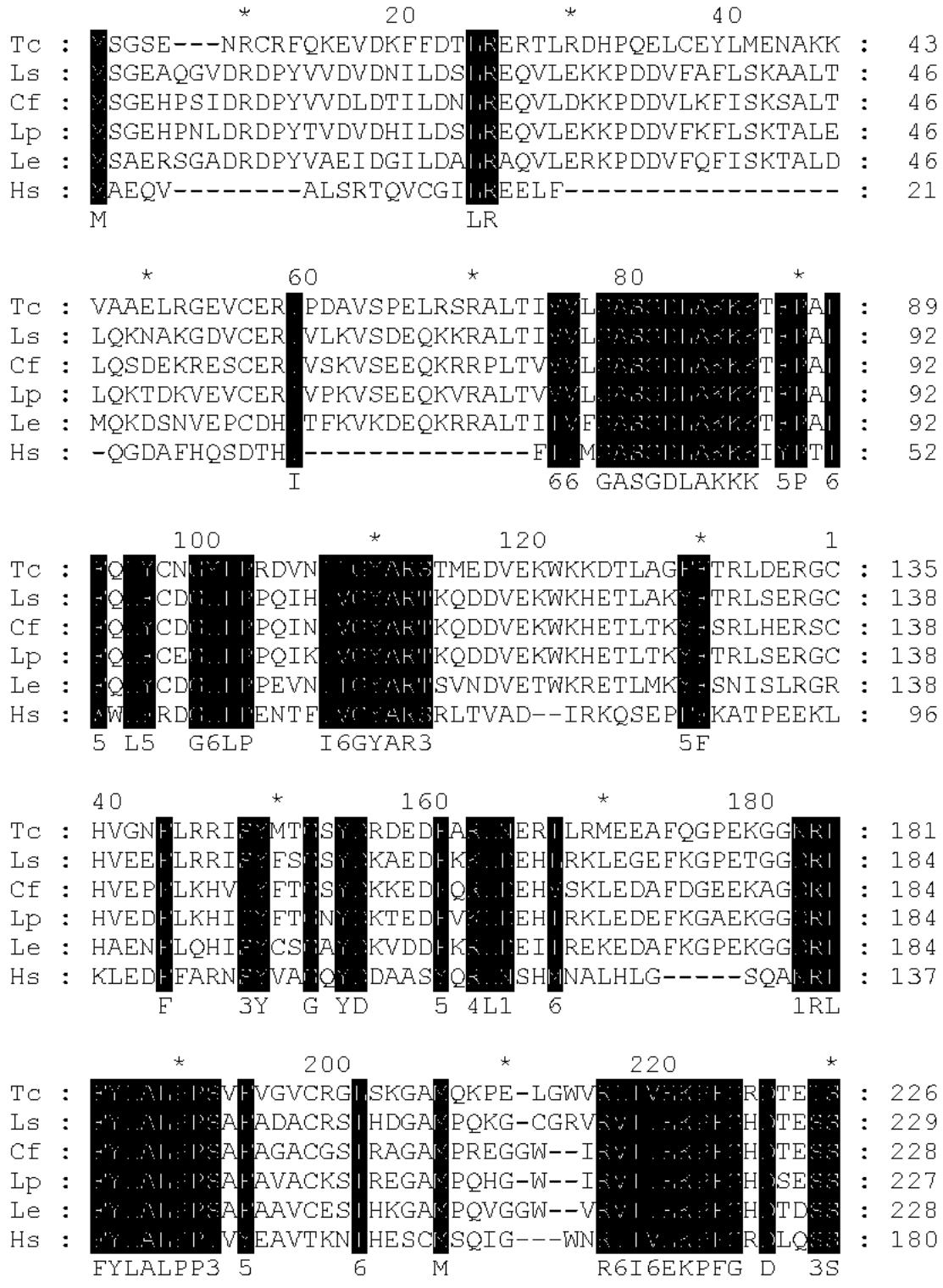

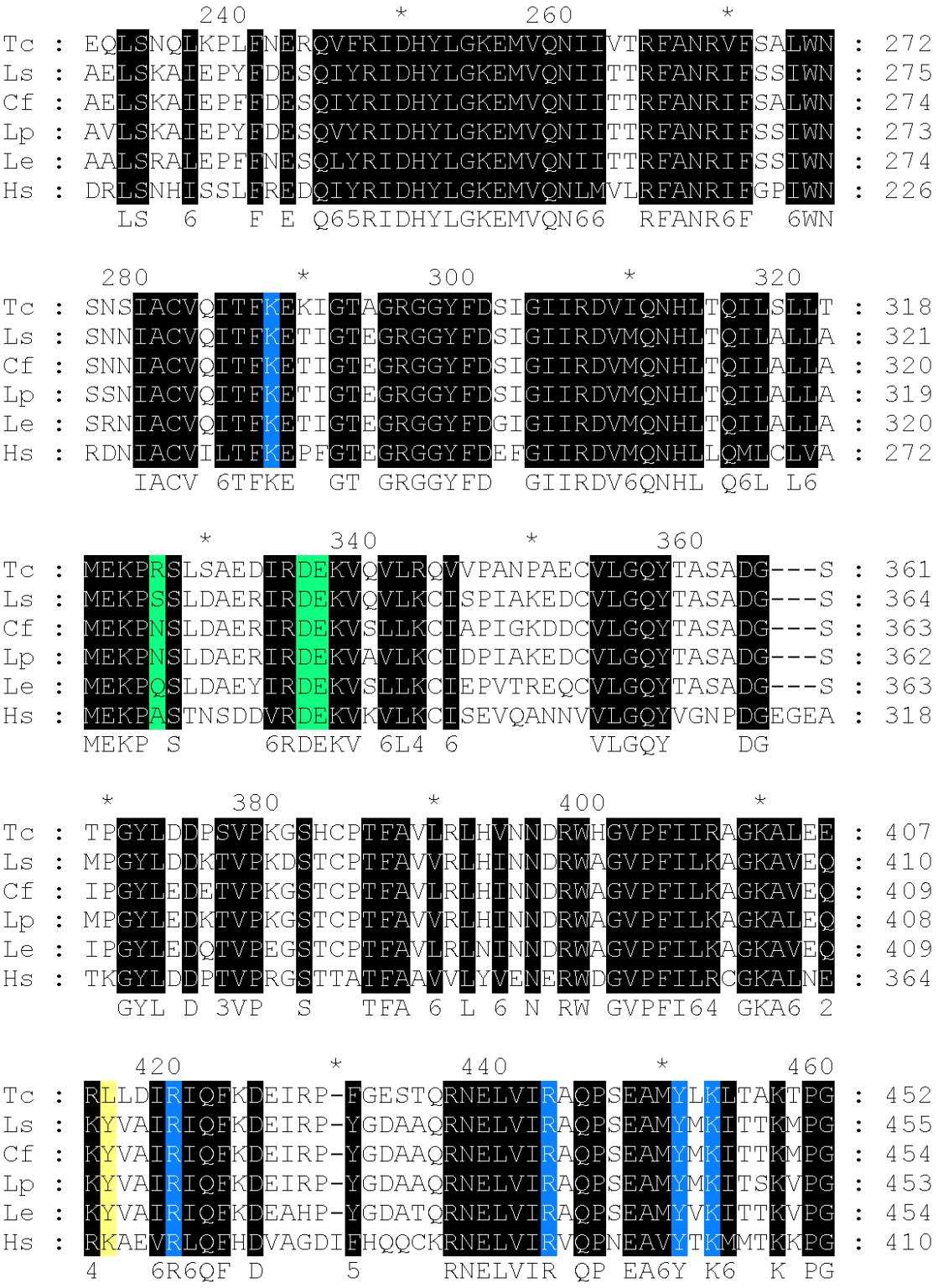
240 * 260 *
Tc : EQLSNQLKPLFNERQVFRIDHYLGKEMVQNIIVTRFANRVFSALWN : 272
Ls : AELSKAIEPYFDESQIYRIDHYLGKEMVQNIITTRFANRIFSSIWN : 275
Cf : AELSKAIEPFFDESQIYRIDHYLGKEMVQNIITTRFANRIFSALWN : 274
Lp : AVLSKAIEPYFDESQVYRIDHYLGKEMVQNIITTRFANRIFSSIWN : 273
Le : AALSRALEPFFNESQLYRIDHYLGKEMVQNIITTRFANRIFSSIWN : 274
Hs : DRLSNHISSLFREDQIYRIDHYLGKEMVQNLMVLRFANRIFGPIWN : 226
LS 6 F E Q65RIDHYLGKEMVQN66 RFANR6F 6WN
280 * 300 * 320
Tc : SNSIACVQITFKEKIGTAGRGGYFDSIGIIRDVIQNHLTQILSLLT : 318
Ls : SNNIACVQITFKETIGTEGRGGYFDSIGIIRDVMQNHLTQILALLA : 321
Cf : SNNIACVQITFKETIGTEGRGGYFDSIGIIRDVMQNHLTQILALLA : 320
Lp : SSNIACVQITFKETIGTEGRGGYFDSIGIIRDVMQNHLTQILALLA : 319
Le : SRNIACVQITFKETIGTEGRGGYFDGIGIIRDVMQNHLTQILALLA : 320
Hs : RDNIACVILTFKEPFGTEGRGGYFDEFGIIRDVMQNHLLQMLCLVA : 272
IACV 6TFKE GT GRGGYFD GIIRDV6QNHL Q6L L6
* 340 * 360
Tc : MEKPRSLSAEDIRDEKVQVLRQVVPANPAECVLGQYTASADG---S : 361
Ls : MEKPSSLDAERIRDEKVQVLKCISPIAKEDCVLGQYTASADG---S : 364
Cf : MEKPNSLDAERIRDEKVSLLKCIAPIGKDDCVLGQYTASADG---S : 363
Lp : MEKPNSLDAERIRDEKVAVLKCIDPIAKEDCVLGQYTASADG---S : 362
Le : MEKPQSLDAEYIRDEKVSLLKCIEPVTREQCVLGQYTASADG---S : 363
Hs : MEKPASTNSDDVRDEKVKVLKCISEVQANNVVLGQYVGNPDGEGEA : 318
MEKP S 6RDEKV 6L4 6 VLGQY DG
* 380 * 400 *
Tc : TPGYLDDPSVPKGSHCPTFAVLRLHVNNDRWHGVPFIIRAGKALEE : 407
Ls : MPGYLDDKTVPKDSTCPTFAVVRLHINNDRWAGVPFILKAGKAVEQ : 410
Cf : IPGYLEDETVPKGSTCPTFAVLRLHINNDRWAGVPFILKAGKAVEQ : 409
Lp : MPGYLEDKTVPKGSTCPTFAVVRLHINNDRWAGVPFILKAGKALEQ : 408
Le : IPGYLEDQTVPEGSTCPTFAVLRLNINNDRWAGVPFILKAGKAVEQ : 409
Hs : TKGYLDDPTVPRGSTTATFAAVVLYVENERWDGVPFILRCGKALNE : 364
GYL D 3VP S TFA 6 L 6 N RW GVPFI64 GKA6 2
420 * 440 * 460
Tc : RLLDIRIQFKDEIRP-FGESTQRNELVIRAQPSEAMYLKLTAKTPG : 452
Ls : KYVAIRIQFKDEIRP-YGDAAQRNELVIRAQPSEAMYMKITTKMPG : 455
Cf : KYVAIRIQFKDEIRP-YGDAAQRNELVIRAQPSEAMYMKITTKMPG : 454
Lp : KYVAIRIQFKDEIRP-YGDAAQRNELVIRAQPSEAMYMKITSKVPG : 453
Le : KYVAIRIQFKDEAHP-YGDATQRNELVIRAQPSEAMYVKITTKVPG : 454
Hs : RKAEVRLQFHDVAGDIFHQQCKRNELVIRVQPNEAVYTKMMTKKPG : 410
4 6R6QF D 5 RNELVIR QP EA6Y K6 K PG

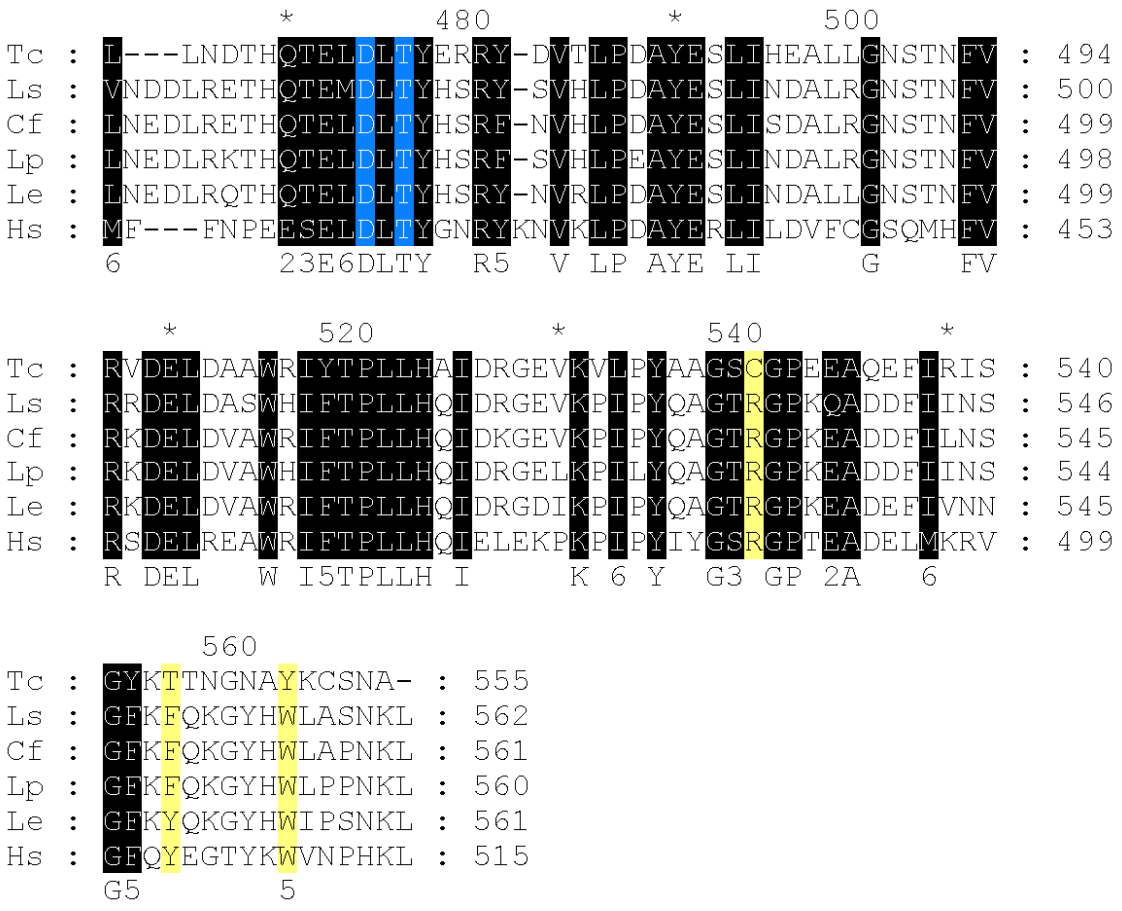
480
500
520
540
560
Tc : L---LNDTHQTELDLTYERRY-DVTLPDAYESLIHEALLGNSTNFV : 494
Ls : VNDDLRETHQTEMDLTYHSRY-SVHLPDAYESLINDALRGNSTNFV : 500
Cf : LNEDLRETHQTELDLTYHSRF-NVHLPDAYESLISDALRGNSTNFV : 499
Lp : LNEDLRKTHQTELDLTYHSRF-SVHLPEAYESLINDALRGNSTNFV : 498
Le : LNEDLRQTHQTELDLTYHSRY-NVRLPDAYESLINDALLGNSTNFV : 499
Hs : MF---FNPEESELDLTYGNRYKNVKLPDAYERLILDVFCGSQMHFV : 453
6 23E6DLTY R5 V LP AYE LI G FV
RVDELDAAWRIYTPLLHAIDRGEVKVLPYAAGSCGPEEAQEFIRIS : 540
RRDELDASWHIFTPLLHQIDRGEVKPIPYQAGTRGPKQADDFIINS : 546
RKDELDVAWRIFTPLLHQIDKGEVKPIPYQAGTRGPKEADDFILNS : 545
RKDELDVAWHIFTPLLHQIDRGELKPILYQAGTRGPKEADDFIINS : 544
RKDELDVAWRIFTPLLHQIDRGDIKPIPYQAGTRGPKEADEFIVNN : 545
RSDELREAWRIFTPLLHQIELEKPKPIPYIYGSRGPTEADELMKRV : 499
R DEL W I5TPLLH I K 6 Y G3 GP 2A 6
GYKTTNGNAYKCSNA- : 555
GFKFQKGYHWLASNKL : 562
GFKFQKGYHWLAPNKL : 561
GFKFQKGYHWLPPNKL : 560
GFKYQKGYHWIPSNKL : 561
GFQYEGTYKWVNPHKL : 515
G5 5

Figure S2

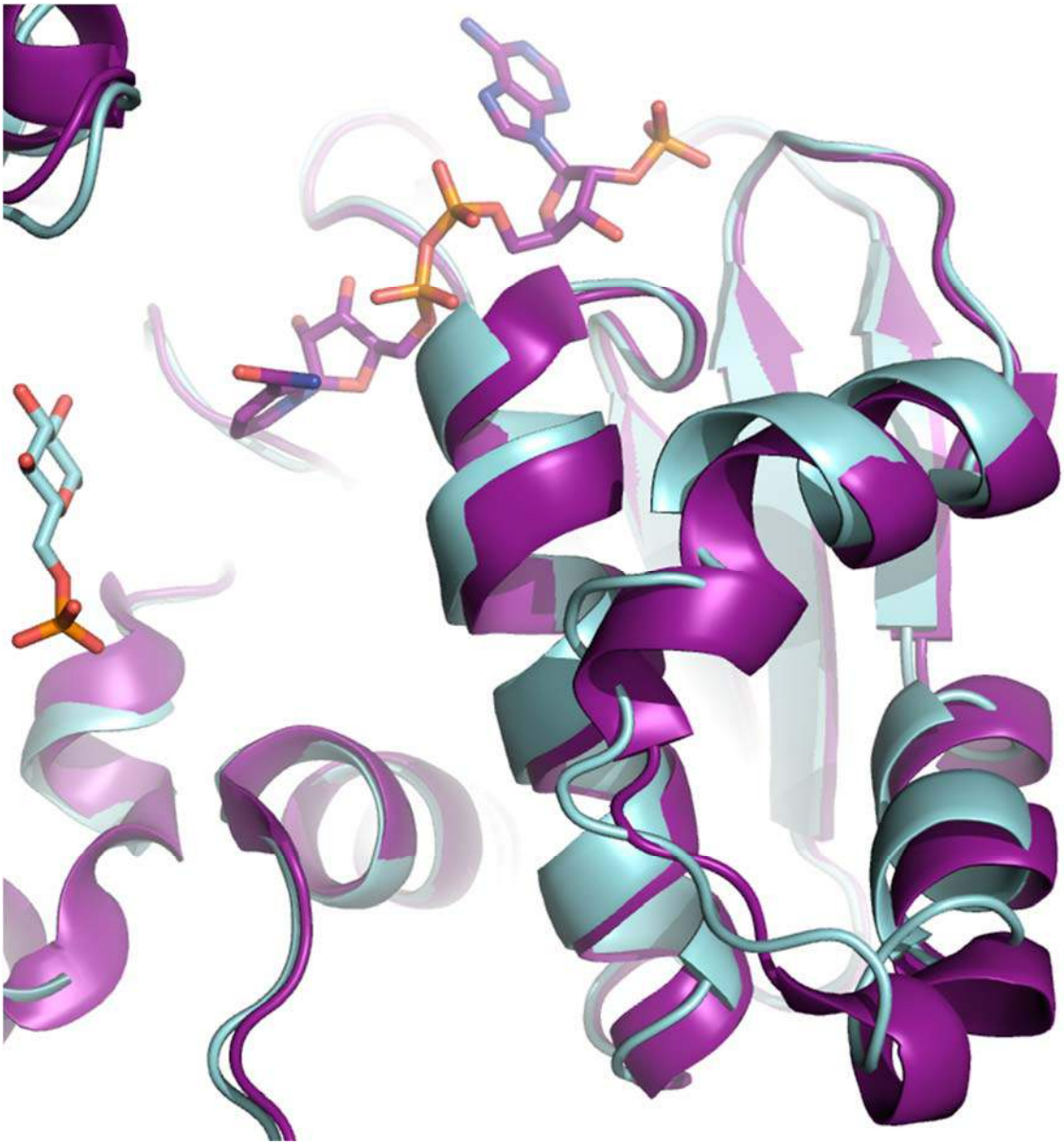

Figure S3

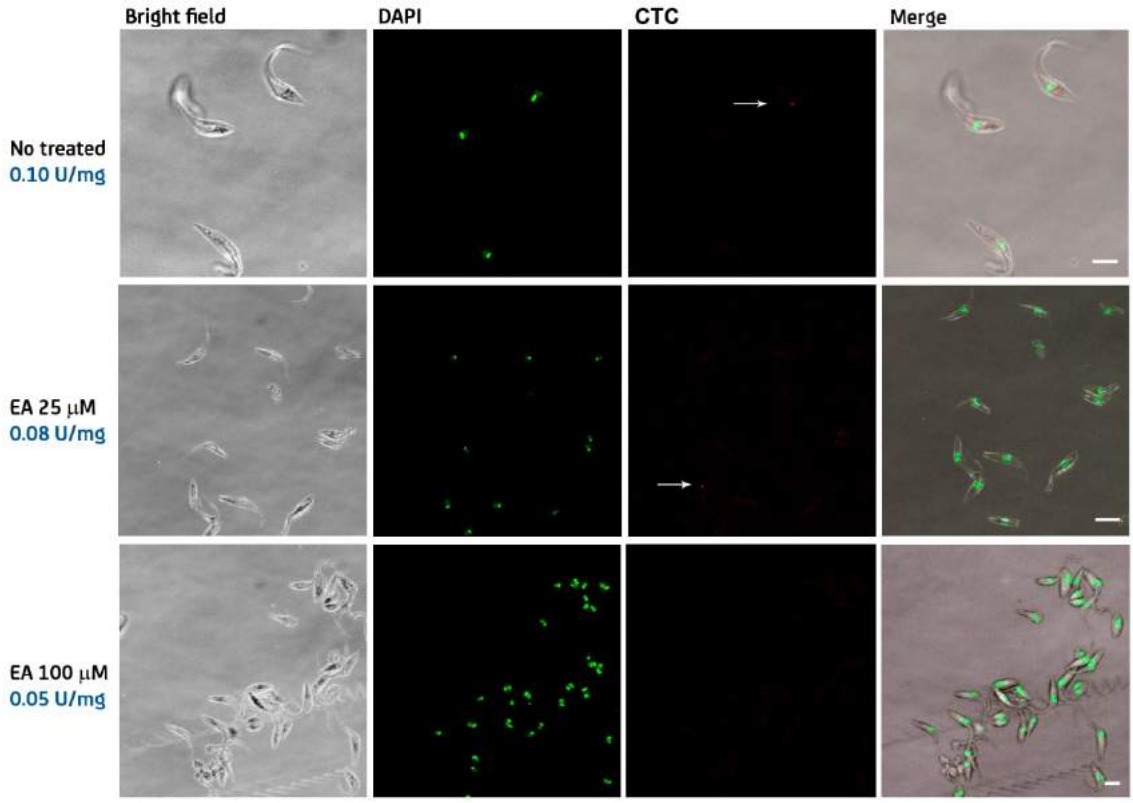
Bright field
DAPI
CTC
Merge
No treated
0.10 U/mg
EA 25 μM
0.08 U/mg
EA 100 μM
0.05 U/mg

Figure S4

Figure S5

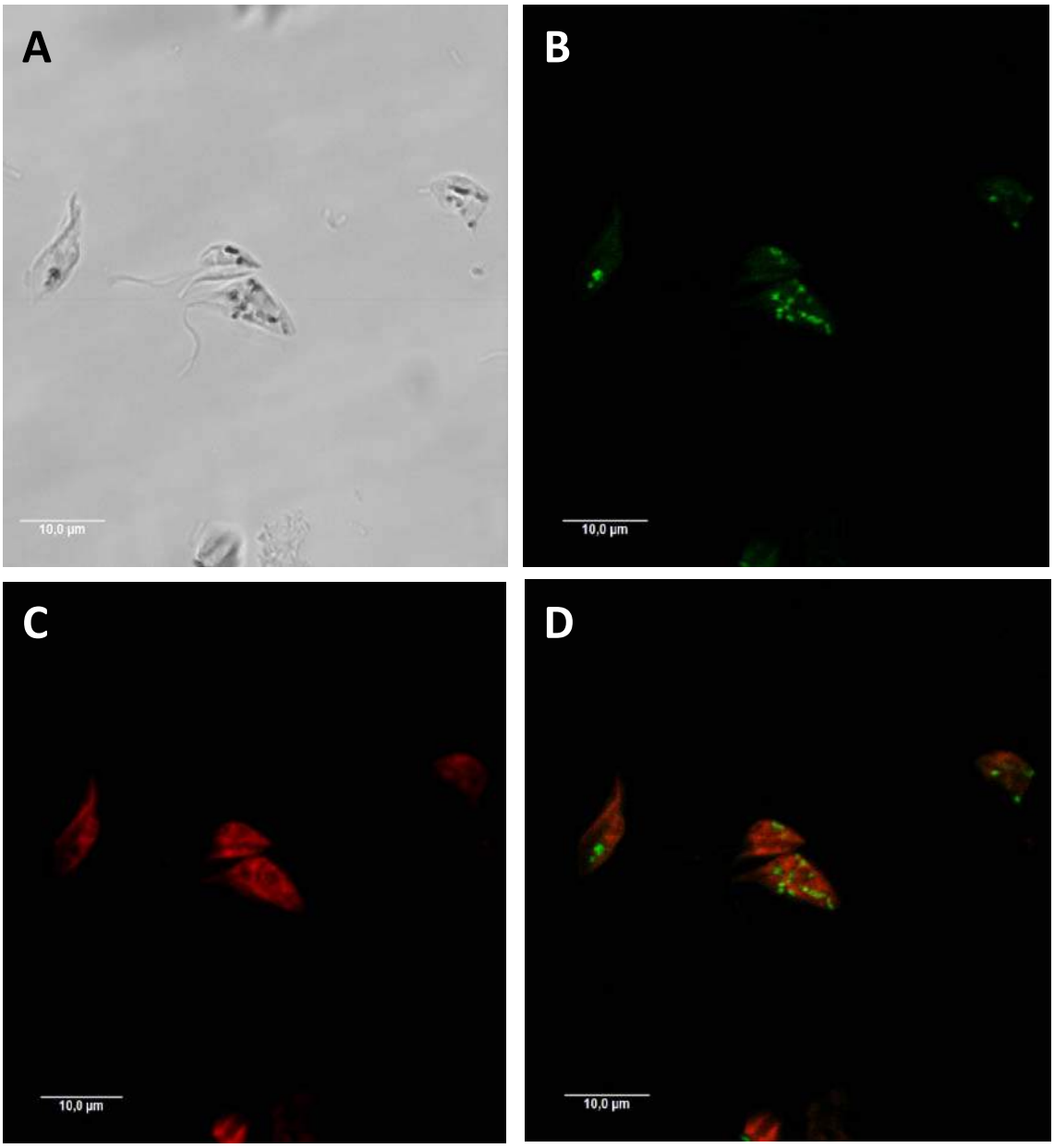

Figure S6

discusión general

Capítulo 4

DISCUSION GENERAL

Como bien se ha detallado en las secciones anteriores la G6PDH es una enzima central en el metabolismo del parásito, ya que participa de tres vías esenciales para su supervivencia. Su función principal radica en convertir a la G6P en 6PGL y generar poder reductor en forma de NADPH. En los últimos años su rol ha ganado relevancia y se la ha postulado como potencial blanco para el desarrollo de fármacos para el tratamiento de las tripanosomiasis.

Esta tesis ha contribuido de manera sustancial no solo con su caracterización enzimática y su descripción estructural, sino también en la elucidación de los mecanismos de acción de una familia de inhibidores; Aportando datos novedosos al área de la biología estructural de esta enzima.

4.1 La relevancia biológica de la estructura tetrámerica de la G6PDH de T. cruzi

Estudios realizados con G6PDH de diferentes organismos (Andrews, 1965; Beydemir, Sükrü et al., 2003; Comakli et al., 2015; Rowland et al., 1994; Shreve and Levy, 1977) muestran que estas enzimas adoptan principalmente una estructura cuaternaria homodimérica (Ranzani and Cordeiro, 2017). Al menos para la enzima de *L. mesenteroides* y la humana se había reportado que la forma monomérica es inactiva a pesar de contener los sitios de unión a sustrato y cofactor. La G6PDH humana también es capaz de formar tetrámeros los cuales presentan actividad enzimática, aunque esta conformación de la proteína representa una proporción pequeña en condiciones fisiológicas (Babalola et al., 1976). La capacidad de la enzima humana para modificar su estado oligomérico se debe a cierta inestabilidad en las interacciones que se dan entre sus subunidades, las cuales son extremadamente sensibles a variaciones en las condiciones fisicoquímicas del medio y a la presencia de diferentes ligandos (Bonsignore et al., 1970, 1971a, 1971b). El análisis estructural de la G6PDH de lactobacilo y humana puso en evidencia la importancia de la interacción entre elementos estructurales de las diferentes subunidades para moldear el sitio activo de la proteína, y como estos efectos alostéricos estabilizan tanto el dímero como la actividad catalítica de la enzima (Rowland et al., 1994). Como hemos mencionado anteriormente la G6PDH juega un rol fundamental en el metabolismo ya que es responsable de la generación de productos cuyo destino es muy diverso, por ejemplo; síntesis de ribonucleotidos, mantenimiento de la homeostasis redox, síntesis de lípidos o intermediarios de la glicólisis. Por esta razón no es extraño observar que la misma ha desarrollado diferentes estrategias de regulación de su expresión o actividad, entre ellas la regulación por producto, des/ acetilación o des/ fosforilación de residuos claves asi como, oxidación o reducción de cisteínas, inducción de la expresión génica frente a determinados estímulos, así como la regulación de su estado oligomérico. Siendo las dos últimas abordadas en este trabajo.

Al inicio de esta tesis la información disponible sobre el comportamiento oligomérico de la TcG6PDH era escasa e indicaba que, al igual que la gran mayoría de las proteínas homólogas de otros organismos (Andrews, 1965; Beydemir, Sükrü et al., 2003, 2003; Comakli et al., 2015; Ranzani and Cordeiro, 2017; Rowland et al., 1994; Shreve and Levy, 1977), la proteína del parásito presentaba una conformación dimérica. Sin embargo, pudimos demostrar que la misma adopta una conformación tetramérica, la cual es altamente refractaria a las condiciones fisicoquímicas del medio o a la presencia de ligandos que alteran el estado cuaternario de la proteína humana (Igoillo-Esteve and Cazzulo, 2006). Sólo una disminución en el pH (~5,5) con-

duce a la disociación del tetrámero de TcG6PDH en especies moleculares de menor masa, compatibles con dímeros y trímeros, indicando que interacciones de tipo electrostáticas son las que gobiernan la unión entre los dímeros. La actividad enzimática de la especie dimérica fue un 70% inferior a la determinada para el tetrámero, lo cual sugería que variaciones en el estado oligomérico repercuten a nivel de sitio activo de la enzima, aunque no podíamos descartar que parte de la pérdida de actividad se debiera a la protonación de residuos catalíticos claves como la H309 o la K217. Además, demostramos que una fracción de las subunidades de los dímeros interaccionan entre sí formando enlaces disulfuros que involucran a cisteínas de la extensión N-terminal de la proteína. Esto planteó varias incógnitas como ser la identidad de los aminoácidos involucrados en la formación del tetrámero estable y de los residuos que participan de los enlaces disulfuro intermoleculares en el dímero, así como la naturaleza de los eventos moleculares que son responsables de la disminución de actividad en el dímero.

Al comienzo de esta tesis existían datos cristalográficos para las deshidrogenasas del lactobacilo *Leuconostoc mesenteroides* (Kotaka et al., 2005; Rowland et al., 1994) y de *Homo sapiens* (Au et al., 1999, 2000). A pesar que las mismas podrían haber sido empleadas como templados moleculares para el desarrollo de modelos estructurales de la TcG6PDH, las propiedades bioquímicas descritas anteriormente para la enzima del parásito dejaban entrever lo limitado de esta estrategia para la obtención de información precisa y distintiva de la misma. Por ello es que nos embarcamos en la obtención de información a nivel atómico, en colaboración con la Unidad de Cristalografía de Proteínas del Institut Pasteur de Montevideo logramos cristalizar y resolver la estructura tridimensional del mutante truncado Δ37N-TcG6PDH en su forma apo y en presencia de G6P con valores de resolución de 2,85 Å (PDB 4EI9) y 3,35 Å (PDB 4EM5), respectivamente. Al igual que lo observado en solución, el arreglo espacial cristalino de la TcG6PDH se vuelve a corresponder con el de un tetrámero. Cada dímero se encuentra formado por dos subunidades idénticas en secuencia pero que presentan asimetría a nivel estructural (ej: presencia/ausencia de puentes disulfuro intramoleculares: C53-C135, así como corrimientos en regiones móviles). En lo que refiere al dominio catalítico, existen regiones que se encuentran altamente conservadas en todas las G6PDs como ser el péptido de 9 residuos RIDHYLGKE (de unión a G6P), o el sitio de unión a nucleótidos GxxGGDLA (localizada en el N-terminal) o la secuencia EKPxG (conteniendo a la P218 y K217) involucrada en la catálisis. A pesar de encontrar estas regiones invariantes en los sitios activos, notamos diferencias a nivel de los elementos estructurales que lo conforman que nos permitirán en parte explicar el comportamiento diferencial entre la proteína de *T. cruzi* y su contraparte humana.

Identificamos que a diferencia de la proteína humana, la región de tetramerización de la TcG6PDH consiste de una cavidad polar conformada y estabilizada por, fundamentalmente, interacciones electrostáticas entre 2 dímeros simétricos. Si bien muchos de estos residuos se encuentran conservados entre la enzima humana y la del parásito, encontramos que un residuo básico de esta última (R323) se encuentra mutado por una alanina en la proteína humana. Analizando los datos estructurales identificamos que la R323 forma puentes salinos con D332 y E333 de una segunda subunidad, de la misma forma que la R265 interacciona con la D390 de la otra subunidad y viceversa; lo que implica una ganancia de 12 interacciones electrostáticas por tetrámero de TcG6PDH. El reemplazo de la R323 por una glicina convirtió a la TcG6PDH en una proteína dimérica con una actividad específica significativamente inferior a la de la especie tetramérica y en el mismo orden al observado para los ensayos realizados con la forma salvaje a pH 5.5. Estos hallazgos confirmaron que el ensamble tetramérico es de naturaleza electroestática y le confiere estabilidad al sitio activo de la TcG6PDH.

Al investigar la región que contiene a R323 notamos que esta no presenta una estructura secundaria definida y que se encuentra contigua a la hélice α13 que contiene a los residuos H309 y D304, ambos esenciales para la actividad de la enzima (Cosgrove et al., 1998), la cual a su vez conecta con la cadena β15 en cuyo extremo se encuentra el E285 interaccionando con la G6P. Esto nos llevó a proponer que la conformación de dichos elementos en el mutante R323G es seguramente desestabilizada por la pérdida de estructura cuaternaria lo cual explicaría la disminución en la eficiencia catalítica de la enzima. Esto no estaría ocurriendo en el dímero de la enzima humana ya que esta región de la proteína, así como varios residuos que interaccionan con G6P, serían estabilizados por él efecto alostérico del $NADP^+$ estructural. De hecho, varios residuos que coordinan la unión del glucósido ocupan posiciones adyacentes a residuos que a su vez sirven de anclaje al $NADP^+$ estructural (Kotaka et al., 2005). En lo que refiere a esta región en la proteína humana, existen evidencias experimentales de pacientes con mutaciones en residuos que participan en la unión de este segundo $NADP^+$, lo cual se asocia a parámetros cinéticos desfavorables (Filosa et al., 1992; Gómez-Manzo et al., 2015; Mizukawa et al., 2011). La introducción de un residuo clave en la unión de $NADP^+$ estructural mejoró los parámetros cinéticos del dímero de TcG6PDH. Si bien esta mutación (C528R) no logró restaurar completamente la capacidad catalítica de la enzima, probablemente porque este mutante no reconstruye por completo este sitio alostérico de unión a $NADP^+$, este resultado es un indicio claro del rol estabilizador que dicha región cumple en la actividad de la enzima.

Un aspecto interesante que surgió de nuestro estudio es que las secuencias de G6PDH correspondientes a organismos no Kinetoplástidos que hemos analizado carecen de un residuo básico ocupando la posición de la R323 de *T. cruzi*, mientras que la naturaleza básica del aminoácido ocupando dicha posición en las secuencias pertenecientes a la gran mayoría de las especies de Kinetoplástidos estuvo conservada. Llamativamente, la excepción fueron las G6PDH de especies (ej. *C. fasciculata*, *Leptonomas* sp. y *L. enrietti*) de este linaje incapaces de establecer infección en humanos inmunocompetentes. Este hallazgo sumado al rol clave de la R323 en la estabilización del tetrámero de la TcG6PDH nos llevó a plantear la posible universalidad de dicha conformación cuaternaria en las G6PDH de Kinetoplástidos. Por otro lado, del análisis de las secuencias de G6PDH de Kinetoplástidos surge una interesante asociación: los organismos que presentan un residuo básico en dicha posición presentan un menor grado de conservación de los residuos que conforman el sitio alostérico de $NADP^+$ y viceversa. Sobre esta base de evidencias *in silico* y a partir del dato obtenido para el dímero con un sitio de $NADP^+$ parcialmente reconstituido, es que nos permitimos especular que las G6PDH capaces de formar tetrámeros pueden prescindir del sitio y función estabilizadora del $NADP^+$ estructural. Desde el punto de vista evolutivo, el hecho que varios (8 de 11) de los residuos que interaccionan con el $NADP^+$ estructural se encuentren conservados en las G6PDH de Kinetoplástidos indica que la mutación en la posición 323 que tuvo lugar en la mayoría de las secuencias de G6PDH de especies patógenas fue un evento posterior a la divergencia de este linaje de la rama eucariota. Ahora si este fenómeno está asociado o no a la adquisición de parasitismo por parte de los Kinetoplástidos es una hipótesis que valdría la pena ser estudiada a futuro, comenzando por investigar la estructura oligomérica de la G6PDH de Leptomonas y/o Crithidia.

Desde el punto de vista biológico, sabemos que la expresión de la TcG6PDH, asi como su actividad se ven incrementadas en los estadios infectivos (tripomastigotas) y replicativos (amastigota). En este sentido, la estabilidad estructural y funcional que le otorga la conformación tetramérica a la enzima del parásito representa una ventaja selectiva ya que de esta forma el patógeno se aseguraría un abastecimiento adecuado de equivalentes de reducción y de R5P, ya que se ha planteado que esta enzima constituye la etapa limitante de la PPP (Igoillo-Esteve and Cazzulo, 2006; Maugeri and Cazzulo, 2004). Este no es detalle menor ya estos organismos presentan una tasa de proliferación superior al de células de mamíferos y durante su ciclo de vida se ven enfrentados a estrés oxidativo, por ej. como parte de la respuesta inmune del huésped. Como se discute más adelante, la G6PDH de *T. cruzi* ha incluso desarrollado un

mecanismo de regulación redox que se traduce en una activación adicional de la actividad enzimática frente a condiciones de estrés oxidativo.

4.2 Regulación redox de la TcG6PDH y efecto alostérico de la extensión N-terminal

Previamente se reportó que el gen de la G6PDH presenta dos posibles codones de inicio de la traducción (Igoillo-Esteve and Cazzulo, 2006). Por un lado está la secuencia completa del gen que codifica para la versión salvaje o "larga" de la proteína que constaría de unos 555 residuos. Por otro lado, unas 114 bases (o 38 residuos) corriente abajo del codón de inicio de la forma larga de la G6PDH se ubica un segundo codón que codifica para una metionina. La traducción a partir de esta segunda metionina daría lugar a un polipéptido de 518 residuos, denominado como la forma "corta" o truncada (Δ37N-G6PDH) de la G6PDH. In vitro, ambas proteínas resultaron ser funcionales aunque, a nivel celular, la forma larga mostró ser la isoforma mayoritaria expresada por el parásito (Igoillo-Esteve and Cazzulo, 2006). La presencia de una extensión N-terminal al plegamiento de Rossmann se repite en las secuencias de G6PDH de todos los Kinetoplástidos con secuencias disponibles y también en las isoformas plastídicas de cianobacterias y plantas (Duffieux et al., 2000; Wenderoth et al., 1997; Wendt et al., 2000). Para las G6PDH de Kinetoplástidos, dichas extensiones comparten un 52% de identidad de secuencia entre sí y en las cuales se destaca la presencia de residuos cargados.

La actividad de la forma salvaje, pero no la truncada, de TcG6PDH resultó ser sensible a agentes reductores (Igoillo-Esteve and Cazzulo, 2006). Un comportamiento similar se había reportado anteriormente para la isoforma plastídica, pero no así para la citosólica, de la G6PDH de ciertos organismos fotosintéticos (Wenderoth et al., 1997). En los organismos fotosintéticos, la regulación redox de la G6PDH de cloroplastos cumple un rol metabólico importante en el ciclo de Calvin (fijación de carbono). El mecanismo de regulación implica la inactivación reversible de la G6PDH por el sistema ferredoxina/tiorredoxina durante la etapa de luz, en la cual $NADP^+$ es reducido a través del flujo de electrones de la fotosíntesis y su posterior activación durante la fase oscura del ciclo (Wendt et al., 2000). Los residuos de cisteína que son blanco de dicha (in)activación no se hayan conservados (Cardi et al., 2016).

Un estudio previo, había reportado que la forma salvaje de la TcG6PDH perdía actividad cuando era expuesta a altas concentraciones de distintos agentes reductores (fisiológico: GSH, y no fisiológicos: el ditiol DTT o el monotiol β-mercaptoetanol), mientras que, de manera opuesta, la

forma truncada Δ37N- de esta proteína era activada por estos tratamientos (Igoillo-Esteve and Cazzulo, 2006). En base a estos resultados los autores propusieron que la forma nativa de la G6PDH de *T. cruzi* estaría sujeta a un mecanismo de regulación redox similar al de los organismos fotosintéticos. No obstante, los detalles moleculares de esta regulación resultaban desconocidos, parte de los cuales fueron abordados en este trabajo de tesis.

Nuestros resultados revelaron que la cisteína 8 de la región N-terminal está implicada en la formación de disulfuros entre las subunidades que forman el dímero de TcG6PDH y que este enlace covalente es responsable de la incrementada actividad de la enzima en condiciones no reductoras. Dicho tipo de enlace requiere de un segundo residuo de cisteína. Las cisteínas: C34, C528 y C552 eran potenciales candidatos ya que se encuentran localizados en regiones de la proteína expuestas al solvente. Sin embargo, ninguno de ellos participa en la formación del puente disulfuro intermolecular. Una posibilidad es que sea la misma C8 de cada subunidad del dímero la que forme un homodisulfuro con la C8 de la subunidad opuesta. Sin embargo, tampoco podemos descartar que C53 o C135 estén involucrados en dicha interacción entre subunidades, ya que como se observa en la estructura de la forma truncada de la proteína (PDB 4EM5), dichos residuos son proclives a formar disulfuros intramoleculares. De todas formas, está claro que la cisteína que participa en la regulación redox de la actividad en la TcG6PDH no está conservada con la descrita para cianobacterias ni formas plastídicas de vegetales y que por lo tanto el mecanismo molecular implicado en el control de la actividad enzimática difiere entre dichas proteínas. El reemplazo de C8 por una serina impide la formación del puente disulfuro intermolecular, llevando a una disminución de la eficiencia catalítica de la enzima por ambos sustratos, en gran medida debido al incremento en las K_M y la disminución en el k_{cat} para $NADP^+$. Un comportamiento cinético similar, en particular en lo que refiere a los cambios en afinidad por sustratos, fue obtenido para la forma salvaje de la enzima ensayada bajo condiciones reductoras. Esto indica que la oxidación de la TcG6PDH tiene por principal efecto incrementar la afinidad por los sustratos.

Con el fin de obtener información estructural que nos brindara pistas sobre cómo esta región de la proteína estaría influenciando el sitio activo de la enzima es que trabajamos arduamente en la obtención de cristales de buena calidad para la forma salvaje de la TcG6PDH en condiciones no reductoras. Identificamos condiciones de obtención de cristales homogéneos y de tamaño aceptable que nos permitieron resolver la estructura de la forma salvaje de la TcG6PDH. Sin embargo, estos datos no aportaron información adicional sobre el segmento N-terminal ya que en estas regiones no se obtuvieron buenos mapas de densidad electrónica para el mismo,

seguramente porque se trata de una región con gran dinámica o flexibilidad (datos no publicados). También generamos cristales para el mutante C8S de la forma salvaje en su forma apo y en complejo con $NADP^+$, los cuales fueron enviados al sincrotrón de Soleil (Saint-Aubin, Francia), pero los mismos no difractaron adecuadamente como para permitir resolver la estructura de la proteína.

Ante esta limitación decidimos analizar las diferentes estructuras cristalinas disponibles para la enzima de *T. cruzi* y la humana, así como un modelo catalítico de la primera, prestando especial atención al dominio N-terminal de la enzima. El análisis realizado muestra que varias regiones de este dominio poseen gran dinámica conformacional la cual es influenciada por la unión de sustratos y la formación de disulfuros intramoleculares (presentes en la forma truncada TcG6PDH). Varios de estos elementos estructurales móviles conectan con el extremo N-terminal y contienen residuos claves en la unión de sustratos y/o en la catálisis (Kotaka et al., 2005; Ortiz et al., 2016; Rowland et al., 1994). Entre ellos se destacan L80, K83 y K84, localizados entre β1 y α2, e importantes en dar forma al sitio catalítico y la unión de G6P. Si bien a nivel de secuencia K217 aparece más alejada de la región N-terminal (K217 se ubica en el loop que conecta β5 con α8), en realidad este residuo se halla en estrecho contacto con esta región a partir de una red de puentes de hidrógeno (K217-E216-Y183) que lo aproximan a β1. De hecho, el modelo de dinámica molecular del complejo ternario, complementado con el análisis cinético del mutante K217I, demostró que este residuo, al igual que la cis-Pro que lo sucede (P218), juega un rol clave en la catálisis, posiblemente actuando como una segunda base complementaria a H309 en la transferencia del hidrogenión de G6P a $NADP^+$. Por lo tanto, proponemos que cambios conformacionales en la extensión N-terminal de TcG6PDH producto de la formación/ruptura del enlace disulfuro entre C8 y otra cisteína de la subunidad opuesta podrían desencadenar cambios en la dinámica de los elementos contiguos del dominio Rossmann, los cuales afectarían a residuos importantes para la unión de ligandos y catálisis. Alternativamente, la extensión N-terminal podría estar afectando la accesibilidad de los sustratos al sitio activo mediante impedimento estérico. Esta hipótesis es aún compatible con las alteraciones cinéticas observadas para las distintas formas de TcG6PDH ya que de acuerdo al mecanismo y modelo catalítico la unión de ligandos induce cambios conformacionales a nivel del sitio catalítico. Por lo tanto, una unión de baja afinidad o alterada de uno o ambos sustratos no sería un estímulo suficiente para disparar dichas adaptaciones estructurales, necesarias para que tenga lugar la catálisis. Si bien aún estamos lejos de comprender los detalles moleculares de esta regulación, esta tesis contribuyó a dilucidar uno de los tioles involucrados en este mecanismo así como el

impacto de la misma sobre la actividad enzimática, además de aportar posibles modelos mecanísticos. La activación de la proteína de *T. cruzi* en condiciones no reductoras es moderada y se puede observar un aumento del 20% de actividad enzimática con respecto al mutante de C8S. Teniendo en cuenta que el ambiente intracelular es reductivo, nos permite estipular que este tipo de regulación significa una ventaja en condiciones de estrés oxidativo como las generadas por la respuesta inmune del hospedero. En este sentido *T. cruzi* no sólo depende de la inducción de la expresión de la proteína para adaptarse a este nuevo ambiente sino que, rápidamente empleando este mecanismo puede regular su actividad, incrementándola aproximadamente un 20%. Si bien es un aumento discreto creemos podría ser una rápida solución ya que otros estudios indican que tras la inducción de stress oxidativo se observa un incremento de un 10% de la tasa de utilización de la PPP (Maugeri and Cazzulo, 2004).

Dado que los elementos/residuos que ejercen control alostérico sobre la actividad de TcG6PDH son únicos para la proteína de este patógeno y otros tripanosomátidos, en principio esto los convierte en posibles blancos moleculares para el desarrollo de inhibidores selectivos. En la sección final se realiza un análisis crítico de dicho potencial.

4.3 El modo de unión de los compuestos esteroideos a TcG6PDH implica el bloqueo estérico de la catálisis

A nivel de las enfermedades no transmisibles, la búsqueda de inhibidores contra la G6PDH estuvo motivada porque la misma ha sido propuesta como un blanco farmacológico para el tratamiento del cáncer ya que varios estudios destacan niveles elevados de esta enzima en tumores de distinto origen, y lo cual en general está asociado a resistencia a quimioterápicos como a metástasis (Jiang et al., 2011). En el caso de las enfermedades infecciosas, la G6PDH de los patógenos humanos *P. falciparum* y *T. cruzi* despertaron interés dada la relevancia de dichas enzimas en la supervivencia y virulencia de ambos parásitos (Gupta et al., 2011a; Jortzik et al., 2011). Las campañas de búsqueda de posibles candidatos farmacológicos contra la G6PDH ha dado lugar a la identificación de varias moléculas inhibidoras que además de diferir en sus estructuras químicas presentan, mecanismos de acción variado incluyendo aquellos de tipo competitivo, no competitivo y acompetitivo, ver Figura 5 (Mercaldi et al., 2014; Preuss et al., 2012a, 2012b). Estos últimos son considerados como inhibidores ideales, ya que los mismos interfieren con la catálisis y no con la unión de los sustratos a la enzima. De hecho, la unión de los inhibidores acompetitivos a la enzima requiere la formación previa de un complejo enzima-

sustrato por el cual los mismos presentarán una gran afinidad, no siendo el caso para la forma apo de la enzima (Cornish-Bowden, 1986). El hecho que estos inhibidores no compitan con los sitios de unión de sustratos sino que, por el contrario, su unión a la enzima se ve beneficiada por la unión del ligando nativo a la misma, tiene importantes implicancias biológicas. A nivel *in vivo*, la inhibición de la enzima conlleva a la acumulación de sustrato lo cual desplaza el equilibrio hacia una mayor formación del complejo enzima-sustrato que es el blanco molecular del inhibidor, por lo que a lo largo del tiempo se verá un incremento gradual de la fracción de enzima inhibida. En resumen, el poder de estos inhibidores radica en que su inhibición no puede ser competida por sustratos sino que la acumulación *in vivo* de los mismos ejerce un *loop* positivo de inhibición enzimática.

Los compuestos esteroides como la epiandrosterona (EA) y la dehidroepiandrosterona (DHEA) y sus derivados (Cordeiro and Thiemann, 2010; Cordeiro et al., 2009; Hamilton et al., 2012; Marks and Banks, 1960), a así como más recientemente nuevas series de quinazolinonas y tienopirimidinas (Cordeiro and Thiemann, 2010; Cordeiro et al., 2009; Gupta et al., 2011b, 2011a; Mercaldi et al., 2014) han sido reportados como inhibidores acompetitivos de la G6PDH humana y/o la enzima de *T. cruzi*. Para el caso de los esteroides, la 16-Br epiandrosterona presentó una marcada potencia y selectividad contra la enzima del patógeno respecto de la humana (Cordeiro and Thiemann, 2010), planteando la posibilidad de selectividad en el modo de unión del mismo. A la fecha de iniciada esta tesis se carecía de evidencia estructural sobre el sitio de unión de estos inhibidores a G6PDH de cualquier especie. Años más tarde, el grupo del Dr. Hamilton de la Universidad de Manchester (Inglaterra) publicó la síntesis y caracterización de nuevos análogos de esteroides que aún no habían sido explorados contra la G6PDH de organismos patógenos (Hamilton et al., 2012). Consideramos por lo tanto interesante estudiar el modo de unión de los esteroides a la TcG6PDH y la actividad de una selección de análogos de EA evaluados contra la enzima humana, de manera tal de poder inferir si es posible guiar el diseño de moléculas, que pertenecientes a esta familia, que presenten buena potencia y selectividad contra la G6PDH del patógeno.

En primera instancia, nuestros mayores esfuerzos estuvieron dirigidos a la obtención de cristales de la forma truncada de la TcG6PDH en complejo con EA y DHEA mediante la estrategia de inmersión de cristales o “soaking”. Lamentablemente, los cristales se dañaban al entrar en contacto con estos derivados esteroideos. Por lo tanto, optamos por una estrategia que combinó el modelado *in silico* del modo de unión de diferentes esteroides a la TcG6PDH con a una validación bioquímica de los modelos generados. Los estudios computacionales fueron

realizados en colaboración con el grupo del Dr. Maurizio Botta de la Universidad de Siena (Italia), mientras que en nuestro grupo llevamos a cabo el análisis y validación bioquímica de dichos modelos mediante el estudio de los parámetros cinéticos y de inhibición de la TcG6PDH en su forma salvaje y distintos mutantes para los distintos compuestos esteroides estudiados.

La inhibición de tipo acompetitiva puede darse tanto con la unión del inhibidor en una región próxima o alejada al sitio activo de la enzima, siendo lo importante que esta no interfiera con la unión de los sustratos pero sí con la catálisis. Existen algunos ejemplos de inhibidores alostéricos que se unen en sitios lejanos al sitio activo y mediante cambios conformacionales logran alterar a distancia la actividad de la enzima (Ghosh and Fishman, 1966). Por lo tanto, en primer lugar se exploró la presencia de potenciales bolsillos de unión a ligandos sobre la estructura cristalina completa de la TcG6PDH unida a G6P (PDB 4EM5), que resultó en la identificación de 7 potenciales sitios de unión a ligandos, ubicándose próximos al sitio activo aquellos 3 que presentaban los scores más altos. Esto permitió confinar la búsqueda del sitio de unión de esteroides a esta zona de la proteína. Tal como se mencionó anteriormente, la unión a la proteína de este tipo de inhibidores requiere de la formación del complejo ternario y dado que se carecía de dicha información para G6PDH, primero fue necesario generar y validar el modelo de complejo ternario obtenido. El modelo fue generado a partir de los datos cristalográficos de la TcG6PDH con G6P unido (PDB 4EM5) y las coordenadas de la unión del $NADP^+$ provenientes de la estructura de la enzima humana. Luego, se realizó el *docking* con los diferentes derivados esteroideos, donde la estabilidad de dichos complejos fue evaluada mediante dinámica molecular. Según lo observado, la EA se posiciona entre ambos sustratos interaccionando con los residuos L80, K83 y K84 (localizados en la región N-terminal que conecta con el dominio de unión a nucleótidos). Validamos dicho modelo mediante la generación de mutantes puntuales de dichos residuos, observándose que dichas sustituciones impactan negativamente en la afinidad por el inhibidor. De esta forma se pudo comprobar que el residuo K84 participa de la unión del sustrato, además de interaccionar por puente de hidrogeno con la EA. Que la lisina 80 provee de un ambiente hidrofóbico para estabilizar la EA y posicionarla correctamente próxima al sitio catalítico. Y finalmente se probamos, que L80 y K83 forman parte de un motivo (hélice-α1) que da forma al sitio catalítico de la TcG6PDH y participa también en la unión de $NADP^+$ durante la catálisis.

Observamos que presentan mejor selectividad por la proteína del parásito se posicionan próximo al sitio catalítico sin interferir con la unión de los sustratos, y son capaces de desestabilizar dicho

sitio e impedir estéricamente la aproximación de los sustratos, necesaria para que tenga lugar la catálisis.

El modelado *in silico* también nos permitió comprender el rol del bromo en la posición 16 del androstano, pudimos observar que las interacciones entre el halógeno voluminoso y el $NADP^+$, no solo mejoran la estabilidad de la unión del inhibidor, sino que aumentan su efecto estérico, interfiriendo de manera eficaz con la catálisis. Esto explica porque la 16BrEA es al menos 10 veces más potente que EA contra la TcG6PDH (Cordeiro and Thiemann, 2010). Por otro lado, el hecho que la enzima humana sea significativamente menos sensible (un factor de 65 veces) a la inhibición por 16BrEA que TcG6PDH sugiere la existencia de diferentes modos de unión dependiendo de la especie.

Los estudios de SAR realizados con diferentes análogos esteroideos nos permitieron identificar que posiciones y grupos químicos contribuyen a la selectividad por la proteína del parásito (Hamilton et al., 2012). Por ejemplo, notamos que las sustituciones por grupos polares y voluminosos en la posición 3β del androstano son bien toleradas y mejoran la inhibición de TcG6PDH. Mientras que, la inclusión en la posición 17 de un grupo polar como la hidroxil ketona (β-COCH2OH) mejora la inhibición de la hG6PDH pero afecta negativamente la unión a la proteína del parásito. También pudimos determinar que la presencia de un grupo sulfamida en la posición 3β contribuiría a estabilizar la unión del esteroide mejorando el grado de interferencia con la catálisis y la selectividad por la TcG6PDH.

En paralelo evaluamos los potenciales sitios de unión de EA, con la hG6PDH y la G6PDH de *Leishmania mexicana*. Este abordaje tuvo como fin obtener evidencias estructurales sobre la selectividad de especie observada en nuestros experimentos y la reportada previamente por otros grupos (Cordeiro et al., 2009; Gupta et al., 2011b). Los derivados esteroideos como la DHEA o EA presentan actividad inhibitoria frente a las G6PDHs de *Trypanosoma cruzi* y *brucei* pero no muestran efecto sobre las G6PDHs provenientes de *Leishmania mexicana*, *Spinacia oleracia*, *Sccharomyces cervisae* o del lactobacilo *Leuconostoc mesenteroides* (Cordeiro et al., 2009; Gupta et al., 2011b; Marks and Banks, 1960). Los resultados del docking de EA con la LmG6PDH evidenciaron que EA se une de manera transitoria y muy inestable a regiones alejadas de los sitios de unión de los sustratos, imposibilitando así la interferencia del compuesto con la catálisis, lo que fortalece nuestra hipótesis de especificidad de especie por parte de algunos de los derivados esteroideos.

Un abordaje similar se empleó para investigar el sitio de unión de EA y varios de sus derivados a la G6PDH humana. Nuestros datos indican que EA se une de manera estable a una región próxima al sitio catalítico que no se corresponde con la determinada para la enzima de *T. cruzi,* ver figura 6. Si bien aun nos resta validar bioquímicamente dicho modelo estos resultados son compatibles con la selectividad especie-específica mostrada por EA y algunos de sus derivados contra estas enzimas.

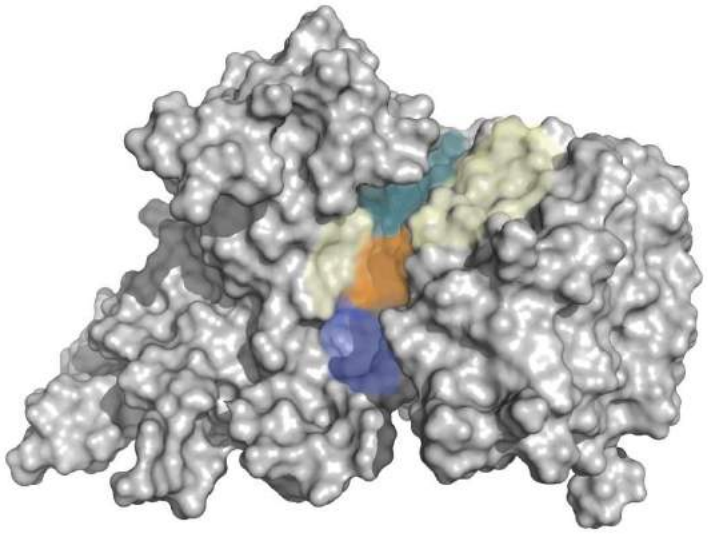

Figura 6. Sitio de unión a Epiandrosterona.
La imagen corresponde a la superposición de tres G6PDHs, donde se muestran en amarillo el sitio de unión a cofactor y sustrato, en verde el sitio de unión de EA para la proteína humana, en anaranjado el sitio de unión del esteroide al modelo catalítico de la proteína de *T. cruzi.* Y en violeta el sitio de unión a EA para un modelo de la G6PDH de *Leishmania mexicana.*

En principio, el conjunto de estos resultados no deja de sorprender dado que las secuencias de las G6PDH de estos organismos muestran una conservación de secuencia cercana al 100% a nivel del sitio catalítico y de unión a sustratos. No obstante, los estudios de relación estructura-actividad llevados a cabo con distintas formas de la TcG6PDH (tetrámero, dímero, condiciones reductoras y no reductoras, C8S, Δ37N-) y con la enzima humana (Filosa et al., 1992; Gómez-Manzo et al., 2014, 2015; Mizukawa et al., 2011; Ortiz et al., 2016) demuestran que la conformación del sitio activo no está determinada únicamente por los residuos catalíticos o aquellos que interaccionan con los ligandos sino que también por residuos secundarios e influenciables por la estructura cuaternaria de la proteína. Por lo tanto no es extraño que ambas enzimas difieran en su mecanismo enzimático con la G6PDH de *T. cruzi* ajustándose a uno del tipo bi-bi secuencial ordenado, donde la enzima presenta preferencia por unir en primer lugar $NADP^+$ y luego G6P para dar lugar a la formación del complejo ternario (Jortzik et al., 2011),

mientras que la humana sigue un mecanismo de equilibrio rápido de tipo bi-bi al azar o Theorell Chance, donde los sustratos se unen a la enzima de manera indistinta e independiente uno del otro para formar el complejo catalítico (Birke et al., 1989).

Que el mecanismo de acción sea ordenado sugiere que previo a la unión de G6P es necesaria la unión del $NADP^+$, que probablemente induzca cambios conformaciones a nivel del sitio de unión de G6P que permitan el correcto posicionamiento del mismo para la catálisis. Seguramente así como estos mismos residuos secundarios al sitio activo pueden influenciar el mecanismo de reacción de la enzima, estos también pueden condicionar la interacción con inhibidores.

A la fecha de iniciada la tesis, existía un reporte demostrando que la causa principal del efecto tripanocida de EA contra *T. brucei* era debido a la inhibición de la G6PDH (Cordeiro et al., 2009). Sin embargo, esto no había sido verificado para *T. cruzi*. Para abordar esta interrogante, debido a la baja concentración de G6PDH en epimastigotas no detectable por WB o inmunifluorescencia indirecta, se adaptó un ensayo citoquímico empleado originalmente para detectar actividad G6PDH en células de mamífero (Frederiks et al., 2006). Esto nos permitió detectar la presencia de la G6PDH y a su vez confirmar que efectivamente EA inhibe la actividad G6PDH endógena o inducible artificialmente (copia ectópica del gen de G6PDH inducible por tetraciclina) en epimastigotas de diferentes cepas de *T. cruzi*. Además el análisis de las imágenes de citoquímica indicaba que la proteína presentaba una localización citosólica, la cual fue confirmada mediante ensayos de inmufluorescencia indirecta con anticuerpos específicos contra esta enzima y diferentes marcadores de estructuras subcelulares celulares (mitocondria, núcleo, membrana) en una cepa sobreexpresante de G6PDH. Estos resultados coinciden en parte con un trabajo anterior del grupo del Dr. Cazzulo (Universidad de San Martín, Argentina) que mediante la sobreexpresión de la TcG6PDH fusionada a una proteína GFP había reportado que la TcG6PDH se localizaba principalmente en el citosol y también en glicosomas, a pesar que esta proteína carece de secuencias de señal de exportación al glicosoma (PTS1 o PTS2) (Duffieux et al., 2000; Igoillo-Esteve and Cazzulo, 2006), para las formas amastigosta, tripoamastigota y tripoamastigota metacíclico (Igoillo-Esteve, 2005). Dado que la fusión de un tag proteico a una proteína multimérica como lo es la TcG6PDH puede alterar su estado oligomérico nativo y/o enmascarar sitios de exportación, es que realizamos varios intentos por co-localizar con glicosomas la proteína expresada sin tag en *T. cruzi*. Sin embargo los anticuerpos recibidos no fueron lo suficientemente específicos para cumplir ese propósito. No obstante, aún no podemos descartar que TcG6PDH presente una distribución subcelular similar a la determinada para *T. brucei*. Esta distribución dual también se observa en células de mamíferos, donde las

proporciones de localización en citosol y peroxisomas, varían dependiendo del tipo celular o si se trata de células normales o tumorales (Frederiks et al., 2006).

En resumen, este estudio permitió definir el sitio de unión de esteroides a la TcG6PDH, aproximarnos a comprender las bases estructurales que determinan la especificidad de varios análogos por esta enzima, identificar derivados selectivos contra la proteína del patógeno, confirmar G6PDH como blanco molecular de la acción tripanocida de EA y proponer como predominantemente citosólica a la localización de esta proteína en epimastigotas de *T. cruzi*.

4.4 Implicancias de los hallazgos de esta tesis para el diseño de inhibidores selectivos contra la G6PDH de tripanosomátidos

Los aportes de este trabajo representan información valiosa para el diseño de nuevas estrategias para la inhibición selectiva de la G6PDH de tripanosomátidos.

Comprobamos que existen diferencias relevantes a nivel de conformación oligomérica entre la TcG6PDH y su contraparte humana. Por un lado tenemos a la proteína humana que presenta un equilibrio muy dinámico y sensible a las condiciones del ambiente que involucra la interconversión de tres especies, monómero (inactivo), dímero y tetrámero (activos), siendo la forma dimérica la predominante en condiciones fisiológicas. En contraposición tenemos a la proteína de *T. cruzi* que presenta una conformación tetramérica no covalente muy estable, donde la disrupción de la misma lleva a la formación de especies diméricas que son significativamente menos activas (70% menos activas que el tetrámero). La interfase tetramérica de la proteína de *T. cruzi* presenta una cavidad polar capaz de admitir la entrada de moléculas pequeñas, además de estar estabilizada por interacciones simétricas, lo que significa que de identificar un compuesto o generar un péptido que sea capaz de desestabilizar la interacción R323/D332/E333, podría conducir a la ruptura del tetrámero y de esta manera disminuir significativamente su actividad. La ventaja de esta técnica es que la selectividad del "compuesto hipotético" por la proteína del parásito no es tan relevante, visto que la proteína humana no sólo carece de esta cavidad polar en su interfase tetramérica (requisito indispensable para poder unir inhibidores) sino que en caso de disociar su estructura tetramérica no estaríamos afectando su actividad, porque como mencionamos anteriormente el dímero es activo. Para validar la factibilidad de esta estrategia de inactivación antes debería comprobarse si *T. cruzi* sería capaz de subsistir sólo con un 30% de actividad G6PDH en condiciones normales

o de estrés, como podría representar su exposición a un fármaco citotóxico (por ej. terapia combinada). Alternativamente, podría trabajarse en el diseño de moléculas que a su vez interfieran con la dimerización de la proteína. Esta propuesta está fundamentada en las bases de la inactivación que ejerce la proteína oncogénica p53 de células mamíferas sobre la G6PDH. En células normales, p53 interacciona con la hG6PDH, induciendo un cambio conformacional capaz de desensamblar el estado dimérico (forma activa) de la enzima y mantenerla en su estado monomérico (inactivo), esta unión ocurre de manera transitoria y conlleva a la pérdida de un 20% de la actividad enzimática (Jiang et al., 2011). Se ha observado que para algunos tipos de cáncer, p53 presenta mutaciones específicas que le impiden desensamblar el dímero de la G6PDH, lo que se acompaña de un incremento en la actividad de hG6PDH que se correlaciona con diferentes pronósticos y sitios de metástasis. Haciendo uso de la información derivada de esta interacción selectiva entre ambas proteínas, el grupo de Obiol ha reportado la generación de un péptido de 14 residuos que es capaz de impedir la formación del dímero dando lugar a la inactivación de la G6PDH (Obiol-Pardo et al., 2014) Si bien resulta atractiva esta estrategia, consideramos que el descubrimiento de moléculas con características de fármacos (bajo peso molecular, equilibrio entre polaridad y lipofilicidad) capaces de monomerizar o dimerizar a la TcG6PDH podría ser complejo.

Otra de las características diferenciales que presenta esta enzima es la capacidad de incrementar en un 20% su actividad en condiciones no reductoras. Este tipo de regulación se encuentra confinada a una región N-terminal común a los kinetoplástidos (datos no mostrados) que contiene a la cisteína 8, que es exclusiva de la proteína de *T. cruzi*. Si bien esto permitiría diseñar inhibidores selectivos contra esta enzima, esta estrategia de inhibición, al igual que la de disrupción del tetrámero, requiere de estudios adicionales que demuestren que impedir un incremento del 20% en la actividad de la TcG6PDH es deletérea para la sobrevida del parásito. Además, vale la pena recordar que se ha reportado que frente a estrés oxidativo *T. cruzi* es capaz de incrementar la expresión de la misma, lo cual hace suponer que inhibir su activación podría ser compensada con una mayor expresión de la misma. También debe tenerse en cuenta que al tratarse de una región exclusiva de la enzima de *T. cruzi* un abordaje de este tipo no sería luego trasladable a otras especies.

A pesar que las G6PDHs presentan una elevada conservación de secuencia a nivel de sitio catalítico, existen diferencias estructurales y variaciones en los residuos secundarios que dan forma al sitio activo. Uno de los aportes más importantes de este proyecto fue la resolución de la estructura tridimensional de la TcG6PDH así como la identificación del sitio de unión de los

derivados esteroides. A su vez pudimos confirmar que la selectividad especie-especifica observada para algunos derivados esteroideos (serie de derivados esteroideos específicos de hG6PDH, 16 BrEA, y la refractariedad de LmG6PDH frente a EA y DHEA) tiene su correlación a nivel estructural. Por otro lado, existe evidencia experimental que muestra que derivados esteroideos son capaces de inhibir a la G6PDH de *T. cruzi* y *T. brucei*, y pre-clínica donde el tratamiento de animales chagásicos con DHEA se ha correlacionado con una disminución significativa de la parasitemia y mejor pronóstico de sobrevida de los animales infectados (Filipin et al., 2010; Santos et al., 2010). Tal como lo sugiere nuestro estudio, los esteroides aún presentan potencial como *scaffolds* que pueden ser optimizados para incrementar su selectividad contra las G6PDH de tripanosomas y para anular su actividad hormonal. Ejemplos de esto último lo constituyen los análogos producidos por el Dr. Donald Pourier los cuales carecen de actividad androgénica y estrogénica (Maltais et al., 2015; Poirier, 2013) y sería interesante testear contra TcG6PDH.

Contar con la información estructural y los modelos generados en este proyecto, aporta herramientas e información valiosa para investigar el sitio de unión de los recién descubiertos, inhibidores acompetitivos de TcG6PDH que son no esteroideos y pertenecen a las familias de las quinazolinonas y las tienopirimidinas. Estos compuestos presentan la ventaja de no presentar efectos secundarios androgénicos. Además se reportó que el compuesto más potente del grupo de las quinazolinonas presenta actividad tripanocida similar a la del benznidazol y compite con el sitio de unión de la EA (Mercaldi et al. 2014). Según estos resultados podemos inferir que esta quinazolinona se estaría uniendo a la misma región que EA, la cual identificamos en este trabajo de tesis. Esto es muy alentador en términos de diseño racional de fármacos ya que los modelos estructurales con los cuales contamos han sido validados bioquímicamente y permitirían realizar *dockings* para guiar el diseño racional de fármacos selectivos y potentes.

En base a los aspectos diferenciales que hemos identificado para la G6PDH humana y del patógeno podemos destacar que la estrategia más viable para el desarrollo de moléculas con potencial farmacológico debería centrarse en inhibidores acompetitivos que presenten un mecanismo de unión selectivo, tal como parece ser el caso de los esteroides (o quinazolinas).

4.5 ¿Es la G6PDH de Trypanosoma cruzi un buen blanco de fármacos?

Para validar a la TcG6PDH como blanco molecular de fármacos se deben cumplir varios requisitos, entre ellos: debe ser indispensable para el parásito, estar ausente o en su defecto, no ser esencial para el hospedero, y además ésta debe presentar diferencias bioquímicas o estructurales con su contraparte humana que permitan el diseño de fármacos selectivos y potentes (Gashaw et al., 2011; Wyatt et al., 2011). Estas características se detallan y discuten para la TcG6PDH de manera crítica y a continuación, ver figura 7.

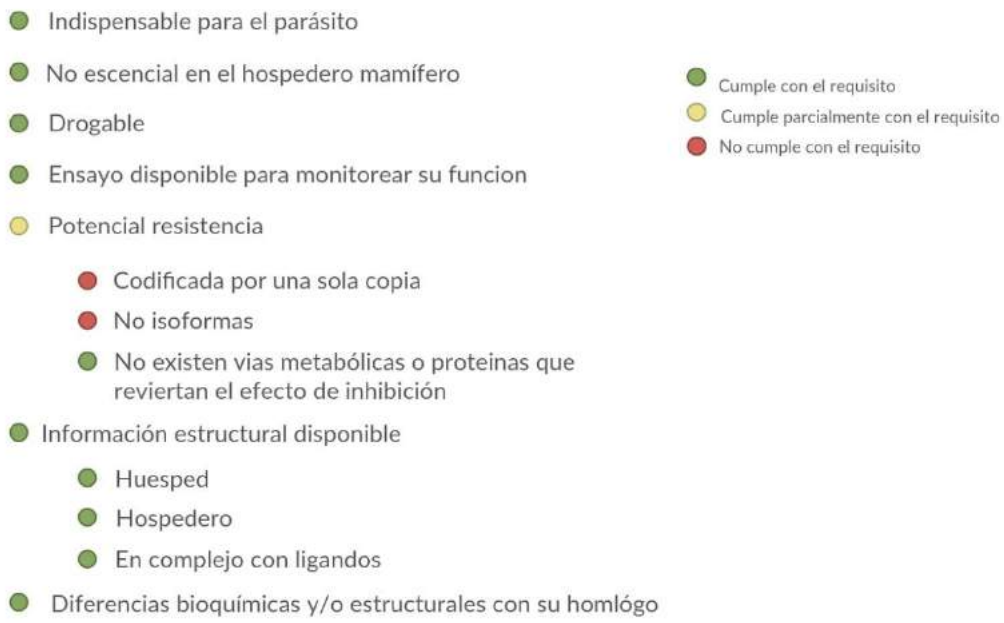

Figura 7. **Requisitos necesarios para ser un buen blanco de fármacos.**
Se muestran los requisitos que debe cumplir la TcG6PDH para ser validada como potencial blanco de fármacos. En círculos y código de colores se muestra el grado de cumplimiento de dichos requisitos.

Como mencionamos anteriormente, la TcG6PDH cumple un rol central en el metabolismo del parasito y suprimir su actividad conduce a su muerte. Como se pudo probar para los tripanosomas, la inhibición selectiva de la misma afecta simultáneamente tres vías metabólicas vitales. A pesar que la hG6PDH cumple funciones similares a la proteína del parasito, bajo condiciones fisiológicas su actividad es totalmente dispensable para los humanos. De hecho, la deficiencia de G6PDH es la enzimopatía más común en nuestra población, afectando a más de 400 millones de personas en el mundo y cuyo fenotipo se caracteriza principalmente por una anemia hemolítica que puede presentar distintos grados de severidad dependiendo el grado de inactivación de la enzima. Inclusive, se ha observado que en regiones endémicas para malaria

esta enzimopatía muestra los fenotipos más severos, aportando resistencia contra *Plasmodium falciparum*, lo que significa una ventaja adaptativa para los portadores. Si bien esta dependencia parcial del ser humano por la enzima permitiría reducir el nivel de exigencia farmacológica para los compuestos candidatos, en realidad la deficiencia en G6PDH y los riesgos para la salud que una inhibición adicional de la enzima podría acarrear en los pacientes, no hace más que destacar que el diseño de inhibidores contra la enzima del patógeno debe apuntar a la creación de compuestos altamente selectivos.

Tal como lo destaca la presencia de inhibidores contra esta enzima, la TcG6PDH presenta regiones que son accesibles a moléculas que pueden unirse a las mismas e interferir con la actividad o estabilidad de la proteína. Además de cumplir este requisito, la existencia de inhibidores selectivos para la TcG6PDH (ej. ciertos derivados de esteroideos, tioenopirimidinas o quinazolinonas) sugiere que dichos sitios no están compartidos con la enzima del hospedador o bien son sustancialmente diferentes.

Por otro lado, para ser considerado como un buen blanco debe ser posible contar con un método versátil para evaluar su funcionalidad. La G6PDH cumple con dicho requerimiento, ya que existen ensayos enzimáticos directos para monitorear su función, como es el caso del seguimiento de la producción de NADPH por espectrofotometría o fluorescencia. También se puede acoplar la medición de su actividad a la reacción de la diaforasa (Preuss et al., 2012b), lo cual rinde un ensayo más robusto y significativamente menos costoso que el anteriormente mencionado. Otras de las limitantes que debe sortear un buen blanco de fármacos son los bajos niveles de expresión de proteína activa y los problemas de estabilidad. En este sentido, tanto en trabajos anteriores a esta tesis (Ortíz, 2012; Whenert, 2012) como durante la misma, se han logrado optimizar los niveles de expresión y purificación de la TcG6PDH así como también identificar condiciones óptimas para su almacenamiento a largo plazo.

Otro punto importante es que el blanco molecular posea una baja probabilidad de dar lugar al desarrollo de resistencia. Al respecto, es ideal que el blanco no esté codificado por más de una copia ni que presente distintas isoformas. Además no debería tratarse de una especie abundante en las formas infectivas del parásito o presentar redundancia funcional con otras proteínas o vías metabólicas accesorias que subroguen su función. De todas estas características, los puntos débiles que presenta la proteína de *T. cruzi* es hallarse codificada por 3 genes, lo cual por otro lado destaca la relevancia funcional que la misma tiene para el parásito, y que sus niveles de expresión se ven incrementados en las formas infectivas o bajo condiciones de estrés oxidativo.

Por otro lado, creemos que es poco probable que otras proteínas productoras de NADPH (malato deshidrogenasa, isocitrato desidrogenasa y glutamato deshidrogenasa) puedan revertir el efecto letal que conlleva la inhibición de la G6PDH ya que su inhibición no solo afecta el *pool* de NADPH, sino que también impacta en la síntesis de ribonucleótidos y en la generación de intermediarios de la glicolisis.

El tener acceso a información estructural del blanco molecular se considera ventajoso ya que facilita el diseño racional de inhibidores selectivos así como el screening virtual de grandes bibliotecas de compuestos. Tal como quedó demostrado en este trabajo de tesis, el contar con la estructura de la G6PDH del huésped y el patógeno nos permitió estudiar en detalle ambas estructuras, posibilitando la identificación de regiones relevantes para la modulación especie-específica de la actividad enzimática y la interacción con ligandos, así como la realización de estudios de dinámica molecular que facilitaron comprender el modo de unión de ciertos inhibidores. De la caracterización estructural y bioquímica se desprende que la TcG6PDH presenta características diferenciales respecto de la enzima humana como ser la región N-terminal con función reguladora redox o el residuo R323 responsable de la tetramerización, así como la ausencia de sitio de unión de NADP estructural o la disposición de los residuos secundarios que dan forma al sitio activo de la proteína. Tal como se mencionó en la sección anterior, la disrupción de la estructura oligomérica de la proteína como estrategia de inhibición de la actividad enzimática no es la más adecuada, y tampoco parece serlo el bloqueo de la formación del disulfuro intermolecular que activa a la proteína. Sin embargo, diferencias sutiles en el sitio activo de la enzima de *T. cruzi* podrían explotarse con el fin de ganar selectividad en la inhibición de esta enzima, tal como lo indican nuestros resultados con los análogos de EA.

Por último, considerar a la G6PDH como buen blanco de fármacos va más allá de la evidencia experimental y los resultados teóricos, sino también abarca los posibles efectos adversos que pueden ocasionar sus inhibidores en el hospedero. Y no menos importante, para esta enfermedad catalogada dentro de las NTDs también se debe considerar el aspecto económico con respecto a posibilidades de producción y accesibilidad de los nuevos fármacos.

Teniendo en cuenta todo lo anteriormente mencionado podemos validar a la G6PDH de *Trypanosoma cruzi* como blanco para el diseño racional de fármacos antichagásicos.

perspectivas y conclusiones

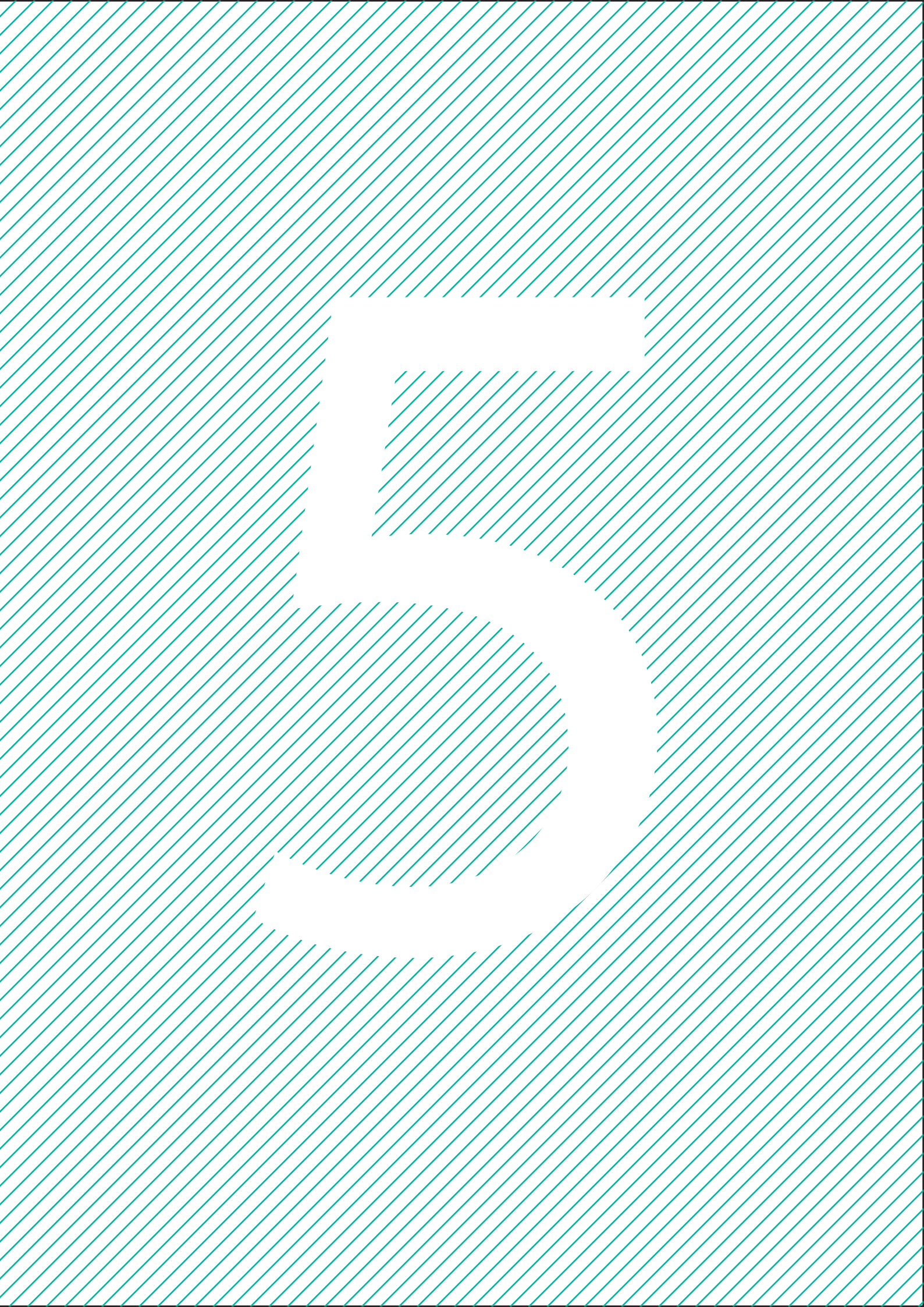

Capítulo 5

CONCLUSIONES Y PERSPECTIVAS

5.1 Conclusiones

En línea con la necesidad de contar con fármacos más seguros y eficaces para tratar la enfermedad de Chagas, se concretaron los objetivos planteados en este Proyecto de Doctorado.

En este trabajo de tesis se emplearon diferentes abordajes para cumplir con los objetivos propuestos, entre los cuales incluimos: estudios bioquímicos, fisicoquímicos y estructurales; evaluamos interacciones proteína-ligando, determinamos parámetros cinéticos de las formas salvajes y diferentes mutantes puntuales o de deleción y establecimos su relevancia biológica mediante la validación química con EA. También, estudiamos el modo y mecanismo de acción de diferentes inhibidores y analizamos en detalle los sitios de unión a ligandos y los comparamos con otras G6PDHs para identificar que aminoácidos son esenciales para la catálisis. Todos estos estudios nos proporcionaron información que puede ser muy útil para guiar el diseño racional de fármacos. A su vez, para evaluar la actividad biológica de los inhibidores a nivel celular, diseñamos un ensayo citoquímico específico para la detección *in situ* de actividad G6PDH. Se caracterizó bioquímica y estructuralmente la glucosa-6-fosfato deshidrogenasa que mostró ser esencial para el metabolismo energético y biosintético de *Trypanosoma cruzi*.

Entre los resultados obtenidos se destaca la resolución de la estructura tridimensional de la forma truncada de la G6PDH de *T. cruzi*, lo que significó un aporte muy importante al área de la parasitología y de las ciencias biomédicas en general. Contar con la primer estructura reportada para una G6PDH proveniente de un organismo patógeno, nos abrió las puertas para llevar adelante nuevos estudios con inhibidores además de brindar información valiosa para comprender el rol biológico de la misma.

Por otro lado la combinación del análisis estructural junto con la caracterización bioquímica y los ensayos *in silico* con inhibidores representó un aporte muy valioso al área de la farmacología, ya que sientan las bases para el diseño racional de nuevos compuestos y/o la optimización de otros ya existentes. Esto incrementa las posibilidades de generar nuevos fármacos o terapias combinadas, más eficaces, selectivas y accesibles que podrían ser la solución a este viejo problema.

En suma, se generó una batería de resultados variados que complementados con los generados por otros grupos nos permitieron validar a la glucosa-6-fosfato deshidrogenasa de *Trypanosoma cruzi* como blanco para el diseño racional de fármacos anti-chagásicos.

5.2 Perspectivas

- Puesta a punto de un método para el screening *in vitro* para la identificación potenciales inhibidores de la TcG6PDH, adaptando a formato HTS el ensayo enzimático acoplado a la reacción de la diaforasa, que emplea NADPH como sustrato para convertir resazurina en el compuesto fluorescente resorfurina. Se emplearán los inhibidores mencionados en este trabajo, para luego proceder a la evaluación de nuestra propia biblioteca de compuestos (más de 850 entidades químicas). Finalmente, se planea realizar un cribado masivo de compuestos contra la TcG6PDH empleando técnicas de alto rendimiento en unidades robóticas.
- Detectar si alguno de los 50 hits obtenidos del screeninig virtual* de más de 6 millones de compuestos que se realizó empleando como templado la estructura 3D de la TcG6PDH y el *scaffold* del inhibidor epiandrosterona (EA) se comporta como potencial inhibidor de la TcG6PDH. *Para ello se planea* evaluar *in vitro* y en cultivo de parásitos parte de los 50 hits obtenidos.
- Dado que la obtención de datos estructurales para cristales de la forma larga de la TcG6PDH ha sido infructuosa, intentaremos resolver esta región N-terminal mediante la generación de modelos estructurales *in silico,* así como comprender su función mediante la identificación del segundo residuo de cisteína involucrado en le formación del disulfuro intermolecular empleando la estrategia de mutantes puntuales.
- Evaluar el blanco molecular y modo de acción de los inhibidores identificados empleando ARNi de TbG6PDH generados por la estudiante.

“If you assume that there is no hope, you guarantee that there will be no hope. If you assume that there is an instinct for freedom, that there are opportunities to change things, then there is a possibility that you can contribute to making a better world.”

-Noam Chomsky-

REFERENCIAS

Abdulla, M.-H., Lim, K.-C., Sajid, M., McKerrow, J.H., and Caffrey, C.R. (2007). Schistosomiasis mansoni: novel chemotherapy using a cysteine protease inhibitor. PLoS Med. *4*, e14.

Ali, N., Anwar, M., Ayyub, M., Bhatti, F.A., Nadeem, M., and Nadeem, A. (2005). Frequency of glucose-6-phosphate dehydrogenase deficiency in some ethnic groups of Pakistan. J. Coll. Physicians Surg.--Pak. JCPSP *15*, 137–141.

Allison, A.C., and Clyde, D.F. (1961). Malaria in African children with deficient erythrocyte glucose-6-phosphate dehydrogenase. Br. Med. J. *1*, 1346–1349.

Altcheh, J., Moscatelli, G., Mastrantonio, G., Moroni, S., Giglio, N., Marson, M.E., Ballering, G., Bisio, M., Koren, G., and García-Bournissen, F. (2014). Population Pharmacokinetic Study of Benznidazole in Pediatric Chagas Disease Suggests Efficacy despite Lower Plasma Concentrations than in Adults. PLoS Negl. Trop. Dis. *8*.

Alving, A.S., Carson, P.E., Flanagan, C.L., and Ickes, C.E. (1956). Enzymatic deficiency in primaquine-sensitive erythrocytes. Science *124*, 484–485.

Andrews, P. (1965). The gel-filtration behaviour of proteins related to their molecular weights over a wide range. Biochem. J. *96*, 595–606.

Arese, P., and De Flora, A. (1990). Pathophysiology of hemolysis in glucose-6-phosphate dehydrogenase deficiency. Semin. Hematol. *27*, 1–40.

Au, S.W., Naylor, C.E., Gover, S., Vandeputte-Rutten, L., Scopes, D.A., Mason, P.J., Luzzatto, L., Lam, V.M., and Adams, M.J. (1999). Solution of the structure of tetrameric human glucose 6-phosphate dehydrogenase by molecular replacement. Acta Crystallogr. D Biol. Crystallogr. *55*, 826–834.

Au, S.W., Gover, S., Lam, V.M., and Adams, M.J. (2000). Human glucose-6-phosphate dehydrogenase: the crystal structure reveals a structural NADP(+) molecule and provides insights into enzyme deficiency. Struct. Lond. Engl. 1993 *8*, 293–303.

Aufderheide, A.C., Salo, W., Madden, M., Streitz, J., Buikstra, J., Guhl, F., Arriaza, B., Renier, C., Wittmers, L.E., Fornaciari, G., et al. (2004). A 9,000-year record of Chagas' disease. Proc. Natl. Acad. Sci. U. S. A. *101*, 2034–2039.

Babalola, A.O., Beetlestone, J.G., and Luzzatto, L. (1976). Genetic variants of human erythrocyte glucose-6-phosphate dehydrogenase. Kinetic and thermodynamic parameters of variants A, B, and A- in relation to quaternary structure. J. Biol. Chem. *251*, 2993–3002.

Bakker, B.M., Westerhoff, H.V., and Michels, P.A. (1995). Regulation and control of compartmentalized glycolysis in bloodstream form Trypanosoma brucei. J. Bioenerg. Biomembr. *27*, 513–525.

Bakker, B.M., Mensonides, F.I., Teusink, B., van Hoek, P., Michels, P.A., and Westerhoff, H.V. (2000). Compartmentation protects trypanosomes from the dangerous design of glycolysis. Proc. Natl. Acad. Sci. U. S. A. *97*, 2087–2092.

Barderi, P., Campetella, O., Frasch, A.C., Santomé, J.A., Hellman, U., Pettersson, U., and Cazzulo, J.J. (1998). The NADP+-linked glutamate dehydrogenase from Trypanosoma cruzi: sequence, genomic organization and expression. Biochem. J. *330 (Pt 2)*, 951–958.

Barrett, M.P. (1997). The pentose phosphate pathway and parasitic protozoa. Parasitol. Today Pers. Ed *13*, 11–16.

Barrett, M.P., Burchmore, R.J.S., Stich, A., Lazzari, J.O., Frasch, A.C., Cazzulo, J.J., and Krishna, S. (2003). The trypanosomiases. Lancet Lond. Engl. *362*, 1469–1480.

Barrios, P., Más, M., Giachetto, G., Basjmadjián, Y., Rodríguez, M., Viera, A.L., Baroloco, A.L., and Sayaguez, B. (2015). Enfermedad de Chagas: transmisión vertical. Descripción de casos clínicos. Rev. Médica Urug. *31*, 209–213.

Benítez, D., Medeiros, A., Fiestas, L., Panozzo-Zenere, E.A., Maiwald, F., Prousis, K.C., Roussaki, M., Calogeropoulou, T., Detsi, A., Jaeger, T., et al. (2016). Identification of Novel Chemical Scaffolds Inhibiting Trypanothione Synthetase from Pathogenic Trypanosomatids. PLoS Negl. Trop. Dis. *10*.

Bernard Pécoul, Fumiko Hirabayashi, and Isabela Riberiro (2009). Eisai and DNDi Enter into a Collaboration and License Agreement To Develop a New Drug for Chagas Disease.

Betke K, Beutler E, Brewer GJ, Kirkman HN, Luzzatto L, and Ramot B (1967). WHO | Standardization of procedures for the study of glucose-6-phosphate dehydrogenase : report of a WHO Scientific Group [meeting held in Geneva from 5 to 10 December 1966] (Geneva: WHO).

Beutler, E. (1994). G6PD deficiency. Blood *84*, 3613–3636.

Beydemir, Sükrü, Yilmaz, Hayrullah, Çiftçi, Mehmet, Bakan, Ebubekir, and Küfrevioglu, Ö. Irfan (2003). Purification of Glucose 6-Phosphate Dehydrogenase From Goose Erythrocytes and Kinetic Properties. Turk. J. Vet. Anim. Sci. *27*, 1179–1185.

Bhardwaj, R., Sharma, P.K., Jadon, S.P.S., and Varshney, R. (2012). A combination of 2-deoxy-D-glucose and 6-aminonicotinamide induces cell cycle arrest and apoptosis selectively in irradiated human malignant cells. Tumour Biol. J. Int. Soc. Oncodevelopmental Biol. Med. *33*, 1021–1030.

Birke, S., Kim, H.W., Periclou, A., Schorsch, B., Grouse, D., and Craney, C. (1989). Kinetics of human erythrocyte glucose-6-phosphate dehydrogenase dimers. Biochim. Biophys. Acta *999*, 243–247.

Blattner, J., Dörsam, H., and Clatyon, C.E. (1995). Function of N-terminal import signals in trypanosome microbodies. FEBS Lett. *360*, 310–314.

Bonsignore, A., Lorenzoni, I., Cancedda, R., and De Flora, A. (1970). Distinctive patterns of NADP binding to dimeric and tetrameric glucose 6-phosphate dehydrogenase from human red cells. Biochem. Biophys. Res. Commun. *39*, 142–148.

Bonsignore, A., Cancedda, R., Lorenzoni, I., Cosulich, M.E., and De Flora, A. (1971a). Human erythrocyte glucose 6-phosphate dehydrogenase. Physical properties. Biochem. Biophys. Res. Commun. *43*, 94–101.

Bonsignore, A., Cancedda, R., Nicolini, A., Damiani, G., and De Flora, A. (1971b). Metabolism of human erythrocyte glucose-6-phosphate dehydrogenase. VI. Interconversion of multiple molecular forms. Arch. Biochem. Biophys. *147*, 493–501.

Budihardjo, I.I., Boerner, S.A., Eckdahl, S., Svingen, P.A., Rios, R., Ames, M.M., and Kaufmann, S.H. (2000). Effect of 6-aminonicotinamide and other protein synthesis inhibitors on formation of platinum-DNA adducts and cisplatin sensitivity. Mol. Pharmacol. *57*, 529–538.

Burleigh, B.A., and Woolsey, A.M. (2002). Cell signalling and Trypanosoma cruzi invasion. Cell. Microbiol. *4*, 701–711.

Cardi, M., Zaffagnini, M., De Lillo, A., Castiglia, D., Chibani, K., Gualberto, J.M., Rouhier, N., Jacquot, J.-P., and Esposito, S. (2016). Plastidic P2 glucose-6P dehydrogenase from poplar is modulated by thioredoxin m-type: Distinct roles of cysteine residues in redox regulation and NADPH inhibition. Plant Sci. Int. J. Exp. Plant Biol. *252*, 257–266.

Cavalli, A., Lizzi, F., Bongarzone, S., Brun, R., Luise Krauth-Siegel, R., and Bolognesi, M.L. (2009). Privileged structure-guided synthesis of quinazoline derivatives as inhibitors of trypanothione reductase. Bioorg. Med. Chem. Lett. *19*, 3031–3035.

Cazorla, S.I., Frank, F.M., Becker, P.D., Arnaiz, M., Mirkin, G.A., Corral, R.S., Guzmán, C.A., and Malchiodi, E.L. (2010). Redirection of the immune response to the functional catalytic domain of the cystein proteinase cruzipain improves protective immunity against Trypanosoma cruzi infection. J. Infect. Dis. *202*, 136–144.

Chen, E.Y., Cheng, A., Lee, A., Kuang, W.J., Hillier, L., Green, P., Schlessinger, D., Ciccodicola, A., and D'Urso, M. (1991). Sequence of human glucose-6-phosphate dehydrogenase cloned in plasmids and a yeast artificial chromosome. Genomics *10*, 792–800.

Childs, B., Zinkham, W., Browne, E.A., Kimbro, E.L., and Torbert, J.V. (1958). A genetic study of a defect in glutathione metabolism of the erythrocyte. Bull. Johns Hopkins Hosp. *102*, 21–37.

Chudzik, D.M., Michels, P.A., de Walque, S., and Hol, W.G. (2000). Structures of type 2 peroxisomal targeting signals in two trypanosomatid aldolases. J. Mol. Biol. *300*, 697–707.

Comakli, V., Akkemik, E., Ciftci, M., and Kufrevioglu, O.I. (2015). Purification and characterization of glucose 6-phosphate dehydrogenase enzyme from rainbow trout (Oncorhynchus mykiss) liver and investigation of the effects of some metal ions on enzyme activity. Toxicol. Ind. Health *31*, 403–411.

Comini, M., Menge, U., Wissing, J., and Flohé, L. (2005). Trypanothione synthesis in crithidia revisited. J. Biol. Chem. *280*, 6850–6860.

Comini, M.A., Krauth-Siegel, R.L., and Flohé, L. (2007). Depletion of the thioredoxin homologue tryparedoxin impairs antioxidative defence in African trypanosomes. Biochem. J. *402*, 43–49.

Conners, E.E., Vinetz, J.M., Weeks, J.R., and Brouwer, K.C. (2016). A global systematic review of Chagas disease prevalence among migrants. Acta Trop. *156*, 68–78.

Contreras, M.C., Schenone, H., and Rojas, A. (1988). [Positivity of xenodiagnosis in subjects with positive indirect hemagglutination reaction in Chagas' disease, according to the titers of that reaction]. Bol. Chil. Parasitol. *43*, 22–24.

Cordeiro, A.T., and Thiemann, O.H. (2010). 16-bromoepiandrosterone, an activator of the mammalian immune system, inhibits glucose 6-phosphate dehydrogenase from Trypanosoma cruzi and is toxic to these parasites grown in culture. Bioorg. Med. Chem. *18*, 4762–4768.

Cordeiro, A.T., Thiemann, O.H., and Michels, P.A.M. (2009). Inhibition of Trypanosoma brucei glucose-6-phosphate dehydrogenase by human steroids and their effects on the viability of cultured parasites. Bioorg. Med. Chem. *17*, 2483–2489.

Cornish-Bowden, A. (1986). Why is uncompetitive inhibition so rare? A possible explanation, with implications for the design of drugs and pesticides. FEBS Lett. *203*, 3–6.

Cosgrove, M.S., Naylor, C., Paludan, S., Adams, M.J., and Levy, H.R. (1998). On the mechanism of the reaction catalyzed by glucose 6-phosphate dehydrogenase. Biochemistry (Mosc.) *37*, 2759–2767.

Cronín, C.N., Nolan, D.P., and Voorheis, H.P. (1989). The enzymes of the classical pentose phosphate pathway display differential activities in procyclic and bloodstream forms of Trypanosoma brucei. FEBS Lett. *244*, 26–30.

Dormeyer, M., Reckenfelderbäumer, N., Ludemann, H., and Krauth-Siegel, R.L. (2001). Trypanothione-dependent synthesis of deoxyribonucleotides by Trypanosoma brucei ribonucleotide reductase. J. Biol. Chem. *276*, 10602–10606.

Duffieux, F., Van Roy, J., Michels, P.A., and Opperdoes, F.R. (2000). Molecular characterization of the first two enzymes of the pentose-phosphate pathway of Trypanosoma brucei. Glucose-6-phosphate dehydrogenase and 6-phosphogluconolactonase. J. Biol. Chem. *275*, 27559–27565.

El-Sayed, N.M., Myler, P.J., Blandin, G., Berriman, M., Crabtree, J., Aggarwal, G., Caler, E., Renauld, H., Worthey, E.A., Hertz-Fowler, C., et al. (2005). Comparative genomics of trypanosomatid parasitic protozoa. Science *309*, 404–409.

Fairlamb, A.H., Blackburn, P., Ulrich, P., Chait, B.T., and Cerami, A. (1985). Trypanothione: a novel bis(glutathionyl)spermidine cofactor for glutathione reductase in trypanosomatids. Science *227*, 1485–1487.

Faria, J., Loureiro, I., Santarém, N., Cecílio, P., Macedo-Ribeiro, S., Tavares, J., and Cordeiro-da-Silva, A. (2016). Disclosing the essentiality of ribose-5-phosphate isomerase B in Trypanosomatids. Sci. Rep. *6*, 26937.

Filipin, M.D.V., Caetano, L.C., Brazão, V., Santello, F.H., Toldo, M.P.A., and do Prado, J.C. (2010). DHEA and testosterone therapies in Trypanosoma cruzi-infected rats are associated with thymic changes. Res. Vet. Sci. *89*, 98–103.

Filosa, S., Calabrò, V., Vallone, D., Poggi, V., Mason, P., Pagnini, D., Alfinito, F., Rotoli, B., Martini, G., and Luzzatto, L. (1992). Molecular basis of chronic non-spherocytic haemolytic anaemia: a new G6PD variant (393 Arg----His) with abnormal KmG6P and marked in vivo instability. Br. J. Haematol. *80*, 111–116.

Finzi, J.K., Chiavegatto, C.W.M., Corat, K.F., Lopez, J.A., Cabrera, O.G., Mielniczki-Pereira, A.A., Colli, W., Alves, M.J.M., and Gadelha, F.R. (2004). Trypanosoma cruzi response to the oxidative stress generated by hydrogen peroxide. Mol. Biochem. Parasitol. *133*, 37–43.

Flohé, L. (2012). The trypanothione system and its implications in the therapy of trypanosomatid diseases. Int. J. Med. Microbiol. IJMM *302*, 216–220.

Francisco, A.F., Lewis, M.D., Jayawardhana, S., Taylor, M.C., Chatelain, E., and Kelly, J.M. (2015). Limited Ability of Posaconazole To Cure both Acute and Chronic Trypanosoma cruzi Infections Revealed by Highly Sensitive In Vivo Imaging. Antimicrob. Agents Chemother. *59*, 4653–4661.

Frearson, J.A., Wyatt, P.G., Gilbert, I.H., and Fairlamb, A.H. (2007). Target assessment for antiparasitic drug discovery. Trends Parasitol. *23*, 589–595.

Frederiks, W.M., van Marle, J., van Oven, C., Comin-Anduix, B., and Cascante, M. (2006). Improved localization of glucose-6-phosphate dehydrogenase activity in cells with 5-cyano-2,3-ditolyl-

tetrazolium chloride as fluorescent redox dye reveals its cell cycle-dependent regulation. J. Histochem. Cytochem. Off. J. Histochem. Soc. *54*, 47–52.

Friedman, M.J., Roth, E.F., Nagel, R.L., and Trager, W. (1979). The role of hemoglobins C, S, and Nbalt in the inhibition of malaria parasite development in vitro. Am. J. Trop. Med. Hyg. *28*, 777–780.

Fry, A.J., Towner, P., Holman, G.D., and Eisenthal, R. (1993). Transport of D-fructose and its analogues by Trypanosoma brucei. Mol. Biochem. Parasitol. *60*, 9–18.

Furuya, T., Kessler, P., Jardim, A., Schnaufer, A., Crudder, C., and Parsons, M. (2002). Glucose Is Toxic to Glycosome-Deficient Trypanosomes. Proc. Natl. Acad. Sci. U. S. A. *99*, 14177–14182.

Galland, N., Demeure, F., Hannaert, V., Verplaetse, E., Vertommen, D., Van der Smissen, P., Courtoy, P.J., and Michels, P.A.M. (2007). Characterization of the role of the receptors PEX5 and PEX7 in the import of proteins into glycosomes of Trypanosoma brucei. Biochim. Biophys. Acta *1773*, 521–535.

Gashaw, I., Ellinghaus, P., Sommer, A., and Asadullah, K. (2011). What makes a good drug target? Drug Discov. Today *16*, 1037–1043.

Ghosh, N.K., and Fishman, W.H. (1966). On the mechanism of inhibition of intestinal alkaline phosphatase by L-phenylalanine. I. Kinetic studies. J. Biol. Chem. *241*, 2516–2522.

Gómez-Manzo, S., Terrón-Hernández, J., De la Mora-De la Mora, I., González-Valdez, A., Marcial-Quino, J., García-Torres, I., Vanoye-Carlo, A., López-Velázquez, G., Hernández-Alcántara, G., Oria-Hernández, J., et al. (2014). The Stability of G6PD Is Affected by Mutations with Different Clinical Phenotypes. Int. J. Mol. Sci. *15*, 21179–21201.

Gómez-Manzo, S., Marcial-Quino, J., Vanoye-Carlo, A., Enríquez-Flores, S., De la Mora-De la Mora, I., González-Valdez, A., García-Torres, I., Martínez-Rosas, V., Sierra-Palacios, E., Lazcano-Pérez, F., et al. (2015). Mutations of Glucose-6-Phosphate Dehydrogenase Durham, Santa-Maria and A+ Variants Are Associated with Loss Functional and Structural Stability of the Protein. Int. J. Mol. Sci. *16*, 28657–28668.

Gonçalves, J.G.F., Dias Silva, V.J., Calzada Borges, M.C., Prata, A., and Correia, D. (2010). Mortality indicators among chronic Chagas patients living in an endemic area. Int. J. Cardiol. *143*, 235–242.

Gordon, G., Mackow, M.C., and Levy, H.R. (1995). On the mechanism of interaction of steroids with human glucose 6-phosphate dehydrogenase. Arch. Biochem. Biophys. *318*, 25–29.

Grunau, S., Mindthoff, S., Rottensteiner, H., Sormunen, R.T., Hiltunen, J.K., Erdmann, R., and Antonenkov, V.D. (2009). Channel-forming activities of peroxisomal membrane proteins from the yeast Saccharomyces cerevisiae. FEBS J. *276*, 1698–1708.

Gualdron-López, M., Vapola, M.H., Miinalainen, I.J., Hiltunen, J.K., Michels, P.A.M., and Antonenkov, V.D. (2012). Channel-Forming Activities in the Glycosomal Fraction from the Bloodstream Form of Trypanosoma brucei. PLoS ONE *7*.

Guerra-Giraldez, C., Quijada, L., and Clayton, C.E. (2002). Compartmentation of enzymes in a microbody, the glycosome, is essential in Trypanosoma brucei. J. Cell Sci. *115*, 2651–2658.

Gupta, S., Igoillo-Esteve, M., Michels, P.A.M., and Cordeiro, A.T. (2011a). Glucose-6-phosphate dehydrogenase of trypanosomatids: characterization, target validation, and drug discovery. Mol. Biol. Int. *2011*, 135701.

Gupta, S., Cordeiro, A.T., and Michels, P.A.M. (2011b). Glucose-6-phosphate dehydrogenase is the target for the trypanocidal action of human steroids. Mol. Biochem. Parasitol. *176*, 112–115.

Güther, M.L.S., Urbaniak, M.D., Tavendale, A., Prescott, A., and Ferguson, M.A.J. (2014). High-confidence glycosome proteome for procyclic form Trypanosoma brucei by epitope-tag organelle enrichment and SILAC proteomics. J. Proteome Res. *13*, 2796–2806.

Haanstra, J.R., van Tuijl, A., Kessler, P., Reijnders, W., Michels, P.A.M., Westerhoff, H.V., Parsons, M., and Bakker, B.M. (2008). Compartmentation prevents a lethal turbo-explosion of glycolysis in trypanosomes. Proc. Natl. Acad. Sci. U. S. A. *105*, 17718–17723.

Haanstra, J.R., Bakker, B.M., and Michels, P.A.M. (2014). In or out? On the tightness of glycosomal compartmentalization of metabolites and enzymes in Trypanosoma brucei. Mol. Biochem. Parasitol. *198*, 18–28.

Haanstra, J.R., González-Marcano, E.B., Gualdrón-López, M., and Michels, P.A.M. (2016). Biogenesis, maintenance and dynamics of glycosomes in trypanosomatid parasites. Biochim. Biophys. Acta *1863*, 1038–1048.

Hamilton, N.M., Dawson, M., Fairweather, E.E., Hamilton, N.S., Hitchin, J.R., James, D.I., Jones, S.D., Jordan, A.M., Lyons, A.J., Small, H.F., et al. (2012). Novel steroid inhibitors of glucose 6-phosphate dehydrogenase. J. Med. Chem. *55*, 4431–4445.

Hannaert, V., Saavedra, E., Duffieux, F., Szikora, J.-P., Rigden, D.J., Michels, P.A.M., and Opperdoes, F.R. (2003). Plant-like traits associated with metabolism of Trypanosoma parasites. Proc. Natl. Acad. Sci. U. S. A. *100*, 1067–1071.

Hauschild, R., and von Schaewen, A. (2003). Differential regulation of glucose-6-phosphate dehydrogenase isoenzyme activities in potato. Plant Physiol. *133*, 47–62.

Heise, N., and Opperdoes, F.R. (1999). Purification, localisation and characterisation of glucose-6-phosphate dehydrogenase of Trypanosoma brucei. Mol. Biochem. Parasitol. *99*, 21–32.

Igoillo-Esteve, M. (2005). Clonado, expresión, caracterización y localización subcelular de las dos deshidrogenasas de la Vía de las Pentosas Fosfato en Trypanosoma cruzi (Glucosa 6 -fosfato deshidrogenasa y 6 -fosfogluconato deshidrogenasa). UNIVERSIDAD NACIONAL DE GENERAL SAN MARTIN.

Igoillo-Esteve, M., and Cazzulo, J.J. (2006). The glucose-6-phosphate dehydrogenase from Trypanosoma cruzi: its role in the defense of the parasite against oxidative stress. Mol. Biochem. Parasitol. *149*, 170–181.

Irigoín, F., Cibils, L., Comini, M.A., Wilkinson, S.R., Flohé, L., and Radi, R. (2008). Insights into the redox biology of Trypanosoma cruzi: Trypanothione metabolism and oxidant detoxification. Free Radic. Biol. Med. *45*, 733–742.

Jiang, P., Du, W., Wang, X., Mancuso, A., Gao, X., Wu, M., and Yang, X. (2011). p53 regulates biosynthesis through direct inactivation of glucose-6-phosphate dehydrogenase. Nat. Cell Biol. *13*, 310–316.

Jimenez, V. (2014). Dealing with environmental challenges: mechanisms of adaptation in Trypanosoma cruzi. Res. Microbiol. *165*, 155–165.

Jortzik, E., Mailu, B.M., Preuss, J., Fischer, M., Bode, L., Rahlfs, S., and Becker, K. (2011). Glucose-6-phosphate dehydrogenase-6-phosphogluconolactonase: a unique bifunctional enzyme from Plasmodium falciparum. Biochem. J. *436*, 641–650.

Keegan, F.P., Sansone, L., and Blum, J.J. (1987). Oxidation of glucose, ribose, alanine, and glutamate by Leishmania braziliensis panamensis. J. Protozool. *34*, 174–179.

Kirsch, M., Talbiersky, P., Polkowska, J., Bastkowski, F., Schaller, T., de Groot, H., Klärner, F.-G., and Schrader, T. (2009). A mechanism of efficient G6PD inhibition by a molecular clip. Angew. Chem. Int. Ed Engl. *48*, 2886–2890.

Köhler, E., Barrach, H.-J., and Neubert, D. (1970). Inhibition of NADP dependent oxidoreductases by the 6-aminonicotinamide analogue of NADP. FEBS Lett. *6*, 225–228.

Kotaka, M., Gover, S., Vandeputte-Rutten, L., Au, S.W.N., Lam, V.M.S., and Adams, M.J. (2005). Structural studies of glucose-6-phosphate and NADP+ binding to human glucose-6-phosphate dehydrogenase. Acta Crystallogr. D Biol. Crystallogr. *61*, 495–504.

Kovářová, J., and Barrett, M.P. (2016). The Pentose Phosphate Pathway in Parasitic Trypanosomatids. Trends Parasitol. *32*, 622–634.

Krauth-Siegel, R.L., and Leroux, A.E. (2012). Low-molecular-mass antioxidants in parasites. Antioxid. Redox Signal. *17*, 583–607.

Krauth-Siegel, R.L., Arscott, L.D., Schönleben-Janas, A., Schirmer, R.H., and Williams, C.H. (1998). Role of active site tyrosine residues in catalysis by human glutathione reductase. Biochemistry (Mosc.) *37*, 13968–13977.

Krazy, H., and Michels, P.A.M. (2006). Identification and characterization of three peroxins--PEX6, PEX10 and PEX12--involved in glycosome biogenesis in Trypanosoma brucei. Biochim. Biophys. Acta *1763*, 6–17.

Kwiatkowski, D.P. (2005). How Malaria Has Affected the Human Genome and What Human Genetics Can Teach Us about Malaria. Am. J. Hum. Genet. *77*, 171–192.

Lannes-Vieira, J., Araújo-Jorge, T.C. de, Soeiro, M. de N.C., Gadelha, P., and Corrêa-Oliveira, R. (2010). The Centennial of the Discovery of Chagas Disease: Facing the Current Challenges. PLoS Negl. Trop. Dis. *4*, e645.

Lee, B.Y., Bacon, K.M., Bottazzi, M.E., and Hotez, P.J. (2013). Global economic burden of Chagas disease: a computational simulation model. Lancet Infect. Dis. *13*, 342–348.

Leroux, A.E., Maugeri, D.A., Opperdoes, F.R., Cazzulo, J.J., and Nowicki, C. (2011a). Comparative studies on the biochemical properties of the malic enzymes from Trypanosoma cruzi and Trypanosoma brucei. FEMS Microbiol. Lett. *314*, 25–33.

Leroux, A.E., Maugeri, D.A., Cazzulo, J.J., and Nowicki, C. (2011b). Functional characterization of NADP-dependent isocitrate dehydrogenase isozymes from Trypanosoma cruzi. Mol. Biochem. Parasitol. *177*, 61–64.

Lewis, M.D., Fortes Francisco, A., Taylor, M.C., Burrell-Saward, H., McLatchie, A.P., Miles, M.A., and Kelly, J.M. (2014). Bioluminescence imaging of chronic Trypanosoma cruzi infections reveals tissue-specific parasite dynamics and heart disease in the absence of locally persistent infection. Cell. Microbiol. *16*, 1285–1300.

Longo, L., Vanegas, O.C., Patel, M., Rosti, V., Li, H., Waka, J., Merghoub, T., Pandolfi, P.P., Notaro, R., Manova, K., et al. (2002). Maternally transmitted severe glucose 6-phosphate dehydrogenase deficiency is an embryonic lethal. EMBO J. *21*, 4229–4239.

Lubert Stryer (1999). Biochemistry (New York: W H Freeman & Co).

Maloney, P., Hedrick, M., Peddibhotla, S., Hershberger, P., Milewski, M., Gosalia, P., Li, L., Preuss, J., Sugarman, E., Hood, B., et al. (2010a). A 2nd Selective Inhibitor of Plasmodium falciparum Glucose-6-Phosphate Dehydrogenase (PfG6PDH) - Probe 2. In Probe Reports from the NIH Molecular Libraries Program, (Bethesda (MD): National Center for Biotechnology Information (US)), p.

Maloney, P., Hedrick, M., Peddibhotla, S., Hershberger, P., Milewski, M., Gosalia, P., Li, L., Preuss, J., Sugarman, E., Hood, B., et al. (2010b). A Selective Inhibitor of Plasmodium falciparum Glucose-6-Phosphate Dehydrogenase (PfG6PDH). In Probe Reports from the NIH Molecular Libraries Program, (Bethesda (MD): National Center for Biotechnology Information (US)), p.

Maltais, R., Trottier, A., Delhomme, A., Barbeau, X., Lagüe, P., and Poirier, D. (2015). Identification of fused 16β,17β-oxazinone-estradiol derivatives as a new family of non-estrogenic 17β-hydroxysteroid dehydrogenase type 1 inhibitors. Eur. J. Med. Chem. *93*, 470–480.

Mancilla, R., and Naquira, C. (1964). COMPARATIVE METABOLISM OF C14-GLUCOSE IN TWO STRAINS OF TRYPANOSOMA CRUZI. J. Protozool. *11*, 509–513.

Marks, P.A., and Banks, J. (1960). INHIBITION OF MAMMALIAN GLUCOSE-6-PHOSPHATE DEHYDROGENASE BY STEROIDS. Proc. Natl. Acad. Sci. U. S. A. *46*, 447–452.

Maugeri, D.A., and Cazzulo, J.J. (2004). The pentose phosphate pathway in Trypanosoma cruzi. FEMS Microbiol. Lett. *234*, 117–123.

Maugeri, D.A., Cazzulo, J.J., Burchmore, R.J.S., Barrett, M.P., and Ogbunude, P.O.J. (2003). Pentose phosphate metabolism in Leishmania mexicana. Mol. Biochem. Parasitol. *130*, 117–125.

McKerrow, J., Doyle, P., Engel, J., Podust, L., Robertson, S., Ferreira, R., Saxton, T., Arkin, M., Kerr, I., Brinen, L., et al. (2009). Two approaches to discovering and developing new drugs for Chagas disease. Mem. Inst. Oswaldo Cruz *104*, 263–269.

Mercaldi, G.F., Ranzani, A.T., and Cordeiro, A.T. (2014). Discovery of new uncompetitive inhibitors of glucose-6-phosphate dehydrogenase. J. Biomol. Screen. *19*, 1362–1371.

Mielniczki-Pereira, A.A., Chiavegatto, C.M., López, J.A., Colli, W., Alves, M.J.M., and Gadelha, F.R. (2007). Trypanosoma cruzi strains, Tulahuen 2 and Y, besides the difference in resistance to oxidative stress, display differential glucose-6-phosphate and 6-phosphogluconate dehydrogenases activities. Acta Trop. *101*, 54–60.

Mikami, D., Kurihara, H., Kim, S.M., and Takahashi, K. (2013). Red algal bromophenols as glucose 6-phosphate dehydrogenase inhibitors. Mar. Drugs *11*, 4050–4057.

Mikami, D., Kurihara, H., Ono, M., Kim, S.M., and Takahashi, K. (2016). Inhibition of algal bromophenols and their related phenols against glucose 6-phosphate dehydrogenase. Fitoterapia *108*, 20–25.

Miller, L.H. (1994). Impact of malaria on genetic polymorphism and genetic diseases in Africans and African Americans. Proc. Natl. Acad. Sci. U. S. A. *91*, 2415–2419.

Mizukawa, B., George, A., Pushkaran, S., Weckbach, L., Kalinyak, K., Heubi, J.E., and Kalfa, T.A. (2011). Cooperating G6PD mutations associated with severe neonatal hyperbilirubinemia and cholestasis. Pediatr. Blood Cancer *56*, 840–842.

Molina, I., Salvador, F., and Sánchez-Montalvá, A. (2014a). Posaconazole versus benznidazole for chronic Chagas' disease. N. Engl. J. Med. *371*, 966.

Molina, I., Gómez i Prat, J., Salvador, F., Treviño, B., Sulleiro, E., Serre, N., Pou, D., Roure, S., Cabezos, J., Valerio, L., et al. (2014b). Randomized trial of posaconazole and benznidazole for chronic Chagas' disease. N. Engl. J. Med. *370*, 1899–1908.

Molina, I., Salvador, F., Sánchez-Montalvá, A., Treviño, B., Serre, N., Sao Avilés, A., and Almirante, B. (2015). Toxic Profile of Benznidazole in Patients with Chronic Chagas Disease: Risk Factors and Comparison of the Product from Two Different Manufacturers. Antimicrob. Agents Chemother. *59*, 6125–6131.

Motulsky AG (1961). Glucose-6-phosphate dehydrogeanse deficiency haemolytic disease of the newborn and malaria. Lancet Lond. Engl. *1*, 1168–1169.

Moyersoen, J., Choe, J., Kumar, A., Voncken, F.G.J., Hol, W.G.J., and Michels, P.A.M. (2003). Characterization of Trypanosoma brucei PEX14 and its role in the import of glycosomal matrix proteins. Eur. J. Biochem. *270*, 2059–2067.

Murta, S.M., and Romanha, A.J. (1998). In vivo selection of a population of Trypanosoma cruzi and clones resistant to benznidazole. Parasitology *116 (Pt 2)*, 165–171.

Murta, S.M., Gazzinelli, R.T., Brener, Z., and Romanha, A.J. (1998). Molecular characterization of susceptible and naturally resistant strains of Trypanosoma cruzi to benznidazole and nifurtimox. Mol. Biochem. Parasitol. *93*, 203–214.

Naylor, C.E., Gover, S., Basak, A.K., Cosgrove, M.S., Levy, H.R., and Adams, M.J. (2001). NADP+ and NAD+ binding to the dual coenzyme specific enzyme Leuconostoc mesenteroides glucose 6-phosphate dehydrogenase: different interdomain hinge angles are seen in different binary and ternary complexes. Acta Crystallogr. D Biol. Crystallogr. *57*, 635–648.

Née, G., Zaffagnini, M., Trost, P., and Issakidis-Bourguet, E. (2009). Redox regulation of chloroplastic glucose-6-phosphate dehydrogenase: a new role for f-type thioredoxin. FEBS Lett. *583*, 2827–2832.

Neuberger, G., Maurer-Stroh, S., Eisenhaber, B., Hartig, A., and Eisenhaber, F. (2003). Motif refinement of the peroxisomal targeting signal 1 and evaluation of taxon-specific differences. J. Mol. Biol. *328*, 567–579.

Noireau, F., Diosque, P., and Jansen, A.M. (2009). Trypanosoma cruzi: adaptation to its vectors and its hosts. Vet. Res. *40*, 26.

Notaro, R., Afolayan, A., and Luzzatto, L. (2000). Human mutations in glucose 6-phosphate dehydrogenase reflect evolutionary history. FASEB J. Off. Publ. Fed. Am. Soc. Exp. Biol. *14*, 485–494.

Obiol-Pardo, C., Alcarraz-Vizán, G., Díaz-Moralli, S., Cascante, M., and Rubio-Martinez, J. (2014). Design of an interface peptide as new inhibitor of human glucose-6-phosphate dehydrogenase. J. Mol. Graph. Model. *49*, 110–117.

Oppenheim, A., Jury, C.L., Rund, D., Vulliamy, T.J., and Luzzatto, L. (1993). G6PD Mediterranean accounts for the high prevalence of G6PD deficiency in Kurdish Jews. Hum. Genet. *91*, 293–294.

Opperdoes, F.R., Baudhuin, P., Coppens, I., De Roe, C., Edwards, S.W., Weijers, P.J., and Misset, O. (1984). Purification, morphometric analysis, and characterization of the glycosomes (microbodies) of the protozoan hemoflagellate Trypanosoma brucei. J. Cell Biol. *98*, 1178–1184.

Ortíz, C. (2012). Caracterización Bioquímica y Estructural de la Glucosa 6-fosfato deshidrogenasa de Tripanosoma cruzi. Universidad de la República.

Ortiz, C., Moraca, F., Medeiros, A., Botta, M., Hamilton, N., and Comini, M.A. (2016). Binding Mode and Selectivity of Steroids towards Glucose-6-phosphate Dehydrogenase from the Pathogen Trypanosoma cruzi. Mol. Basel Switz. *21*, 368.

Parodi-Talice, A., Monteiro-Goes, V., Arrambide, N., Avila, A.R., Duran, R., Correa, A., Dallagiovanna, B., Cayota, A., Krieger, M., Goldenberg, S., et al. (2007). Proteomic analysis of metacyclic trypomastigotes undergoing Trypanosoma cruzi metacyclogenesis. J. Mass Spectrom. JMS *42*, 1422–1432.

Piacenza, L., Zago, M.P., Peluffo, G., Alvarez, M.N., Basombrio, M.A., and Radi, R. (2009). Enzymes of the antioxidant network as novel determiners of Trypanosoma cruzi virulence. Int. J. Parasitol. *39*, 1455–1464.

Piacenza, L., Peluffo, G., Alvarez, M.N., Martínez, A., and Radi, R. (2013). Trypanosoma cruzi Antioxidant Enzymes As Virulence Factors in Chagas Disease. Antioxid. Redox Signal. *19*, 723–734.

Pinazo, M.-J., Espinosa, G., Gállego, M., López-Chejade, P.L., Urbina, J.A., and Gascón, J. (2010). Successful treatment with posaconazole of a patient with chronic Chagas disease and systemic lupus erythematosus. Am. J. Trop. Med. Hyg. *82*, 583–587.

Piñeyro, M.D., Parodi-Talice, A., Arcari, T., and Robello, C. (2008). Peroxiredoxins from Trypanosoma cruzi: virulence factors and drug targets for treatment of Chagas disease? Gene *408*, 45–50.

Poirier, D. (2013). Synthesis and biological testing of steroid derivatives as inhibitors. J. Steroid Biochem. Mol. Biol. *137*, 174–175.

Preuss, J., Maloney, P., Peddibhotla, S., Hedrick, M.P., Hershberger, P., Gosalia, P., Milewski, M., Li, Y.L., Sugarman, E., Hood, B., et al. (2012a). Discovery of a Plasmodium falciparum glucose-6-phosphate dehydrogenase 6-phosphogluconolactonase inhibitor (R,Z)-N-((1-ethylpyrrolidin-2-yl)methyl)-2-(2-fluorobenzylidene)-3-oxo-3,4-dihydro-2H-benzo[b][1,4]thiazine-6-carboxamide (ML276) that reduces parasite growth in vitro. J. Med. Chem. *55*, 7262–7272.

Preuss, J., Hedrick, M., Sergienko, E., Pinkerton, A., Mangravita-Novo, A., Smith, L., Marx, C., Fischer, E., Jortzik, E., Rahlfs, S., et al. (2012b). High-throughput screening for small-molecule inhibitors of plasmodium falciparum glucose-6-phosphate dehydrogenase 6-phosphogluconolactonase. J. Biomol. Screen. *17*, 738–751.

Preuss, J., Richardson, A.D., Pinkerton, A., Hedrick, M., Sergienko, E., Rahlfs, S., Becker, K., and Bode, L. (2013). Identification and characterization of novel human glucose-6-phosphate dehydrogenase inhibitors. J. Biomol. Screen. *18*, 286–297.

Raineri, R., and Levy, H.R. (1970). On the specificity of steroid interaction with mammary glucose 6-phosphate dehydrogenase. Biochemistry (Mosc.) *9*, 2233–2243.

Rakitzis, E.T., and Papandreou, P. (1998). Reactivity of 6-phosphogluconolactone with hydroxylamine: the possible involvement of glucose-6-phosphate dehydrogenase in endogenous glycation reactions. Chem. Biol. Interact. *113*, 205–216.

Ranzani, A.T., and Cordeiro, A.T. (2017). Mutations in the tetramer interface of human glucose-6-phosphate dehydrogenase reveals kinetic differences between oligomeric states. FEBS Lett.

Rodriguez, J.B., Falcone, B.N., and Szajnman, S.H. (2016). Detection and treatment of Trypanosoma cruzi: a patent review (2011-2015). Expert Opin. Ther. Pat. *26*, 993–1015.

Rokka, A., Antonenkov, V.D., Soininen, R., Immonen, H.L., Pirilä, P.L., Bergmann, U., Sormunen, R.T., Weckström, M., Benz, R., and Hiltunen, J.K. (2009). Pxmp2 is a channel-forming protein in Mammalian peroxisomal membrane. PloS One *4*, e5090.

Romao, S., Castro, H., Sousa, C., Carvalho, S., and Tomás, A.M. (2009). The cytosolic tryparedoxin of Leishmania infantum is essential for parasite survival. Int. J. Parasitol. *39*, 703–711.

Rosa, R., Basmadjián, Y., González-Murguiondo, M., González-Arias, M., and Salvatella, R. (2001). Actualización clínico-epidemiológica y terapéutica de la enfermedad de Chagas en Uruguay. Rev. Médica Urug. *17*, 125–132.

Roth, E.F., Raventos-Suarez, C., Rinaldi, A., and Nagel, R.L. (1983). Glucose-6-phosphate dehydrogenase deficiency inhibits in vitro growth of Plasmodium falciparum. Proc. Natl. Acad. Sci. U. S. A. *80*, 298–299.

Rowland, P., Basak, A.K., Gover, S., Levy, H.R., and Adams, M.J. (1994). The three-dimensional structure of glucose 6-phosphate dehydrogenase from Leuconostoc mesenteroides refined at 2.0 A resolution. Struct. Lond. Engl. 1993 *2*, 1073–1087.

Ruwende, C., Khoo, S.C., Snow, R.W., Yates, S.N., Kwiatkowski, D., Gupta, S., Warn, P., Allsopp, C.E., Gilbert, S.C., and Peschu, N. (1995). Natural selection of hemi- and heterozygotes for G6PD deficiency in Africa by resistance to severe malaria. Nature *376*, 246–249.

Salomao, K., Menna-Barreto, R.F.S., and de Castro, S.L. (2016). Stairway to Heaven or Hell? Perspectives and Limitations of Chagas Disease Chemotherapy. Curr. Top. Med. Chem. *16*, 2266–2289.

Salvatella R (2009). Enfermedad de Chagas, algunos aspectos de su situación epidemiológica a los 100 años de su descripción. A 100 Años de la enfermedad de Chagas contribuciones desde Uruguay (OPS).

Sánchez, L.V., and Ramírez, J.D. (2013). Congenital and oral transmission of American trypanosomiasis: an overview of physiopathogenic aspects. Parasitology *140*, 147–159.

Sanchez-Burgos, G., Mezquita-Vega, R.G., Escobedo-Ortegon, J., Ramirez-Sierra, M.J., Arjona-Torres, A., Ouaissi, A., Rodrigues, M.M., and Dumonteil, E. (2007). Comparative evaluation of therapeutic DNA vaccines against Trypanosoma cruzi in mice. FEMS Immunol. Med. Microbiol. *50*, 333–341.

Santos, C.D., Loria, R.M., Oliveira, L.G.R., Kuehn, C.C., Toldo, M.P.A., Albuquerque, S., and do Prado, J.C. (2010). Effects of dehydroepiandrosterone-sulfate (DHEA-S) and benznidazole treatments during acute infection of two different Trypanosoma cruzi strains. Immunobiology *215*, 980–986.

Schliebs, W., and Kunau, W.-H. (2006). PTS2 co-receptors: diverse proteins with common features. Biochim. Biophys. Acta *1763*, 1605–1612.

Shin, E.S., Park, J., Shin, J.-M., Cho, D., Cho, S.Y., Shin, D.W., Ham, M., Kim, J.B., and Lee, T.R. (2008). Catechin gallates are NADP+-competitive inhibitors of glucose-6-phosphate dehydrogenase and other enzymes that employ NADP+ as a coenzyme. Bioorg. Med. Chem. *16*, 3580–3586.

Shreve, D.S., and Levy, H.R. (1977). On the molecular weight of human glucose 6-phosphate dehydrogenase. Biochem. Biophys. Res. Commun. *78*, 1369–1375.

Silber, A.M., Tonelli, R.R., Lopes, C.G., Cunha-e-Silva, N., Torrecilhas, A.C.T., Schumacher, R.I., Colli, W., and Alves, M.J.M. (2009). Glucose uptake in the mammalian stages of Trypanosoma cruzi. Mol. Biochem. Parasitol. *168*, 102–108.

Sokolova, A.Y., Wyllie, S., Patterson, S., Oza, S.L., Read, K.D., and Fairlamb, A.H. (2010). Cross-resistance to nitro drugs and implications for treatment of human African trypanosomiasis. Antimicrob. Agents Chemother. *54*, 2893–2900.

Stoffel, S.A., Alibu, V.P., Hubert, J., Ebikeme, C., Portais, J.-C., Bringaud, F., Schweingruber, M.E., and Barrett, M.P. (2011). Transketolase in Trypanosoma brucei. Mol. Biochem. Parasitol. *179*, 1–7.

Stuart, K., Brun, R., Croft, S., Fairlamb, A., Gürtler, R.E., McKerrow, J., Reed, S., and Tarleton, R. (2008). Kinetoplastids: related protozoan pathogens, different diseases. J. Clin. Invest. *118*, 1301–1310.

Tarleton, R.L., and Zhang, L. (1999). Chagas disease etiology: autoimmunity or parasite persistence? Parasitol. Today Pers. Ed *15*, 94–99.

Taylor, M.C., Lewis, M.D., Fortes Francisco, A., Wilkinson, S.R., and Kelly, J.M. (2015). The Trypanosoma cruzi vitamin C dependent peroxidase confers protection against oxidative stress but is not a determinant of virulence. PLoS Negl. Trop. Dis. *9*, e0003707.

Teusink, B., Walsh, M.C., van Dam, K., and Westerhoff, H.V. (1998). The danger of metabolic pathways with turbo design. Trends Biochem. Sci. *23*, 162–169.

Tishkoff, S.A., Varkonyi, R., Cahinhinan, N., Abbes, S., Argyropoulos, G., Destro-Bisol, G., Drousiotou, A., Dangerfield, B., Lefranc, G., Loiselet, J., et al. (2001). Haplotype diversity and linkage disequilibrium at human G6PD: recent origin of alleles that confer malarial resistance. Science *293*, 455–462.

Tyler, K.M., and Engman, D.M. (2001). The life cycle of Trypanosoma cruzi revisited. Int. J. Parasitol. *31*, 472–481.

Urbina, J.A. (2009). Ergosterol biosynthesis and drug development for Chagas disease. Mem. Inst. Oswaldo Cruz *104 Suppl 1*, 311–318.

Veitch, N.J., Maugeri, D.A., Cazzulo, J.J., Lindqvist, Y., and Barrett, M.P. (2004). Transketolase from Leishmania mexicana has a dual subcellular localization. Biochem. J. *382*, 759–767.

Verma, A., Chandra, S., Suthar, M.K., Doharey, P.K., Siddiqi, M.I., and Saxena, J.K. (2016). $NADP^+$ binding effects tryptophan accessibility, folding and stability of recombinant B. malayi G6PD. Int. J. Biol. Macromol. *85*, 645–654.

Verplaetse, E., Rigden, D.J., and Michels, P.A.M. (2009). Identification, characterization and essentiality of the unusual peroxin 13 from Trypanosoma brucei. Biochim. Biophys. Acta *1793*, 516–527.

Volkman, S.K., Barry, A.E., Lyons, E.J., Nielsen, K.M., Thomas, S.M., Choi, M., Thakore, S.S., Day, K.P., Wirth, D.F., and Hartl, D.L. (2001). Recent origin of Plasmodium falciparum from a single progenitor. Science *293*, 482–484.

de Walque, S., Kiel, J.A., Veenhuis, M., Opperdoes, F.R., and Michels, P.A. (1999). Cloning and analysis of the PTS-1 receptor in Trypanosoma brucei. Mol. Biochem. Parasitol. *104*, 106–119.

Wang, X.-T., Lam, V.M.S., and Engel, P.C. (2005). Marked decrease in specific activity contributes to disease phenotype in two human glucose 6-phosphate dehydrogenase mutants, G6PD(Union) and G6PD(Andalus). Hum. Mutat. *26*, 284.

Wenderoth, I., Scheibe, R., and von Schaewen, A. (1997). Identification of the cysteine residues involved in redox modification of plant plastidic glucose-6-phosphate dehydrogenase. J. Biol. Chem. *272*, 26985–26990.

Wendt, U.K., Wenderoth, I., Tegeler, A., and Von Schaewen, A. (2000). Molecular characterization of a novel glucose-6-phosphate dehydrogenase from potato (Solanum tuberosum L.). Plant J. Cell Mol. Biol. *23*, 723–733.

Whenert, E. (2012). Screening of storage conditions for the Glucose-6-phosphate dehydrogenase of Trypanosoma cruzi. Beuth Hochschule für Technik.

Wyatt, P.G., Gilbert, I.H., Read, K.D., and Fairlamb, A.H. (2011). Target validation: linking target and chemical properties to desired product profile. Curr. Top. Med. Chem. *11*, 1275–1283.

Yoshida, N. (2009). Molecular mechanisms of Trypanosoma cruzi infection by oral route. Mem. Inst. Oswaldo Cruz *104 Suppl 1*, 101–107.

Zago, M.P., Hosakote, Y.M., Koo, S.-J., Dhiman, M., Piñeyro, M.D., Parodi-Talice, A., Basombrio, M.A., Robello, C., and Garg, N.J. (2016). TcI Isolates of Trypanosoma cruzi Exploit the Antioxidant Network for Enhanced Intracellular Survival in Macrophages and Virulence in Mice. Infect. Immun. *84*, 1842–1856.

Zhao, Z.-B., Liu, Y., and Yao, Y. (2014). Computational determination of binding structures and free energies of glucose 6-phosphate dehydrogenase with novel steroid inhibitors. J. Mol. Graph. Model. *51*, 168–172.

Zhelev, Z., Ivanova, D., Bakalova, R., Aoki, I., and Higashi, T. (2016). Inhibition of the Pentose-phosphate Pathway Selectively Sensitizes Leukemia Lymphocytes to Chemotherapeutics by ROS-independent Mechanism. Anticancer Res. *36*, 6011–6020.

AGRADECIMIENTOS

Los resultados presentados en este trabajo de tesis fueron generados entre diciembre de 2012 y febrero de 2016. La mayoría de ellos fueron publicados en revistas internacionales arbitradas y presentados en congresos nacionales e internacionales, tanto en formato de poster como de presentación oral. Es importante destacar que en el marco de este proyecto tuve la oportunidad de co-dirigir la Tesis de grado de Evelyn Whenert, 2012.

Este proyecto contó con el apoyo del Institut Pasteur y varios investigadores del ambito nacional e internacional. Quisiera destacar el aporte de la Dra. Andrea Medeiros (Facultado de Medicina) co-directora de mi tesis de Maestría que contribuyó a sentar las bases de este proyecto de Doctorado, el Dr. Juan José Cazzulo de la Universidad de Rosario- Argentina; Dra. Francesca Moraca de la Universidad de Siena, Italia; Lic. Evelyn Whenert de Beuth Hochschule für Technik, Alemania, Dr. Horacio Botti, Lic. Nicole Larrieux y Dr. Alejandro Buzzchiazo del laboratorio de Cristalografía de Proteínas.
Asi como a los miembros de las Unidades Técnicas del IP-Montevideo, principalmente a las unidades de Proteínas Recombinantes (UPR), Cristalografía de Proteínas (PXF), Biología Celular (UBC), Biología Molecular (BM) y Microscopía.

El trabajo de tesis fue financiado por varias instituciones: ANII, mediante el programa INNOVA, SNB y SNI; PEDECIBA, mediante becas movilidad y asistencia a congresos; CAP, mediante becas de finalización postgrado. Asi como, Institut Pasteur Montevideo (IPM), Institut Pasteur International Network (RIIP), COST-ACtion CM0801, UCyR, CNPq, Universidad de Heildelberg, entre otros.

Sin lugar a dudas, esta Tesis fue posible gracias al apoyo de muchas personas y por ello quisiera agradecer especialmente:
Al Tribunal de tesis por su buena disposición y la gentiliza de aceptar corregir este trabajo.
A Marcelo por ser el Sr. Miyagi durante todos estos años.
A Andrea por estar siempre presente.
A mis compañeros del Labocho.
A la gente del IP, sin olvidarme de Bea, Claudio, Inchausti y Mario.
A la gente de Alemania y de EEUU.

Y a mis otros colaboradores incondicionales...
Mis padres y Mogli; mi familia grande y mis amigos.
A Martín.
A Morita y León.